L-Aspartate is a high-quality nitrogen source of *Escherichia coli*: regulation and physiology

DISSERTATION

ZUR ERLANGUNG DES GRADES

DOKTOR DER NATURWISSENSCHAFTEN

AM FACHBEREICH BIOLOGIE

DER JOHANNES GUTENBERG-UNIVERSITÄT MAINZ

CHRISTOPHER SCHUBERT

GEBOREN AM 04. NOVEMBER 1993 IN BENSHEIM

MAINZ, MÄRZ 2021

Dekan: Prof. Dr. Eckhard Thines

1. Berichterstatter: Prof. Dr. Gottfried Unden

2. Berichterstatter: Prof. Dr. Ralf Heermann

Tag der mündlichen Prüfung: 09.09.2021

Contents

A Abstract

Escherichia coli is a highly adaptable bacterium, which can utilize diverse carbon and nitrogen sources. In aerobic growth, the L-Asp transporter DcuA and the aspartate ammonia-lyase AspA catalyze a collaborative nitrogen shuttle in which L-Asp is transported into the bacterial cell and directly deaminated to form ammonium and fumarate. Ammonium is assimilated in the GS-GOGAT pathway, while fumarate is exported. In anaerobic growth, fumarate can be used to drive fumarate respiration, which transforms L-Asp to an electron acceptor and nitrogen source, emphasizing the importance of L-Asp. AspA was stimulated by GlnB saturated with either 2-oxoglutarate and ATP, a bound UMP, or both. GlnB stimulates AspA deamination activity twofold, providing ammonium under nitrogen-limited conditions to supply the bacterial cell with a nitrogen source. The DcuA-AspA-GS-GOGAT pathway is able to produce L-Asp, L-Gln, L-Glu, and ammonium, which completely satisfies the nitrogen requirement of *E. coli*. L-Asp was found in millimolar concentration in the mouse intestine, which highlights its physiological relevance.

DctA is an aerobic C_4-dicarboxylate transporter which has a high affinity for succinate. Reporter gene assays of *aspAp* and *dctAp* expression, demonstrated a high sensitivity of the expression to the presence of different carbon sources, such as sugars, sugar alcohols, and C_4-dicarboxylates. cAMP-CRP fine-tunes the expression of genes involved in the catabolism of substrates other than glucose, including *aspA* and *dctA,* in response to carbon availability. Bioinformatics revealed a mutation of the CRP-binding site in the dominant first half site of *dctAp*, explaining the higher repression in the presence of glycerol and D-xylose. In addition, DctA showed interaction with $EIIA^{Glc}$ of the glucose:phosphotransferase system, which is supposed to inhibit C_4-dicarboxylate uptake in aerobic growth when upper and lower glycolytic substrates are available.

Enzymes that catalyze sequential reactions in metabolic pathways can be organized into sequential complexes ('metabolons') capable of channeling metabolic intermediates and increasing metabolic efficiency. Interaction between DcuA-AspA, DcuB-AspA, and DcuB-FumB was demonstrated and was suggested to drive nitrogen assimilation and fumarate respiration.

The sensor histidine kinase DcuS was modeled using various bioinformatic tools to investigate the interaction between the DcuS linker region and DctA helix 8b. The interaction model postulated a salt bridge between two residues to stabilize the interaction. In addition, the DcuS model, multiple sequence alignment, and current research indicated an L-Proline hinge in the N-terminal α-helix of the cytoplasmic PAS domain.

B Zusammenfassung

Escherichia coli ist ein anpassungsfähiges Bakterium, das verschiedene Kohlenstoff- und Stickstoffquellen verwerten kann. Bei aerobem Wachstum katalysieren der L-Asp-Transporter DcuA und die Aspartase AspA einen Stickstoff-Shuttle, bei dem L-Asp in die Bakterienzelle transportiert und direkt zu Ammonium und Fumarat deaminiert wird. Ammonium wird über den GS-GOGAT-Weg assimiliert, während Fumarat exportiert wird. Bei anaerobem Wachstum wird Fumarat für die Fumarat-Atmung verwendet, wodurch L-Asp einen Elektronenakzeptor (Fumarat) und eine Stickstoffquelle (Ammonium) liefert. AspA wird durch GlnB stimuliert, das entweder mit 2-Oxoglutarat und ATP oder UMP oder beidem gesättigt ist. GlnB steigert die AspA-Desaminierungsaktivität zweifach, wodurch unter Stickstoff-limitierten Bedingungen Ammonium bereitgestellt wird, um die Bakterienzelle mit einer Stickstoffquelle zu versorgen. Der DcuA-AspA-GS-GOGAT-Weg ist in der Lage, L-Asp, L-Gln, L-Glu und Ammonium zu produzieren, was den Stickstoffbedarf von *E. coli* vollständig deckt. L-Asp wurde in millimolarer Konzentration im Mäusedarm gefunden, was seine physiologische Relevanz unterstreicht. Der aerobe C_4-Dicarboxylat-Transporter DctA hat eine hohe Affinität für Succinat. Reportergen-Tests von *aspAp* und *dctAp* zeigten eine hohe Sensitivität der Expression gegenüber verschiedene Kohlenstoffquellen. cAMP-CRP reguliert die Expression von Genen, die am Katabolismus von nicht-PTS Substraten beteiligt sind, wie im Fall von *aspA* und *dctA*. Die bioinformatische Analyse zeigte eine Mutation der CRP-Bindungsstelle in der dominanten ersten Halbseite von *dctAp*, was die höhere Repression in Gegenwart von Glycerin und D-Xylose erklärt. Darüber hinaus zeigte DctA eine Interaktion mit $EIIA^{Glc}$, was vermutlich die Aufnahme von C_4-Dicarboxylaten im aeroben Wachstum hemmt, wenn obere und untere glykolytische Substrate verfügbar sind. Enzyme, die aufeinanderfolgende Reaktionen in Stoffwechselwegen katalysieren, können in sequentiellen Komplexen ('Metabolons') organisiert sein, die eine effiziente Weiterleitung von Intermediaten und dementsprechend die metabolische Effizienz erhöhen. Eine Interaktion zwischen DcuA-AspA, DcuB-AspA und DcuB-FumB wurde nachgewiesen, die Metabolons zur effizienten Bildung von Fumarat aus C_4-Dicarboxylaten für die Fumarat-Atmung vermuten lässt. Die Sensor-Histidin-Kinase DcuS wurde mit bioinformatischen Methoden modelliert, um die Interaktion zwischen der DcuS-Linker-Region und der DctA-Helix 8b zu untersuchen. Das Interaktionsmodell postuliert eine Salzbrücke zwischen zwei Resten zur Stabilisierung der Interaktion. Das DcuS-Modell, multiple Sequenz-Alignments und experimentelle Daten weisen auf ein L-Prolin-Scharnier in der N-terminalen α-Helix der cytoplasmatischen PAS-Domäne hin.

C List of publications

Strecker, A., **Schubert, C.**, Zedler, S., Steinmetz, P. & Unden, G. 2018. DcuA of aerobically grown *Escherichia coli* serves as a nitrogen shuttle (L-aspartate/fumarate) for nitrogen uptake. *Mol Microbiol*, **109**(6), 801-811.

Wissig, J., Grischin, J., Bassler, J., **Schubert, C.**, Friedrich, T., Bähre, Schultz, J.E. & Unden, G. 2019. CyaC, a redox-regulated adenylate cyclase of *Sinorhizobium meliloti* with a quinone responsive diheme-B membrane anchor domain. *Mol Microbiol*, **112**(1), 16-28.

Schubert, C., Zedler, S., Strecker, A. & Unden, G. 2020. L-Aspartate as a high-quality nitrogen source in *Escherichia coli*: Regulation of L-aspartase by the nitrogen regulatory system and interaction of L-aspartase with GlnB. *Mol Microbiol*, **115**(4), 526-538.

Stopp, M., Steinmetz, P. A., **Schubert, C.**, Griesinger, C., Schneider, D. & Unden, G. 2021. Transmembrane signaling and cytoplasmic signal conversion by dimeric transmembrane helix 2 and a linker domain of the DcuS sensor kinase. *J Biol Chem* **296**, 100148.

Schubert, C.*, Winter, M. G.*; Ebert-Jung, A., Kierszniowska, S., Nagel-Wolfrum, K., Schramm, T., Link, H., Winter, S. & Unden, G. 2021 C_4-dicarboxylates and L-aspartate utilization by *Escherichia coli* K-12 in the mouse intestine: L-aspartate as a major substrate for fumarate respiration and as a nitrogen source. *Environ Microbiol*, **23**(5), 2564-2577.

Schubert, C. & Unden, G. 2021. C_4-dicarboxylate metabolons: Interaction of C_4-dicarboxylate transporters of *Escherichia coli* with cytosolic enzymes and regulators. doi: bioRxiv 2021.03.01.433382. (**Preprint publication**)

Stopp, M., **Schubert, C.*** & Unden, G. (2021) Conversion of the Sensor Kinase DcuS to the Fumarate Sensitive State by Interaction of the Bifunctional Transporter DctA at the TM2/PASC-Linker Region. *Microorganisms* **9**, 1397

***Share first co-author and contributed equally to this work.**

1 Introduction

Gram-negative and facultatively anaerobic *Escherichia coli* is a model organism belonging to the phylum Proteobacteria. *E. coli* has high adaptability and can obtain energy for growth from a variety of substrates in the presence or absence of the electron acceptor oxygen. Efficient utilization of the available substrates requires gene regulation in response to external environmental factors. Aerobic and anaerobic respiration or fermentation use electron acceptors that allow metabolism with significantly different energy yields. Based on the energy yield, the expression of the genes of the respective enzymes is regulated hierarchically (Gunsalus 1992). The ubiquitous electron donor with a low redox potential is hydrogen ($E^{o'}$= -0.413 V). Oxygen has the highest redox potential ($E^{o'}$= +0.82 V) and allows the highest energy yield. In the absence of oxygen, anaerobic respiration uses alternative electron acceptors according to their redox potential, which in turn defines the energy yield. The redox potential decreases from nitrate ($E^{o'}$= +0.43 V) to dimethyl sulfoxide (DMSO, $E^{o'}$= +0.16 V), trimethylamine oxide (TMAO, $E^{o'}$= +0.13 V) and fumarate ($E^{o'}$= +0.03 V).

The regulatory system for the transition between aerobic or anaerobic respiration and fermentation involves the global sensor FNR (fumarate nitrate reductase) and the two-component system ArcB-ArcA (anoxic redox control) (Spiro and Guest 1990; Green *et al.* 1991; Iuchi and Lin 1992). ArcB indirectly detects the redox status of the cell via the redox state of the quinones and represses genes involved in aerobic respiration. FNR is a transcriptional regulator that controls hundreds of genes, mainly repressing genes involved in aerobic metabolism while inducing genes involved in anaerobic metabolism. FNR is a dimeric protein containing a [4Fe-4S] cluster that decays to a [2Fe-2S] cluster in the presence of oxygen. FNR with a [2Fe-2S] cluster loses the ability to dimerize and bind to DNA (Khoroshilova *et al.* 1995). Apart from ArcBA and FNR, there are other regulatory mechanisms of alternative electron acceptors. The two-component systems, consisting of a sensor histidine kinase and a response regulator, NarX-NarL and NarQ-NarP, stimulate nitrate respiration genes in the presence of nitrate and nitrite. Both repress genes involved in anaerobic respiration of alternative electron acceptors (Rabin and Stewart 1993; Stewart *et al.* 2003). The utilization of the electron acceptor TMAO is regulated by the two-component system TorS-TorR (Jourlin *et al.* 1996). The presence of fumarate is detected by DcuS-DcuR (C_4-dicarboxylate uptake sensor/regulator), which induces the expression of genes involved in fumarate respiration, such as terminal fumarate reductase and associated transport proteins (Zientz *et al.* 1998).

1.1 Interplay of carbon and nitrogen metabolism

The main objective of carbohydrate metabolism is to provide ATP for energy-dependent reactions and carbon skeletons for biosynthesis and assimilation purposes. *E. coli* is a glycolytic bacterium in which glucose is the preferred substrate. Besides glucose, regulation is based on the available carbon source, which is usually organized according to energy density (Stülke and Hillen 1999; Leuze *et al.* 2012). The energy density is defined by how early a carbon source is introduced into the central metabolic pathway (Fig. 1), which consists of several sections: First, the glycolysis with the main task of hexose degradation. Glycolysis can be divided into the upper and lower glycolytic pathways, with the fructose-bisphosphate aldolase reaction representing the boundary. Second, the pentose phosphate pathway channels pentoses into the upper and lower glycolytic pathways, and third, the tricarboxylic acid (TCA) cycle, including pyruvate dehydrogenase, which links the reactions of glycolysis and the TCA cycle. The TCA cycle provides a plethora of precursors for different biosynthetic pathways. One of the most important intermediates of the TCA cycle is 2-oxoglutarate (2-OG) (Fig. 1). This substrate is not only a central indicator of the nitrogen and carbon status of *E. coli* but also the precursor of nitrogen assimilation and an emerging master regulator (Yuan *et al.* 2009; van Heeswijk *et al.* 2013; Huergo and Dixon 2015). Nitrogen assimilation revolves around 2-OG and the amino acids L-Glu and L-Gln. All three substrates have the same C_5-carbon skeleton derived from the TCA cycle. The nitrogen metabolism is dependent on the carbon metabolism, as this provides the carbon skeleton to assimilate ammonium. Both metabolisms are very closely linked in *E. coli*, and accordingly their regulation, which will be explained in more detail in the following sections. Another important intermediate is oxaloacetate, which together with PEP can be considered as the starting point of gluconeogenesis and is crucial for the synthesis of amino sugars for the lipopolysaccharide layer of the outer membrane in *E. coli*.

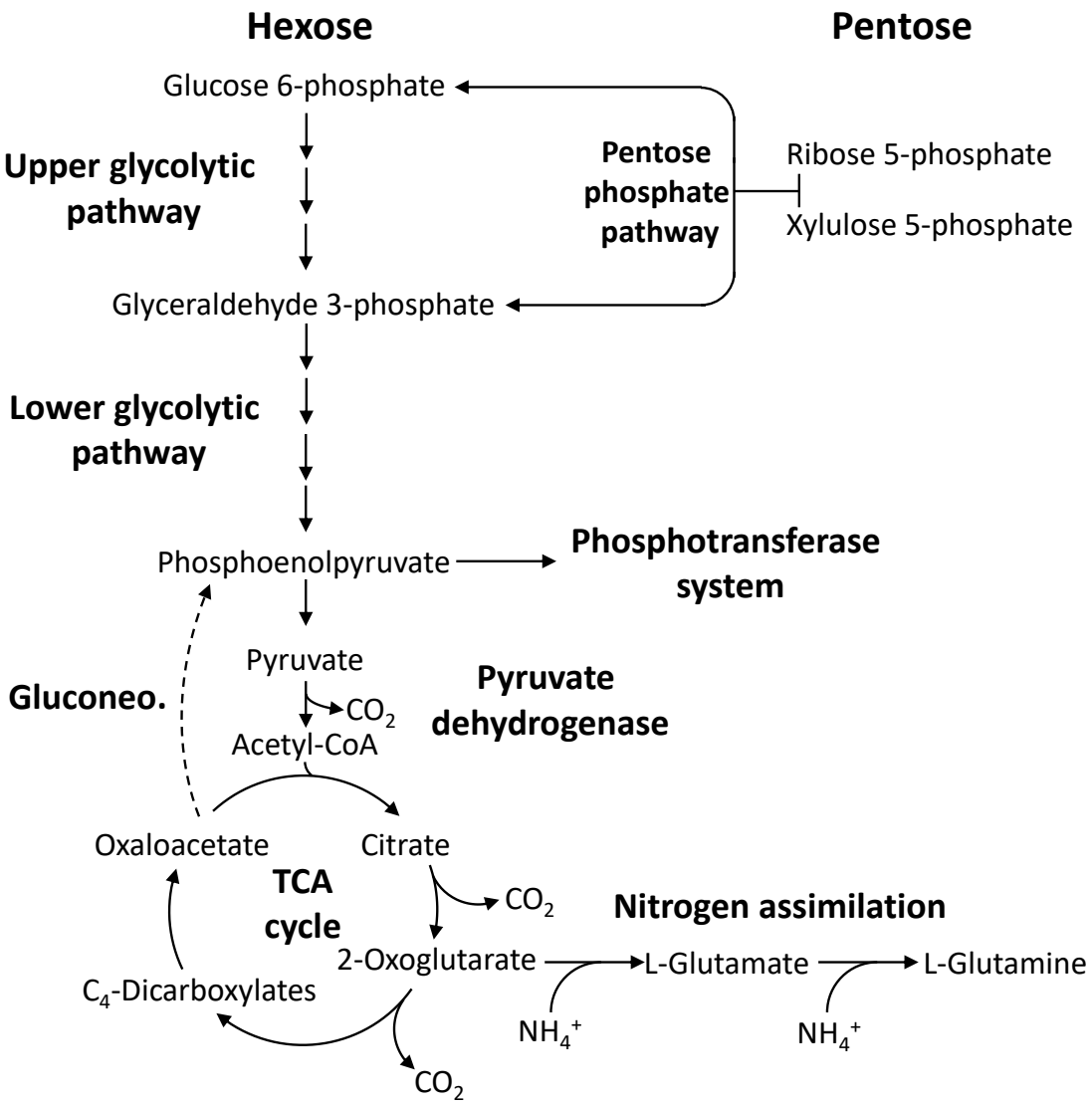

Fig. 1: Central metabolic pathway of *E. coli*. Glycolysis can be divided into the upper and lower glycolytic pathways, with pentoses being introduced via the pentose phosphate pathway. Phosphoenolpyruvate is the phosphoryl group donor of the phosphotransferase system. The TCA cycle provides various precursors for nitrogen assimilation (2-oxoglutarate) and gluconeogenesis (oxaloacetate). Abbreviations: Gluconeo.: gluconeogenesis.

1.2 C_4-dicarboxylate metabolism in *E. coli*

1.2.1 Aerobic C_4-dicarboxylate metabolism in *E. coli*

E. coli is a glucophilic bacterium, but can additionally use a variety of different sugars, sugar alcohols, and C_4-dicarboxylates, such as L-malate, fumarate, succinate, oxaloacetate, L-tartrate, and L-Asp as an energy and carbon source (Unden *et al.* 2016). C_4-dicarboxylate metabolism differs according to oxygen availability.

In the presence of oxygen, C_4-dicarboxylates are transported inside the bacterial cell and introduced into the TCA cycle of *E. coli* (Fig. 2) (Maloney *et al.* 1974). In general, C_4-dicarboxylates are gluconeogenic substrates and provide little energy, requiring the pyruvate/phosphoenolpyruvate (PEP) bypass to serve as a carbon source (Hermsen *et al.* 2015; Surmann *et al.* 2020). The major aerobic C_4-dicarboxylate transporter is DctA at neutral pH and is replaced by DauA under acidic conditions (pH 5) (Kay and Kornberg 1971; Janausch *et al.* 2001; Karinou *et al.* 2013). In recent years, DcuA was identified as the main L-Asp transporter in aerobic growth. DcuA-AspA catalyze a nitrogen shuttle in which L-Asp is deaminated to release ammonium and fumarate, while fumarate is excreted in an antiport against L-Asp (Fig. 3) (Strecker *et al.* 2018). Ammonium is assimilated in the glutamine synthetase (GS, GlnA) glutamine 2-oxoglutarate aminotransferase (GOGAT, GltBD) pathway. C_4-dicarboxylates are completely oxidized to carbon dioxide in two consecutive TCA cycles. Oxidation of these substrates produces reducing equivalents in the form of ubiquinol (QH_2) and reduced nicotinamide adenine dinucleotide (NADH), both of which are subsequently used as electron donors in the aerobic respiratory chain. Succinate has the highest energy yield of the C_4-dicarboxylates. Immediately after succinate uptake, succinate dehydrogenase oxidizes succinate to fumarate, producing a QH_2 (Fig. 3). The oxidation of reducing equivalents is coupled with the translocation of protons across the membrane, establishing an electrochemical proton motive force. This electrochemical gradient is used to synthesize ATP by ATP synthase or to drive other proton potential-dependent reactions such as the electrogenic uptake of C_4-dicarboxylates.

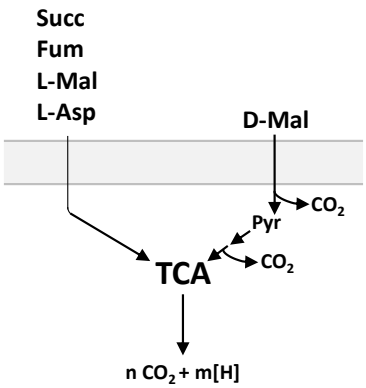

Fig. 2: Stylized aerobic C_4-dicarboxylate metabolism. Modified according to Unden *et al.* (2016).

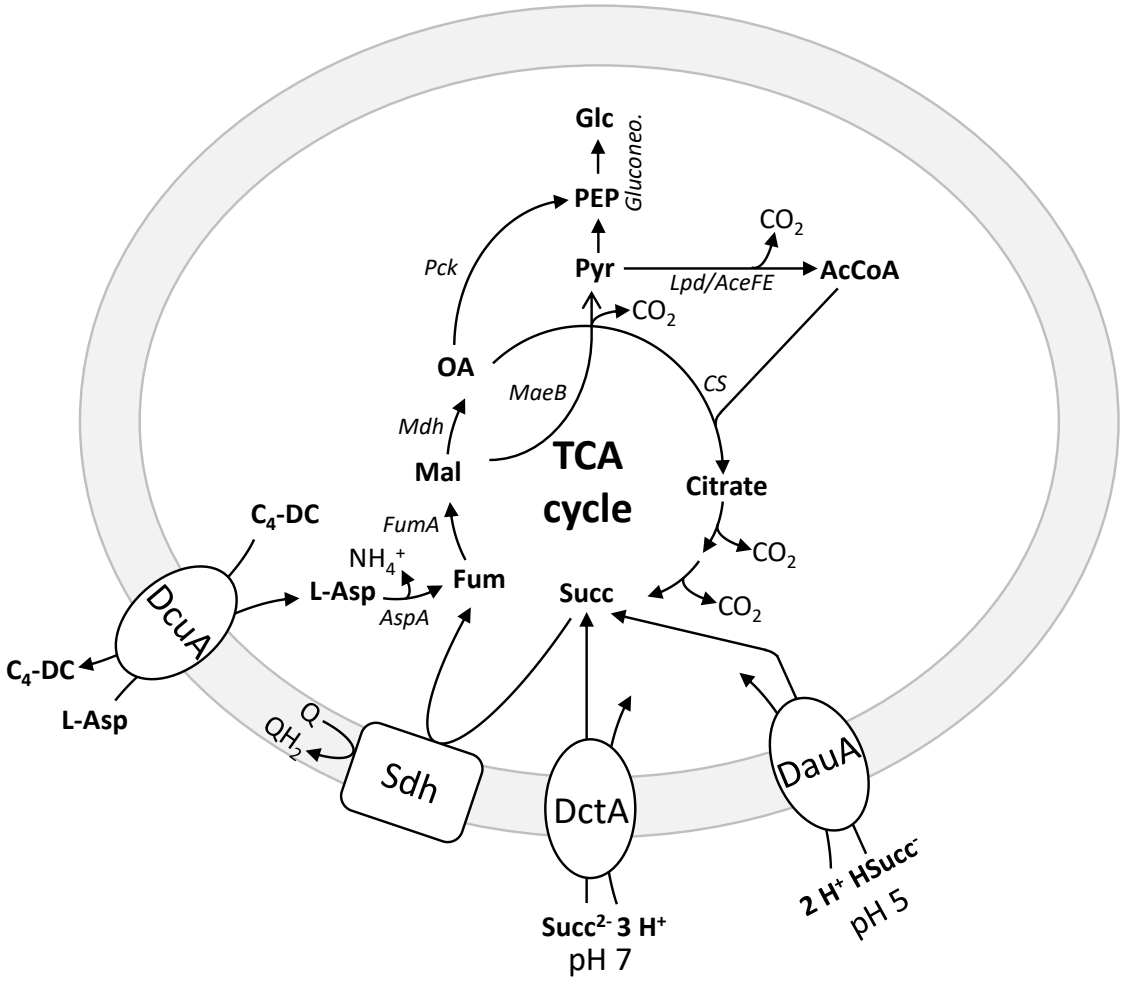

Fig. 3: Aerobic C_4-dicarboxylate metabolism in *E. coli*. Abbreviations: Glc: glucose; Gluconeo.: gluconeogenesis; PEP: phosphoenolpyruvate; Pck: phosphoenolpyruvate carboxykinase; OA: oxaloacetate; Lpd/AceFE: pyruvate dehydrogenase; AcCoA: acetyl-CoA; CS: citrate synthase; MaeB: $NADP^+$-dependent malate dehydrogenase; Mdh: malate dehydrogenase; FumA: fumarase A; AspA: aspartate ammonia-lyase; C_4-DC: C_4-dicarboxylate; Q/QH_2: ubiquinone/ubiquinol; Sdh: succinate dehydrogenase SdhABCD.

1.2.2 Anaerobic C_4-dicarboxylate metabolism in *E. coli*

In the absence of oxygen, C_4-dicarboxylates can be used as the electron acceptor in fumarate respiration. In general, C_4-dicarboxylates are converted either directly to fumarate in a one-step reaction or to fumarate via oxaloacetate (Fig. 4). However, *E. coli* requires additional substrates such as H_2, glycerol, or glucose for fumarate respiration. The latter two provide glyceraldehyde 3-phosphate and NADH, which is an electron donor for fumarate respiration (Guest 1979). Fumarate reductase

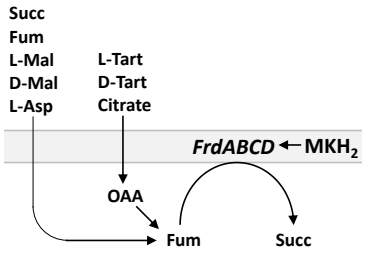

Fig. 4: Stylized anaerobic C_4-dicarboxylate metabolism. Modified according to Unden *et al.* (2016).

(FrdABCD) reduces fumarate to succinate with menaquinol as the electron donor. The fumarate reductase reaction itself does not translocate protons. Due to the absence of succinate dehydrogenase (SdhCDAB) under anaerobic conditions and the division of the TCA cycle into the oxidative and reductive branches, succinate is not further metabolized. Accordingly, succinate is exported as the end product of fumarate respiration (Fig. 5) (Spiro and Guest 1991; Park *et al.* 1995; Prohl *et al.* 1998), preferentially by the succinate exporter DcuC (Zientz *et al.* 1996; Zientz *et al.* 1999). The main anaerobic C_4-dicarboxylate antiporter for fumarate respiration with externally supplied C_4-dicarboxylates is DcuB, catalyzing a C_4-dicarboxylate:succinate antiport (Engel *et al.* 1992; Kleefeld *et al.* 2009). L-Malate is dehydrated by fumarase B (FumB) to fumarate. L-Asp is deaminated by aspartase (AspA), producing ammonium and fumarate. The main objective of anaerobic C_4-dicarboxylate metabolism is the conversion of C_4-dicarboxylates to fumarate (Fig. 5). In aerobic and anaerobic growth, C_4-dicarboxylates can be used as a carbon source. Anaerobic metabolism is optimized to convert C_4-dicarboxylate to fumarate, which drives fumarate respiration (Fig. 4 and Fig. 5) (Unden *et al.* 2016).

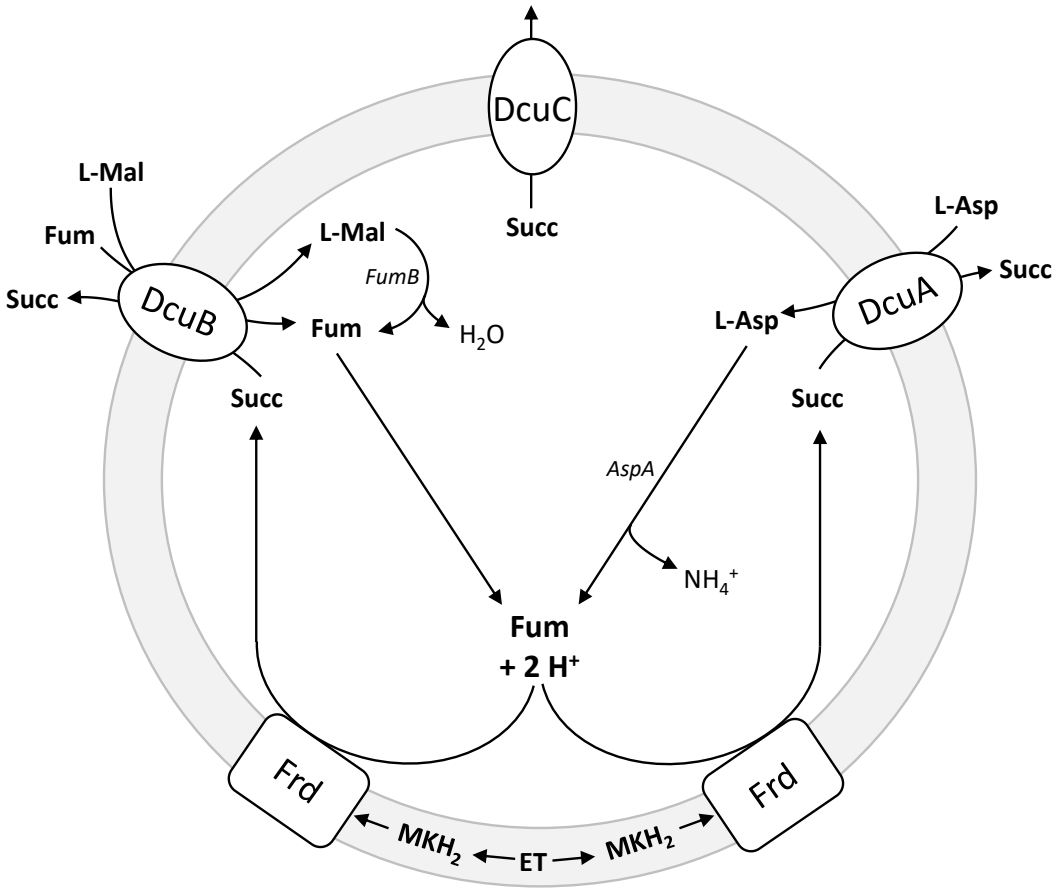

Fig. 5: Anaerobic C_4-dicarboxylate metabolism in *E. coli.* Abbreviations: L-Mal: L-malate; Fum: fumarate; Succ: succinate; FumB: fumarase B; Frd: fumarate reductase FrdABCD; MKH_2; menaquinol.

1.2.3 Aerobic and anaerobic respiratory chain of *E. coli*

The main function of central metabolism, consisting of glycolysis and the TCA cycle, is to oxidize carbon sources to carbon dioxide and provide building blocks for biosynthesis and reducing equivalents. The most important reducing equivalents are NAD^+ and ubiquinone (Q) or menaquinone (MK). $NADH+H^+$ and QH_2 or MKH_2 serve as electron donors to drive electron transport to the terminal electron acceptor to establish an electrochemical proton motive force across the cytoplasmic membrane. Electron transport is coupled with translocation of protons, against a concentration gradient into the periplasmic space. An electrochemical potential is defined by the concentration difference and the charge equilibrium of the hydrogen protons. The proton gradient is used to drive proton potential-dependent transport and ATP synthesis. This principle applies to both the aerobic and anaerobic respiratory chain (Fig. 6A and B).

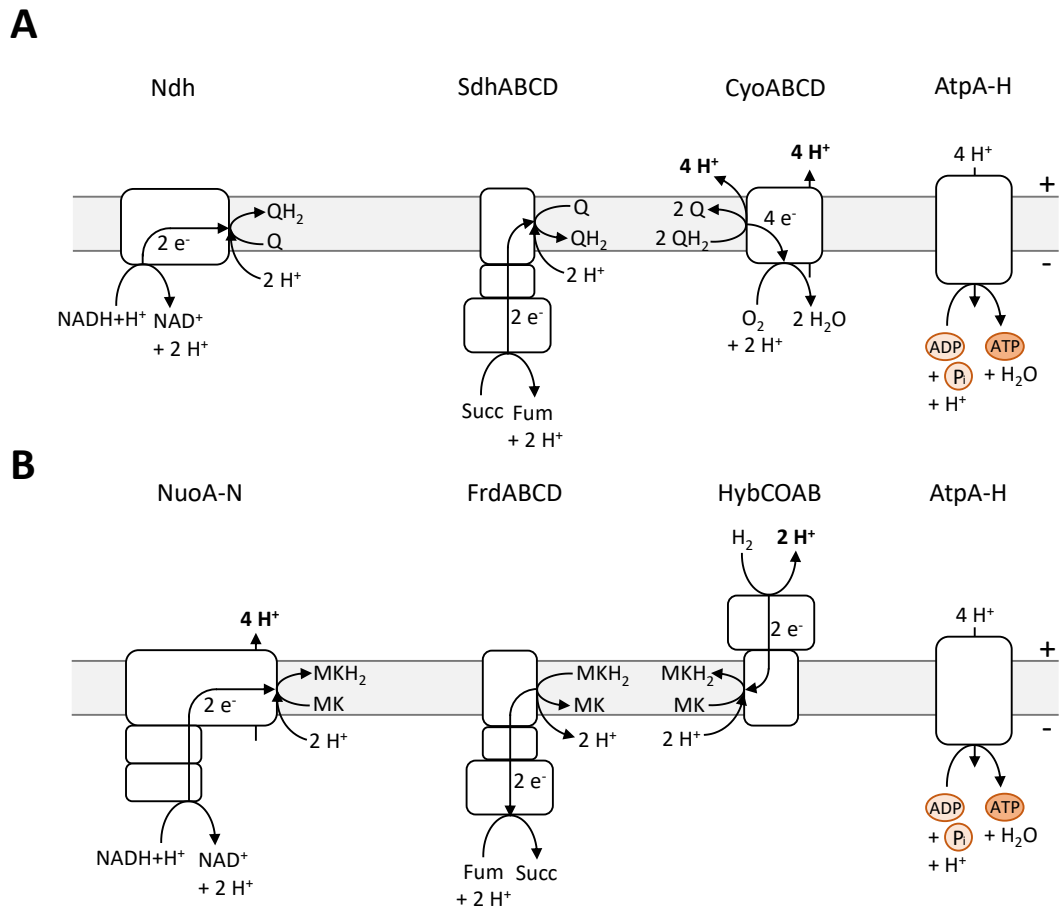

Fig. 6: Aerobic (A) and anaerobic (B) respiratory chain of *E. coli*. Abbreviations: Ndh: NADH:quinone oxidoreductase II; SdhABCD: succinate dehydrogenase; CyoABCD: cytochrome *bo*$_3$ ubiquinol oxidase; AtpA-H: ATP synthase; e^-: electron; Q/QH_2: ubiquinone/ubiquinol; MK/MKH_2: menaquinone/menaquinol; NuoA-N: NADH:quinone oxidoreductase I; FrdABCD: fumarate reductase; HybCOAB: hydrogenase 2.

In the presence of oxygen, cytochrome *bo*$_3$ oxidase is expressed and reduces O_2 with four H^+ and four electrons derived from two QH_2, releasing two H_2O molecules. This redox reaction is coupled to the translocation of eight H^+ (Fig. 6A). The electrons originate from NADH dehydrogenase I and II (NuoA-N and Ndh) and succinate dehydrogenase (SdhABCD), which oxidize either NADH or succinate. The electrons are transferred to the redox mediator ubiquinone (Q), forming ubiquinol (UQH_2). Ubiquinol is lipophilic and therefore can freely diffuse in the cytoplasmic membrane and carry electrons to the cytochrome *bo*$_3$ oxidase (Fig. 6A). Under oxygen-limited conditions, cytochrome *bd* oxidase is active, which does not couple the reduction of O_2 to the translocation of protons, but the redox loop with QH_2/Q is still present (Cotter *et al.* 1990).

Similarly, there are two forms of NADH dehydrogenase NADH-I (NuoA-N) and NADH-II (Ndh). NADH I translocates four H^+ per two electrons across the cytoplasmic membrane, while NADH-II does not couple electron transport to proton translocation (Calhoun and Gennis 1993). NADH dehydrogenase I is active in aerobic and fumarate respiration, whereas NADH dehydrogenase II is involved in nitrate and aerobic respiration (Tran *et al.* 1997). ATP synthase catalyzes the synthesis of ATP (Fig. 6A and B) by the free energy resulting from the proton motive force (Senior 1990). The proton motive force generates subunit rotation by driving conformational change at each of the three catalytic sites. This mechanical force is coupled to the synthesis of ATP, the ubiquitous energy source in all life. During fermentation, ATP synthase can function as a H^+ pump which couples the hydrolysis of ATP with the translocation of protons across the membrane (Trchounian 2004). NADH-I is active in fumarate respiration, which couples electron transport with proton translocation and represents the only site for proton translocation in NADH-fumarate respiration (Fig. 6B). The redox mediator ubiquinone is replaced by menaquinone, which has a more negative standard redox potential. In addition, a hydrogenase (HybCOAB) that converts molecular H_2 into two H^+ in the periplasmic space reduces MK to MKH_2, establishing a proton gradient. Electrons derived from MKH_2 are used to reduce fumarate by fumarate reductase (FrdABCD), producing the end product succinate, which is subsequently exported by Dcu transporters (Fig. 5 and Fig. 6B).

1.3 Two-component systems in *E. coli*

Two-component systems (TCS) consist of a sensor histidine kinase (HK) and a response regulator (RR). Due to a significant diversity in bacterial and archaeal genomes, TCS and RR are found in large abundance in sequence databases (Ortet *et al.* 2015). Furthermore, TCS are also present in eukaryotes, predominantly in unicellular organisms. They are not present in the animal kingdom, making TCS an interesting target for antibiotics.

In a prototypical TCS, HK and RR serve as a link between the detection of an environmental stimulus or a cellular signal and an appropriate cellular response. The communication between HK and RR is based on a phosphoryl group transfer, whereby the phosphoryl group of the conserved L-His residue of the HK is transferred to the L-Asp residue of the RR. Some HKs may also have a phosphatase function that transforms the RR in a dephosphorylated state under non-inductive conditions (Igo *et al.* 1989). Due to the great diversity of input signals and cellular responses, there is a significant variability at the signal input and signal output domains.

A membrane bound TCS has different domains for the functions of signal detection, signal transmission, and catalysis (Fig. 7). The sensor domain is located in the periplasm. PDC domains are characterized according to the sensor domains of the sensor-histidine kinases of PhoQ, DcuS, and CitA (PDC) (Janausch *et al.* 2002). Membrane bound TCS are anchored in the membrane by transmembrane helices. On the cytoplasmic side, signal transduction domains follow, e.g., a HAMP domain, as in the chemotaxis sensor Aer (Garcia *et al.* 2016) or a cytoplasmic PAS domain, which is used for signal transmission. In the case of DcuS, the cytoplasmic PAS domain acts as a signal integration domain that receives input from the sensor domain and the coregulator (Witan *et al.* 2012a; Witan *et al.* 2012b; Monzel *et al.* 2013). The catalytic domain (cat. domain) autophosphorylates the DHp domain (dimerization and histidine phosphotransfer), following the transphosphorylation of the RR (Fig. 7). In some systems, the kinase domain may have additional phosphatase activity (Casino *et al.* 2010; Cheung

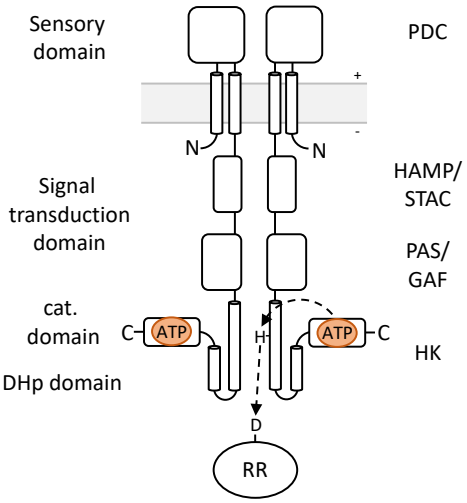

Fig. 7: Model of a prototypical membrane bound sensor histidine kinase. The course of autophosphorylation and transphosphorylation is indicated by dotted lines. Modified according to Zschiedrich *et al.* (2016).

and Hendrickson 2010; Zschiedrich *et al.* 2016). The genome of *E. coli* encodes 36 two-component systems (Blattner *et al.* 1997; Oshima *et al.* 2002), 21 of which are annotated in EcoCyc (Keseler *et al.* 2017) and 14 of which are further characterized.

1.3.1 The C_4-dicarboxylate-sensitive two-component system DcuS-DcuR

The DcuS-DcuR two-component system (TCS) consists of the membrane-anchored sensor histidine kinase DcuS and the response regulator DcuR. DcuSR controls the expression of genes involved in the catabolism of C_4-dicarboxylates, e.g., fumarate, L-malate, succinate, L-tartrate, and L-Asp, in aerobiosis and anaerobiosis. Under aerobic conditions, the expression of *dctA* is induced, whereas in absence of oxygen, the expression of *frdABCD* (fumarate reductase operon), the citrate-sensitive two-component system *citA-citB*, and the colocalized genes *dcuB* and *fumB* is stimulated (Fig. 8) (Zientz *et al.* 1998; Golby *et al.* 1999; Abo-Amer *et al.* 2004; Janausch *et al.* 2004). The expression of *dcuS* and *dcuR* is negatively regulated by NarX-NarL and positively regulated by cAMP-CRP (Goh *et al.* 2005; Oyamada *et al.* 2007). DcuS-DcuR is the only TCS where the HK and RR have independent promoters (Olivera *et al.* 2010). DcuS has two coregulators, DctA and DcuB, which convert DcuS to the C_4-dicarboxylate-responsive state. Under aerobic conditions, DcuS and DctA form sensor complexes, while DcuB replaces DctA during anaerobic growth. In the absence of coregulators, DcuS is constitutively active, with DcuR-controlled genes induced in a stimulus-independent manner (Davies *et al.* 1999; Janausch *et al.* 2004; Kleefeld *et al.* 2009; Witan *et al.* 2012a; Steinmetz *et al.* 2014; Wörner *et al.* 2016). Proteomics and reporter gene assays revealed additional DcuR targets induced in response to fumarate, such as *aspA* (Surmann *et al.* 2020). C_4-dicarboxylates bind to the periplasmic PAS domain (PASp). PASp is membrane anchored by two transmembrane helices (TM1 and TM2). The signal is transduced across the membrane to the cytoplasmic PAS domain (PASc) which controls the autophosphorylation activity of the kinase domain (Fig. 8).

Previous studies have already resolved functional and structural aspects of the signal transduction pathway. One of these was a compaction of the substrate binding pocket of PASp confirmed by crystallization and NMR studies (Cheung and Hendrickson 2008; Salvi *et al.* 2017). This compaction is transferred via PASp-α6 to TM2 resulting in a piston type displacement towards the periplasm (Monzel and Unden 2015). The incoming conformational shift is converted by PASc to a different structural rearrangement, controlling the kinase activity. Biochemical data revealed that the linker region, connecting TM2 and the

N-terminal α-helix of PASc, is essential for signal transduction and conversion (Stopp 2021; Stopp *et al.* 2021).

Mass spectrometry revealed the cellular concentrations of DcuS, which was present at approximately 10-20 molecules per cell. The copies per cell of the coregulators DctA and DcuB significantly exceed those of DcuS (Wörner *et al.* 2017). Both DcuB and DctA had at least a copy number of 200 molecules per cell, which was increased 12.7-fold and 2.7-fold, respectively, in the induced state (Wörner *et al.* 2017). For the cellular concentration of DcuR, copy numbers per genome were also quantified. When *E. coli* is cultured in LB-medium, DcuR is estimated to reach copy numbers of about 100 molecules per genome (Ishihama *et al.* 2014). Considering that *E. coli* cultivated in LB medium can have approx. eight fully replicated chromosomes (Liu *et al.* 2014), it can be assumed that DcuR reaches a copy number of several hundred copies per cell.

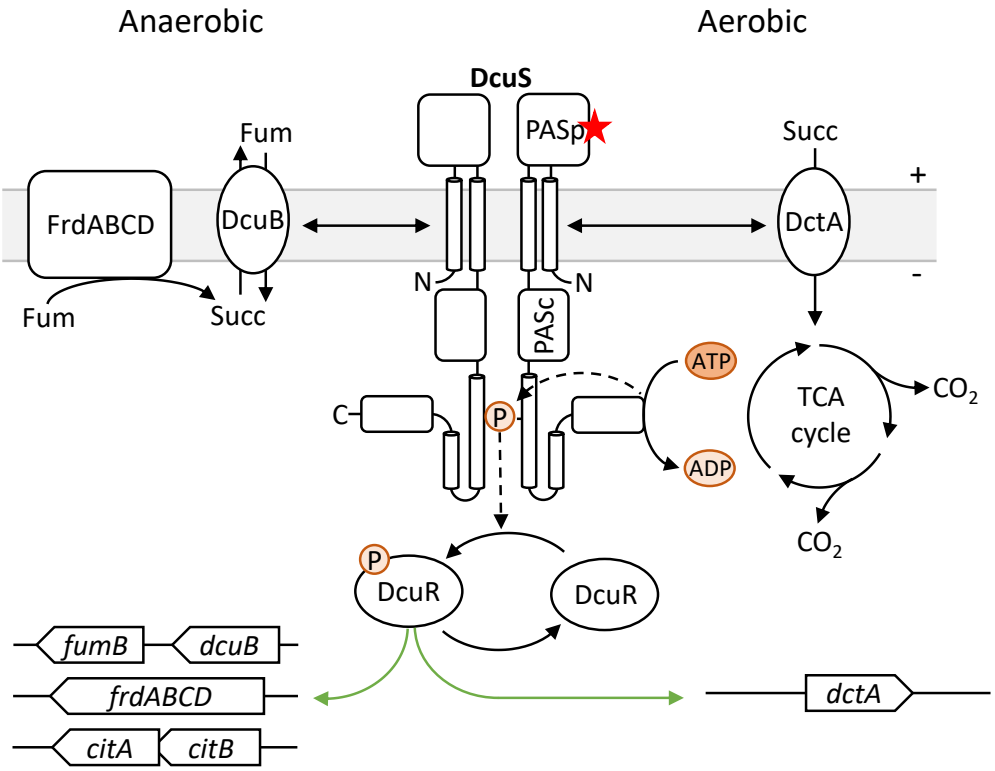

Fig. 8: Functionality of the DcuS-DcuR two-component system. The PASp domain senses C_4-dicarboxylates (red star) in the periplasmic space, resulting in compaction of the binding pocket and subsequent conformational changes and structural rearrangements that relay the signal to the kinase domain, leading to autophosphorylation of the DHp domain. The phosphoryl group is transferred to DcuR and DcuR-regulated genes are stimulated.

1.4 The phosphoenolpyruvate:glucose phosphotransferase system

The phosphoenolpyruvate (PEP):carbohydrate phosphotransferase system (PTS) carries out both catalytic and regulatory functions (Deutscher *et al.* 2014). The PTS catalyzes the transport and phosphorylation of a variety of sugars and sugar derivatives, but also divers regulatory functions related to carbon metabolism. *E. coli* is a glucophilic bacterium and the PTS is therefore optimized for glucose uptake. The PTS transfers a phosphoryl group from the donor phosphoenolpyruvate (PEP) via EI, HPr and $EIIA^{Glc}$ to the glucose transporter EIIBC (Fig. 9). The phosphorylation status of $EIIA^{Glc}$ depends on the availability of glucose. In the presence of glucose, phosphorylated $EIIA^{Glc}$ transfers the phosphoryl group to EIIB, which immediately phosphorylates glucose to glucose-6-phosphate (G6P) upon entry, a process known as group translocation (Fig. 9). In this state, $EIIA^{Glc}$ is predominantly dephosphorylated and can inhibit transporters of secondary metabolism such as the lactose permease LacY. In the absence of glucose, $EIIA^{Glc}$ is primarily phosphorylated and can stimulate cAMP production by adenylate cyclase (CyaA) (Fig. 9). cAMP is the allosteric effector of the transcriptional regulator CRP, cAMP-CRP complexes can induce metabolic genes of secondary metabolism, such as *lacZYA* operon for lactose catabolism. In general, sugars and sugar derivatives are divided into PTS sugars that are transported by the PTS, e.g., glucose, mannitol, and mannose, while non-PTS sugars are not. PTS-sugars other than glucose have different transport enzymes, whereas the phosphoryl group donor PEP is the same, highlighting the PEP/pyruvate ratio as an important indicator of carbon metabolism (Deutscher *et al.* 2006).

In a recent study, the PTS was shown to involve bacterial metabolic status in quorum sensing (QS) regulation via an HPr-LsrK interaction (Fig. 9) (Ha *et al.* 2018). The autoinducer-2 (AI-2) kinase LsrK phosphorylates AI-2, which is essential for internalization and sequestration (Roy *et al.* 2010; Pereira *et al.* 2012). The *in vivo* ratio of HPr and HPr-P is closely related to the rate of sugar uptake, similar to $EIIA^{Glc}$ and $EIIA^{Glc}$-P. HPr is predominantly unphosphorylated in the exponential growth phase. In this state, HPr interacts with LsrK and decreases the phosphorylation of AI-2 up to 25-fold, which inhibits the expression of the *lsr* operon (Ha *et al.* 2018). The phosphorylation state of HPr directly links metabolic state to QS of bacteria, which is critical because QS accompanies transitions between planktonic and sessile growth (Ha *et al.* 2018).

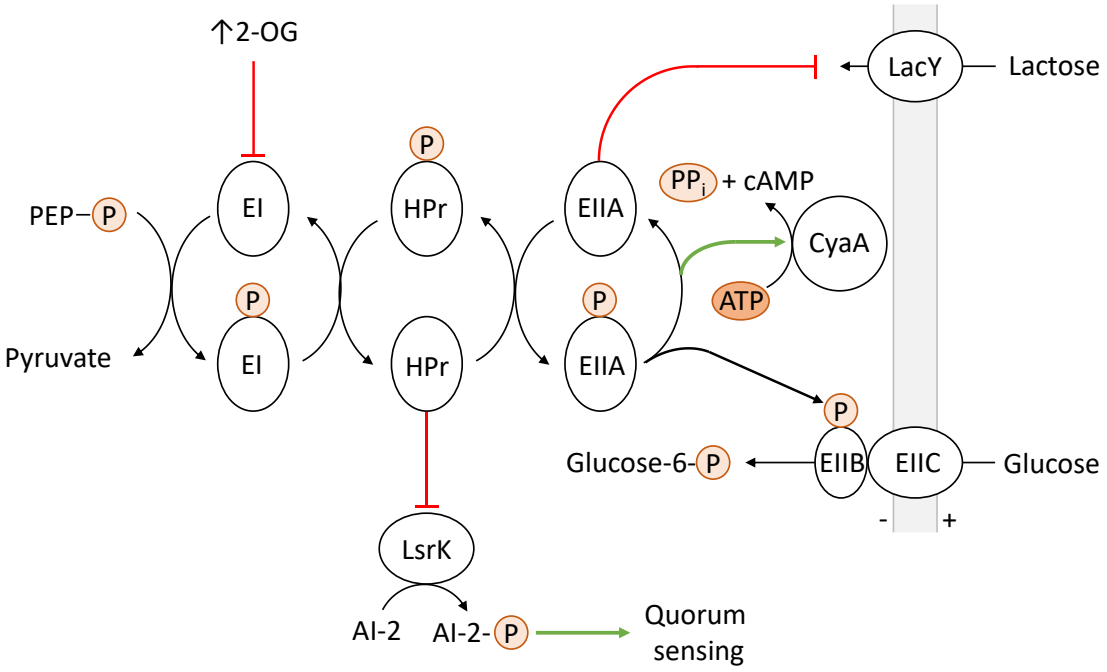

Fig. 9: The phosphoenolpyruvate:glucose phosphotransferase system PTS of *E. coli*. Abbreviations: PEP: phosphoenolpyruvate; EI: enzyme I *ptsI*; HPr: phosphocarrier protein HPr *ptsH*; EIIA: enzyme IIA *crr*; EIIBC: glucose specific PTS permease *ptsG*; P: phosphoryl group; 2-OG: 2-oxoglutarate; LsrK: auto-inducer-2 (AI-2) kinase; CyaA: adenylate cyclase; LacY: lactose permease.

2-oxoglutarate (2-OG) is an important substrate in the nitrogen regulatory system of *E. coli*. Intracellular 2-OG levels indicate either nitrogen-limited or nitrogen-saturated conditions (van Heeswijk *et al.* 2013). Variations in the nitrogen source can lead to drastic changes in intracellular 2-OG levels (Yuan *et al.* 2009; Doucette *et al.* 2011). 2-OG has been shown to bind competitively with a K_M of approximately 2.2 mM to the C-terminal domain of EI at the binding site of PEP (Fig. 9). This feedback inhibition reduces the intracellular EI-PEP complexes and limits sugar uptake by the PTS (Venditti *et al.* 2013) and maintains homeostasis and maximizes nutrient utilization by limiting excess carbon uptake (Goyal *et al.* 2010; Doucette *et al.* 2011). Both examples show that PTS is a central regulatory system in *E. coli* that not only controls carbon uptake but also integrates information from other regulatory systems, such as QS.

1.4.1 The cAMP-CRP signal transduction pathway

The transcriptional regulator CRP (cAMP receptor protein) regulates the expression of over 180 genes in *E. coli* (Grainger *et al.* 2005). The majority of these genes are involved in catabolism of secondary carbon sources, such as lactose, glycerol, and maltose. Additionally, CRP is involved in a multitude of other processes, e.g., nitrogen assimilation (Mao *et al.*

2007), osmoregulation and virulence (Balsalobre *et al.* 2006). CRP is activated via binding of the allosteric effector cAMP and can subsequently bind to DNA (Deutscher *et al.* 2014).

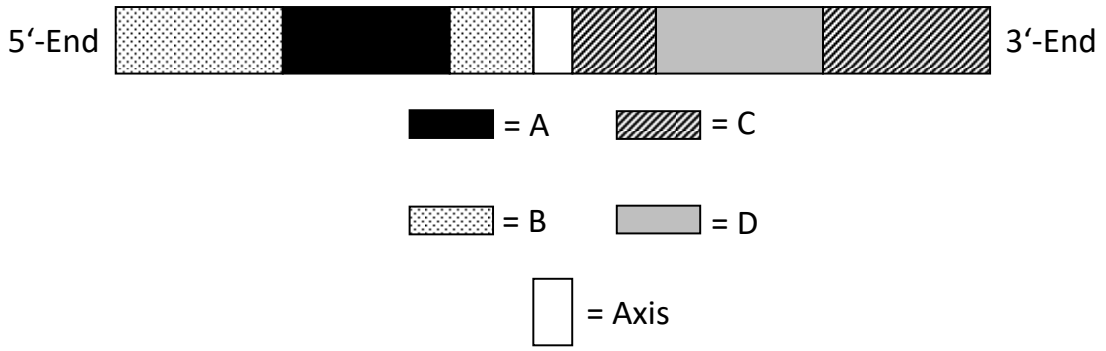

Fig. 10: Simplified presentation of a CRP-binding site. Specific regions within the CRP-binding site are highlighted and annotated: (**A**) conserved TGTGA motif, (**B**) flanking sequence proximal to the conserved TGTGA motif, (**C**) flanking sequence distal to the conserved TGTGA motif, (**D**) and inverted repeat motif. Modified according to Pyles *et al.* (1998).

CRP is a homodimer and belongs to the CRP-FNR superfamily of transcription factors (Green *et al.* 2000; Körner *et al.* 2003). The C-terminal domain of CRP carries a helix-turn-helix (HTH) motif for DNA-binding. Upon binding of cAMP, the C-terminal helix and DNA-binding domain are elongated and reorganized, freeing the DNA recognition helix (Popovych *et al.* 2009; Sharma *et al.* 2009), followed by insertion of the HTH recognition helices into two adjacent DNA major grooves (Kim *et al.* 1992). In the case of the consensus sequence, CRP induces a nucleic acid bend of 87° (Ebright *et al.* 1989; Parkinson *et al.* 1996). The introduced bend is either symmetric (e.g., *lac* promoter) or asymmetric (e.g., *gal* promoter) depending on the symmetry of the DNA-binding sites and the flanking sequences (Fig. 10) (Pyles *et al.* 1998; Pyles and Lee 1998; Lin and Lee 2003). The nucleotide sequence and the location of the CRP-binding site are the key factors for determining gene expression. The DNA association constant for CRP without cAMP is 100 µM, and for the cAMP-CRP complex in the range of 100 nM and 100 pM, highly dependent on the CRP-binding site (Giraud-Panis *et al.* 1992; Harman 2001). Promoter activation by cAMP-CRP can be clustered into three classes (Busby and Ebright 1999; Fic *et al.* 2009). Class I promoters have a single CRP site located upstream of the RNA polymerase (RNAP) binding site and require only CRP to activate transcription. Class II promoters differ from class I promoters in that the CRP-binding site and the RNAP-binding site are shared (-35 promoter sequence). Class III promoters require additional transcriptional activators, either two or more cAMP-CRP complexes or one cAMP-CRP complex and an additional transcriptional activator that synergistically activates transcription (Fic *et al.* 2009).

1.5 The nitrogen regulatory system in *E. coli*

Nitrogen accounts for approximately 14% of the dry weight of bacteria. The carrier molecule of nitrogen is ammonium (NH_4^+), which is assimilated to a carbon skeleton, usually L-Glu or 2-oxoglutarate (2-OG) (Fuchs and Schlegel 2006). *E. coli* has two pathways that catalyze ammonium assimilation. First, the glutamate dehydrogenase (GDH) pathway, which aminates 2-OG to L-Glu, without consuming ATP yet has a low affinity for ammonium (Fig. 11). Second, the glutamine synthetase (GS, GlnA) and glutamate 2-oxoglutarate aminotransferase (GOGAT, GltBD) pathway, which assimilates ammonium to L-Glu, producing one net L-Glu molecule. However, this pathway consumes one ATP for each ammonium assimilated, while it has a relatively high affinity for ammonium (Fig. 11). Both pathways produce one L-Glu molecule, although the GS-GOGAT pathway is the dominant route under physiological conditions (van Heeswijk *et al.* 2013).

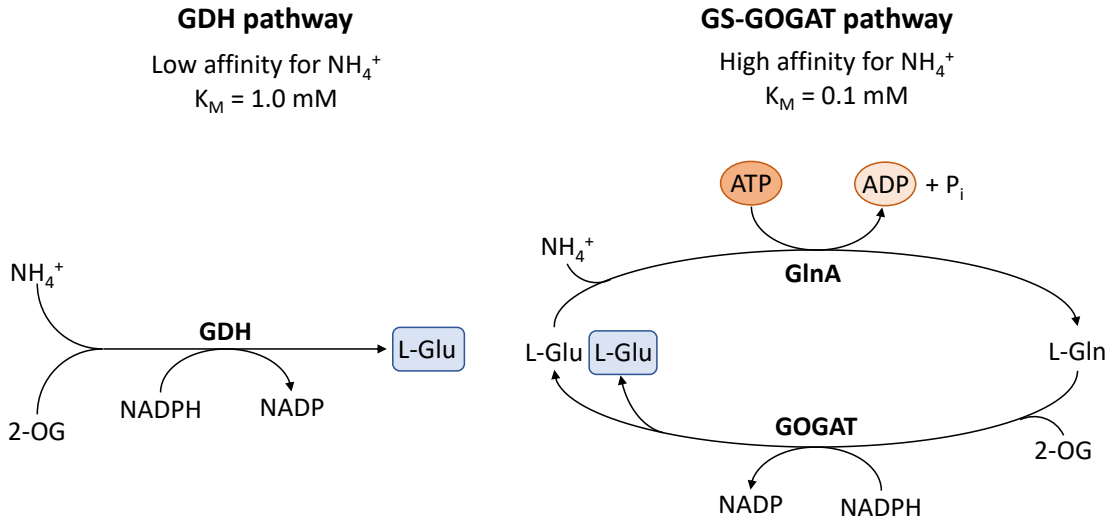

Fig. 11: Nitrogen assimilation by the GDH and the GS-GOGAT pathway of *E. coli*. The glutamate dehydrogenase (GDH) catalyzes the reductive amination of 2-OG, producing one net L-Glu; GDH has a relatively low affinity for ammonium (NH_4^+); no ATP is required. The glutamine synthetase (GS, GlnA) and glutamate 2-oxoglutarate aminotransferase (GOGAT, GltBD) also produces one net L-Glu by reductive amination of L-Glu and subsequent transamination of 2-OG. However, ATP is consumed in the process and NH_4^+ affinity is high. Modified according to van Heeswijk *et al.* (2013).

In the center of this regulatory network is the GlnB protein (alternative name PII). GlnB is known from enteric bacteria but is also present in many other bacteria, archaea, and eukaryotes (Son and Rhee 1987; Arcondéguy *et al.* 2001; Leigh and Dodsworth 2007; Selim *et al.* 2020). GlnB has two important functions in the regulation of the nitrogen assimilation: First, the transcriptional regulation of assimilation genes via the two-component system NtrB-NtrC (Jiang and Ninfa 2007, 2009) and second the regulation of GS at the post-transcriptional level (van Heeswijk *et al.* 2013). GlnB can bind ATP or ADP and 2-OG, both indicators of the carbon and nitrogen state of the bacterial cell, respectively. In addition, GlnB can

be chemically modified via uridylylation catalyzed by the bifunctional uridylyltransferase/uridylyl-removing enzyme GlnD (Ninfa and Magasanik 1986; Atkinson *et al.* 1994; Liu and Magasanik 1995; van Heeswijk *et al.* 2013). Under nitrogen-limited conditions, the intracellular 2-OG levels are increased, while L-Gln levels are decreased. In this state, GlnD uridylylates GlnB, abolishing the stimulation of NtrB phosphatase activity. Phosphorylated NtrC levels rise, leading to a higher expression of genes involved in nitrogen assimilation, e.g., *glnA* (GS) (Fig. 12).

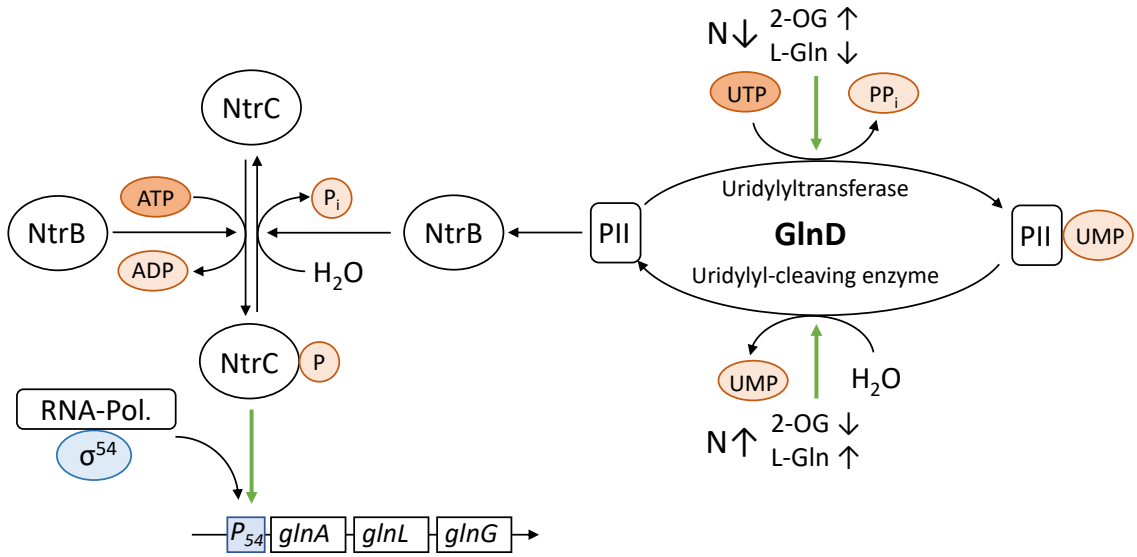

Fig. 12: Transcriptional control of the *glnALG* operon of *E. coli* by the NtrB-NtrC two-component system. The *glnALG* operon encodes the glutamine synthetase (GS, GlnA) and the two-component system NtrB-NtrC consisting of the sensor histidine kinase NtrB (*glnL*) and the response regulator NtrC (*glnG*). The uridylyltransferase (GlnD) perceives the nitrogen status of the bacterial cell and controls the uridylylation of PII (GlnB). Modified according to Fuchs und Schlegel (2006).

Under nitrogen-saturated conditions, the 2-OG level are decreased and the L-Gln levels are increased, resulting in the deuridylylation of GlnB. GlnB induces NtrB phosphatase activity, thereby reducing phosphorylated NtrC and hence the induction of genes involved in nitrogen assimilation (Fig. 12) (Ninfa and Magasanik 1986; Keener and Kustu 1988; Jiang *et al.* 2000; Pioszak *et al.* 2000; Huergo *et al.* 2013). A similar principle applies to the indirect regulation of GS by GlnB. Under nitrogen-saturated conditions, GlnB induces the adenylyltransferase activity of GlnE, leading to adenylylation of GS and subsequent inactivation of ammonium assimilation (Son and Rhee 1987; Rhee *et al.* 1989; van Heeswijk *et al.* 2013). Under nitrogen-limited conditions, GlnB-UMP induces the deadenylase activity of GlnE, resulting in the activation of ammonium assimilation by GS (Fig. 13). GlnD and GlnE are bifunctional proteins that catalyze a reversible covalent modification of either GlnB or GS in response to the intracellular levels of 2-OG, ATP, L-Gln, or to the uridylylation state of GlnB (Garcia *et al.* 1980; Garcia and Rhee 1983). GlnB is at the center of the nitrogen regulatory

network of *E. coli*. The GlnB effector molecules ATP, ADP, and 2-OG, as well as the UMP moiety, make GlnB unique in its ability to translate diverse signaling inputs into adequate cellular responses. This versatility allows *E. coli* to adapt rapidly to changing nitrogen and carbon availability.

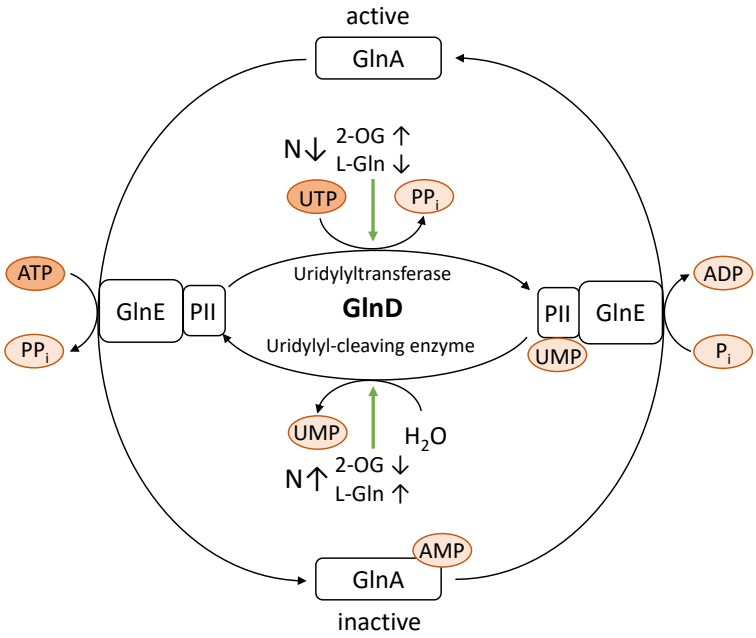

Fig. 13: Regulation of glutamine synthetase by GlnB and GlnE. The glutamine synthetase (GS, GlnA) can be adenylylated at a L-Tyr residue. The covalent modification is based on the nitrogen status. Sensor is the uridylyltransferase (GlnD), which can either uridylylate or deuridylylate GlnB (PII). The PII protein (PII or PII-UMP) controls the activity of the GS via adenylyltransferase (GlnE). Modified according to Fuchs und Schlegel (2006).

1.5.1 Nitrogen regulator GlnB

GlnB has a central role as an energy and nitrogen sensor in *E. coli*. The binding of the effector molecules ATP or ADP and 2-OG enables GlnB to directly sense the current metabolic state of the bacterial cell. Binding of effector molecules leads to a conformational change within GlnB, modulating its interaction with various target proteins (Fokina *et al.* 2010; Radchenko and Merrick 2011; van Heeswijk *et al.* 2013; Forchhammer and Lüddecke 2016). The intracellular indicator of the energy state is ATP or ADP. Both molecules bind competitively to the same binding site. 2-OG is an intermediate of the TCA cycle and the carbon skeleton for ammonium assimilation. 2-OG represents the carbon and nitrogen status of the bacterial cell (Fokina *et al.* 2010; van Heeswijk *et al.* 2013; Oliveira *et al.* 2015; Forchhammer and Lüddecke 2016). The Mg-ATP-dependent 2-OG binding to GlnB triggers a conformational change at the surface exposed T-loop, influencing interactions between GlnB and target proteins, e.g., NtrB, NagB, or ACCase (Ninfa and Magasanik 1986; Jiang and Ninfa 1999; Gerhardt *et al.* 2015; Rodionova *et al.* 2018). GlnB is a trimer and has three binding sites, each located in an inter-cleft of the three subunits. The binding of the effector molecules is anti-cooperative to sense different cellular concentrations of ATP or ADP and 2-OG

(Fokina *et al.* 2010; Ma *et al.* 2014). Saturation of the first binding site in a GlnB trimer continuously leads to small conformational changes in subsequent binding sites, resulting in a decrease in binding affinity and corresponding increase in K_D (Fokina *et al.* 2010; Ma *et al.* 2014; Zeth *et al.* 2014). The binding affinity for ATP is higher than for ADP, additionally 2-OG increases the binding affinity of ATP, which counteracts ADP binding (Fokina *et al.* 2010; Gerhardt *et al.* 2012; Oliveira *et al.* 2015). In addition to direct binding of effector molecules, GlnB can also be covalently modified. The Tyr51 residue undergoes uridylylation under nitrogen-limited conditions catalyzed by the bifunctional enzyme GlnD. Uridylyltransferase and uridylyl-removing activity is dependent on the intracellular L-Gln levels. Under nitrogen-saturated conditions, L-Gln levels are increased, leading to the induction of uridylyl-removing activity. Under nitrogen-limited conditions, GlnB is saturated with ATP and 2-OG and is uridylylated (Fig. 12) (Atkinson *et al.* 1994; Jiang *et al.* 1998; van Heeswijk *et al.* 2013; Forchhammer and Lüddecke 2016).

1.5.2 GlnK regulation of the ammonium transporter AmtB

The ammonium transporter AmtB facilitates the uptake of NH_3/NH_4^+. The GlnB paralogous GlnK (alternative name PII-2) and AmtB are expressed in the same operon. The *glnK-amtB* operon is induced under nitrogen-limited conditions by the two-component system NtrB-NtrC (van Heeswijk *et al.* 1995; van Heeswijk *et al.* 1996; Javelle *et al.* 2004). Ammonium uptake is tightly regulated by GlnK in response to nitrogen status of the bacterial cell (Javelle *et al.* 2004). Under nitrogen-limited conditions, *glnK-amtB* are expressed, while AmtB catalyzes ammonium uptake. The uridylyltransferase GlnD recognizes small amounts of L-Gln and uridylylates GlnK (UTase), while ATP and 2-OG are also bound to GlnK, abolishing the inhibition of AmtB by GlnK (Coutts *et al.* 2002; Radchenko *et al.* 2010). Under nitrogen-saturated conditions, GlnD removes the UMP moiety of GlnK (UR). In this state, GlnK is bound to ADP and inhibits ammonium uptake by AmtB (Fig. 14) (Javelle *et al.* 2004). As a result, *E. coli* is able to rapidly adjust ammonium uptake to meet the nitrogen requirement of the cell.

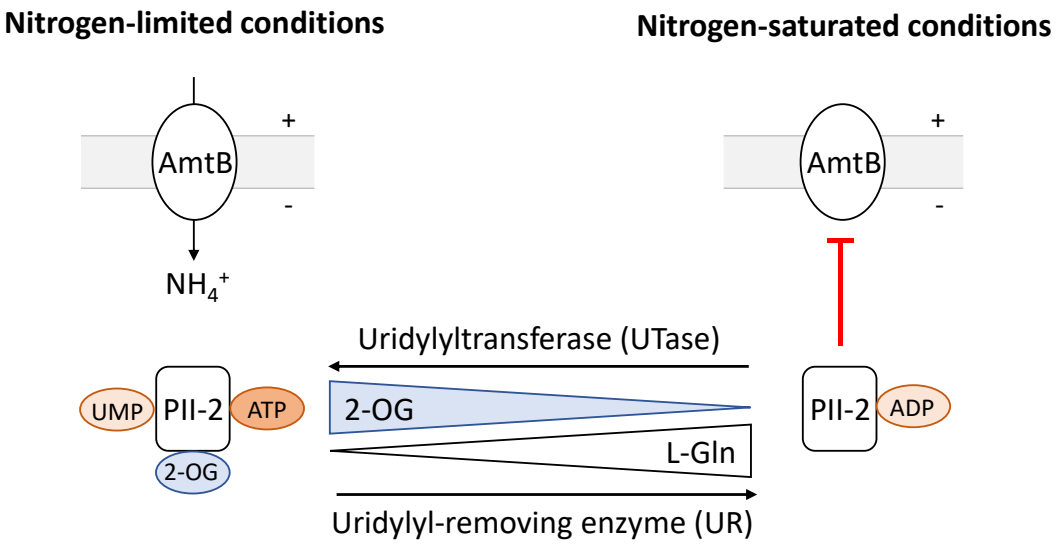

Fig. 14: GlnK (PII-2) regulation of the ammonium transporter AmtB of *E. coli*. Under nitrogen-limited conditions, intracellular 2-OG levels are high and L-Gln levels are low which induce the uridylyltransferase activity of GlnD (UTase). PII-2 (GlnK) is uridylylated and the effector molecules ATP and 2-OG are bound. In this state, PII-2 is unable to inhibit ammonium uptake by AmtB. Under nitrogen-saturated conditions, the intracellular L-Gln levels are high which induce the uridylyl-removing activity of GlnD (UR). PII-2 is deuridylylated and ADP is bound. In this state, PII-2 inhibits ammonium uptake by AmtB.

1.5.3 The GlnB targets: NagB and ACCase

In recent years, additional GlnB targets were identified such as the glucosamine 6-phosphate deaminase NagB and the acetyl-CoA carboxylase (ACCase) (Gerhardt *et al.* 2015; Rodionova *et al.* 2018). GlnB is a versatile regulator because GlnB has several signaling inputs (ATP, ADP, 2-OG, and uridylylation) that represent the metabolic state of the bacterial cell. The signal input causes a conformational change in the surface-exposed signal output domain, which is the T-loop. Acetyl-CoA carboxylase catalyzes the two-step reaction and produces malonyl-CoA, which serves as a building block for fatty acid elongation. The first half reaction comprises of the ATP-dependent carboxylation of biotin, which is covalently attached to ACCase. The second half reaction is the transfer of the carboxyl group from carboxybiotin to acetyl-CoA producing malonyl-CoA (Tong 2013; Gerhardt *et al.* 2015). Previous work showed that GlnB can inhibit ACCase, which is abolished by uridylylation of GlnB (Fig. 15) (Gerhardt *et al.* 2015). Amino sugars are present in many polysaccharides in all kingdoms, e.g., cell surface mucus (Koropatkin *et al.* 2012). NagB catalyzes the last step in the amino sugar catabolic pathway, converting glucosamine 6-phosphate to ammonium and fructose 6-phosphate (Fru-6P). Ammonium is assimilated in the GS-GOGAT pathway, while Fru-6P is introduced into glycolysis. GlnB-UMP stimulates

NagB deaminase activity more than tenfold (Rodionova *et al.* 2018). Both examples emphasize the versatility of GlnB regulation in *E. coli*. Involvement in the regulation of carbon and nitrogen metabolism establishes GlnB as a ubiquitous post-transcriptional regulator of *E. coli* carbon and nitrogen metabolism.

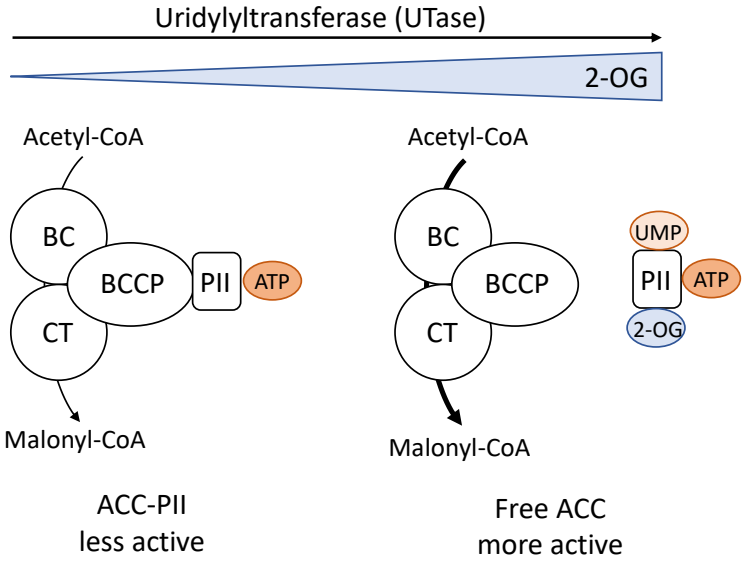

Fig. 15: GlnB stimulation of ACCase activity. Acetyl-CoA carboxylase (ACCase) first assimilates hydrogen carbonate (HCO_3^-) to enzymatically bound biotin under ATP consumption. Second, the carboxyl group (CO_2) is transferred to acetyl-CoA to form malonyl-CoA, the building block of fatty acid biosynthesis (not shown). Under nitrogen-saturated conditions, PII (GlnB) is bound to ATP and inhibits ACCase via protein-protein interaction with the BCCP subdomain. Under nitrogen-limited conditions, PII is uridylylated and saturated with ATP and 2-OG, abolishing repression. Abbreviations: BC: biotin carboxylase; CT: carboxyltransferase; BCCP: biotin carboxyl carrier protein.

1.6 The physiological habitat of *E. coli*

The *E. coli* K-12 strain was predominantly used in this work. K-12 was isolated from feces of a convalescent diphtheria patient at Stanford University in 1922. Subcultures and derivatives of this strain were reported starting in 1936 (Clifton and Morrow 1936; Clifton 1937; Gray and Tatum 1944). Since then, *E. coli* K-12 evolved into an unprecedented model organism in microbiology, because K-12 strains are unable to colonize the human gut, rendering K-12 harmless (Smith 1975). Contrary to the pathogenic relative enterohaemorrhagic *Escherichia coli* (EHEC), the K-12 strain has lost the genes for virulence factors, which makes it ideal for molecular biology work (Mühldorfer and Hacker 1994). *E. coli* K-12 lacks the O antigen which is part of the lipopolysaccharide. The O antigen consists of repeating units of four to five hexoses that are partially branched and is encoded by the *rfb* gene cluster (Liu and Reeves 1994). Additionally, the O antigen plays a major role in the immunogenicity of gram-negative bacteria. EHEC is a zoonotic foodborne pathogen characterized by the ability to produce shiga toxin. Shiga toxins are cytotoxic, bacterial exotoxins that act as translation inhibitors. In humans, EHEC can cause hemorrhagic colitis, hemolytic uremic

syndrome (HUS), or central nervous system failure (Kaper and O'Brien 2014). The intestine is a complex environment in which bacteria are competing against limited resources. Pathogenic *E. coli* must outcompete the gut microbiota for colonization (Kamada *et al.* 2012). Approximately 500 bacterial species are present in the mammalian gut (Moore and Holdeman 1974). Miranda and coworkers (2004) showed that the EHEC reference strain EDL933 colonizes the intestinal mucus layer and utilizes glycolytic substrates for initial growth and maintenance (Wadolkowski *et al.* 1990). The carbon nutrition for pathogenic and commensal *E. coli* strains in the mouse intestine slightly differ. EDL933 and MG1655 both utilize L-arabinose, fructose, and N-acetylglucosamine. Additionally, EDL933 uses galactose, hexuronates, mannose, and ribose, whereas MG1655 utilizes gluconate and N-acetylneuraminic acid (Fabich *et al.* 2008). Ethanolamine in the bovine intestine was identified as a source of nitrogen, which is used by EDL933 to gain a competitive advantage over the gut microbiota. Ethanolamine is converted intracellularly to acetyl-CoA, yielding ammonium which is assimilated in the GS-GOGAT pathway (Bertin *et al.* 2011). Acetyl-CoA is either introduced into the TCA cycle or converted to acetate via acetyl phosphate under energy limitation, yielding ATP (Stojiljkovic *et al.* 1995; Brinsmade and Escalante-Semerena 2004; Starai *et al.* 2005). Bovine small intestine contents (BSIC) contains the majority of proteinogenic amino acids in millimolar concentrations (Bertin *et al.* 2018). It was shown that *E. coli* EDL933 strain utilized L-Asp and L-Thr in BSIC (Bertin *et al.* 2018). qPCR-RT revealed that genes involved in L-Asp metabolism, respectively, *aspA* and *dcuA* are significantly up-regulated in BSIC (Bertin *et al.* 2018). Fumarate respiration is essential for *E. coli* to colonize the gastrointestinal tract of mice (Jones *et al.* 2007; Jones *et al.* 2011). C_4-dicarboxylates, with exception of L-Asp, are found in low micromolar concentrations in the BSIC (Bertin *et al.* 2018). Fumarate can be generated endogenously from carbohydrate degradation via glycolysis, reductive branch of the TCA cycle, and L-Asp (Unden *et al.* 2016). The utilization of L-Asp by AspA provides an electron acceptor and nitrogen source in a one-step reaction, highlighting the significant role of L-Asp as a physiological nutrient (Jones *et al.* 2011; Bertin *et al.* 2018). Kinetics of L-Asp consumption and comparison of gene expression revealed that pathogenic EDL933 is able to metabolize L-Asp much faster than commensal *E. coli*, presumably due to the upregulation of *aspA* and *dcuA* transcripts in BSIC, compared to M9 glucose (Bertin *et al.* 2018).

1.7 Research questions and objectives

Four main topics of C_4-dicarboxylate metabolism and regulation of *E. coli* were studied in this work:

1. Recently, L-Asp was shown to be an important amino acid for *E. coli* strains (Bertin *et al.* 2018) and that *E. coli* contains DcuA, a nitrogen shuttle for L-Asp uptake (Strecker *et al.* 2018). Here, we characterized the physiological role of L-Asp for bacteria, the pathway of nitrogen assimilation, and the transcriptional and post-transcriptional levels of regulation, including regulation by the nitrogen regulator GlnB.

2. DctA represents the major transporter for the uptake of C_4-dicarboxylates by *E. coli* under aerobic conditions. The regulation of *dctA* (and *aspA*) expression and the role of the phosphotransferase system and cAMP-CRP in transcriptional regulation were analyzed by expression studies, biochemical and bioinformatic approaches, and protein interactions between DctA and $EIIA^{Glc}$.

3. Metabolons are assumed to coordinate metabolic pathways, including integration of transport with sequential metabolic reactions. The metabolon concept was investigated by measuring the interaction of the carriers DcuA, DcuB and AmtB with aspartase AspA and fumarase FumB.

4. DcuS of DcuS-DcuR requires the transporters DcuB or DctA as coregulators. Available structural and biochemical data were used by manual modeling and sequence comparison to model the DcuS-DctA interaction, namely the DcuS linker region and DctA helix 8b. Structural analysis revealed that a conformational change through an L-Pro hinge during signal propagation in DcuS is similar to signal transduction observed in other membrane integral sensors.

2 Materials and Methods

2.1 Bacterial strains, plasmids, and oligonucleotide primers

Tab. 1: Bacterial strains and plasmids used in this study

Strain/Plasmid	Genotype	Reference
JM109	*recA1 supE44 endA1 hsdR17 gyrA96 relA1 thi*Δ(*lac-proAB*) F'[*traD36 proAB+*, *lacIq lacZ*Δ*M15*]	Yanisch-Perron *et al.* (1985)
XL1-Blue	F-, *recA1-, (mk+, rk-) supE44, endA1, thi-1*, λ-, *gyrA96, relA1*, (*lac*-) [F-, *proAB, lacIq, Z*Δ*M15* Tn10 (Tet^R)]	Stratgene
	***lacZ*-reporter gene assays**	
MC4100	F- *araD139* Δ(*argF-lac*)*U169, rpsL150, (*Δ*lacZ), relA1 flbB530 deoC1 ptsF25 rbsR*	Silhavy *et al.* (1984)
IMW385	MC4100, *dctAp-lacZ*, Amp^R	Kleefeld (2006)
IMW386	IMW385 but *dctA*::Spc^R, Amp^R	Kleefeld (2006)
IMW670	IMW385 but *glpK*::Kan^R, Amp^R	This study
IMW671	IMW385 but *glpD*::Kan^R, Amp^R	This study
IMW672	IMW385 but *glpR*::Kan^R, Amp^R	This study
IMW676	IMW386 but *glpK*::Kan^R, Amp^R	This study
IMW677	IMW386 but *glpR*::Kan^R, Amp^R	This study
IMW678	IMW385 but *xylB*::Kan^R, Amp^R	This study
IMW679	IMW385 but *xylR*::Kan^R, Amp^R	This study
IMW669	IMW385 but *cyaA*::Kan^R, Amp^R	Best (2018)
IMW680	IMW386 but *xylB*::Kan^R, Amp^R	This study
IMW681	IMW386 but *xylR*::Kan^R, Amp^R	This study
IMW665	IMW386 but *cyaA*::Kan^R , Amp^R	Best (2018)
MC4100λJ100	MC4100, *frdAp-lacZ*, Amp^R	Gunsalus (1992)
IMW682	MC4100λJ100 but *lrp*::Kan^R, Amp^R	This study
IMW237	MC4100, *dcuBp-lacZ*, Amp^R	Zientz *et al.* (1998)
IMW683	IMW237 but *lrp*::Kan^R, Amp^R	This study
IMW503	MC4100, *dcuBp-lacZ*, Δ*dcuB*, Amp^R	Zientz *et al.* (1998)
IMW684	IMW503 but *lrp*::Kan^R, Amp^R	This study
IMW240	MC4100, *dcuCp-lacZ*, Amp^R	Zientz *et al.* (1999)
IMW691	IMW240 but *lrp*::Kan^R, Amp^R	This study
IMW642	MC4100, but *aspAp-lacZ*, Amp^R	Schubert (2016)
IMW675	IMW642, but *lrp*::Kan^R, Amp^R	Schubert *et al.* (2020)
IMW687	IMW642, but *ntrC*::Kan^R, Amp^R	Schubert *et al.* (2020)
IMW688	IMW642, but *rpoS*::Kan^R, Amp^R	Schubert *et al.* (2020)
IMW690	IMW642 but *crp*::Kan^R, Amp^R	Bohn (2019)
	Keio collection strains and mutants	
BW25113	F- *cya-99, araD139, galE15, galK16, rpsL1* (Str^R), *hsdR2, mcrA1, mcrB1*	Baba *et al.* (2006)
JW3896	BW25113 but Δ*glpR*::Kan^R	Baba *et al.* (2006)
JW3897	BW25113 but Δ*glpK*::Kan^R	Baba *et al.* (2006)
JW3389	BW25113 but Δ*glpD*::Kan^R	Baba *et al.* (2006)
JW3536	BW25113 but Δ*xylB*::Kan^R	Baba *et al.* (2006)
JW3541	BW25113 but Δ*xylR*::Kan^R	Baba *et al.* (2006)
JW0872	BW25113 but Δ*lrp*::Kan^R	Baba *et al.* (2006)
JW3496	BW25113 but Δ*dctA*::Kan^R	Baba *et al.* (2006)
JW5735	BW25113 but Δ*dcuA*::Kan^R	Baba *et al.* (2006)
JW4084	BW25113 but Δ*dcuB*::Kan^R	Baba *et al.* (2006)
JW4099	BW25113 but Δ*aspA*::Kan^R	Baba *et al.* (2006)
JW0872	BW25113 but Δ*lrp*::Kan^R	Baba *et al.* (2006)
JW3839	BW25113 but Δ*glnG*::Kan^R	Baba *et al.* (2006)
JW5437	BW25113 but Δ*rpoS*::Kan^R	Baba *et al.* (2006)
JW0911	BW25113 but Δ*aspC*::Kan^R	Baba *et al.* (2006)
JW2537	BW25113 but Δ*glnB*::Kan^R	Baba *et al.* (2006)

JW0440	BW25113 but Δ*glnK*::Kan^R	Baba *et al.* (2006)
AN387	K-12 wild type	Wallace and Young (1977)
JRG2814	AN387 but *dcuB*::Kan^R and *dcuA*::Spc^R	Six *et al.* (1994)
	BACTH strains and plasmids	
BTH101	F- *cya-99, araD139, galE15, galK16, rpsL1* (Str^R), *hsdR2, mcrA1, mcrB1*	Karimova *et al.* (1998)
pUT18	N-Terminal T18 protein fusion plasmid, pUC19 derivative, Amp^R	Karimova *et al.* (2001)
pUT18C	C-Terminal T18 protein fusion plasmid, pUC19 derivative, Amp^R	Karimova *et al.* (2001)
pKT25	C-Terminal T25 protein fusion plasmid, pSU40 derivative, Kan^R	Karimova *et al.* (2001)
pKNT25	N-Terminal T25 protein fusion plasmid, pSU40 derivative, Kan^R	Karimova *et al.* (2001)
pUT18C-Zip	$_{T18}$Zip expression plasmid, pUT18C derivative, Amp^R	Karimova *et al.* (1998)
pKT25-Zip	$_{T25}$Zip expression plasmid, pKT25 derivative, Kan^R	Karimova *et al.* (1998)
pMW2781	DctA$_{T18}$ expression plasmid, pUT18 derivative, Amp^R	Schubert and Unden (2021)
pMW2782	$_{T18}$DctA expression plasmid, pUT18C derivative, Amp^R	Schubert and Unden (2021)
pMW2783	$_{T25}$DctA expression plasmid, pKT25 derivative, Kan^R	Schubert and Unden (2021)
pMW2784	DctA$_{T25}$ expression plasmid, pKNT25 derivative, Kan^R	Schubert and Unden (2021)
pMW2785	EIIA$^{Glc}{}_{T18}$ expression plasmid, pUT18 derivative, Amp^R	Schubert and Unden (2021)
pMW2786	$_{T18}$EIIA^{Glc} expression plasmid, pUT18C derivative, Amp^R	Schubert and Unden (2021)
pMW2787	$_{T25}$EIIA^{Glc} expression plasmid, pKT25 derivative, Kan^R	Schubert and Unden (2021)
pMW2788	EIIA$^{Glc}{}_{T25}$ expression plasmid, pKNT25 derivative, Kan^R	Schubert and Unden (2021)
pMW2367	AspA$_{T18}$ expression plasmid, pUT18 derivative, Amp^R	Schubert *et al.* (2020)
pMW2368	$_{T18}$AspA expression plasmid, pUT18C derivative, Amp^R	Schubert *et al.* (2020)
pMW2373	AspA$_{T25}$ expression plasmid, pKNT25 derivative, Kan^R	Schubert *et al.* (2020)
pMW2774	$_{T25}$AspA expression plasmid, pKT25 derivative, Kan^R	Schubert *et al.* (2020)
pMW2771	$_{T25}$GlnB expression plasmid, pKT25 derivative, Kan^R	Schubert *et al.* (2020)
pMW2773	$_{T18}$GlnB expression plasmid, pUT18C derivative, Amp^R	Schubert *et al.* (2020)
pMW3050	$_{T18}$GlnB (pMW2773), but A49P expression plasmid, pUT18 derivative, Amp^R	Schubert *et al.* (2020)
pMW3051	$_{T25}$GlnB (pMW2771), but A49P expression plasmid, pKT25 derivative, Kan^R	This study
pMW3052	$_{T18}$GlnB (pMW2773), but Y51F expression plasmid, pUT18 derivative, Amp^R	Schubert *et al.* (2020)
pMW3053	$_{T25}$GlnB (pMW2771), but Y51F expression plasmid, pKT25 derivative, Kan^R	This study
pMW2775	$_{T25}$GlnK expression plasmid, pKT25 derivative, Kan^R	Schubert *et al.* (2020)
pMW2776	GlnK$_{T25}$ expression plasmid, pKNT25 derivative, Kan^R	Schubert *et al.* (2020)
pMW2777	$_{T18}$GlnK expression plasmid, pUT18C derivative, Amp^R	Schubert *et al.* (2020)

pMW2778	$GlnK_{T18}$ expression plasmid, pUT18 derivative, Amp^R	Schubert *et al.* (2020)
pMW3091	$_{T25}$AspC expression plasmid, pKT25 derivative, Kan^R	This study
pMW3092	$AspC_{T25}$ expression plasmid, pKNT25 derivative, Kan^R	This study
pMW3093	$_{T18}$AspC expression plasmid, pUT18C derivative, Amp^R	This study
pMW3094	$AspC_{T18}$ expression plasmid, pUT18 derivative, Amp^R	This study
pMW3095	$AmtB_{T25}$ expression plasmid, pKNT25 derivative, Kan^R	This study
pMW3096	$AmtB_{T18}$ expression plasmid, pUT18 derivative, Amp^R	This study
pMW3086	$FumB_{T18}$ expression plasmid, pUT18 derivative, Amp^R	Schubert and Unden (2021)
pMW2376	Expression of $DcuC_{1-229}$-T25-$DcuC_{230-461}$, ($DcuC_{SWT25}$) pKNT25 derivative, Kan^R	Strecker (2018)
pMW1028	Expression of $DcuB_{1-211}$-T25-$DcuB_{213-446}$ ($DcuB_{SWT25}$), pKNT25 derivative, Kan^R	Wörner *et al.* (2016)
Expression plasmids and strains		
BL21(DE3)	F- *ompT*, *gal*, *dcm*, *lon*, *hsdSB*(rB- mB-) λ(DE3[*lacI lacUV5-T7 gene 1 ind1 sam7 nin5*])	Studier and Moffatt (1986)
C43(DE3)	Mutant of BL21(DE3), for expression of membrane proteins	Miroux and Walker (1996)
pASK-IBA3plus	Expression plasmid with tet promoter and C-terminal Strep-tag, Amp^R	IBA lifesciences
pMW3049	pASK-IBA3plus-*aspA*-Strep, Amp^R	Schubert *et al.* (2020)
pMW3055	pASK-IBA3plus-*glnB*-Strep, Amp^R	Schubert *et al.* (2020)
pMW3056	pASK-IBA3plus-*glnK*-Strep, Amp^R	Schubert *et al.* (2020)
pBAD18	expression vector; pBR322 *ori*, L-arabinose-inducible pBAD promoter, Kan^R	Guzman *et al.* (1995)
pMW577	pBAD18 DcuA-PhoA, Kan^R	Bauer *et al.* (2011)
pET28a	Expression vector, pBR ori, T7 promoter, His_6-tag, Kan^R	Guzman *et al.* (1995)
pMW3054	pET28a-His_6-*glnB*-His_6, Kan^R	Schubert *et al.* (2020)
pMW3069	pMW3054 but Y51F, Kan^R	Schubert *et al.* (2020)
pMW3071	pET28a-His_6-*glnK*-His_6, Kan^R	This study
pMW3070	pET28a-His_6-*glnD*-His_6, Kan^R	Schubert *et al.* (2020)
pMW3097	pET28a-His_6-*aspC*-His_6, Kan^R	This study
Phage		
$P1_{kc}$	Bacteriophage for *E. coli* infection	Miller (1992)

I Appendix 2.1 Oligonucleotide primers and sequencing primers

2.2 Chemicals

I Appendix 2.2 Chemicals

2.3 Media, solutions, and buffer

I Appendix 2.3 Media, solutions, and buffers

2.4 Growth of *E. coli*

The appropriate antibiotic was added to all cell cultures. If two antibiotics were added, the final concentration was halved (Tab. 8).

Molecular genetic methods

E. coli strains used for molecular genetic work were cultured overnight in test tubes containing 5 ml LB medium at 37°C with shaking (180 rpm, EXCELLA E24, New Brunswick Scientific). SOC medium was used as recovery medium after electroporation and heat shock transformation.

Bacterial two-hybrid (BACTH) system

Plasmids to study a protein-protein interaction with the BACTH system were cotransformed into *E. coli* BTH101 (Δ*cyaA*), plated out, and grown for 40 h at 30°C on LB agar plates containing IPTG (500 µM) and antibiotics. Pre-cultures were grown aerobically overnight at 30°C in 500 µl LB medium in 48-well plates (Sarstedt). Main cultures were inoculated with 4% (v/v) inoculum and grown to an ΔOD_{578} of 0.5 - 0.7 at 30°C. Expression of bacterial T18 and T25 fusion proteins were induced in both pre- and main cultures with IPTG (500 µM).

Aerobic reporter gene assays

Aerobic reporter gene measurements of *E. coli* containing the *dctAp-lacZ* and *aspAp-lacZ* fusions were performed in 48-well plates. Bacteria were grown aerobically in 500 µl M9 medium with glycerol (50 mM) or LB medium and different effectors (20 mM). Effectors were added as indicated in the experiment and NH_4Cl (20 mM) was present in the M9 medium unless otherwise stated. Pre-cultures were incubated overnight at 37°C with shaking (1150 rpm, Titramax 1000, Heidolph). Main cultures were inoculated at different percentages depending on growth rate and cultivated at 37°C with shaking (1150 rpm) to an ΔOD_{578} of 0.5 - 0.8 (exponential growth phase) or > 1.2 (stationary growth phase).

Anaerobic reporter gene measurement

Anaerobic reporter gene measurements of *E. coli* containing the *dcuBp-lacZ*, *frdAp-lacZ* and *dcuCp-lacZ* fusions were performed in 96-deep-well plates. Bacteria were grown anaerobically in 500 µl enriched M9 medium with glycerol (50 mM) and an electron acceptor (20 mM). Additional effectors were added as indicated in the experiment. Pre-cultures were

grown semi-anaerobically for at least 24 h at 37°C. Main cultures were inoculated at different percentages depending on growth rate. The main cultures in the 96-deep-well plates were degassed in anaerobic chambers for 15 min. Afterwards, the anaerobic chamber was gassed with nitrogen gas (1.2 atm, purity 99.999%, Westfalen AG). Main cultures were incubated for at least 16 h at 37°C to an ΔOD_{578} of 0.5 - 0.8 (exponential growth phase).

Growth studies

Aerobic and anaerobic growth experiments were performed in M9 or enriched M9 medium with a carbon source (50 mM) and effectors (20 mM). NH_4Cl (20 mM) was present in the M9 medium unless otherwise stated. In aerobic growth studies, the main cultures were inoculated with 2-4% (v/v) of 5 ml pre-cultures grown aerobically overnight at 37°C in test tubes with shaking (180 rpm, EXCELLA E24). Main cultures were grown in baffled Erlenmeyer flasks containing 20 ml medium with shaking (120 - 140 rpm, EXCELLA E24). Pre-cultures for anaerobic growth studies were grown in test tubes semi-anaerobically in standing conditions. The main anaerobic cultures were cultured in gas-tight Müller-Krempel flasks containing 20 ml of medium inoculated with 2-8% (v/v) pre-culture. Cultures were then degassed for 15 min and air was replaced with nitrogen gas (1.2 atm; purity >99.999%, Westfalen AG). The ΔOD_{578} was measured hourly or at an endpoint.

2.5 Molecular genetic methods

2.5.1 Polymerase chain reaction (PCR)

The high-fidelity DNA polymerase Phusion® (Thermo Fisher Scientific) was used for *in vitro* gene amplification and site-directed mutagenesis. The primers were synthesized by either Eurofins MWG Operon or Sigma-Aldrich (Tab. 5). The PCR reaction and cycle instructions were applied according to the manufacturer's instructions.

2.5.2 Isolation of plasmids

Plasmids were isolated using the GeneElute HP Plasmid Miniprep Kit (Sigma-Aldrich) according to manufacturer's instructions.

2.5.3 Isolation of genomic DNA

Genomic DNA was isolated using the Bacterial Genomic DNA Kit (Sigma-Aldrich) according to manufacturer's instructions.

2.5.4 Determination of the concentration and purity of DNA samples

The concentration and purity of the DNA samples were determined using a NanoDrop.

2.5.5 Sequencing of DNA samples

The sequencing of DNA samples was carried out by LGC Genomics (Berlin). The sequencing primers (Tab. 6) were synthesized by either Eurofins MWG Operon or Sigma-Aldrich.

2.5.6 Gel electrophoresis

Gel electrophoresis was used to analyze the molecular size of DNA fragments to determine the success of gene amplification or mutagenesis. DNA samples were loaded onto an agarose gel (1% w/v) and separated in 1x TAE buffer at 90 V for 45 min. Addition of Red-Safe™ nucleic acid staining solution (0.0025% v/v, iNtRON Biotechnology) to the agarose gel visualized DNA molecules by intercalation in DNA double helices, resulting in fluorescence emission under UV light. DNA samples were mixed with 1x loading dye (Thermo Fisher Scientific).

2.5.7 Production of competent cells

For electrocompetent and heat shock competent cells, either *E. coli* and glycerol-MOPS buffer, or *E. coli* XL1-Blue and TSB buffer were used, respectively. The pre-culture was grown aerobically at 37°C overnight. The main culture was inoculated with 1-2% (v/v) inoculum and cultivated in baffled Erlenmeyer flasks at 37°C with shaking (120 – 140 rpm, EXCELLA E24) to an ΔOD_{578} of > 0.5. Cells were harvested by centrifugation (6000 x g, 4°C, 10 min) and washed with buffer (10% of the culture volume), which was repeated twice. The cell pellet was resuspended in buffer to the final concentration (1% of the culture volume) and stored at -80°C.

2.5.8 Electroporation

Plasmid DNA (1-5 µl) and electrocompetent cells (50 µl) were mixed in a sterile electroporation cuvette (2 mm electrode gap) and then subjected to a pulse of 2500 V (Eporator®, Eppendorf). The bacterial solution was transferred to 1 ml of prewarmed SOC medium and incubated for at least 1 h at 37°C with shaking (1000 rpm, Thermomixer comfort, Eppendorf). The bacterial solution (25-200 µl or the entire batch) was plated out onto selective LB agar plates and incubated overnight at 37°C.

2.5.9 Heat shock transformation

Heat-competent XL1-Blue cells (50 µl) were mixed with FastDigest (FD) DpnI-digested plasmid DNA (3 µl) on ice. Heat shock was performed at 42°C followed by incubation on ice for 2 min. 1 ml of prewarmed SOC medium was added to the bacterial solution and incubated at 37°C for 90 min with shaking (1000 rpm, Thermomixer comfort, Eppendorf). The entire batch was plated out on selective LB agar plates and incubated aerobically at 37°C overnight.

2.5.10 Site-directed mutagenesis

Site-directed mutagenesis was performed in analogy to the New England BioLabs protocol (Kunkel 1985). Mutations were introduced by PCR using the high-fidelity polymerase Phusion® and mutagenesis primers (Tab. 5). Template DNA was digested for 30 min with the restriction enzyme FD DpnI (Thermo Fisher Scientific) and transformed into XL1-Blue cells by heat shock.

2.5.11 Cloning

The PCR products were purified and digested with restriction enzymes (FasDigest, Thermo Fisher Scientific) according to the manufacturer's instructions. The digested vector was dephosphorylated by fast alkaline phosphatase (FastAP, Thermo Fisher Scientific) to prevent religation. The digested PCR products and vector were ligated in a 1:1 ratio, not exceeding 5 µl of each component. Ligation was performed overnight at 16°C in a reaction volume of 20 µl with T4 DNA ligase (Thermo Fisher Scientific). The ligase was inactivated

at 70°C for 5 min. Then, 5 µl of the ligation solution was transformed in JM109 by electroshock. Individual colonies were picked and grown in an overnight culture at 37°C. The plasmid was isolated and sequenced to verify the success of the cloning procedure.

2.5.11.1 Cloning of the BACTH constructs

The bacterial two-hybrid system (BACTH) consists of the two T18 and T25 subunits of an adenylate cyclase from *Bordellia pertussis*, which in combination with a C- and N-terminal fusion protein yield a total of four fusion proteins (Fig. 16) (Karimova *et al.* 1998; Karimova *et al.* 2001). Vectors pUT18C and pUT18 are ampicillin-resistant (Amp^R), whereas pKT25 and pKNT25 are kanamycin-resistant (Kan^R). In pKNT25 and pUT18, the proteins are N-terminally fused to the fragments, while in pKT25 and pUT18C they are C-terminally fused. As an example, the possible fusion proteins with *aspA* are shown (Fig. 16). The corresponding genes were amplified from genomic DNA derived from *E. coli* BW25113. The oligonucleotide primers (Tab. 5) contained restriction sites in the overhanging regions that were used to clone the genes into the multiple cloning site of the respective expression plasmid. All operons are controlled by an IPTG-inducible plac-promoter.

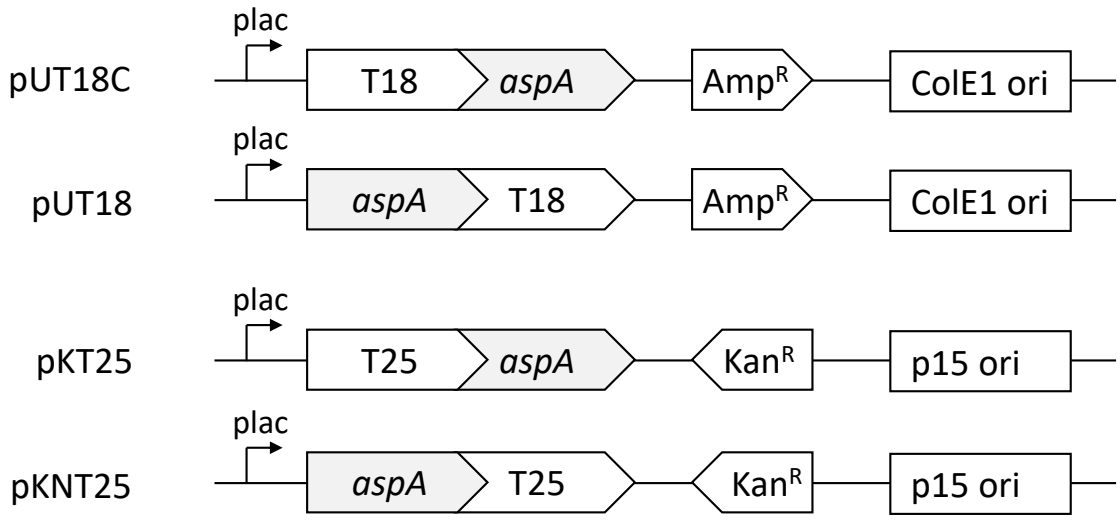

Fig. 16: Schematic representation of the adenylate cyclase-based bacterial two-hybrid (BACTH) constructs.

2.5.11.2 Cloning of the expression plasmids

For *in vitro* studies with isolated proteins, genes were cloned in expression plasmids. pET28a has a kanamycin resistance (Kan^R), an IPTG-inducible T7 promoter, pBR322-origin, and an N- and C-terminal His_6-tag (Rosenberg *et al.* 1987; Studier *et al.* 1990). pASK-IBA3plus

has an ampicillin resistance (Amp^R), an AHT-inducible tet promoter, ColE1-origin, and a C-terminal Strep-tag. Exemplary the pET28a and pASK-IBA3plus constructs of *aspA* are shown (Fig. 17). Genes were amplified using chromosomal DNA from *E. coli* BW25113 as a template, with restriction sites introduced in the overhanging regions of the oligonucleotide primers. DNA fragments and plasmids were cloned as previously described.

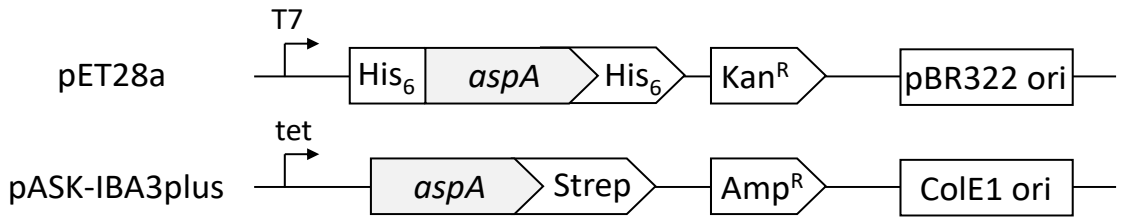

Fig. 17: Schematic representation of the pET28a and pASK-IBA3plus constructs.

2.5.12 Strain construction

In *E. coli*, the nonspecific transducing phage $P1_{kc}$ can be used to transfer regions of the genome up to a size of 80 kBp from a donor strain to a recipient strain. The exchange is accomplished by homologous recombination between the recombinant phage $P1_{kc}$ and the recipient strain. Successful transduction is usually verified qualitatively by antibiotic resistance.

An overnight aerobically grown culture of the donor strain in 5 ml LB medium was centrifuged (6000 rpm, 4°C, 5 min), the supernatant was discarded, and the cell pellet was resuspended in 5 ml MC buffer and incubated at 37°C for 30 min. The bacterial suspension (100 µl) was infected with $P1_{kc}$ phage (100 µl, plaque forming unit, PFU = 10^5) for 15 min at 37°C. Infected cells were then mixed with 3 ml of liquid R-top agar (prewarmed, 50°C) and poured evenly onto an R-agar plate. The plates were incubated for 10 min at room temperature (RT) and afterwards incubated at 37°C until confluent lysis (5-7 h). LB medium (2 ml) was added and incubated for 10 min. The R-top agar and LB medium were transferred to a centrifuge tube, and 500 µl chloroform was added to lyse the remaining bacterial cells. The solution was incubated for 10 min at RT followed by centrifugation (6000 x g, 4°C, 5 min) to separate lysed bacterial cells and the recombinant $P1_{kc}$ lysate. The clear phage lysate was aliquoted into 1.5 ml reaction tubes, 50 µl chloroform was added per 1 ml phage lysate. The clear lysate had a titer of approximately 10^{10} $P1_{kc}$ phages and is stable for several months at 4°C.

For transduction, an overnight aerobically grown culture of the recipient strain in 5 ml LB medium was centrifuged (6000 rpm, 4°C, 5 min), the supernatant was discarded, and the cell pellet was resuspended in 3 ml MC buffer. The bacterial suspension was shaken for 30 min at 37°C, then centrifuged (6000 rpm, 4°C, 5 min.) and resuspended in 1 ml LB medium. The bacterial solution (100 µl) was mixed with dilutions of 100 µl recombinant P1$_{kc}$ lysate (10^7, 10^6, and 10^5) and $CaCl_2$ (10 µl, 0.01 M) and then incubated at 37°C for 30 min. After 1 h at 37°C the infection was stopped by adding Na_3-Citrate (200 µl, 0.1 M) and 500 µl LB medium. The mixture was plated out on selective LB agar plates and incubated overnight at 37°C. Individual colonies were streaked out on selective LB agar plates and incubated overnight at 37°C. The success of P1$_{kc}$ transduction was qualitatively verified by growth on selective agar plates or genomic DNA was isolated, amplified, and sequenced with primers of the respective genomic region.

2.6 Biochemical methods

2.6.1 Adenylate cyclase-based bacterial two-hybrid system (BACTH)

The BACTH system is used for the *in vivo* analysis of protein-protein interactions, based on the successful reconstitution of an adenylate cyclase which restores cAMP-CRP signaling (Karimova *et al.* 1998; Karimova *et al.* 2001; Karimova *et al.* 2005). The adenylate cyclase is derived from the gram-negative bacterium *Bordellia pertussis* and is composed of two fragments T18 and T25, which form the catalytic center of the cyclase (Fig. 18A).

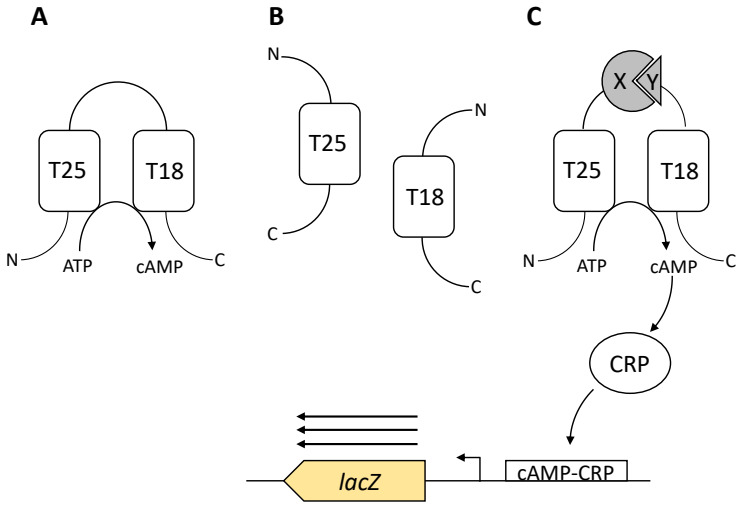

Fig. 18: Schematic representation of the bacterial two-hybrid system (BACTH). (**A**) Wild-type adenylate cyclase from *Bordellia pertussis* which converts ATP to cAMP. (**B**) Individual T25 and T18 domains (**C**) Reconstitution of adenylate cyclase activity by the interaction between fused proteins X and Y. Modified according to Karimova *et al.* (1998).

Individually, both fragments are inactive (Fig. 18B). The fragments can be fused to potential interacting proteins. When proteins X and Y interact under *in vivo* conditions, the adenylate cyclase is reconstituted and the *lacZ* reporter gene is induced, allowing the activity to be determined in a quantitative or qualitative β-galactosidase assay (Fig. 18C).

2.6.2 Quantitative measurement of β-galactosidase activity

Expression of *aspA, dctA, dcuB, dcuC,* and *frdA* was studied in a transcriptional promoter-*lacZ* fusion (e.g., *aspAp-lacZ*) where p stands for promoter. The promoter fragment included the intergenic region between the first three codons of the respective gene and the beginning of the adjacent upstream gene. Bacteria containing the *aspAp-lacZ* and *dctAp-lacZ* reporter gene fusion were grown aerobically for expression studies, whereas bacteria containing *dcuBp-*, *dcuCp-*, and *frdAp-lacZ* fusions were grown anaerobically. Cells for BACTH measurements were grown aerobically in LB medium. Quantitative measurement of β-galactosidase activity was performed with *o*-nitrophenol-β-D-galactopyranoside (ONPG). The enzyme β-galactosidase hydrolyzes ONPG to galactose and *o*-nitrophenol. When sodium carbonate (Na_2CO_3) is added, the pH shifts to the basic range and *o*-nitrophenol (λ_{max} = 352 nm) is deprotonated to *o*-nitrophenolate (λ_{max} = 420 nm), while β-galactosidase is inactivated. Both products show a yellowish coloration, but *o*-nitrophenolate is predominantly detected photometrically at 415 nm. The β-galactosidase activity was determined in Miller-Units (MU) (Miller 1992) and calculated according to the following equation (Eq. 1).

Eq. 1: Calculation of the β-galactosidase activity

$$\beta - \text{galactosidase activity [MU]} = \frac{(1000 * (\Delta E_{415} - \Delta OD_{570after}))}{(t[min] * V[ml] * \Delta OD_{570before})}$$

For the measurement of β-galactosidase activity in microtiter plates (MTP) a modified protocol was used (Griffith and Wolf 2002; Monzel *et al.* 2013). Bacteria (315 µl) were transferred to a MTP and ΔOD_{570} ($\Delta OD_{570before}$) were measured (EL808, Biotek). Chemical cell disruption was performed by adding 200 µl bacterial solution to 800 µl β-galactosidase buffer in a 96-deep-well plate and mixing with a mechanical pipette (E4 XLS Rainin, Mettler-Toledo). Lysed cells (150 µl) were aliquoted in a MTP and incubated for 10 min at 30°C. The assay was started by addition of ONPG (30 µl, 4 mg/ml) and stopped after 20 min incubation at 30°C by addition of Na_2CO_3 (70 µl, 1 M). Finally, extinction at 415 nm (ΔE_{415})

and ΔOD_{570} ($\Delta OD_{570after}$) were measured photometrically (EL808, Biotek). The collected data were used to calculate the MU (Eq. 1).

2.6.3 Membrane Strep protein interaction experiment (mSPINE)

E. coli strain C43 was cotransformed with plasmids, pMW3049 and pMW577, which encoded the fusion proteins AspA-Strep and DcuA-PhoA, respectively. The bacteria were grown aerobically in 400 ml LB medium to an ΔOD_{578} of 0.5. Protein expression was induced for 3 h with L-arabinose (100 µM) and anhydrotetracycline (AHT, 100 µM). To cross-link the proteins *in vivo*, the bacteria were incubated with formaldehyde (0.6% w/v) for 15 min at 37°C with shaking. Next, the bacteria were harvested with centrifugation (11,300 × g, 10 min), and the sediment was washed in Tris-HCl buffer (pH 8, 50 mM). For Strep-Tactin purification, cells were disrupted with a French Press (1,260 psi) in a buffer that contained lauryldimethylamine oxide (LDAO, 0.05% (v/v)). The cell homogenates were clarified by centrifugation (39,100 × g, 30 min, 4°C) and subjected to Strep-Tactin chromatography, 10% SDS-PAGE, and Western blotting. Western blots were probed with anti-Strep fused to HRP and anti-PhoA antisera (IBA Lifesciences, Sigma-Aldrich) (Scheu *et al.* 2010b; Graf *et al.* 2014; Wörner *et al.* 2016).

2.6.4 Transport measurement of radioactive labeled L-[U^{14}C]aspartate

The bacteria were grown to the stationary growth phase, sedimented with centrifugation, washed in aerobic buffer containing sodium potassium phosphate buffer (100 mM, pH 7) and $MgSO_4$ (1 mM), and resuspended in the same buffer at an ΔOD_{578} of 7.0 - 8.0. For the uptake assay, initial transport rates were determined by adding L-[U^{14}C]aspartate (100 µM) to the medium (Strecker *et al.* 2018). After 1 min, 100 µl of sample was stopped with cold LiCl (900 µl, 0.1 M) and then dried via vacuum filtration (Hoefer FH225V ten-pore Manifold filter, Pharmacia Biotech) on a cellulose mixed ester filter (ME24, Ø25 mm, pore size 0.2 µm, Schleicher & Schuell) with two LiCl (1 ml, 0.1 M) wash steps. The filters were dissolved in 4 ml scintillation liquid (Rotiszint ecoplus, Roth) and measured in the scintillation counter (Liquid Scintillation System, LS 6000SC, Beckman). Uptake was calculated, based on the accumulated radioactivity in the bacteria, per gram of dry weight (an ΔOD_{578} of 1 corresponded to 281 mg/l) per minute, and the specific radioactivity (Eq. 2) (Engel *et al.* 1992; Zientz *et al.* 1996).

Eq. 2: Calculation of the uptake rate

$$\text{Uptake rate } \left[\frac{\mu\text{mol}}{\text{g}} * \text{dw}\right] = \frac{\Delta\text{dpm} * 10000}{2000 \left[\frac{\text{dpm}}{\text{nmol}}\right] * \Delta\text{OD}_{570} * 281 \text{ [mg dw]}}$$

2.6.5 Purification of His- and Strep-tagged Proteins

E. coli BL21(DE3) that carried expression plasmids (Tab. 1) for the overproduction of AspA-Strep (pMW3049), GlnB-Strep (pMW3055), GlnK-Strep (pMW3056), His_6-AspC-His_6 (pMW3097), His_6-GlnB-His_6 (pMW3054), His_6-GlnK-His_6 (pMW3071), and His_6-GlnD-His_6 (pMW3070) were cultivated in 400 ml LB at 37°C to an ΔOD_{578} of 0.5. All proteins or genes were derived from *E. coli* BW25113, a K-12 derivative. Expression was induced by incubation with either anhydrotetracycline (AHT, 100 µM) or isopropyl-β-d-1-thiogalactopyranoside (IPTG, 250 µM) for 2.5 h. After expression, the bacteria were sedimented with centrifugation (11,300 × g, 10 min). The pellet was resuspended in buffer containing Tris-HCl (50 mM, pH 8), NaCl (500 mM), glycerol (10% v/v), and imidazole (20 mM) for Ni-NTA purification. Alternatively, the pellet was resuspended in buffer containing Tris-HCl (50 mM, pH 8), NaCl (150 mM), and EDTA (1 mM) for Strep-Tactin purification. Cells were disrupted with a French Press (1,260 psi). Cell homogenates were clarified with centrifugation (39,100 × g, 30 min, 4°C). Proteins were purified on Ni-NTA agarose (Macherey-Nagel) or with a streptavidin affinity column (IBA Lifesciences), as recommended by the suppliers. Strep-tagged proteins were eluted with a Strep buffer containing D-desthiobiotin (2.5 mM) and His-tagged proteins with increased imidazole (250-500 mM) concentration in the buffer. The peak fractions of His-tagged GlnB, GlnK, and GlnD were dialyzed in buffer for Ni-NTA purification without imidazole. Protein concentrations were determined with the Bradford assay, with bovine serum albumin as standard (Bradford 1976).

2.6.6 Protein copurification with His magnetic beads

The *in vitro* interaction between AspA-GlnB and AspA-GlnK was tested with His magnetic beads (Promega) (Huergo *et al.* 2007; Gerhardt *et al.* 2015). All reactions were conducted as suggested by the supplier (Promega). The buffer contained Tris-HCl (50 mM, pH 8), NaCl (0.1 M), glycerol (10% v/v), $MgCl_2$ (5 mM), and imidazole (50 mM). Reactions, equilibration, washing, and elution were conducted in the presence or absence of 2-oxoglutarate

(5 mM) and ATP (3.5 mM). Briefly, His magnetic beads (5 µl) were equilibrated with 100 µl buffer. Then, His_6-GlnB-His_6 or His_6-GlnK-His_6 (each 12 µg) was added as bait, and 55 µg AspA-Strep was added as prey. The proteins were mixed in a 500 µl reaction volume and preincubated at 30°C for 10 min. After preincubation, the samples were mixed with the equilibrated beads and incubated for 5 min at 30°C under agitation (800 rpm, Thermomixer comfort, Eppendorf). The beads were washed twice with 300 µl reaction buffer, and the proteins were eluted with 20 µl reaction buffer containing imidazole (0.5 M) for 5 min. Eluted samples were mixed with sample buffer and analyzed with 15% of SDS-PAGE and Western blotting. Western blots were probed with anti-Strep fused to HRP and anti-His fused to HRP antisera (IBA Lifesciences, Roth)

2.6.7 Uridylylation of GlnB

GlnB was uridylylated with purified GlnD of *E. coli* by a modified procedure (Rodionova *et al.* 2018). Purified His_6-GlnD-His_6 (2 µM) and His_6-GlnB-His_6 (50 µM) were incubated in buffer containing Tris-HCl (50 mM, pH 7.5), KCl (100 mM), $MgCl_2$ (10 mM), DTT (1 mM), uridine-5'-triphosphate (UTP, 2 mM), 2-oxoglutarate (5 mM), and ATP (1 mM) at 37°C for 3 h. Then, the mixture was incubated at 60°C for 10 min followed by centrifugation (12,295 × g, 10 min) to separate denaturated GlnD and GlnB-UMP. GlnB uridylylation was verified by native gel electrophoresis (Fig. 24).

2.6.8 Gas chromatography-mass spectrometry (GC-MS) of mouse samples

The preparation of the mouse intestinal samples of conventional Swiss Webster was performed by Maria Winter (University of Texas). The gut was removed from the abdominal cavity. Subsequently, the intestinal lumen contents in the distal part of the Jejunum (proximal part of the small intestine), the Ileum (distal part of the small intestine) as well as cecum and colon were collected (Fig. 28). The contents of each intestinal section were transferred to an Eppendorf reaction tube containing 500 µl TBS buffer and weighed. The samples were then vortexed for 2 min to break up the pellet. The solids and cells were centrifuged (6,000 x g, 5 min, benchtop centrifuge, Eppendorf). The supernatant was aliquoted and deep-frozen at 80°C until use. The metabolites of the lyophilized sample were extracted with methyl *tert*-butyl ether (MTBE) and methanol and analyzed with a mass spectrometer (Agilent Technologies) consisting of an electron impact ionization source (EI) and a time of

flight (TOF) mass analyzer. The measurement and sample preparation were performed by MetaSysX GmbH according to a modified protocol (Salem *et al.* 2016).

2.6.9 *In vitro* activity of AspA in a coupled enzymatic AST assay

AspA activity was monitored with isolated protein by determining the L-Asp consumed or produced in a discontinuous enzymatic assay. Samples (50 µl) were taken at different time points, and enzymes were inactivated by incubating at 95°C for 10 min. Then, the L-Asp concentration was quantified with a coupled enzymatic L-Asp:2-OG aminotransferase (AST) assay at RT (Bergmeyer *et al.* 1983). For testing the effect of GlnB or GlnK, purified AspA (350 nM) and GlnB or GlnK (1 µM) were mixed in 500 µl of assay buffer. For the amination reaction, this assay buffer consisted of Tricin (50 mM, pH 8.5), L-Asp (1 mM), NH_4Cl (20 mM), fumarate (10 mM), $MgCl_2$ (5 mM), and dithiothreitol (DTT, 1 mM). For the deamination reaction, the assay buffer contained HEPES (50 mM, pH 8), L-Asp (5 mM), $MgCl_2$ (5 mM), and DTT (1 mM). Reactions were initiated by adding L-Asp or NH_4Cl.

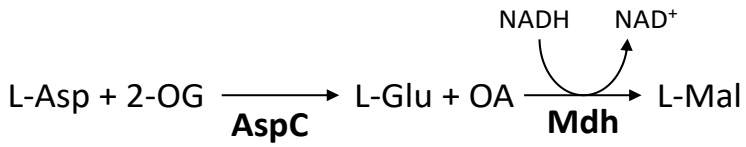

Fig. 19: Reactions of the coupled enzymatic AST assay. Abbreviations: 2-OG: 2-oxoglutarate; AspC: L-Asp:2-OG aminotransferase AST; OA: oxaloacetate; Mdh: malate dehydrogenase; L-Mal: L-malate.

The coupled reaction of AspC and malate dehydrogenase Mdh consumes NADH (Fig. 19). NADH (λ_{max} = 340 nm) and NAD^+ (λ_{max} = 260 nm) have distinct absorption peaks, allowing quantification according to the Beer-Lambert law (Beer 1852).

Determination of L-Asp in the medium or buffer

Bacteria were grown aerobically to the stationary phase at 37°C in minimal M9 medium, with or without NH_4Cl, supplemented with glycerol (50 mM) and L-Asp (20 mM). After centrifugation, the supernatant was analyzed for L-Asp in an AST enzymatic assay (Bergmeyer *et al.* 1983).

2.6.10 SDS-PAGE and semi-dry Western blotting

SDS-PAGE (sodium dodecyl sulfate polyacrylamide gel electrophoresis) is an analytical method for the separation of proteins on an electric field. The Mini-PROTEAN system (Bio-

Rad) was used for SDS-PAGE at a constant voltage of 150 V for approx. 90 min. Proteins were transferred to a nitrocellulose membrane (Whatman, GE Healthcare) by semi-dry Western blotting. For semi-dry Western blotting, two layers of filter paper, nitrocellulose membrane, SDS gel, and two layers of filter paper were placed between the anode and cathode on a semi-dry blotter (Bio-Rad). All components were soaked in transfer buffer. Transfer was performed under 45 mA for 90 min per nitrocellulose membrane. The proteins are chemically denatured by the SDS and thus acquire a negative charge, causing the denatured proteins to diffuse from the cathode to the anode and consequently transfer to the nitrocellulose membrane. For native-PAGE, SDS was omitted from each buffer and the protocol according to Atkinson *et al*. (1994) was used.

2.6.11 Antibody staining

After semi-dry Western blotting, free binding sites on the nitrocellulose membrane were saturated by incubation in blocking buffer (3% w/v BSA, 0.1% v/v Tween 20) on a tumbling shaker overnight at 4°C (Polymax 1040, Heidolph). The nitrocellulose membrane was incubated for 1 h with the antibody buffer (1% w/v BSA, 0.1% v/v Tween 20) containing the respective antibody at a dilution of 1:10,000. Unbound antibody was then removed via three 5 min wash steps with wash buffer (0.1% v/v Tween 20). If necessary, this step was repeated with the secondary antibody. During the incubation phases, the nitrocellulose membrane was shaken on a tumbling shaker (Polymax 1040, Heidolph). Immunostaining was performed with horse-radish peroxidase (HRP)-coupled anti-His, anti-Strep, and anti-IgG-mouse polyclonal antiserum (Roth, IBA Lifesciences, Sigma-Aldrich) or with anti-PhoA antibodies produced in mouse (Sigma-Aldrich). For visualization, a chemiluminescent substrate was applied (Immobilon Western HRP substrate, Merck Millipore), followed by exposure to an X-ray film (Advansta).

2.7 Bioinformatics

2.7.1 Programs and servers

Tab. 2: Programs and servers used in this study

Program/Server	Description	Reference
EggNOG v5.0	Database for orthologous groups and functional annotations	(Huerta-Cepas *et al.* 2016) http://eggnog5.embl.de/#/app/home
UCSF Chimera	Visualization of protein structures	(Pettersen *et al.* 2004) https://www.cgl.ucsf.edu/chimera/
NCBI Blast	Comparison of nucleotide and protein sequences	(Altschul *et al.* 1990) https://blast.ncbi.nlm.nih.gov/Blast.cgi
OligoCalc	Calculation of melting temperatures and much more	(Kibbe 2007) http://biotools.nubic.northwestern.edu/OligoCalc.html
RCSB Protein Database	Database with protein structures	(Berman *et al.* 1999) https://www.rcsb.org/
Unipro UGENE	Bioinformatics software with different alignment functions	(Okonechnikov *et al.* 2012) http://ugene.net/
EcoCyc	Database of the *E. coli* genome with functional annotations	(Keseler *et al.* 2017) https://ecocyc.org/
BRENDA	A comprehensive enzyme information system	(Jeske *et al.* 2019) https://www.brenda-enzymes.org/
Regulon DB	*E. coli* K-12 transcriptional regulatory network	(Gama-Castro *et al.* 2016) http://regulondb.ccg.unam.mx/
GRAVY Calculator	Grand average of hydropathy (GRAVY) value for protein sequences	http://www.gravy-calculator.de/
Sequence massager	Nucleic acid sequence 'massager'	http://bio-model.uah.es/en/lab/cybertory/analysis/massager.htm
UniProt	The Universal Protein Resource (UniProt) is a comprehensive resource for protein sequence and annotation data	(UniProt Consortium 2019) https://www.uniprot.org/
Clone Manager	Cloning and amplification planning	http://www.scied.com/index.htm
FinchTV	Chromatogram viewer	https://digitalworldbiology.com/FinchTV
Translation	DNA translation	https://web.expasy.org/translate/
Protein MW calculator	Molecular weight calculator	http://www.sciencegateway.org/tools/proteinmw.htm
Heatmapper	Web-enabled heat mapping	(Babicki *et al.* 2016)

3 Results

3.1 The physiology and regulation of L-aspartate metabolism in *E. coli*

3.1.1 L-Asp is an optimal nitrogen source for *E. coli*

L-Asp is an important precursor for numerous biosynthetic pathways, including biosynthesis of UMP and NAD^+ and of various amino acids (Jensen *et al.* 2008; Osterman 2009). The degradation of L-Asp requires only one step compared to other amino acids, producing free ammonium and fumarate catalyzed by AspA. Ammonium is assimilated in the glutamine synthetase (GS, GlnA) and glutamine 2-oxoglutarate aminotransferase (GOGAT, GltBD) reaction, producing L-Glu (van Heeswijk *et al.* 2013). Fumarate is excreted in a L-Asp:fumarate antiport by DcuA under aerobiosis (Strecker *et al.* 2018), whereas fumarate can be used as an electron acceptor in anaerobic growth (Six *et al.* 1994). The quality of L-Asp as a nitrogen source was investigated by comparing aerobic *E. coli* growth in response to ammonium and amino acids, including L-Asp, as the sole nitrogen source. The bacteria were grown in minimal M9 medium with glycerol as the carbon source. The selection of amino acids was based on their physiological significance and turn-over rates in the reference enterohaemorrhagic *E. coli* (EHEC) strain EDL933, and other microbiota found in the bovine small intestine contents (BSIC) (Bertin *et al.* 2018). The growth rates for the nitrogen source ammonium, L-Asp, L-Asn, and L-Gln were very similar (Fig. 20A). L-Asn is deaminated to L-Asp in the periplasm of *E. coli* by asparaginase AnsB (Cedar and Schwartz 1967; Willis and Woolfolk 1974). L-Gln was used as a reference because of its central role in nitrogen metabolism. However, in BSIC, L-Gln is found only at low concentrations and is therefore of minor significance for *E. coli*. L-Ala compared to L-Asp has a similar fast degradation pathway. L-Ala can be converted directly to ammonium and pyruvate, though the growth rate was inferior to L-Asp. L-Ser and L-Thr which are also degraded by EDL933 and the bovine small intestine microbiota (Bertin *et al.* 2018), supported growth rate with only one-third of optimal nitrogen sources such as ammonium, L-Asp, L-Gln, and L-Asn (Fig. 20A).

In a previous work, it was shown that ammonium is a preferred source of nitrogen and represses the utilization of L-Asp (Strecker *et al.* 2018). In similar competition experiments, the effect of other amino acids on L-Asp utilization was tested. Bacteria were grown in minimal M9 medium and glycerol with either L-Asp as the sole nitrogen source or paired with L-Ala, L-Gln, or L-Thr. The presence of L-Ala had no effect on L-Asp consumption. L-Gln

and L-Thr lowered L-Asp consumption by 39% and 37%, respectively (Fig. 20B). Interestingly, L-Thr did not support growth as, for example, L-Gln did, but still lowered L-Asp consumption (Fig. 20A and B). Both L-Asp and L-Gln supported rapid growth as high-quality nitrogen sources, with L-Gln being used preferentially over L-Asp. Overall, L-Asp is a high-quality nitrogen source that supports rapid growth of *E. coli*.

The utilization of L-Asp as the nitrogen source can be via two pathways. In the first pathway, ammonium is released from L-Asp by the deamination reaction of AspA. The free ammonium is assimilated by the GS-GOGAT pathway, producing L-Glu. In the second pathway, the amide group of L-Asp can be transferred directly to 2-oxoglutarate, producing L-Glu and oxaloacetate, which is catalyzed by the aspartate aminotransferase AspC. To differentiate between these two pathways, bacteria were cultured aerobically in minimal M9 medium with L-Asp as the sole nitrogen source. Additionally, genes involved in the degradation of L-Asp were genetically inactivated. The *dcuA*-deficient mutant showed the highest growth reduction, whereas the aerobic C_4-dicarboxylate transporter DctA had wild-type growth (Fig. 20C), confirming previous findings that DcuA is the main L-Asp transporter in *E. coli* (Strecker *et al.* 2018). *aspA*-deficiency halved growth, while *aspC*-deficiency had a minor effect (Fig. 20C). In conclusion, DcuA is essential for growth on L-Asp, while AspA is an important enzyme for the effective degradation of L-Asp as a nitrogen source.

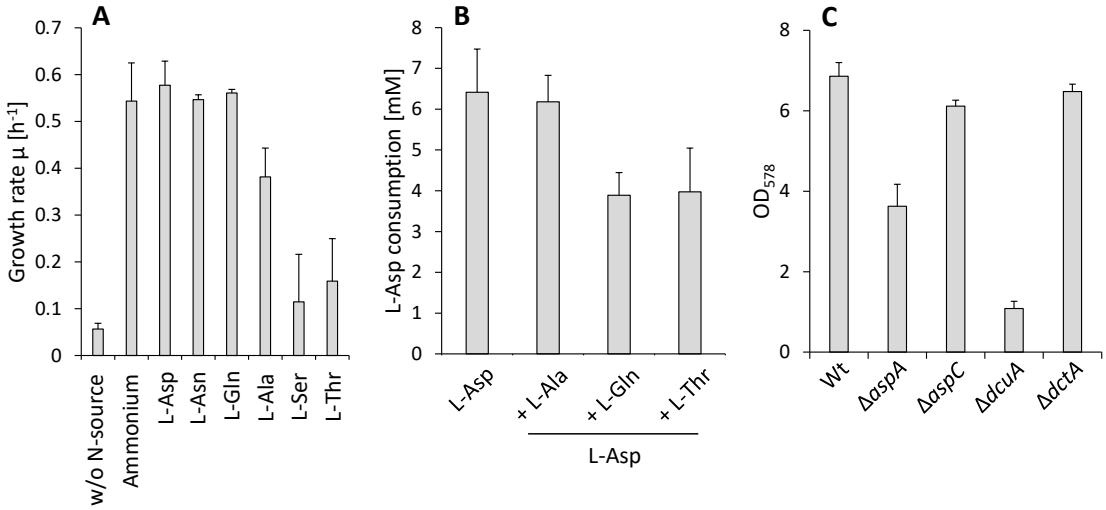

Fig. 20: Growth of *E. coli* with different amino acids as the nitrogen source. (**A**) *E. coli* BW25113 (wild type) was grown in NH_4Cl-deficient M9 medium with glycerol (50 mM) and the indicated amino acids or NH_4Cl (20 mM), as the nitrogen source. Growth rates (μ, h^{-1}) were calculated from growth curves. (**B**) BW25113 were grown aerobically to an OD_{578} of 2 in NH_4Cl-deficient M9 medium with glycerol (50 mM) and L-Asp as the sole nitrogen source or paired with either L-Ala, L-Gln, or L-Thr (20 mM). L-Asp in the supernatant was measured before and after growth with the aspartate aminotransferase (AST) assay (Bergmeyer *et al.* 1983). The difference is shown. (**C**) Wild type (Wt) and mutant BW25113 bacteria were grown for 24 h to the stationary growth phase in NH_4Cl-deficient M9 medium with glycerol (50 mM) and L-Asp (20 mM) as the sole nitrogen source. Growth is expressed in terms of optical density at 578 nm (OD_{578}). Gene deficiency (Δ) abbreviations: *aspA*: aspartase; *aspC*: aspartate aminotransferase; *dcuA*: L-Asp/succinate antiporter; *dctA*: C_4-dicarboxylate transporter.

3.1.2 *aspAp-lacZ* expression is independent of nitrogen regulators

Previous work showed that the expression of *aspA* depends on cAMP-CRP activation (Tsai *et al.* 2018; Surmann *et al.* 2020). Furthermore, *aspA* is negatively regulated by NarL of the NarX-NarL two-component system and positively regulated by DcuR and FNR (Golby *et al.* 1998b; Goh *et al.* 2005; Surmann *et al.* 2020). The *aspA* and *dcuA* genes colocalize on the *E. coli* genome. An *aspA-dcuA* cotranscript is produced, but it is of minor significance for the expression of the genes (Golby *et al.* 1998b). Transcription of *dcuA* is constitutive (Golby *et al.* 1998b; Strecker *et al.* 2018). The utilization of L-Asp as the nitrogen source was influenced by the presence of other amino acids (Fig. 20B). To investigate whether this effect can be explained by transcriptional regulation of *aspA*, the effect on *aspAp-lacZ* expression by different nitrogen sources and compositions of growth medium as well as transcriptional regulators of nitrogen metabolism was tested. The *aspA* promoter was fused to the reporter gene *lacZ* encoding the β-galactosidase. Bacteria containing the chromosomal *aspAp-lacZ* reporter gene fusion were grown aerobically in minimal M9 medium and glycerol in presence of different effectors to the exponential growth phase (OD_{578} = 0.5). In addition, bacteria were grown in nitrogen deficient M9 medium and glycerol with different nitrogen sources as the effector. Overall, the *aspAp-lacZ* expression was not significantly affected by the presence of effectors (Fig. 21A).

In addition, the response regulator NtrC of the NtrB-NtrC two-component system (alternative name GlnL-GlnG), the transcriptional regulator Lrp, and the alternative σ-factor RpoS, involved in general stress response, were tested. The transcriptional regulators were genetically inactivated in the *aspAp-lacZ* reporter strain. Bacteria were grown in minimal M9 medium and glycerol with either NH_4Cl or L-Asp as the sole nitrogen source to the exponential growth phase (OD_{578} = 0.5). In both cases, the *lrp*- and *ntrC*-deficient mutants showed wild-type growth, while an increase of *aspAp-lacZ* expression was observed in the *rpoS*-deficient mutant (Fig. 21B). Overall, alteration of transcriptional regulators involved in nitrogen metabolism had no effect on *aspAp-lacZ* expression, whereas the σ-factor of the general stress response negatively affected expression in the exponential growth phase. Prior work has shown that *aspA* transcription is regulated by Lrp. These data were based on global transcriptional analyses, for example, using chromatin immunoprecipitation (ChIP)-sequencing (Hung *et al.* 2002; Cho *et al.* 2008; Kroner *et al.* 2019). This observation could not be confirmed by direct testing in the *aspAp-lacZ* expression analysis (Fig. 21B).

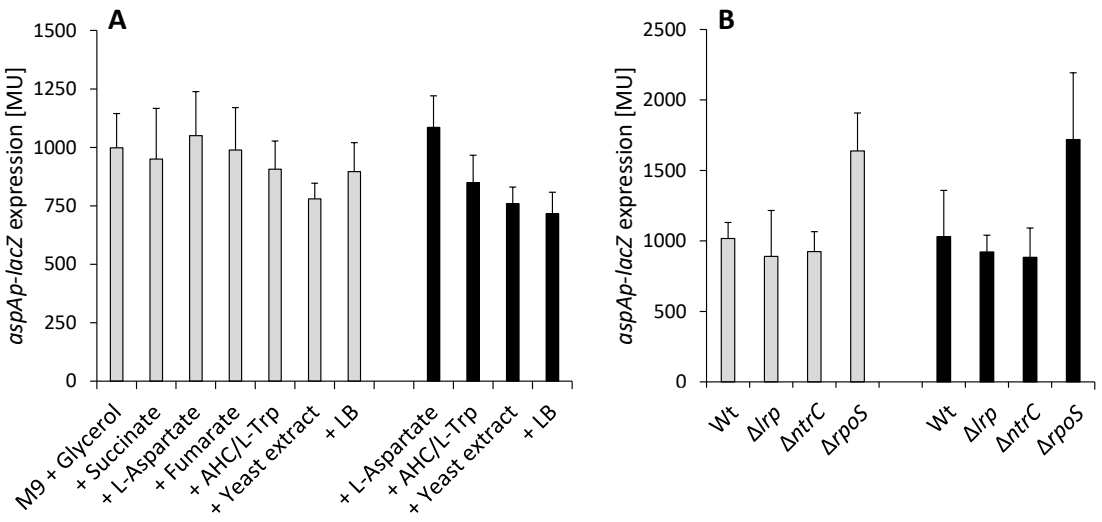

Fig. 21: *aspAp-lacZ* expression in response to varying carbon and nitrogen sources (A), and transcriptional regulators (B). Bacteria were grown in M9 medium (gray bars) and NH_4Cl-deficient M9 medium (black bars) and glycerol (50 mM) to the exponential growth phase (OD_{578} = 0.5). The β-galactosidase activity was measured and is expressed in Miller-Units (MU). (**A**) *aspAp-lacZ* expression were measured in *E. coli* strain IMW642. The indicated nutrients were added, at the following concentrations: succinate (20 mM), L-Asp (20 mM), fumarate (20 mM), acid hydrolyzed casein (AHC, 0.1 % w/v) with L-Trp (0.005 % w/v), yeast extract (5 g/l), and lysogeny broth (LB, 5 g/l). (**B**) L-Asp (20 mM) was used as the sole nitrogen source (black bars). IM642 were rendered deficient (Δ) in the following genes: *lrp*: leucine-responsive transcriptional regulator; *ntrC*: response regulator of NtrB-NtrC; and *rpoS*: the general stress response σ-factor.

3.1.3 L-Asp consumption of *E. coli* is influenced by GlnB

Since neither *dcuA* nor *aspA* were transcriptionally affected by nitrogen availability or by transcriptional regulators, L-Asp transport and utilization were tested. Previous work identified DcuA as the main L-Asp transporter in *E. coli* (Strecker *et al.* 2018). At the center of the *E. coli* nitrogen regulatory network is the protein GlnB (PII) by controlling the activity of glutamine synthetase (GS) of the GS-GOGAT pathway through regulating the adenylyltransferase/adenylyl-removing enzyme GlnE (van Heeswijk *et al.* 2013). The GlnB homolog GlnK (PII-2) regulates the ammonium transporter AmtB via protein-protein interaction (Javelle *et al.* 2004). The utilization of L-Asp as the nitrogen source was influenced by the presence of other amino acids (Fig. 20B). In this context, it was investigated whether L-Asp uptake by DcuA is affected by GlnB or GlnK. The initial rates of L-[$U^{14}C$]Asp uptake in *E. coli* and mutants lacking *glnB* and *glnK* were measured. Bacteria were cultivated aerobically in minimal M9 medium and glycerol with L-Asp as the sole nitrogen source or paired with ammonium. The advantage of initial rate measurements is the minimized interference of transport by cellular metabolism of the substrate and by other cellular parameters. The uptake rates of L-[$U^{14}C$]Asp did change slightly in the wild type in response to ammonium, whereas in the *glnB* and *glnK* mutant the uptake rates remained similar in both conditions

(Fig. 22A). Overall, GlnB and GlnK had no effect on L-Asp uptake by DcuA, indicating that AspA is the likely candidate for regulation.

E. coli wild type and mutants lacking *glnB* and *glnK* were grown in nitrogen-deficient M9 medium and glycerol with L-Asp as the sole nitrogen source or paired with ammonium to the stationary growth phase (OD_{578} = 2). The supernatant was collected and L-Asp consumption before and after growth was measured using the aspartate aminotransferase (AST) assay (Bergmeyer *et al.* 1983). The wild type consumed 5.4 mM L-Asp, whereas the presence of ammonium decreased L-Asp consumption to 3.8 mM. In the *glnB* mutant, L-Asp consumption in the presence of ammonium was wild-type, whereas L-Asp consumption increased significantly in the absence of ammonium. The *glnK*-deficient mutant had no significant effect on L-Asp consumption; the amounts of L-Asp consumed were wild-type (Fig. 22B). In conclusion, the L-Asp consumption rates of *E. coli* revealed that the nitrogen regulatory protein GlnB affects L-Asp utilization, whereas GlnK had no impact. These results suggest that the target of GlnB regulation is the aspartase AspA.

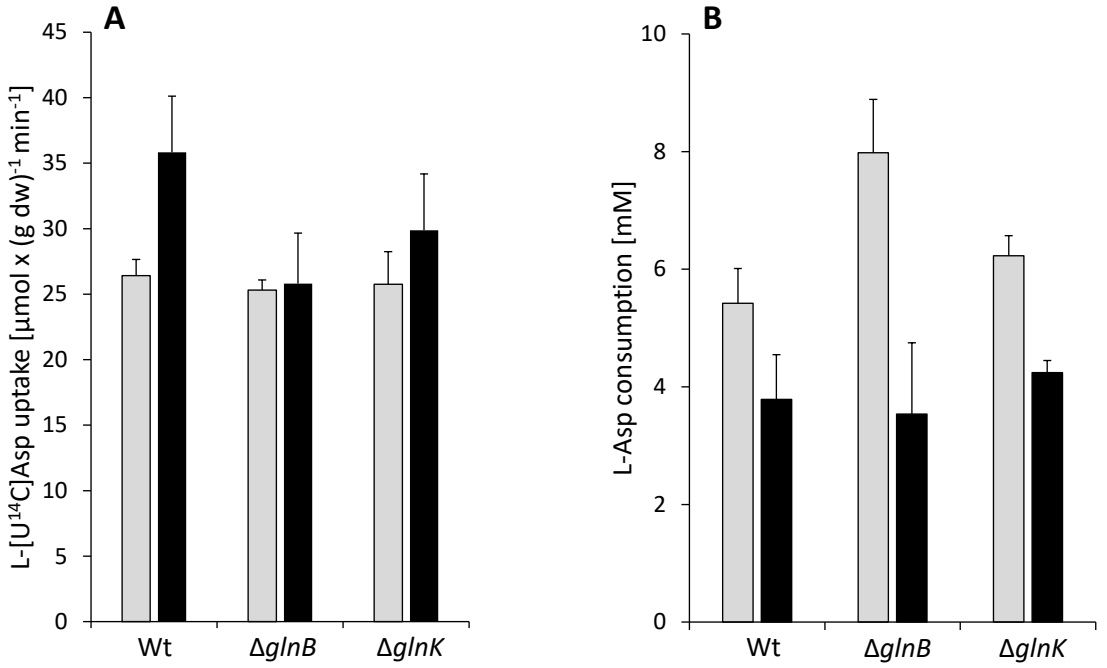

Fig. 22: Effect of GlnB and GlnK on L-Asp uptake and consumption. Bacteria were grown aerobically in NH_4Cl-deficient M9 medium and glycerol (50 mM) with L-Asp (20 mM; gray bars) or paired with NH_4Cl (20 mM each; black bars).(**A**) *E. coli* BW25113, and *E. coli* deficient (Δ) in GlnB (JW2537; Δ*glnB*) or GlnK (JW0440; Δ*glnK*) were washed and resuspended, then incubated with 100 µM L-[U^{14}C]Asp for 1 min. L-Asp uptake was determined with rapid filtration. (**B**) L-Asp consumption by *E. coli* BW25113 (Wt), JW2537, and JW0440 was measured in the supernatant before and after growth (OD_{578} = 2) using the AST assay, the difference is given (Bergmeyer *et al.* 1983).

3.1.4 AspA-GlnB interaction is dependent on effector molecules

L-Asp utilization was affected by the regulatory protein GlnB, whereas L-Asp uptake was not affected by DcuA (Fig. 22A and B). L-Asp serves as a direct precursor for numerous amino acids, NAD^+ und UMP biosynthesis (Michal 1999; Jensen *et al.* 2008; Osterman 2009). This diversity of L-Asp metabolism complicates the interpretation of the previous experiments as to what type of regulation GlnB exerts. For this reason, the interaction between AspA and GlnB were tested *in vivo* and *in vitro*. GlnB controls its target proteins, such as GlnE, NtrB, NagB, and ACCase, through direct protein-protein interaction (Jiang and Ninfa 1999; van Heeswijk *et al.* 2013; Gerhardt *et al.* 2015; Rodionova *et al.* 2018). Therefore, the interaction between AspA and GlnB were tested in a bacterial adenylate cyclase-based two-hybrid system (BACTH). Fusion proteins of AspA and GlnB with either T25 or T18 domains of *Bordetella pertussis* adenylate cyclase were constructed. In this system, restoration of cyclase activity requires interaction between the fused proteins, leading to cAMP production that ultimately induces the *lacZ* reporter gene.

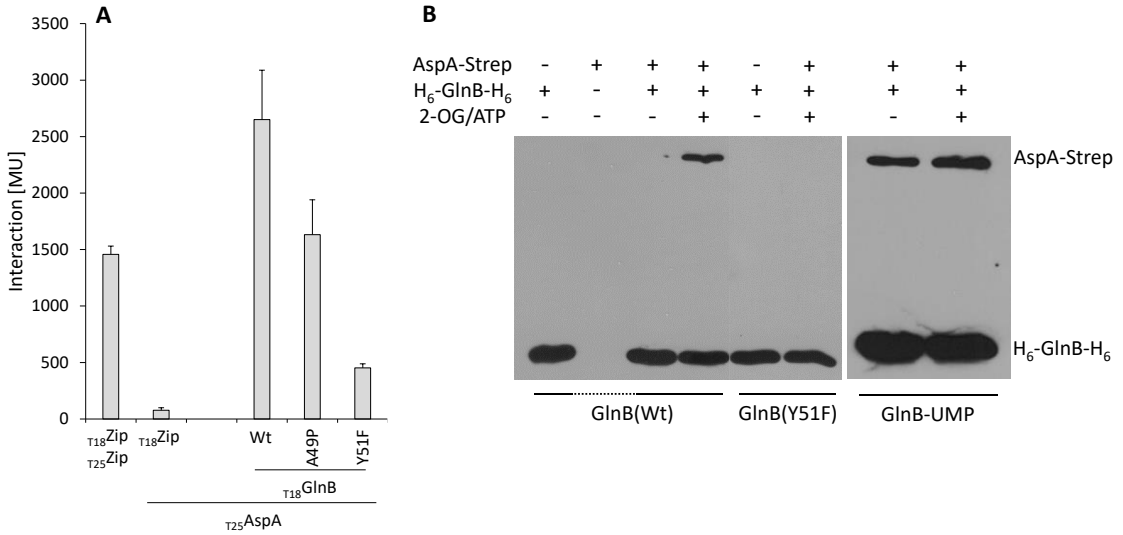

Fig. 23: Interaction of AspA with GlnB and GlnB mutants *in vivo* (A) and *in vitro* (B). (A) *E. coli* BTH101 (Δ*cyaA*) was cotransformed pairwise with plasmids encoding fusions of T25 to AspA ($_{T25}$AspA) and fusions of T18 to GlnB and GlnB mutants ($_{T18}$GlnB, A49P and Y51F). The combinations are shown on the x-axis. The leucine zipper pair $_{T18}$Zip and $_{T25}$Zip are applied as a positive control (Karimova *et al*. 1998; Karimova *et al*. 2001), the pair $_{T18}$Zip/$_{T25}$AspA as the negative control for background β-galactosidase activity. The corresponding plasmids are derivatives of pUT18C and pKT25 (Tab. 1). The strains were grown aerobically in LB medium. β-Galactosidase activities were quantified in Miller-Units (MU). (**B**) Purified AspA-Strep (55 µg) and His_6-tagged GlnB (H_6-GlnB-H_6), either GlnB (Wt) or GlnB (Y51F) or uridylylated GlnB-UMP (each 12 µg) were incubated in buffer, with or without 2-oxoglutarate (2-OG, 5 mM) and ATP (3.5 mM). H_6-GlnB-H_6 was precipitated with the addition of His magnetic beads. The (co)purified proteins were separated with SDS-PAGE and identified in Western Blots, with antisera against the Strep-tag and His_6-tag. The bands corresponding to AspA-Strep (56.0 kDa) and H_6-GlnB-H_6 (16.2 kDa) are indicated.

The strains showed high activities of β-galactosidase for the strain that produced AspA and GlnB, indicating interaction of the proteins (Fig. 23A). The GlnB mutants A49P and Y51F are located in the T-Loop, which plays a crucial role in the protein-protein interaction with target proteins (Gerhardt *et al.* 2015). GlnB A49P is known to cause loss of interaction with the sensor histidine kinase NtrB (Martínez-Argudo and Contreras 2002; Zhang *et al.* 2007). The strain that expressed the GlnB mutant A49P showed a much weaker interaction with AspA compared with wild-type GlnB (Fig. 23A). Residue Trp51 of GlnB represents the site for GlnB uridylylation (Rhee *et al.* 1989; Jaggi *et al.* 1996). The GlnB mutant Y51F showed almost a complete loss of interaction compared with GlnB A49P (Fig. 23A). These results confirm that the interaction between AspA and GlnB involves the T-Loop.

The interaction between GlnB and target proteins is dependent on the effector molecules ATP, ADP, and 2-OG. Moreover, GlnB can be chemically modified via uridylylation by GlnD (Jiang *et al.* 1998). GlnB is a homotrimer, whereby each monomer harbors three characteristic T-, B-, and C-loops. The B- and C-loops are involved in the binding of effector molecules. Ligand binding induces conformational changes in the T-loop that modulate interaction with target proteins. Thus, GlnB is able to modulate the enzyme activity of target proteins to the current metabolic state and requirement of *E. coli* (Huergo *et al.* 2013; van Heeswijk *et al.* 2013). To verify this interaction, Strep-tagged AspA and His_6-tagged GlnB were purified and examined *in vitro* in a copurification experiment using His magnetic beads. The interaction was assayed in presence of the known GlnB effector molecules, ATP and 2-oxoglutarate (2-OG). In addition, uridylylated GlnB and the uridylylation mutant GlnB Y51F were tested against AspA-Strep. When His magnetic beads were treated with His_6-tagged GlnB in the absence of effector molecules, AspA-Strep was not detected in immunostaining. AspA-Strep was copurified with His magnetic beads pretreated with H_6-GlnB-H_6 when ATP and 2-OG were present. In the absence of effector molecules and H_6-GlnB-H_6, Strep-tagged AspA did not bind to His magnetic beads (Fig. 23B). Moreover, AspA-Strep did not copurify when His magnetic beads were pretreated with the uridylylation mutant GlnB Y51F, similar to the BACTH results where a strong reduction of the interaction was observed (Fig. 23A and B). GlnB was uridylylated by GlnD *in vitro*. The successful uridylylation was confirmed by the electrophoretic mobility shift of GlnB-UMP in native protein electrophoresis

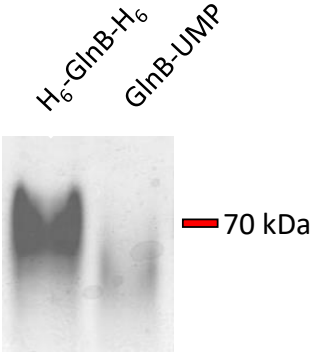

Fig. 24: Native PAGE of GlnB after uridylylation. Native-PAGE of GlnB after uridylylation by GlnD. Uridylylated GlnB runs lower than non-uridylylated GlnB in a non-denaturing PAGE (Atkinson *et al.* 1994)

(Fig. 24). AspA-Strep copurified with uridylylated GlnB-UMP in an effector molecule-independent manner (Fig. 23B), and for both situations, high levels of copurified AspA-Strep were detected in immunostaining. These results suggest that the interaction between AspA and GlnB depends on the presence of either ATP and 2-OG or uridylylated GlnB or both.

3.1.5 AspA activity is positively regulated by GlnB

The previous experiments have shown that GlnB interacts with AspA in the presence of ATP and 2-OG or when GlnB is uridylylated. There are several examples in which GlnB modulates the enzyme activity of target proteins via protein-protein interaction depending on effector molecules and uridylylation state (Gerhardt *et al.* 2015; Rodionova *et al.* 2018). These different signal inputs lead to conformational changes in the T-loop that defines the signal output, resulting in positive or negative regulation of the target protein (Huergo *et al.* 2013). The effect of GlnB on AspA was measured with purified AspA and GlnB proteins *in vitro*. AspA catalyzes either an amination of fumarate (ammonium + fumarate → L-Asp), or in reverse, the deamination of L-Asp (L-Asp → ammonium + fumarate). Both types of reaction were assayed in presence of GlnB, uridylylated GlnB-UMP, and effector molecules.

Addition of 2-OG paired with ATP or ADP alone had no effect on the amination and deamination activity (Fig. 25B). However, the deamination reaction was significantly stimulated by 2.27-fold in the presence of GlnB paired with ATP and 2-OG (Fig. 25A). Comparatively, ATP alone showed a minor effect on the latter activity (1.3-fold). The presence of ADP alone and paired with 2-OG marginally increased the AspA deamination activity. Uridylylated GlnB-UMP stimulated the deamination reaction of AspA twofold both in the presence and absence of 2-OG and ATP (Fig. 25A). The amination reaction remained largely constant or was slightly inhibited in presence of ATP (0.8-fold). Overall, GlnB in presence of ATP and 2-OG, or GlnB-UMP stimulate ammonium formation by AspA (Fig. 25A). These data are consistent with the copurification assay in which either GlnB in the presence of ATP and 2-OG, or GlnB-UMP were able to copurify Strep-tagged AspA (Fig. 23B). Under nitrogen-limited conditions, intracellular 2-OG levels are high and GlnB is predominantly uridylylated (van Heeswijk *et al.* 2013). In this metabolic state, GlnB-UMP stimulates the AspA deamination reaction twofold, releasing ammonium, which is then assimilated in the GS-GOGAT pathway to produce L-Glu.

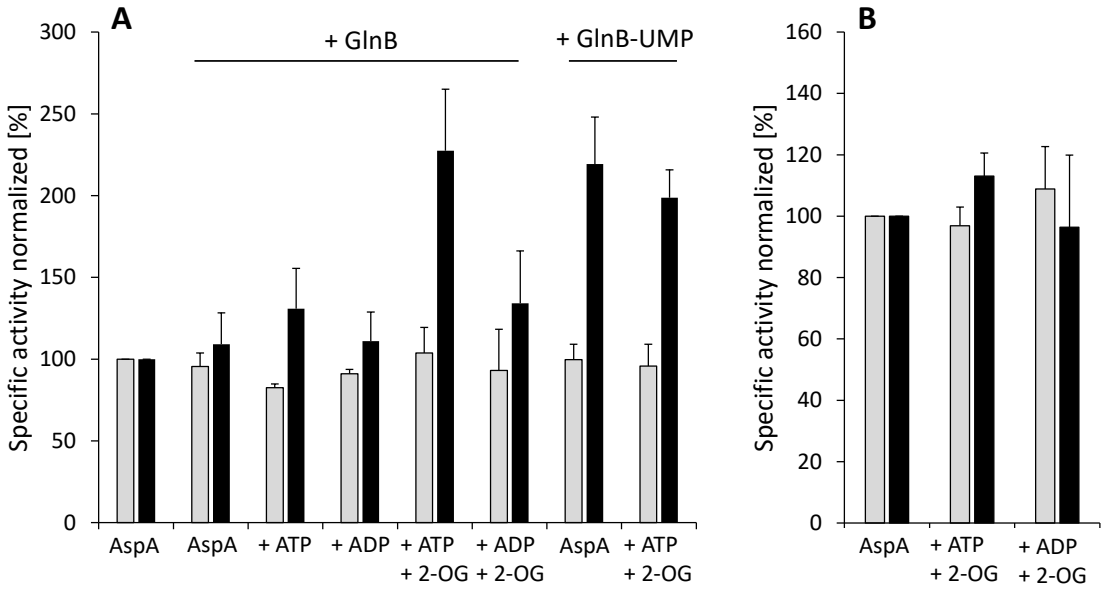

Fig. 25: The effects of GlnB on AspA activity *in vitro*. (A) The activity of purified AspA-Strep was measured with the coupled AST assay (Bergmeyer *et al.*, 1983) in the presence or absence of purified GlnB or GlnB-UMP paired with the effectors 2-oxoglutarate (2-OG, 5 mM), ATP (3.5 mM), and ADP (3.5 mM). The activities are normalized to the activity of AspA alone (100% activity). AspA activity is shown for both amination (fumarate + ammonium → L-Asp, gray bars) and deamination (L-Asp → fumarate + ammonium, black bars) reactions. (**B**) AspA activity in the presence with 2-OG paired with ATP or ADP as control.

3.1.6 AspA-GlnK interaction had no regulatory effect

The GlnB paralog protein GlnK showed interaction with AspA in the adenylate cyclase-based BACTH system, although no effect could be measured on L-Asp utilization *in vivo* (Fig. 22B & Fig. 26A). GlnB in presence of 2-OG and ATP or uridylylated GlnB-UMP stimulated the AspA deamination reaction by twofold (Fig. 25A). The same type of experiment was performed with purified GlnK and AspA. When His magnetic beads were treated with His_6-tagged GlnK, Strep-tagged AspA weakly copurified in the absence of effector molecules. Obviously, interaction between AspA and GlnK is present, but much weaker than with GlnB. In contrast to the AspA-GlnB interaction, which was dependent on 2-OG and ATP, an AspA-GlnK interaction can only be detected in the absence of ATP and 2-OG. In the presence of effector molecules, no Strep-tagged AspA can be detected in immunostaining (Fig. 26B). GlnK alone, as well as paired with 2-OG and ATP showed no significant effect on either the amination or deamination reaction of AspA (Fig. 26C). Thus, the weak interaction observed between AspA and GlnK had no regulatory effect on either AspA activity. This resembles the GlnB target acetyl-CoA carboxylase ACCase, where GlnK interacted with the protein without affecting the ACCase activity (Rodrigues *et al.* 2014; Gerhardt *et al.* 2015).

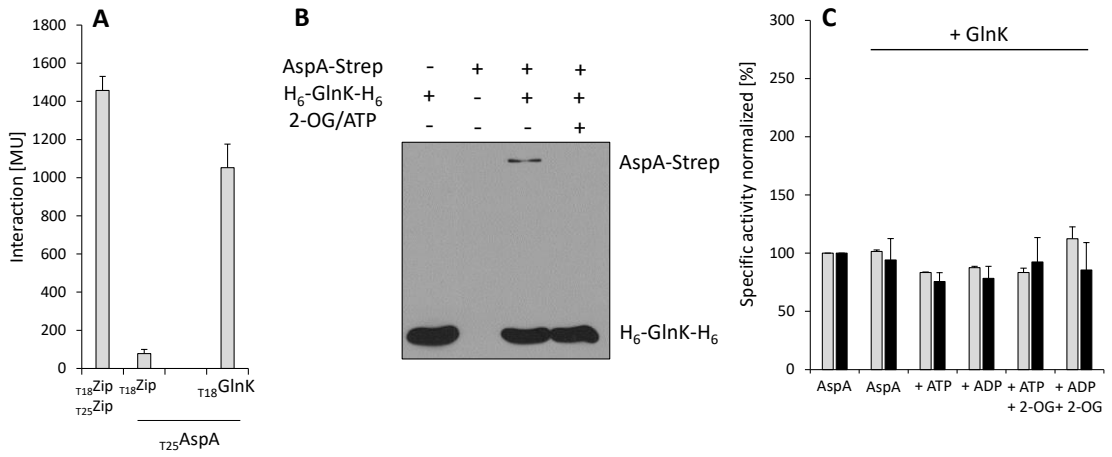

Fig. 26: Interaction of AspA and GlnK *in vivo* (A), copurification to demonstrate the interaction between AspA and GlnK *in vitro* (B), and the effects of GlnK on AspA activity *in vitro* (C). (A) *E. coli* BTH101 (Δ*cyaA*) was cotransformed pairwise with plasmids encoding fusions of T25 to AspA ($_{T25}$AspA) and fusions of T18 to GlnK ($_{T18}$GlnK). The combinations are shown on the x-axis. The leucine zipper pair $_{T18}$Zip and $_{T25}$Zip are applied as a positive control (Karimova *et al*. 1998; Karimova *et al*. 2001), the pair $_{T18}$Zip/$_{T25}$AspA as the negative control for background β-galactosidase activity. The corresponding plasmids are derivatives of pUT18C and pKT25 (Tab. 1). The strains were grown aerobically in LB medium. β-Galactosidase activities were quantified in Miller-Units (MU). (**B**) AspA-Strep (55 µg) and H_6-GlnK-H_6 (12 µg) were incubated in buffer, with or without 2-oxoglutarate (2-OG, 5 mM) and ATP (3.5 mM). H_6-GlnK-H_6 was precipitated with the addition of HisMagnetic beads. The (co)purified proteins were separated with SDS-PAGE and identified in Western Blots, with antisera against Strep and His_6. (**C**) The activity of purified AspA was measured with the coupled AST assay (Bergmeyer *et al*. 1983) in the presence or absence of GlnK, without or with the effectors 2-oxoglutarate (2-OG, 5 mM), ATP (3.5 mM), and ADP (3.5 mM). The activities are normalized to the activity of AspA alone (100% activity). AspA activity is shown for both amination (fumarate + ammonia → L-Asp, gray bars) and deamination (L-Asp → fumarate + ammonia, black bars) reactions.

3.1.7 Aspartate aminotransferase AspC interacted with GlnB

The aspartate aminotransferase AspC catalyzes one of the two L-Asp degradation pathways, which was of minor significance (Fig. 20C). AspC is a multifunctional enzyme that catalyzes the synthesis of L-Asp, L-Phe, L-Tyr, and other substrates. AspC catalyzes the reversible transfer of the amide group from L-Asp to 2-oxoglutarate, yielding L-Glu and oxaloacetate (Powell and Morrison 1978). The products of the AspC reaction are at the interface of carbon and nitrogen metabolism. L-Glu can be used to incorporate ammonium in the GS-GOGAT pathway (van Heeswijk *et al.* 2013), whereas oxaloacetate can be utilized for gluconeogenesis through the PEP/pyruvate bypass (Sauer and Eikmanns 2005). The reversible reaction of AspC provides a rapid pathway for the production of L-Asp, an important precursor for UMP biosynthesis, under nitrogen upshift (Jensen *et al.* 2008; Yuan *et al.* 2009). Both AspA and AspC catalyze reactions of interest for nitrogen and carbon metabolism in *E. coli*. GlnB stimulation of AspA deamination activity in the presence of ATP and 2-OG or uridylylated GlnB-UMP was demonstrated (Fig. 25A). Accordingly, an AspC-GlnB interaction was

tested using the adenylate cyclase-based BACTH system. Similar to the BACTH experiments with AspA-GlnB, two GlnB mutants, GlnB A49P and Y51F, were used (Fig. 23A).

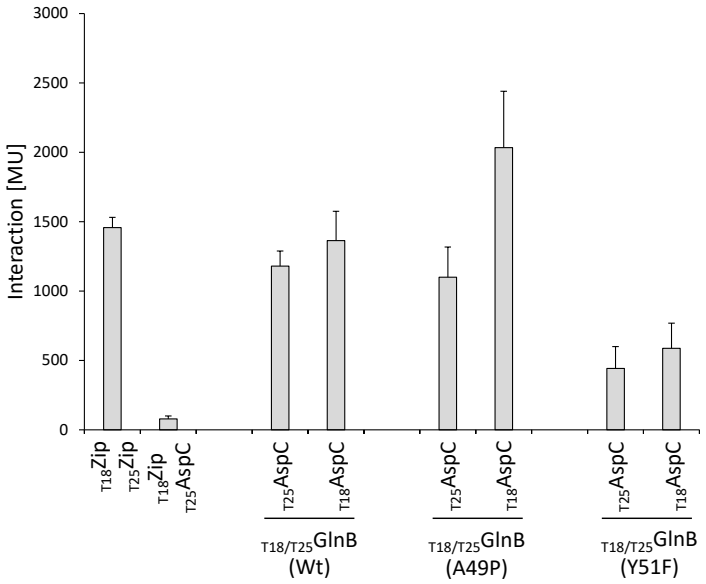

Fig. 27: **Interaction of AspC with GlnK and GlnK mutants.** *E. coli* BTH101 (Δ*cyaA*) was cotransformed pairwise with plasmids encoding fusions of T25 to AspC or GlnB ($_{T25}$AspC, $_{T25}$GlnB) and fusions of T18 to AspC or GlnB ($_{T18}$AspC, $_{T18}$GlnB). The combinations are shown on the x-axis. The leucine zipper pair $_{T18}$Zip and $_{T25}$Zip are applied as a positive control (Karimova *et al*. 1998; Karimova *et al*. 2001), the pair $_{T18}$Zip/$_{T25}$AspC as the negative control for background β-galactosidase activity. The corresponding plasmids are derivatives of pUT18C and pKT25 (Tab. 1). The strains were grown aerobically in LB medium. β-Galactosidase activities were quantified in Miller-Units (MU).

The strains producing the AspC and GlnB fusions showed high activities of β-galactosidase for both pairs, indicating an interaction of the proteins (Fig. 27). The GlnB A49P mutation is located in the T-loop and showed in one combination wild-type interaction, while the alternation of the T25 and T18 fragments caused a twofold increase in interaction. In contrast, GlnB A49P caused a decrease in interaction with AspA. The uridylylation mutant GlnB Y51F showed a twofold decrease in interaction with AspC, a similar observation was made for interaction with AspA (Fig. 23A and Fig. 27) (Rhee *et al.* 1989; Jaggi *et al.* 1996). The data showed that the AspC-GlnB interaction also involves the T-loop and is presumably specific. In addition, the GlnB paralog GlnK was tested for interaction with AspC in the adenylate cyclase-based BACTH system. The β-galactosidase activity was significantly lower than with GlnB and AspA-GlnK, but still some combinations exceeded the background activity of the negative control (I. Appx. 3.1.7).

3.2 L-Asp as a nitrogen source and electron acceptor in the mouse intestine

3.2.1 GC-MS of primary metabolites in the mouse intestine

The intestine is a highly complex and competitive environment in which *E. coli* must compete with the gut microbiota for efficient colonization (Miranda *et al.* 2004; Kamada *et al.* 2012). Analysis of the bovine small intestine contents revealed high levels of proteinogenic amino acids (Bertin *et al.* 2018). A similar analysis was performed for the mouse model of conventional Swiss Webster mice. Intestinal contents of mice were collected at four distinct position by collaborator Maria Winter (University Texas) (Fig. 28). Samples were dissolved in TBS buffer and vortexed, then the mixture was centrifuged, and the supernatant was removed, aliquoted and deep-frozen. The metabolites of the lyophilized sample were extracted with methyl *tert*-butyl ether (MTBE) and methanol. Samples were analyzed for their content of primary metabolites using gas chromatography-mass spectrometry (GC-MS) by MetaSysX (Potsdam). The metabolites were quantified relatively in normalized intensities, with exception of the C_4-dicarboxylates fumarate, L-malate, and succinate. These were determined in absolute concentrations using a calibration curve. With this set of reference substrates and the assumption that the extraction and detection of the remaining substrates, especially amino acids, are comparable to C_4-dicarboxylates, the extrapolation of their absolute contents was performed. Absolute contents were calculated in mmol kg^{-1} dry weight; concentrations are shown for simpler presentation. The regions for sampling were divided into proximal and distal part of the small intestine (PI and DI), cecum (CE) and colon (CO) (Fig. 28).

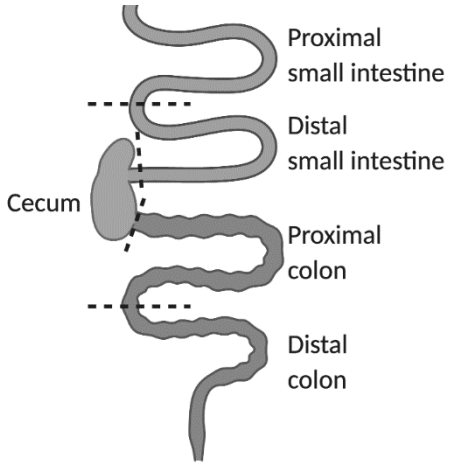

Fig. 28: Schematic overview of the mouse intestine and sampling areas.

3.2.1.1 Aminogram of the mouse intestine

The bovine gastrointestinal tract contains high amounts of proteinogenic amino acids. Previous work showed that L-Asp is a preferentially utilized substrate for enterohemorrhagic *E. coli* strain EDL933 in bovine small intestinal contents, with DcuA and AspA being the key enzymes involved in L-Asp utilization (Bertin *et al.* 2018). Analysis of the intestinal contents of conventional Swiss Webster mice revealed similarly high levels of proteinogenic

amino acids (Fig. 29). In addition, about 40 substrates were found, of which amino acids represent the largest group. Four regions of the gastrointestinal tract were examined, the proximal and distal parts of the small intestine (PI and DI), the cecum (CE), and the colon (CO) (Fig. 28). A total of 127 mM amino acids in the proximal part and 77 mM in the distal part of the small intestine were quantified. The cecum and colon parts are largely negligible with 11 mM and 10 mM amino acids, respectively (Fig. 29A). Most amino acids are found in the proximal and distal parts of the small intestine in the range of 4 to 17 mM, L-Ala showed the highest levels, whereas L-Cys and L-Asn were present in very low amounts (Fig. 29B). In addition to L-Ala; L-Pro, L-Val, and L-Leu also showed high concentrations in both sections of the small intestine. Amino acid concentrations decreased continuously from the proximal part through the distal part of the small intestine to the cecum and colon, with the lowest amount of amino acids observed in the colon (Fig. 29A). The concentration of L-Asp in the proximal part was 4 mM, which decreased to 2 mM in the distal part of the small intestine. In the cecum and colon, 1.3 and 0.4 mM were measured, respectively (Fig. 29B). These results are similar to the L-Asp levels found in bovine small intestine, where approximately 3.8 mM L-Asp was quantified. Similar to what has already been shown for the bovine small intestine (Bertin *et al.* 2018), the mouse intestine exhibited a similar amino acid-rich environment, with amino acid levels exceeding those of the bovine small intestine. In the proximal and distal parts of the small intestine in mice, 127 mM and 77 mM amino acids were found, respectively, compared to 41.3 mM for the bovine small intestine. This discrepancy can be explained by the initial dilution of the bovine intestine samples, which halves the concentrations presented (Bertin *et al.* 2018).

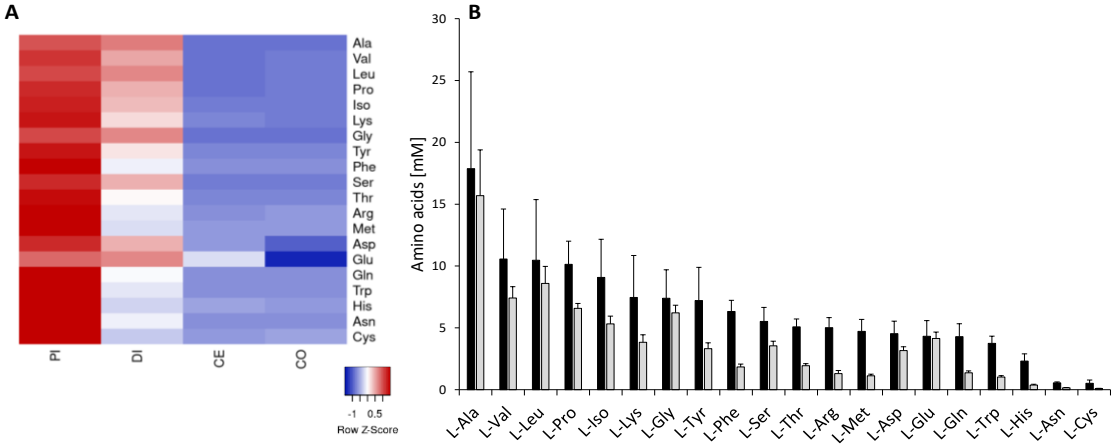

Fig. 29: Heatmap of the intestinal amino acids (A) and aminogram of the proximal and distal part of the small intestine (B). (**A**) Heatmaps were prepared with the online tool Heatmapper (Babicki *et al.* 2016) of the proximal part (PI) and the distal part (DI) of the small intestine, cecum (CE), and colon (CO). (**B**) Aminogram of the proteinogenic amino acids quantified in the proximal (black bars) and distal part (gray bars) of the small intestine. Four samples from different male mice were analyzed for each section of the mouse intestine.

The availability of different nitrogen sources and the competition with other microorganisms in the animal gut makes it even more essential to specialize in the degradation of single amino acids in order to coexist with other bacterial species (Freter *et al.* 1983).

3.2.1.2 Distribution of intermediate substrates in the mouse intestine

The aminogram revealed an amino acid-rich environment, especially in the proximal and distal part of the small intestine (Fig. 29B). In addition, many intermediates or end products were found in the small intestine. A total of 20 mM in the proximal and 28 mM substrates in the distal part of the small intestine were quantified (Fig. 30A and B). The most abundant substrate in all sampling areas of the mouse intestine is L-lactate, accounting for 77% of the total in the proximal part and 80% in the distal part of the small intestine. L-Lactate concentrations significantly exceeded L-Ala levels in the distal part of the small intestine at 22.5 mM (L-Ala = 15.7 mM) (Fig. 30B). Substrates in the low single-digit millimolar range were quantified for the cecum and colon. The high amounts of L-lactate found in the small intestine were presumably produced by lactic acid fermentation from Lactobacillaceae and excreted as an end product. Lactobacillaceae are by far the most common family in the small intestine (Yang *et al.* 2019). In the cecum and colon, L-lactate levels collapsed severely due to butyrate fermentation of L-lactate and acetate by Clostridia (Bourriaud *et al.* 2005; Detman *et al.* 2019). Clostridia are only found in these sections of the mouse intestine (Yang *et al.* 2019). Short chain fatty acids (SCFA), such as butyrate, acetate, and propionate, are assimilated by the mammalian host and provide high portions of total energy gained from the diet, especially in ruminants (Mortensen and Clausen 1996; Scheppach *et al.* 2001). In humans, SCFA are implicated as a preferred energy source for colonic mucosa and protection against colitis and colorectal cancer (McIntyre *et al.* 1993; Archer *et al.* 1998; Wächtershäuser and Stein 2000; Pryde *et al.* 2002). In addition, D-glyceric acid and urea are found in low millimolar range. Urea is one of the three most important nitrogenous waste products in humans, along with creatine and uric acid. A total of 3.5 mM urea, 0.14 mM creatine, and 0.27 mM uric acid were quantified in all four intestinal sections combined. Urea is degraded by microorganisms in the intestine, releasing ammonia that can be utilized as a nitrogen source (Wrong 1978). The remaining substrates were measured only in very low micromolar concentrations (Fig. 30A).

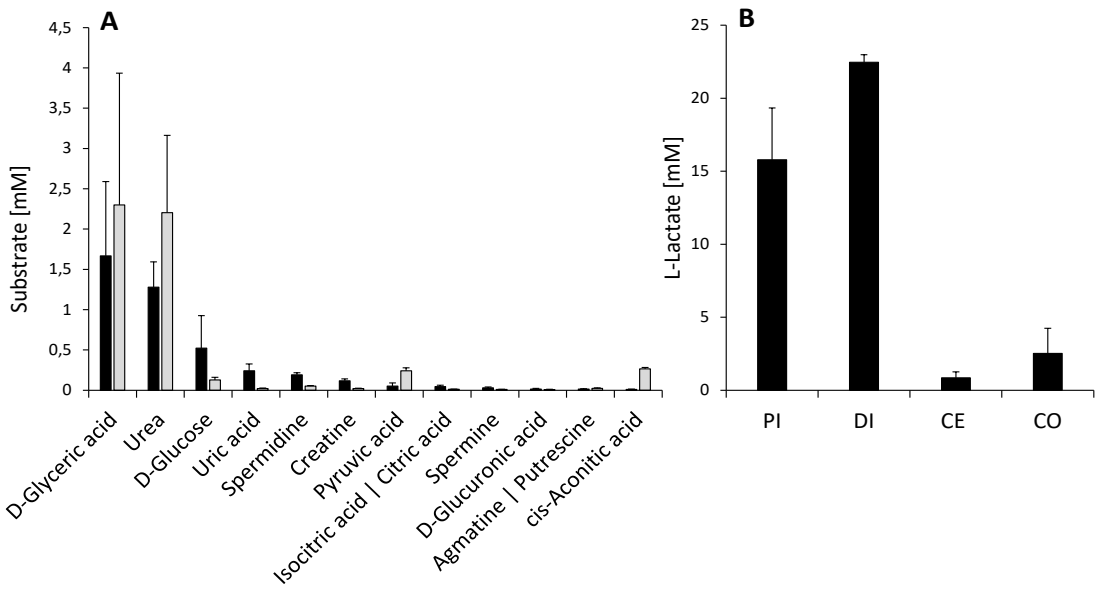

Fig. 30: Distribution of intermediate substrates and end products in the mouse intestine. (**A**) Absolute concentrations of intermediate substrates and end products in the proximal (black bars) and distal part (gray bars) of the small intestine. (**B**) L-Lactate concentrations in the mouse intestine. Four samples from different male mice were analyzed for each section of the mouse intestine. Abbreviations: proximal (PI) and distal part (DI) of the small intestine, cecum (CE), and colon (CO).

3.2.1.3 Distribution of C_4-dicarboxylates in the mouse intestine.

E. coli uses nitrate and fumarate in the intestine as electron acceptors for growth. However, the nitrate concentration in the intestinal cecal mucus is limited, rendering fumarate respiration more essential (Jones *et al.* 2007; Jones *et al.* 2011). Analysis of the intestinal samples revealed that L-Asp is by far the most abundant C_4-dicarboxylate, with 4 mM measured in the proximal and 2 mM in the distal part of the small intestine. In the cecum, L-Asp is still present in the millimolar range (1.3 mM), and only in the colon did L-Asp levels drop into the micromolar range (0.4 mM) (Fig. 31A). The L-Asp levels found are comparable to those from bovine small intestine contents (Bertin *et al.* 2018). In contrast, fumarate and L-malate were quantified only in the low micromolar range. The highest succinate concentration was measured in the distal part of the small intestine (410 µM), assuming that fumarate, L-malate, and L-Asp are converted by microbial fumarate respiration to succinate. However, the increase in succinate did not reflect the decrease in L-Asp, L-malate, and fumarate. Most likely, the decrease in succinate levels in the cecum and colon may be caused by host intestinal gluconeogenesis, bacterial succinate fermentation, or oxidative degradation using low levels of diffused oxygen (Jones *et al.* 2007; Jones *et al.* 2011; Vadder *et al.* 2016; Connors *et al.* 2018). DcuA has a K_M of 43 µM for L-Asp, consequently the L-Asp levels found are sufficient to saturate transport by DcuA. The K_M value for fumarate uptake by DcuB is 100 µM (Engel *et al.* 1994). Therefore, DcuB is suitable for the uptake of L-malate in the

proximal and distal parts of the small intestine. The K_M of DcuB for L-Asp is not known, but the high L-Asp levels suggest that DcuB is also involved in L-Asp uptake. The approximate K_M for induction of DcuS-dependent genes is in the millimolar range (Unden *et al.* 2016), suggesting that L-Asp is likely the C_4-dicarboxylate that is predominantly detected under physiological conditions in the mouse intestine. Overall, L-Asp is by far the most abundant C_4-dicarboxylate found in the mouse intestine, possibly rendering L-Asp the most important C_4-dicarboxylate for *E. coli* under physiological conditions. Fumarate respiration is essential for *E. coli* for intestinal colonization (Jones *et al.* 2007; Jones *et al.* 2011); based on the available data, it can be assumed that L-Asp is the main fumarate source for commensal and pathogenic *E. coli*.

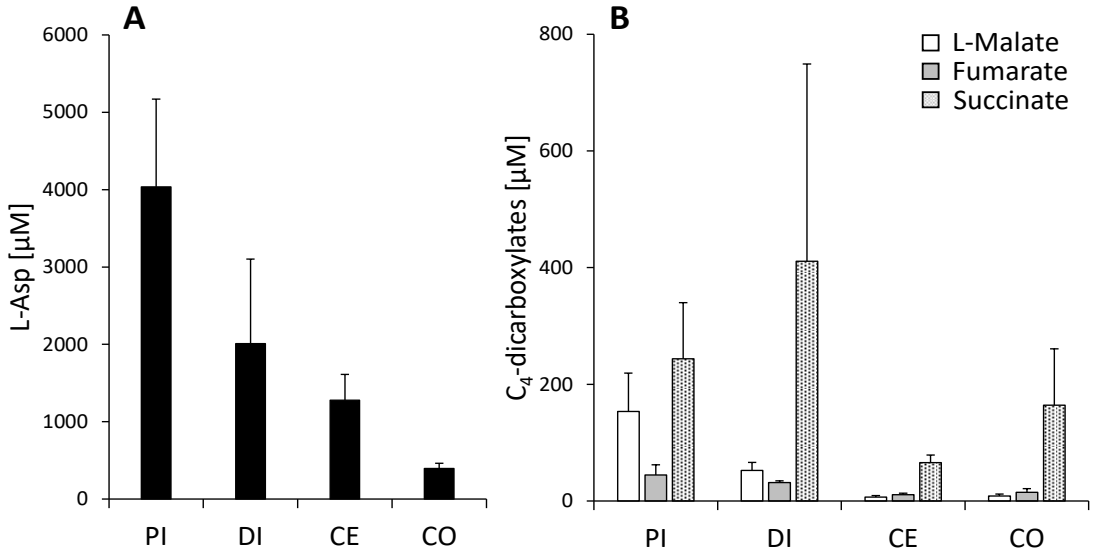

Fig. 31: Concentration of C_4-dicarboxylates L-Asp (A), L-malate, fumarate, and succinate (B) in the mouse intestine. (**A**) L-Asp concentration in the intestinal contents of mice. (**B**) L-Malate, fumarate, and succinate concentrations of the mouse intestine. Four samples from different male mice were analyzed for each section of the mouse intestine. Abbreviations: proximal (PI) and distal part (DI) of the small intestine, cecum (CE), and colon (CO).

3.2.2 Lrp regulation of genes involved in fumarate respiration

In the absence of oxygen, *E. coli* can use fumarate respiration for anaerobic growth, and the succinate formed is excreted as the end product of fumarate respiration. Any C_4-dicarboxylate can be converted to fumarate in a few enzymatic steps, including L-Asp by aspartase AspA (Guest 1979; Unden *et al.* 2016). L-Asp is an important intermediate step for various amino acid biosynthetic pathways, as well as their degradation pathways. Thus, the intracellular production of fumarate is closely linked to amino acid degradation via L-Asp (Michal 1999). The animal gut is an amino acid-rich environment that provides *E. coli* with several possibilities to produce fumarate (Fig. 29) (Bertin *et al.* 2018). Lrp is a global transcriptional

regulator for one third of the *E. coli* genome, responding to L-Leu, L-Met, L-Ala, and other amino acids (Tani *et al.* 2002; Hart and Blumenthal 2011; Kroner *et al.* 2019). These genes are involved in amino acid biosynthesis and catabolism, and other cellular functions (Brinkman *et al.* 2003). Lrp may act as a repressor or activator that can be potentiated or antagonized by L-Leu binding, or L-Leu binding may has no effect at all (Lin *et al.* 1992; Platko and Calvo 1993; Newman and Lin 1995). A global gene expression profile for Lrp showed that the expression of *dcuB* (factor -2.23), *frdA* (factor -1.63), and *dcuC* (factor -1.44) was reduced in a *lrp*-deficient strain (Hung *et al.* 2002). The involvement of Lrp in the expression of *dcuB*, *frdA*, and *dcuC* was investigated using *lacZ* reporter gene fusions to determine whether an Lrp-dependent effect on expression could be observed.

3.2.2.1 *dcuB* and *frdA* are positively regulated by Lrp

Under anaerobiosis, C_4-dicarboxylates are used for fumarate respiration, in which fumarate is reduced to succinate by the fumarate reductase FrdABCD (Guest 1979; Unden *et al.* 2016). The transport of C_4-dicarboxylates is catalyzed by DcuB, which couples C_4-dicarboxylate uptake with the export of succinate (Engel *et al.* 1992; Engel *et al.* 1994). *dcuB* and *frdA* are both anaerobically expressed and positively regulated by the transcriptional regulator FNR and the DcuS-DcuR two-component system in response to C_4-dicarboxylates (Golby *et al.* 1998b; Zientz *et al.* 1998; Golby *et al.* 1999). The animal intestine is an amino acid-rich environment, which means that the supply of fumarate to the cell is not limiting (Jones *et al.* 2007; Jones *et al.* 2011; Bertin *et al.* 2018). Thus, the extent to which the expression of *dcuB* and *frdA* is influenced by the transcriptional regulator Lrp was investigated. Both promoters were fused to the reporter gene *lacZ*, with additional genetic inactivation of *lrp*. Bacteria were cultured anaerobically in minimal M9 medium and glycerol as the carbon source with fumarate as the electron acceptor. Lrp responds to different amino acids, so the expression was tested in the presence of lysogeny broth (LB) which is an undefined complex medium containing a mixture of amino acids. Expression of *dcuBp-lacZ* was examined in two reporter gene strains IMW237 (*dcuBp-lacZ*) and IMW503 (*dcuBp-lacZ*, Δ*dcuB*), both of which contain a chromosomal *dcuBp-lacZ* fusion and in IMW503 *dcuB* is additionally genetically inactivated. Deficiency of *dcuB* leads to constitutively activated DcuS, resulting in fumarate-independent induction of *dcuBp-lacZ* (Kleefeld *et al.* 2009; Steinmetz *et al.* 2014).

As expected, a fumarate-dependent induction of *dcuBp-lacZ* is observed in IMW237, which is lost in IMW503 (Δ*dcuB*). Throughout the experiment, a decrease in *dcuBp-lacZ* expression was observed when *lrp* was genetically inactivated (Fig. 32A). The reduction in *dcuBp-lacZ* expression ranges from a factor of -1.37 to -3.45. These results are in agreement with data from the global gene expression analysis of a *lrp* mutant (factor -2.23) (Hung *et al.* 2002). In summary, the *dcuBp-lacZ* expression analysis revealed positive regulation by the global transcriptional regulator Lrp.

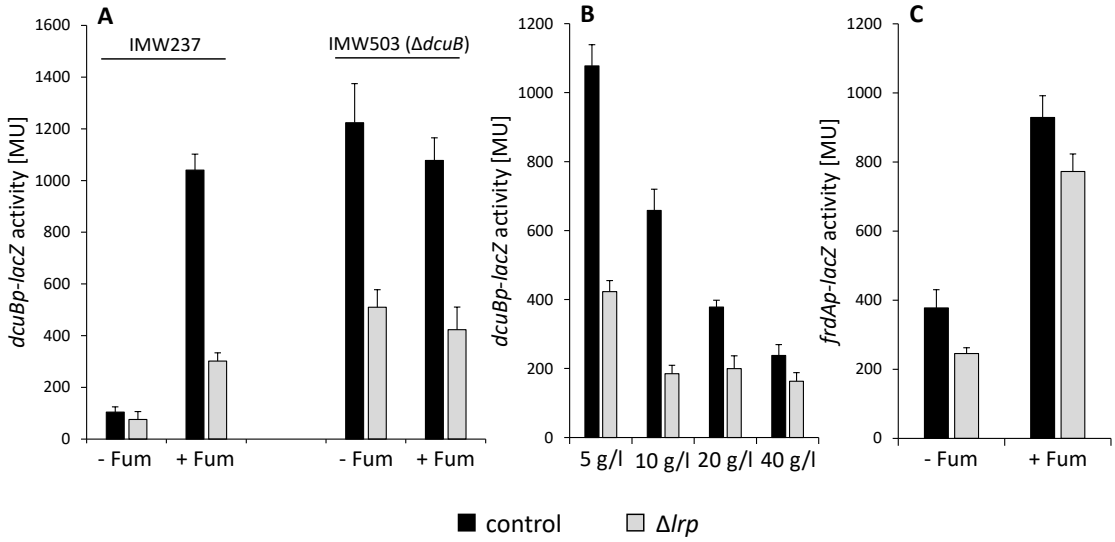

Fig. 32: *dcuBp-lacZ* (A and B) and *frdAp-lacZ* (C) expression of *lrp* mutants in presence LB. Bacteria were grown anaerobically at 37°C in minimal M9 medium and glycerol (50 mM) with fumarate (20 mM). LB was added as an effector (5 g/l), and at increased concentrations (5/10/20/40 g/l). (**A**) Shown are the control activities of IMW237 (*dcuBp-lacZ*) and IMW503 (*dcuBp-lacZ*, Δ*dcuB*) (black bars) and *dcuBp-lacZ* expression in the *lrp* mutant (gray bars). (**B**) Shown are control activities of IMW503 (black bars) and *dcuBp-lacZ* expression in the *lrp* mutant (gray bars). (**C**) Shown are control activities of MC4100λJ100 (*frdAp-lacZ*) (black bars) and activities of *lrp*-deficient IMW682 (*frdAp-lacZ*, Δ*lrp*) (gray bars). The β-galactosidase assay was performed in the stationary growth phase (OD_{578} = 1.5). Activities were quantified in Miller-Units (MU).

In addition, *dcuBp-lacZ* expression was measured in the presence of increased LB concentrations. Bacteria were cultured anaerobically in minimal M9 medium and glycerol with different LB concentrations, which were gradually increased. When LB concentrations beyond 5 g/l were added, a strong repression of *dcuBp-lacZ* expression was observed in IMW503 (Δ*dcuB*) (Fig. 32B). However, in the *lrp*-deficient *dcuBp-lacZ* reporter strain, expression was similar under the elevated LB concentrations, except at 5 g/l LB, where expression was twofold higher. Altogether, *dcuB* shows a clear Lrp-dependent induction by amino acid-containing media, which, however, turns into repression at elevated concentrations. This transition from induction to repression depending on the amino acid concentration is consistent with the character of Lrp (Lin *et al.* 1992; Platko and Calvo 1993; Newman and Lin 1995).

The same type of experiment was performed for *frdA* without using a *dcuB*-deficient reporter gene strain, because the fumarate-dependent induction of *frdAp-lacZ* is significantly lower than in *dcuBp-lacZ* (Zientz *et al.* 1998). Similar to *dcuBp-lacZ*, an Lrp-dependent reduction in *frdAp-lacZ* expression is observed, although noticeably less (Fig. 32C). The reduction in *frdAp-lacZ* expression ranges from a factor of -1.2 to -1.54, which is comparable to data from a global gene expression analysis of a *lrp* mutant (factor -1.63) (Hung *et al.* 2002). Thus, both *dcuB* and *frdA* showed an Lrp-dependent phenotype, indicating activation of *dcuB* and *frdA* transcription in response to the amino acid-rich environment in the animal gut.

3.2.2.2 *dcuC* is not regulated by Lrp

DcuA, DcuB, and DcuC are C_4-dicarboxylate transporters expressed under anaerobiosis. DcuA and DcuB catalyze a C_4-dicarboxylate:succinate antiport during fumarate respiration, with DcuA preferentially transporting L-Asp and DcuB catalyzing the uptake of L-malate or fumarate. DcuC is responsible for succinate efflux during glucose fermentation (Engel *et al.* 1992; Engel *et al.* 1994; Six *et al.* 1994; Zientz *et al.* 1996; Janausch *et al.* 2002; Strecker *et al.* 2018). Therefore, *dcuC* is not subject to catabolite repression by glucose, in contrast to *dcuB* (Zientz *et al.* 1998; Zientz *et al.* 1999). *lrp* was genetically inactivated in the *dcuCp-lacZ* strain. The *dcuC* expression is independent of DcuSR, hence no fumarate was used (Zientz *et al.* 1999). In contrast to *dcuB* and *frdA*, *dcuCp-lacZ* did not show a Lrp-dependent phenotype in expression (Fig. 33). In addition, expression of *dcuCp-lacZ* was largely independent on LB availability. The observation from the global gene expression profile for Lrp that *dcuC* expression is decreased (factor -1.44) in a Lrp-deficient strain could not be confirmed by *dcuCp-lacZ* reporter gene assays (Hung *et al.* 2002).

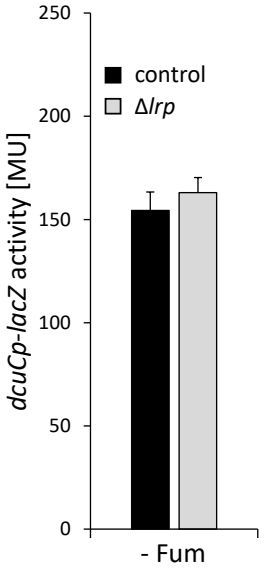

Fig. 33: *dcuCp-lacZ* expression under *lrp*-deficiency in presence LB. Bacteria were cultivated anaerobically at 37°C in M9 medium and glycerol (50 mM) with LB (5 g/l). Shown are control activities (black bars) and *dcuCp-lacZ* expression in the *lrp* mutant (gray bars). The β-galactosidase test was performed in the stationary growth phase (OD_{578} = 1.5). Activities were quantified in Miller-Units (MU).

3.2.3 L-Asp as a nitrogen source for anaerobic growth

E. coli is a facultative anaerobic bacterium that uses fumarate respiration for anaerobic growth (Guest 1979). L-Asp can serve as a substrate for fumarate respiration (Six *et al.* 1994), which requires uptake and conversion to fumarate by DcuA and AspA. DcuA catalyzes an L-Asp:fumarate antiport under aerobiosis, L-Asp is deaminated by AspA to ammonium and fumarate, with fumarate being excreted. This system serves as a nitrogen shuttle to supply nitrogen to the cell without net carbon supply (Strecker *et al.* 2018). It was investigated whether L-Asp can supply *E. coli* with sufficient nitrogen for anaerobic growth, while fumarate respiration is saturated. Bacteria were grown anaerobically in nitrogen-deficient M9 medium and glycerol. Fumarate served as an electron acceptor and either L-Asp or ammonium were supplied as nitrogen sources. The wild type was rendered deficient in either *aspA*, *dcuA* or *dcuB*, and additionally a *dcuAB* double mutant was tested.

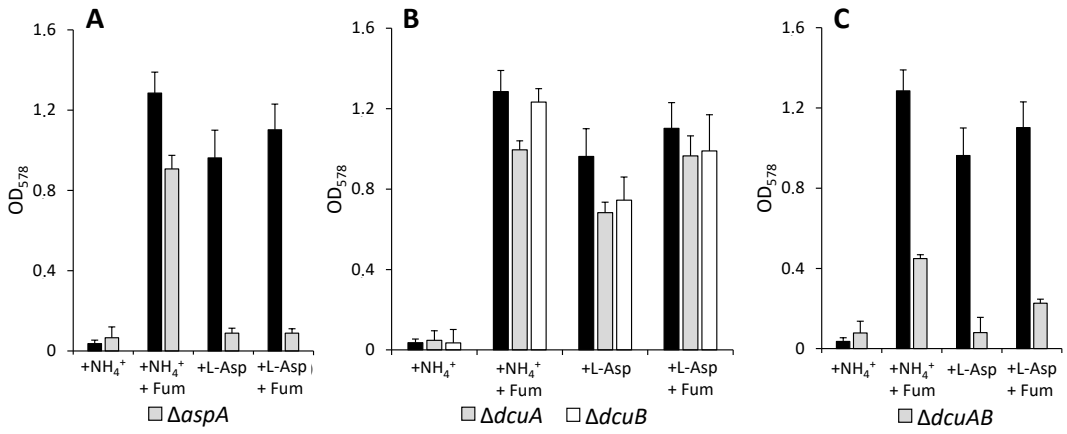

Fig. 34: L-Asp supplied as a nitrogen source in *aspA* and *dcuAB*-deficient strains in anaerobic growth. Bacteria were grown anaerobically in nitrogen-deficient M9 medium and glycerol (50 mM) with either NH_4Cl or L-Asp (each 20 mM) or fumarate (20 mM). *E. coli* wild type (BW25113) is applied as reference for anaerobic growth (black bars). (**A**) JW4099 (Δ*aspA*) (gray bars). (**B**) JW5735 (Δ*dcuA*) (gray bars) and JW4084 (Δ*dcuB*) (white bars). (**C**) JRG2814 (Δ*dcuA* Δ*dcuB*) (gray bars). Bacteria were grown for 24 h, and growth is expressed as optical density at 578 nm (OD_{578}).

In the absence of an electron acceptor, virtually no growth was observed (Fig. 34). Strong growth of the wild type was measured only in the presence of fumarate, with the growth of the *aspA* mutant being slightly reduced (Fig. 34A). When the nitrogen source (ammonium) was replaced by L-Asp, a minor decrease in wild-type growth was observed, while growth of the *aspA* mutant collapsed. The addition of fumarate did not change this observation (Fig. 34A). Overall, L-Asp could serve as a nitrogen source and as an electron acceptor (Fig. 34A). Thus, L-Asp can aerobically and anaerobically saturate the nitrogen consumption of *E. coli*. In addition, AspA is anaerobically required to utilize L-Asp for nitrogen metabolism and fumarate respiration.

DcuA and DcuB share a high sequence similarity and therefore catalyze similar transport reactions (Six *et al.* 1994). Bacteria deficient in either *dcuA* or *dcuB* showed similar growth compared to the wild type, even when L-Asp was used as a nitrogen source instead of ammonium (Fig. 34B). These data suggest that both DcuA and DcuB can compensate for L-Asp uptake when either is deficient, consistent with previous results (Six *et al.* 1994). The *dcuAB* double mutant still showed considerable growth with ammonium and fumarate, suggesting that fumarate uptake may be taken over to some extent by DcuC, as shown previously (Six *et al.* 1994; Zientz *et al.* 1999). However, when ammonium was replaced by L-Asp as a nitrogen source, growth in the *dcuAB* double mutant decreased, whereas slightly higher growth was observed in the presence of fumarate (Fig. 34C). This indicates that DcuC can substitute for fumarate uptake more efficiently than for L-Asp uptake.

Overall, the data showed that L-Asp can also be used anaerobically as a nitrogen source in addition to its role in fumarate respiration. For L-Asp to fulfill this role, one of the two Dcu transporters and the aspartase AspA are required. Both are responsible for the L-Asp uptake and the efficient release of ammonium and fumarate. Interestingly, *aspA* deficiency is more severe than deletion of *dcuA* or *dcuB*, implying that, at least under anaerobic conditions, there is redundancy in the L-Asp uptake, since both Dcu transporters are capable of L-Asp uptake at a rate that stimulates *E. coli* growth. This is not the case under aerobic conditions, where *dcuA*-deficiency is much more severe than *aspA* deletion (Fig. 20C) (Strecker *et al.* 2018). L-Asp is uniquely positioned to saturate both nitrogen metabolism and fumarate respiration in *E. coli*, highlighting the physiological importance of L-Asp as a nitrogen source in the bovine (Bertin *et al.* 2018) and mouse (Fig. 31 and Fig. 34) intestine.

3.3 DcuA-AspA, DcuB-AspA, and AmtB-AspA interaction network

3.3.1 AspA and DcuA copurified in mSPINE

Previous work has shown that DcuA and AspA catalyze a nitrogen shuttle that supplies ammonium to the bacterial cell while excreting fumarate (Strecker *et al.* 2018). This shared function implies a protein-protein interaction between AspA and DcuA for the benefit of this collaborative metabolic pathway. DcuA is a membrane transporter, with both C- and N-termini located in the periplasm (Golby *et al.* 1998a). This eliminates the use of the adenylate cyclase-based BACTH system to study the interaction, since the adenylate cyclase requires cytoplasmic formation. In an alternative approach, DcuA was fused to the bacterial alkaline phosphatase PhoA, which can be used as a tag for immunodetection of membrane proteins

(Bauer *et al.* 2011). PhoA fused to a membrane protein like DcuB, a DcuA paralog, mostly retains its activity (Bauer *et al.* 2011). The DcuA-PhoA fusion allows specific immunodetection with anti-PhoA antisera. In this experiment, Strep-tagged AspA and PhoA-tagged DcuA were simultaneously overexpressed and crosslinked *in vivo* with formaldehyde. *E. coli* strain C43 was cotransformed with plasmids containing AspA-Strep and DcuA-PhoA fusions. Bacteria were grown aerobically in LB medium and expression was induced by the addition of either anhydrotetracycline (AHT) or IPTG. The intact cells were treated with formaldehyde to stimulate protein crosslinking (Sutherland *et al.* 2008). Bacteria were then homogenized and treated with the detergent lauryldimethylamine oxide to solubilize membrane proteins. In extracts from bacteria that produced both, DcuA-PhoA and AspA-Strep comigrated during purification on the Strep-Tactin column. This comigration, or retention of DcuA-PhoA on the column was only observed when the bacteria produced AspA-Strep as well; without AspA-Strep, DcuA-PhoA did not comigrate (Fig. 35). Comigration was observed only when cells were treated with the crosslinking reagent formaldehyde. The data suggested that DcuA-PhoA and AspA-Strep are in close proximity to promote crosslinking, indicating a protein-protein interaction. This interaction would benefit metabolic coupling to promote nitrogen shuttling.

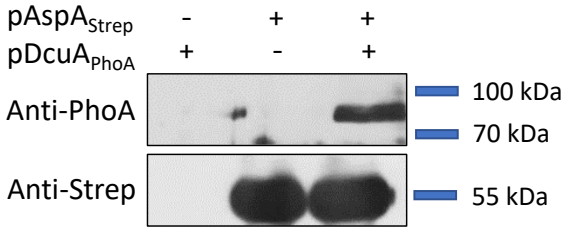

Fig. 35: Copurification to demonstrate the interaction between AspA and DcuA. Constructs were created to produce Strep-tagged AspA (pMW3049) and PhoA-tagged DcuA (pMW577). These plasmids were expressed individually or coexpressed in *E. coli* C43. To crosslink the proteins, bacteria were treated with formaldehyde (0.6% w/v) for 15 min; then bacteria were homogenized and treated with lauryldimethylamine oxide (0.05% v/v). The cell homogenate was applied to a Strep-Tactin column. The D-desthiobiotin (2.5 mM) eluate was subjected to SDS-PAGE and Western blotting. Western blots were probed with antibodies against PhoA (upper panel) and Strep-tag (lower panel). Protein standards are shown on the right-hand side. The calculated molecular masses of AspA-Strep and DcuA-PhoA are 56.0 kDa and 95.2 kDa, respectively.

3.3.2 DcuB-AspA and DcuB-FumB interaction in the BACTH system

The mSPINE experiment indicated protein-protein interaction between DcuA and AspA that would allow efficient nitrogen shuttling (Fig. 35). The *aspA dcuA* and *dcuB fumB* genes are colocalized on the *E. coli* genome and can be cotranscribed (Golby *et al.* 1998b). DcuB anaerobically catalyzes an L-malate:succinate antiport, while L-malate is dehydrated to

fumarate by fumarase B (Six *et al.* 1994; Janausch *et al.* 2002). Similar to DcuA-AspA, an interaction between DcuB and FumB would be beneficial for this metabolic pathway. DcuA and DcuB are paralogous and share a high sequence similarity. Therefore, the adenylate cyclase-based BACTH system was used to investigate whether AspA or FumB show interaction with DcuB. In addition, DcuC was also tested against AspA and FumB to serve as a control, since the sequence similarity between DcuC and DcuAB is much lower (Janausch *et al.* 2002). The N- and C-termini of DcuA, DcuB, and DcuC are located in the periplasm, which theoretically excludes the use of the adenylate cyclase-based BACTH system. To overcome this problem, the T25 fragment of the adenylate cyclase were fused in a cytosolic loop of the Dcu transporters, called a sandwich construct (SWT25) (Bauer 2010; Wörner *et al.* 2016; Strecker 2018). Unfortunately, DcuA was not functional in this construct, but DcuB and DcuC were (Wörner *et al.* 2016; Strecker 2018).

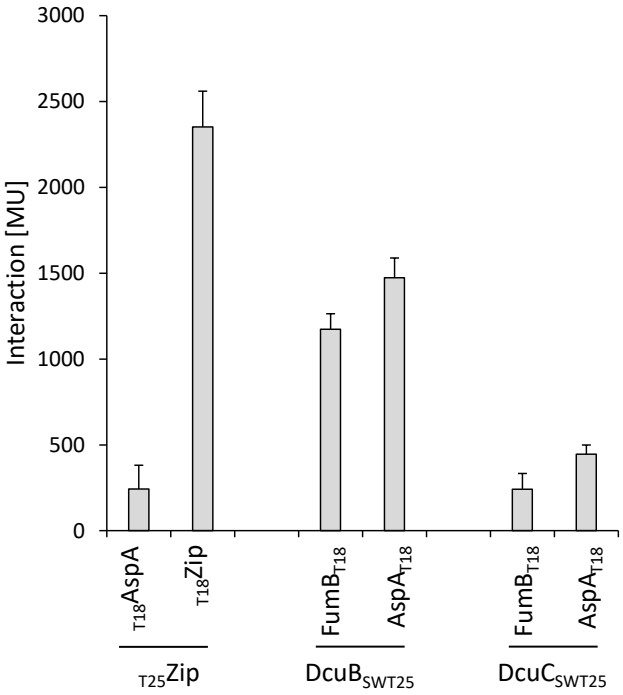

Fig. 36: Interaction between DcuB and DcuC with AspA and FumB in the BACTH system. *E. coli* BTH101 (Δ*cyaA*) was cotransformed pairwise with plasmids encoding T25 sandwich constructs with DcuB and DcuC ($DcuB_{SWT25}$) and fusions of FumB or AspA to T18 ($FumB_{T18}$). The combinations are shown on the x-axis. The leucine zipper pair $_{T18}$Zip and $_{T25}$Zip are applied as a positive control (Karimova *et al.* 1998; Karimova *et al.* 2001), the pair $_{T18}$Zip and $_{T25}$AspA as the negative control for background β-galactosidase activity. The corresponding plasmids are derivatives of pUT18 ($FumB_{T18\ and}$ $AspA_{T18}$) and pKNT25 ($DcuB_{SWT25}$) (Tab. 1). Bacteria were grown anaerobically in LB medium. β-Galactosidase activities were quantified in Miller-Units (MU).

Bacteria producing $DcuB_{SWT25}$ and $FumB_{T18}$ or $AspA_{T18}$ showed high β-galactosidase activity exceeding the negative control of $_{T18}$AspA and $_{T25}$Zip (Fig. 36). This observation was largely independent of the added effectors, L-malate, and L-Asp (data not shown). This

indicates a protein-protein interaction between DcuB-FumB and DcuB-AspA, which is independent of effector molecules. Bacteria producing $DcuC_{SWT25}$ and $FumB_{T18}$ or $AspA_{T18}$ showed a significantly lower β-galactosidase activity than before, which was only slightly higher than background activity in the combination of $DcuC_{SWT25}$ and $AspA_{T18}$ (Fig. 36). Therefore, the data suggested that there is no interaction between DcuC and FumB or AspA. Overall, an interaction between DcuB-FumB and DcuB-AspA was observed. The interaction of AspA with DcuA and DcuB is consistent with their high sequence similarity and the transport of L-Asp by DcuB at rates that support *E. coli* growth (Fig. 34B) (Six *et al.* 1994). Metabolic coupling between a transporter and a cytosolic enzyme would increase the efficiency of the respective pathway. Coupling between DcuA-AspA, DcuB-AspA, and DcuB-FumB would provide the cell with a rapid and efficient metabolic chain to saturate fumarate respiration in anaerobic growth.

3.3.3 AmtB-AspA interaction in the BACTH system

Previous experiments have focused on the deamination reaction of AspA to supply nitrogen to the cell. However, the amination reaction is of equal interest as it incorporates ammonium into fumarate without ATP consumption. The ammonium transporter AmtB is encoded in the *glnK amtB* operon, the expression of which is strongly induced under nitrogen limitation. Under nitrogen excess, GlnK is deuridylylated and blocks ammonium uptake via protein-protein interaction with AmtB (van Heeswijk *et al.* 1996). Normally, nitrogen assimilation is performed via the GS-GOGAT pathway, where ammonium is incorporated into 2-oxoglutarate (2-OG) with consumption of ATP (van Heeswijk *et al.* 2013). In previous work, a metabolic coupling between AmtB and GS has already been postulated with some experimental support (Kleinschmidt and Kleiner 1978; Javelle *et al.* 2005). Metabolic coupling between AmtB and AspA would allow an alternative pathway of nitrogen assimilation that does not consume ATP. AspA and AmtB were tested for interaction in the adenylate cyclase-based BACTH assay. AspA and AmtB were genetically fused to the T25 and T18 domains of *Bordetella pertussis* adenylate cyclase. The BACTH system requires that N- and C-termini are in the cytoplasm to restore adenylate cyclase activity. The N-terminus of AmtB is located in the periplasm, precluding constructs in which T18 and T25 are fused C-terminally to AmtB.

Bacteria producing AspA and AmtB showed high β-galactosidase activity, with two of four combinations exceeding the background activity of the negative control (Fig. 37A). Therefore, the data suggest an interaction between the ammonium transporter AmtB and AspA, which may provide an energy-saving alternative pathway for ammonium assimilation, compared with the GS-GOGAT pathway. AmtB-AspA catalyze ammonium uptake and incorporation producing L-Asp, which is an important precursor for numerous biosynthetic pathways, including UMP and NAD^+ biosynthesis (Fig. 37B) (Jensen *et al.* 2008; Osterman 2009).

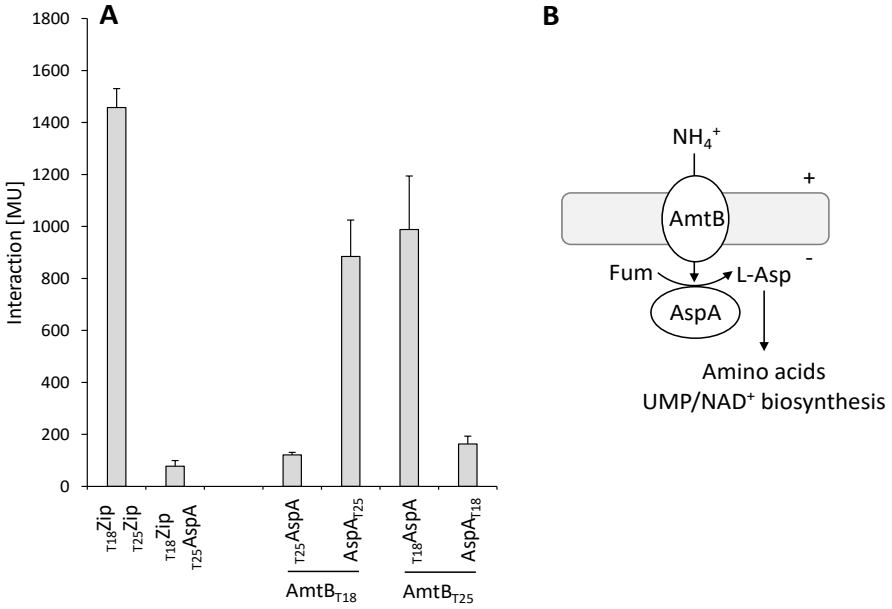

Fig. 37: Interaction of AspA with the ammonia transporter AmtB. (**A**) *E. coli* BTH101 (Δ*cyaA*) was cotransformed pairwise with plasmids encoding fusions of T25 to AspA or AmtB ($_{T25}$AspA) and fusions of T18 to AspA or AmtB ($_{T18}$AspA). The combinations are shown on the x-axis. The leucine zipper pair $_{T18}$Zip and $_{T25}$Zip are applied as a positive control (Karimova *et al*. 1998; Karimova *et al*. 2001), the pair $_{T18}$Zip and $_{T25}$AspA as the negative control for background β-galactosidase activity. The corresponding plasmids are derivatives of pUT18C ($_{T18}$AspA), pUT18 (AspA$_{T18}$ and AmtB$_{T18}$), pKNT25 (AspA$_{T25}$ and AmtB$_{T25}$), and pKT25 ($_{T25}$AspA) (Tab. 1). The strains were grown aerobically in LB medium. β-Galactosidase activities were quantified in Miller-Units (MU). (**B**) Model of the metabolic pathway of AmtB-AspA to supply the cell with L-Asp, an important precursor.

3.4 cAMP-CRP signaling fine-tunes *dctA* and *aspA* expression

The transcriptional regulator CRP regulates the expression of over 100 genes, many of which are involved in the catabolism of secondary substrates other than glucose (Zheng *et al.* 2004; Grainger *et al.* 2005). CRP was the first purified transcriptional regulator and the first protein for which the protein structure was determined (Zubay *et al.* 1970; McKay *et al.* 1982). Following the binding of the allosteric effector cAMP, CRP is able to bind specific DNA sites near the promoter. CRP is a true global transcriptional regulator in *E. coli* and is directly linked to the availability of PTS sugars through its activation via cAMP. In the absence of PTS sugars, cAMP production of the adenylate cyclase CyaA is stimulated and cAMP-CRP induces genes of alternative metabolic pathways to enable the continued growth of *E.* coli (Deutscher *et al.* 2006; Deutscher *et al.* 2014). Previous work has shown that intracellular cAMP levels in *E. coli* fluctuate under different carbon sources (Bennett *et al.* 2009). This allows *E. coli* to continuously fine-tune the expression of cAMP-CRP-dependent genes based on the available carbon source. The role of cAMP-CRP for the transcriptional regulation was studied in more detail for *dctA,* encoding the aerobic C_4-dicarboxylate transporter, and *aspA,* encoding the aspartate ammonia lyase.

3.4.1 *dctAp-lacZ* expression is strongly influenced by carbon sources

DctA is a proton potential stimulated C_4-dicarboxylate transporter, which is responsible for the uptake of fumarate, succinate, L- ,and D-malate, while serving as a coregulator of DcuS (Kay and Kornberg 1969; Kay and Kornberg 1971; Janausch *et al.* 2002; Steinmetz *et al.* 2014). The transcription of *dctA* is controlled by the two-component system DcuS-DcuR. Furthermore, *dctA* is subject to the strong transcriptional control of CRP and ArcBA (Gosset *et al.* 2004; Goh *et al.* 2005). The *dctA* promoter was genetically fused to *lacZ,* encoding the β-galactosidase. The *dctAp-lacZ* expression was examined in the presence of various pentoses, hexoses, disaccharides, sugar alcohols, and C_4-dicarboxylates. The two reporter strains IMW385 (*dctAp-lacZ*) and IMW386 (*dctAp-lacZ, dctA::Spc*^{R}) were used. Similar to the previous experiment, where the Lrp regulation of *dcuBp-lacZ* was elucidated, the *dctA*-deficient reporter strain renders DcuS constitutively active. As a result, DcuSR continuously induces the expression of DcuR target genes, such as *dctA* (Davies *et al.* 1999; Janausch *et al.* 2002; Janausch *et al.* 2004; Kleefeld *et al.* 2009; Steinmetz *et al.* 2014). Bacteria were grown aerobically in LB medium in presence of different carbon sources.

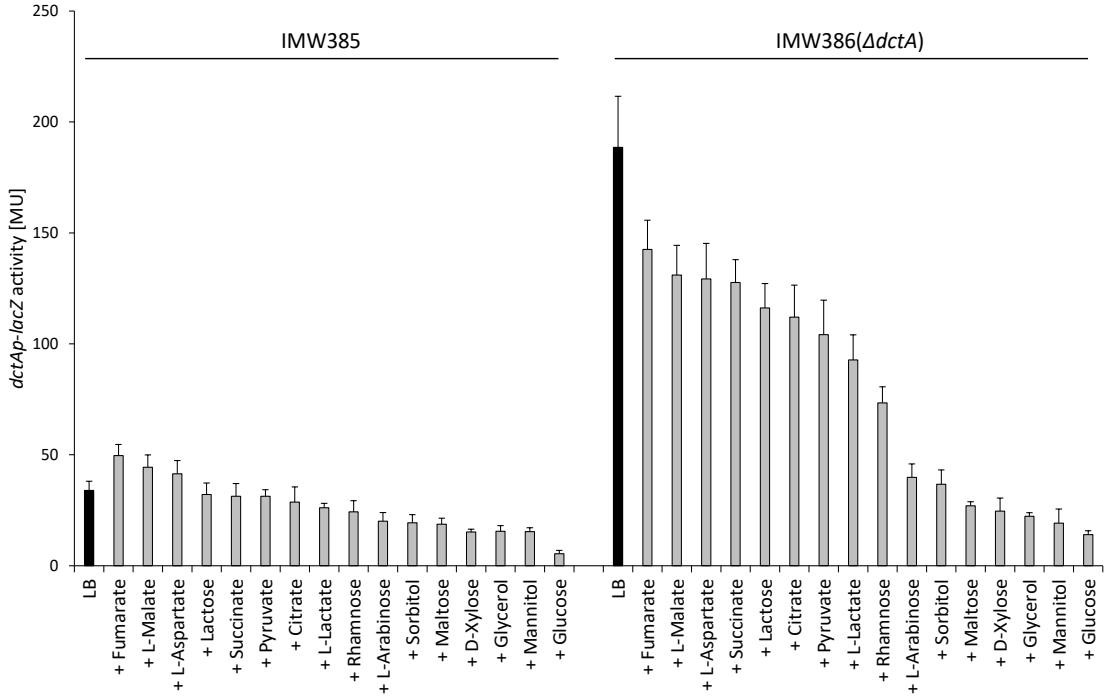

Fig. 38: *dctAp-lacZ* expression in the presence of different carbon sources. Both reporter strains, IMW385 (*dctAp-lacZ*) and IMW386 (*dctAp-lacZ*, Δ*dcuB*), were cultivated aerobically at 37°C in LB medium in presence of different carbon sources (20 mM, gray bars). Control activities in absence of an effector are given (black bars). The β-galactosidase assay was performed in the late exponential growth phase (OD_{578} = 1.5). The β-galactosidase activity is quantified in Miller-Units (MU).

As expected, *dctAp-lacZ* activity is fivefold higher in the *dctA*-deficient reporter strain than in IMW385. In the absence of a coregulator, DcuS cannot be converted to the C_4-dicarboxylate-responsive state, leading to the observation that only IMW385 shows C_4-dicarboxylate-dependent induction of *dctAp-lacZ* (Fig. 38). Starting with lactose, the repression of *dctAp-lacZ* expression in reporter strain IMW385 increased continuously, with glucose showing maximal repression. The *dctAp-lacZ* expression is significantly higher and independent of C_4-dicarboxylate-dependent induction via DcuSR in the reporter strain IMW386 (Δ*dctA*), leading to the interesting observation that even C_4-dicarboxylates repressed *dctAp-lacZ* expression compared to growth in LB (Fig. 38). In general, *dctAp-lacZ* expression is decreased in IMW386 (Δ*dctA*) among all carbon sources tested, suggesting that the C_4-dicarboxylate uptake by DctA is repressed by many substrates in aerobic growth. Notably, the order in which carbon sources repress *dctAp-lacZ* expression in both strains is quite similar.

When the activities of the experiment of Fig. 38 were normalized to the activity in LB and plotted for IMW385 and IMW386 (Δ*dctA*) against each other, it becomes evident that the *dctAp-lacZ* activity in IMW386 (Δ*dctA*) was more repressed under each carbon source than in IMW385 (Fig. 39). Interestingly, among each carbon source tested, a 20-40% stronger repression was observed in IMW386 (Δ*dctA*) than in IMW385. This observation indicates

that cAMP-CRP regulation is superior to DcuR regulation, and even a higher basal activity of *dctAp-lacZ* could not counteract this hierarchy.

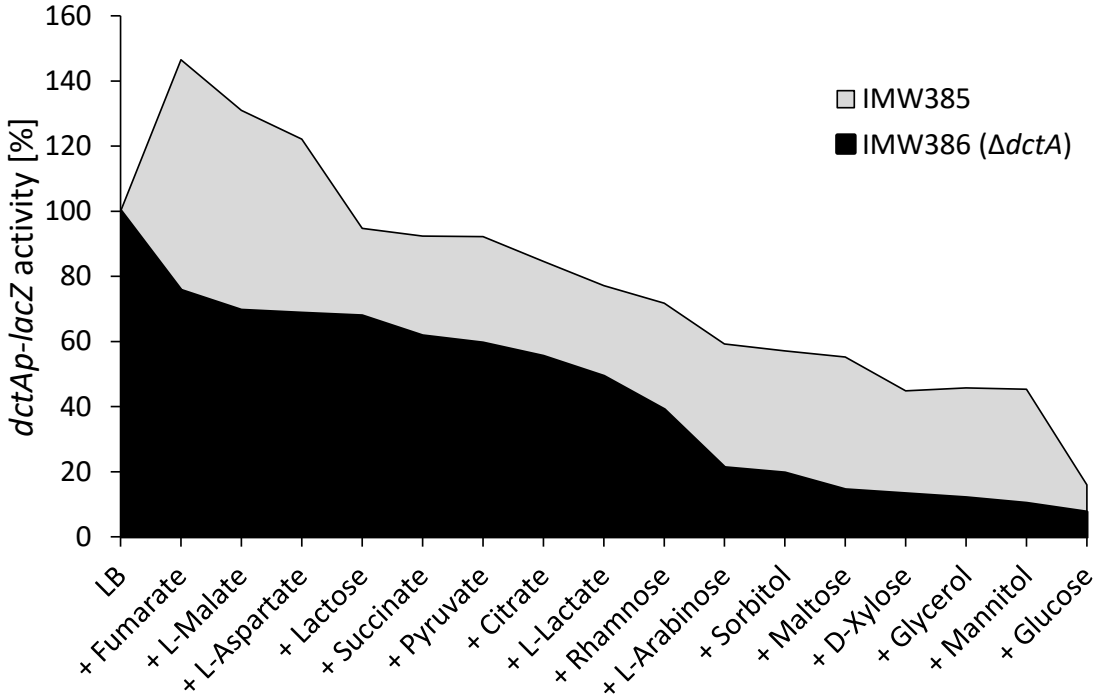

Fig. 39: Repression of *dctAp-lacZ* activity of IMW385 and IMW386 in comparison. The activities of both reporter strains, IMW385 (*dctAp-lacZ*, gray) and IMW386 (*dctAp-lacZ*, Δ*dcuB*, black) were plotted in %. The activities are normalized to the activity of LB medium in absence of an effector (100% activity).

For better understanding, the carbon sources from Fig. 38 are arranged according to their repression of *dctAp-lacZ* in IMW385 and IMW386 (Δ*dctA*) (Fig. 40). The hexoses, glucose, and mannitol that are transported by the phosphotransferase system (PTS sugar) showed the highest repression of *dctAp-lacZ*. Maltose, glycerol, and D-xylose stood out as non-PTS sugars in direct comparison (Fig. 40). The PTS sugar sorbitol showed weaker repression than the pentose L-arabinose. These substrates have in common that they are introduced into the upper glycolytic pathway, in the case of L-arabinose and D-xylose via the pentose phosphate pathway (Mayer and Boos 2005). These substrates are followed by the alpha-keto acid pyruvate and rhamnose, and eventually the C_4 dicarboxylates, the disaccharide lactose, and citrate. The C_4-di-/tricarboxylates and lactose showed the weakest repression of *dctAp-lacZ*. Pyruvate and rhamnose, on the other hand, ranked slightly above them (Fig. 40). In direct comparison, the sugar alcohol glycerol

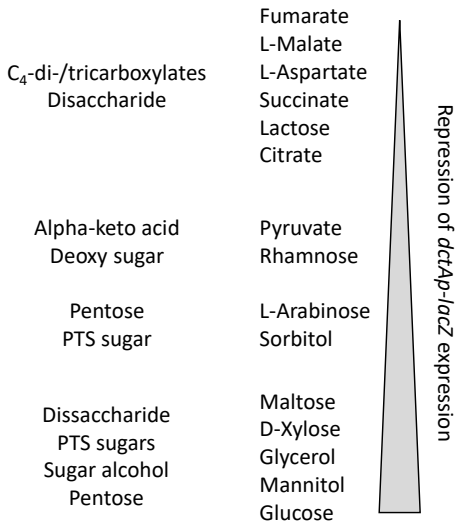

Fig. 40: Classification of carbon sources. All tested carbon sources were sorted according to the repression intensity of *dctAp-lacZ* expression. The substrate class is described on the left side.

and the pentose D-xylose were conspicuous. In general, carbon sources can be divided into upper and lower glycolytic substrates based on repression. Upper glycolytic substrates are introduced before the fructose 1,6-bisphosphate aldolase reaction, catalyzing the reversible aldol cleavage of fructose 1,6-bisphosphate, producing dihydroxyacetone phosphate and D-glyceraldehyde 3-phosphate. Lower glycolytic substrates and the gluconeogenic substrates showed much weaker repression. Gluconeogenic substrates are C_4-di-/tricarboxylates which require gluconeogenesis to serve as a carbon source via the PEP/pyruvate bypass (You *et al.* 2013; Hermsen *et al.* 2015; Surmann *et al.* 2020). Glycerol is a lower glycolytic substrate, whereas the pentose phosphate pathway by which D-xylose is degraded produces both an upper and a lower glycolytic substrate as end products (Mayer and Boos 2005). Interestingly, D-xylose and glycerol cluster among the PTS sugars by repression intensity and both showed excessively strong repression of *dctAp-lacZ* compared to more characteristically similar substrates, for instance, L-arabinose and pyruvate (Fig. 40). To further elucidate D-xylose- and glycerol-mediated repression of *dctAp-lacZ*, both were studied in mutants deficient in transcriptional regulation and degradation of the respective substrate.

3.4.1.1 *dctA* is repressed by glycerol 3-phosphate

Glycerol is a sugar alcohol that is extensively used as a carbon source in minimal M9 medium because of its low cost and low impact on transcriptional regulation (da Silva *et al.* 2009). Glycerol uptake is catalyzed by GlpF and phosphorylation by GlpK, producing glycerol-3-phophate. Glycerol dehydrogenase GlpD oxidizes glycerol 3-phosphate to dihydroxyacetone phosphate and shuttles electrons via cofactor FAD to reduce ubiquinone (Schryvers *et al.* 1978; Yeh *et al.* 2008). Dihydroxyacetone phosphate is then further metabolized in the lower glycolytic part of glycolysis. Most likely, an intermediate of the glycerol metabolism is responsible for *dctAp-lacZ* repression. Thus, the metabolic genes of glycerol catabolism, namely the glycerol kinase *glpK*, glycerol 3-phosphate dehydrogenase *glpD*, and the transcriptional regulator *glpR* were genetically inactivated in both *dctAp-lacZ* reporter strains. Bacteria were cultivated aerobically in LB medium with glycerol added as an effector.

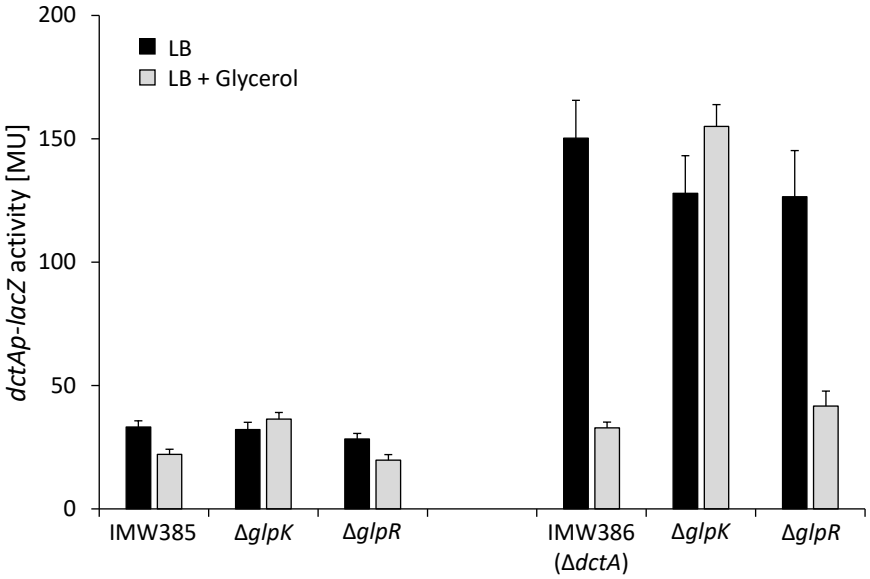

Fig. 41: *dctAp-lacZ* expression of *glpK* and *glpR* deficient mutants. Bacteria containing the *dctAp-lacZ* fusion (IMW385 and IMW386 (Δ*dctA*)) and mutants were cultivated aerobically at 37°C in LB medium (black bars) and in presence of glycerol (20 mM, gray bars) to the late exponential growth phase (OD_{578} = 1.5). The β-galactosidase activity is quantified in Miller-Units (MU).

The *glpD* mutants could not be cultured under the growth conditions used (data not shown). It is possible that intracellular accumulation of the intermediate glycerol 3-phosphate is toxic to *E. coli*. The *dctAp-lacZ* expression decreased 1.5-fold and 4.5-fold in the presence of glycerol in IMW385 and IMW386 (Δ*dctA*), respectively. The *glpR* mutants showed a similar phenotype as the parent strains IMW385 and IMW386 (Δ*dctA*). This phenotype is absent when *glpK* is genetically inactivated. The glycerol-dependent repression of *dctAp-lacZ* is largely resolved in the *glpK* mutants (Fig. 41). The data suggested that glycerol-dependent repression of *dctAp-lacZ* is not mediated by the transcriptional regulator GlpR but is caused by glycerol 3-phosphate. This type of glycerol 3-phosphate-dependent repression has already been observed for the transcriptional regulator of the maltose operon *malT* (Eppler *et al.* 2002).

3.4.1.2 *dctA* is possibly regulated by the transcriptional regulator XylR

D-Xylose is an aldopentose and the main component of hemicellulose, xylan. It is found in the cell wall of plants and grasses (Mellerowicz and Gorshkova 2012). D-Xylose enters the cell either through proton motive force or a high-affinity, ATP-driven transport system. The isomerase XylA converts D-xylose to D-xylulose and subsequently the xylulokinase XylB phosphorylates it to D-xylulose 5-phosphate, an intermediate of the pentose phosphate pathway (Mayer and Boos 2005). The pentose phosphate pathway is one of the three main pathways of central metabolism and provides *E. coli* with various precursors for vitamins

and amino acids (Sprenger 1995; Mayer and Boos 2005). This pathway produces fructose 6-phosphate and D-glyceraldehyde 3-phosphate as end products, which are fed into the upper and lower part of glycolysis. Analogous to the experiments on glycerol-dependent repression of *dctAp-lacZ*, the xylulokinase *xylB* and the transcriptional regulator *xylR* were genetically inactivated in both reporter strains. Bacteria containing the *dctAp-lacZ* fusion were grown aerobically in LB medium with D-xylose added as an effector.

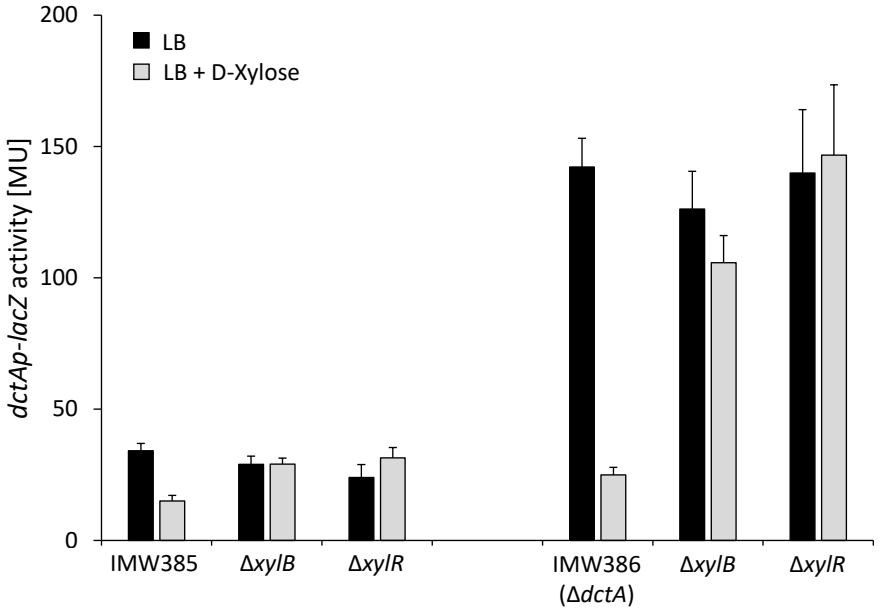

Fig. 42: *dctAp-lacZ* expression of *xylB* or *xylR* deficient mutants. Bacteria containing the *dctAp-lacZ* fusion (IMW385 and IMW386 (Δ*dctA*)) and mutants were cultivated aerobically at 37°C in LB medium (black bars) and in presence of D-xylose (20 mM, gray bars) to the late exponential growth phase (OD_{578} = 1.5). The β-galactosidase activity is quantified in Miller-Units (MU).

D-Xylose-dependent repression is observed in IMW385 but is lost in the Δ*xylB* and Δ*xylR* mutants. This observation is confirmed by IMW386 (Δ*dctA*), where *dctAp-lacZ* expression is reduced 5.7-fold in the presence of D-xylose, however genetic inactivation of *xylB* and *xylR* alleviates D-xylose-dependent repression (Fig. 42). In both cases, glycerol and D-xylose repression of *dctAp-lacZ* is lost in the respective kinase mutant (Fig. 41 and Fig. 42). In addition, *xylR* inactivation also mitigates the D-xylose repression of *dctAp-lacZ*. Based on the present observations, the transcriptional regulator XylR, bound to D-xylose, negatively regulates *dctA*. Equivalently, the product of XylB, xylose 5-phosphate, or a subsequent intermediate showed repression of *dctAp-lacZ*. These data suggest that both XylR and xylose 5-phosphate repress *dctA*, unlike glycerol, where glycerol 3-phosphate was identified as the substrate responsible for repression (Fig. 41). XylR is a transcriptional regulator that induces genes involved in the degradation of D-xylose, such as the *xylAB* operon (Song and Park 1997). XylR-dependent repression was also observed for the *rbs* operon, while the *xylAB* operon is the target of AraC regulation, the transcriptional regulator

of the L-arabinose catabolism (Desai and Rao 2010).The *rbs* operon codes for genes that are important for the degradation of D-ribose (Kang *et al.* 1998). D-Xylose repression of *dctAp-lacZ* could not be characterized in more detail. Nevertheless, these data further elucidated the relationship between pentoses and C_4-dicarboxylate metabolism, especially since pentoses are carbon sources and fumarate respiration is essential under physiological conditions in the animal gut (Jones *et al.* 2007; Fabich *et al.* 2008; Jones *et al.* 2011). This indicates that the aerobic C_4-dicarboxylate transporter DctA is of minor significance even in the presence of oxygen in the animal gut (Levitt 1970; He *et al.* 1999).

3.4.2 *aspAp-lacZ* expression is susceptible to different sugars

The aspartate ammonia-lyase AspA is a cytosolic enzyme which catalyzes the reversible deamination of L-Asp, forming fumarate and ammonium. The expression of *aspA* is positively regulated by cAMP-CRP and FNR, and repressed by NarL (Spiro and Guest 1991; Golby *et al.* 1998b; Goh *et al.* 2005). NarL is the response regulator of the NarX-NarL two-component system, which senses nitrate (Egan and Stewart 1990). *aspA* and *dcuA* are colocalized, and cotranscripts are possible but not common (Golby *et al.* 1998b). Recent data suggested a positive regulation by the DcuS-DcuR two-component system (Surmann *et al.* 2020). The promoter of *aspAp* was fused to *lacZ* coding for the β-galactosidase. The expression of *aspAp-lacZ* was examined in minimal M9 medium and glycerol in presence of different carbon sources.

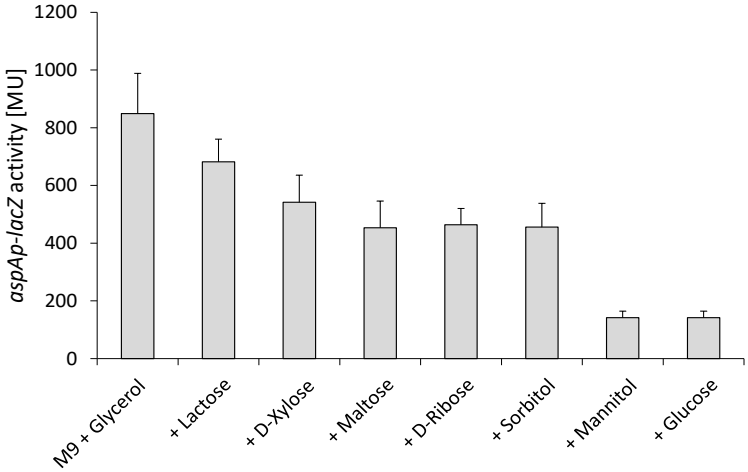

Fig. 43: *aspAp-lacZ* expression in presence of different carbon sources. Bacteria containing the *aspAp-lacZ* fusion (IMW642) were cultivated aerobically at 37°C in M9 medium and glycerol (50 mM) with different effectors (20 mM) to the exponential growth phase (OD_{578} = 0.5). The β-galactosidase activity was quantified in Miller-Units (MU).

A similar pattern as for *dctAp-lacZ* (Fig. 38) is observed for *aspAp-lacZ* expression (Fig. 43). A clear distinction between PTS (mannitol and glucose) and non-PTS sugars (lactose, D-xylose, and D-ribose) is evident (Fig. 43). Notably, glycerol and D-xylose showed much weaker repression than for *dctAp-lacZ* (Fig. 38). Expression analysis of *aspAp-lacZ* and *dctAp-lacZ* shows a hierarchical gene regulation based on the available carbon source, which is regulated by cAMP-CRP. The *aspA* and *dctA* expression is reliant on cAMP-CRP activation. To investigate the extent to which the expression of *dctA* and *aspA* is dependent on cAMP-CRP, the reporter strains were rendered deficient in cAMP-CRP signaling.

3.4.3 *aspA* and *dctA* expression is dependent on cAMP-CRP activation

cAMP-CRP is essential for the activation of genes involved in catabolism of substrates other than glucose (Kolb *et al.* 1993; Deutscher *et al.* 2006; Fic *et al.* 2009). Both PTS and non-PTS sugars affect the phosphorylation status of $EIIA^{Glc}$ and thus cAMP production via the adenylate cyclase CyaA (Hogema *et al.* 1998). Consistent with this, cAMP levels were shown to fluctuate in the presence of PTS sugars as well as non-PTS sugars (Bennett *et al.* 2009). These properties give cAMP-CRP the ability to continuously fine-tune regulation of genes involved in alternative metabolic pathways in response to available carbon sources. The reliance of *aspAp-lacZ* and *dctAp-lacZ* expression on cAMP-CRP activation was investigated. In IMW385 (*dctAp-lacZ*), IMW386 (*dctAp-lacZ*, Δ*dctA*), and IMW642 (*aspAp-lacZ*), either the gene encoding CRP or the adenylate cyclase CyaA was genetically inactivated. cAMP-CRP activation is impaired in both mutants. As a comparison, expression of the parent strain was tested in the presence of glucose.

The presence of glucose or interference of the cAMP-CRP signaling pathway led to a drastic reduction in reporter gene activity (Fig. 44). *aspAp-lacZ* expression decreased 6.5- and 8.3-fold, while *dctAp-lacZ* declined 6.3- and 6.2-fold in presence of glucose and in the *crp* or *cyaA* mutant, respectively (Fig. 44A and B). Under *dctA*-deficiency, *dctAp-lacZ* activity decreased 13.4-fold in presence of glucose and 13.8-fold in the *cyaA* mutant (Fig. 44C). The *dctAp-lacZ* expression is increased 5.56-fold in the *dctA*-deficient strain, this value is halved to 2.6-fold in the presence of glucose (Fig. 44B and C). The expectation was to observe a comparable ratio of *dctAp-lacZ* expression with and without glucose in both reporter strains.

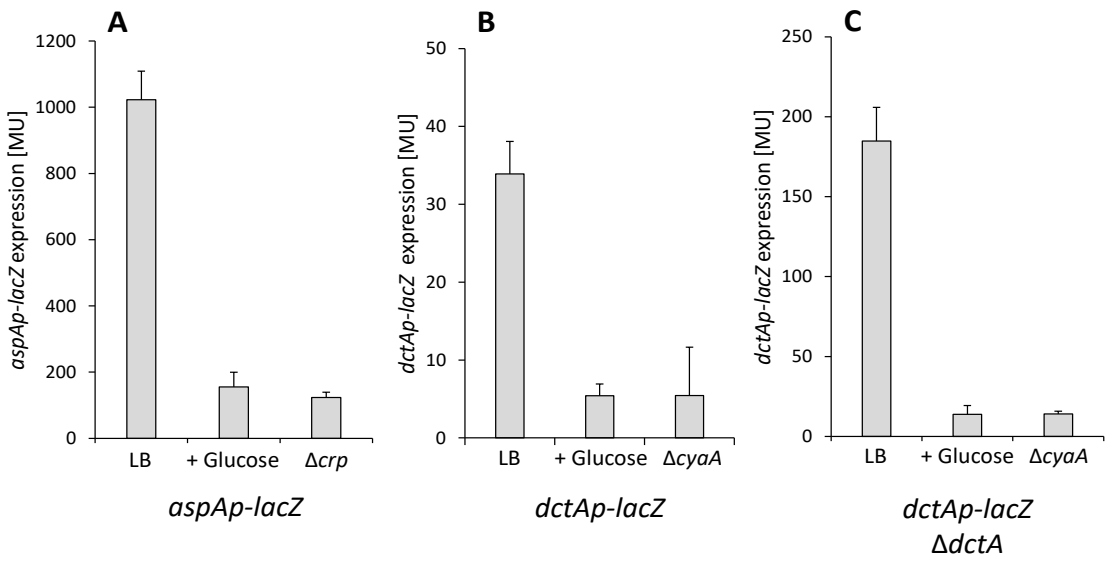

Fig. 44: Dependence of *aspAp-lacZ* and *dctAp-lacZ* expression on cAMP-CRP activation. Bacteria were cultivated aerobically at 37°C in LB medium and glucose (20 mM) to the late exponential growth phase (OD_{578} = 1.2). β-Galactosidase activity was quantified in Miller-Units (MU). (**A**) IMW642 (*aspAp-lacZ*) and IMW690 (IMW642, Δ*crp*); (**B**) IMW385 (*dctAp-lacZ*) and IMW669 (IMW385, Δ*cyaA*); (**C**) IMW386 (*dctAp-lacZ*, Δ*dctA*) and IMW665 (IMW386, Δ*cyaA*).

However, significantly stronger repression by interference of cAMP-CRP activation is observed in the strain with the higher basal activity, IMW386 (Δ*dctA*). This indicates that C_4-dicarboxylate-dependent induction by DcuS-DcuR is inferior to cAMP-CRP activation. Overall, transcription of *dctA* and *aspA* is highly dependent on cAMP-CRP, suggesting that the variability in expression is due to fine-tuning of the cAMP-CRP signal transduction pathway in response to carbon source availability. When cAMP-CRP complexes are not present in sufficient amounts, *dctA* and *aspA* are transcribed very poorly. Both *dctA* and *aspA* showed similar expression in presence of glucose and cAMP-CRP-deficiency, indicating similar CRP-binding sites in the promoter region.

3.4.4 Distribution matrix of the conservations of CRP-binding sites

The expression of *aspA* and *dctA* are affected by numerous carbon sources. The level of repression correlates roughly with the energy density of the carbon source (Fig. 38 and Fig. 43). When a carbon source is fed into the upper part of glycolysis, a stronger repression of reporter gene activity was observed than when a carbon source is fed into the lower part of glycolysis (Fig. 40). This gradual transcriptional regulation in response to different carbon sources is mainly regulated by the cAMP-CRP pathway (Fig. 44). Both the promoter region of *aspAp* and *dctAp* contain only one CRP-binding site (Golby *et al.* 1998b; Davies *et al.* 1999). The CRP-binding sites of *aspAp* and *dctAp* were aligned against the CRP consensus sequence (Fig. 45B) (Ebright *et al.* 1989). The CRP-binding site of *aspAp* and *dctAp* showed

a conservation of 68% and 59%, respectively (Fig. 45B). In order to contextualize both values, all known CRP-binding sites from *E. coli* were aligned against the CRP consensus sequence in a multiple sequence alignment (MSA) (Fig. 45A).

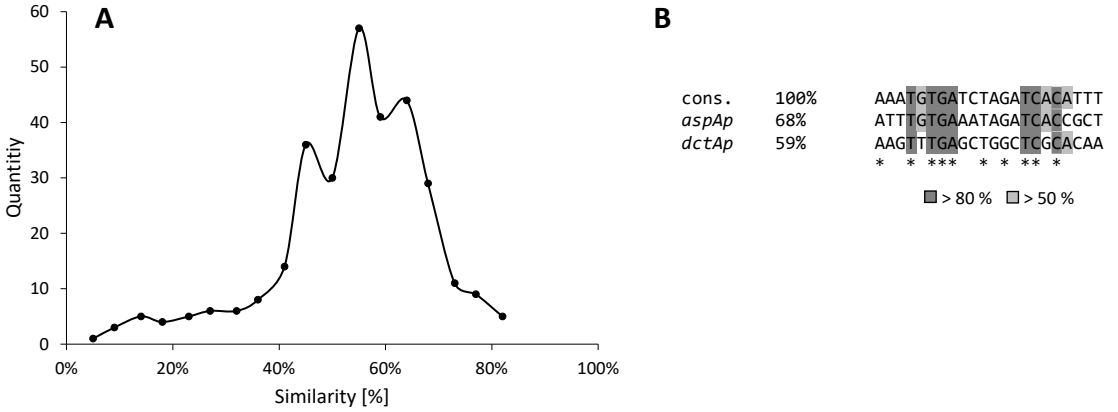

Fig. 45: Conservation distribution of CRP-binding sites in *E. coli* (A) and alignment of *dctAp* and *aspAp* CRP-binding sites against the consensus (B). (**A**) 312 CRP-binding sites from RegulonDB were acquired and aligned using Unipro UGENE (Okonechnikov *et al.* 2012; Gama-Castro *et al.* 2016). The degree of conservation was plotted against the number of times occurred. (**B**) A section of the multiple sequence alignment showing the CRP-binding sites of *aspAp*, *dctAp* and the consensus (Ebright *et al.* 1989).

A total of 312 CRP-binding sites from *E. coli* were obtained via RegulonDB and used for the MSA, whereby duplicates and shortened binding sites were removed from the data set (Gama-Castro *et al.* 2016). The similarity of all CRP-binding sites to the CRP consensus sequence was calculated. The conservation values were visualized via a distribution matrix (Fig. 45A). The distribution of the conservation values of the CRP-binding sites resembles a Gaussian curve. Surprisingly, both CRP-binding sites of *aspAp* and *dctAp* are located either near or at the peak. This observation is not surprising, as expression analysis showed that both *dctA* and *aspA* are similarly dependent on cAMP-CRP activation. Overall, the conservation of the CRP-binding sites and dependence on transcriptional activation by cAMP-CRP were similar (Fig. 44 & Fig. 45B), however, conservation of the CRP-binding site is only one factor; another key factor is the position on the promoter region (Fic *et al.* 2009).

3.4.5 Classification of *aspAp* and *dctAp* CRP-binding sites

The transcriptional regulator CRP binds to a 22-bp symmetrical site and, similar to the integration host factor IHF, induces a DNA bend upon binding (Ebright *et al.* 1989; Parkinson *et al.* 1996). The association constant for CRP without cAMP is approx. 100 µM (Giraud-Panis *et al.* 1992). When cAMP binds to CRP, the association constant for DNA of the cAMP-CRP complex increases drastically between 100 nM to 100 pM, depending on the specific DNA sequence (Harman 2001; Fic *et al.* 2009). cAMP-CRP signaling is one of the

regulatory pillars of carbon catabolite repression (CCR) (Müller-Hill and Oehler 1996; Deutscher *et al.* 2006; Narang and Pilyugin 2007), enabling *E. coli* to gradually utilize carbon sources and thus grow diauxically (Kolb *et al.* 1993; Busby and Ebright 1999). The expression of *dctA* and *aspA* showed a high susceptibility to different carbon sources (Fig. 38 and Fig. 43). Both are reliant on cAMP-CRP activation, hence low levels of expression were observed in mutants lacking cAMP-CRP signaling (Fig. 44).

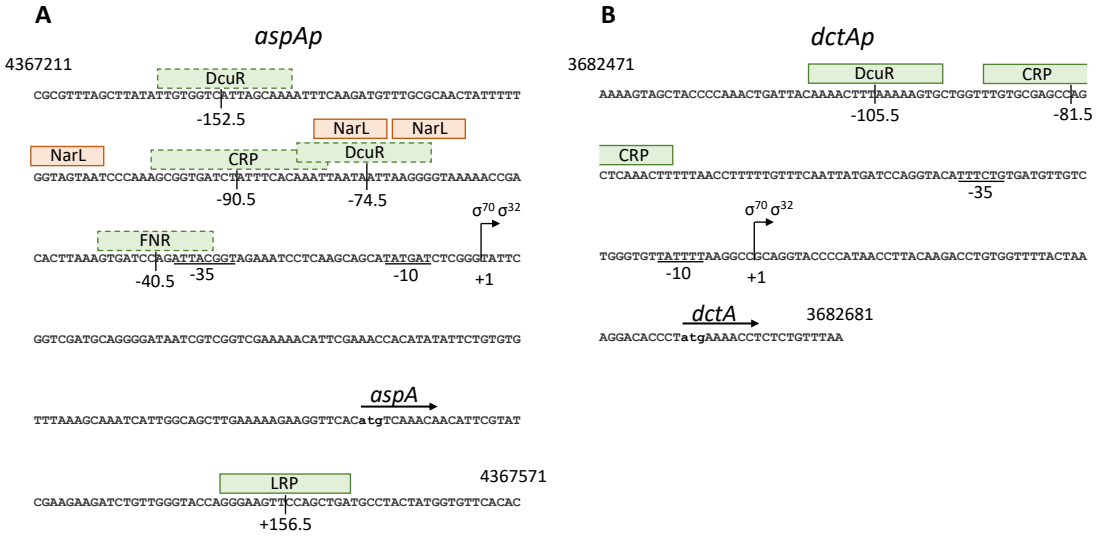

Fig. 46: Schematic model of the *aspAp* (A) and *dctAp* (B) promoter regions. The positions of transcription start, and binding sites of transcriptional regulators are indicated in reference to the +1 transcription start. Binding sites are based on sequence deduction (dashed lines) and experimental data (continuous lines). The region of the *E. coli* genome is noted in the top left and bottom right corner. Coordinates are from EcoCyc and previous data (Golby *et al.* 1998b; Davies *et al.* 1999; Keseler *et al.* 2017).

There are two classes of CRP-dependent promoters: Class I promoters require only CRP activation and have a single binding site in the promoter region, located upstream to which the RNA polymerase (RNAP) binds. Class II promoters differ in this respect, the CRP-binding site is the same as the RNAP site, generally the -35 promoter sequence (Busby and Ebright 1999; Tebbutt *et al.* 2002; Fic *et al.* 2009). Based on the location, *dctAp* as well as *aspAp* can be characterized as class I CRP-dependent promoters. The CRP-binding sites are located upstream of the RNAP-binding site and centered near position -90.5 and -81.5, respectively (Fig. 46A and B). The expression data showed that DcuR regulation of *dctA* is hierarchically inferior to cAMP-CRP activation (Fig. 44B and C). DcuR-binding site is upstream of CRP, indicating that the cAMP-CRP induced DNA bend is essential for positive DcuR regulation. This is consistent with reporter gene analysis, which showed a drastic reduction in IMW386 (Δ*dctA*, Δ*cyaA*) *dctAp-lacZ* activity, despite DcuS being constitutively active (Fig. 44C). Comparing the binding sequences of *aspAp* and *dctAp* with the consensus sequence of CRP, no clear assignment of symmetry is possible. Most likely, DNA bending

may be asymmetric, similar to the *gal* promoter. Expression analysis of *aspAp*, especially *dctAp*, showed fine regulation by cAMP-CRP in response to availability of carbon sources. The CRP-binding sites are positionally and sequentially very similar, which was also confirmed in part by the similar experimental results.

3.4.6 DctA-EIIA^{Glc} interaction in BACTH system

Transcription of the C_4-dicarboxylate transporter *dctA* is dependent on activation by cAMP-CRP (Fig. 44B and C) (Davies *et al.* 1999). Nevertheless, analysis of the cellular concentrations of DctA and DcuS revealed that DctA is always present in several hundred copies per cell to convert DcuS to the C_4-dicarboxylate-responsive state (Wörner *et al.* 2017). This may allow C_4-dicarboxylate uptake by DctA in aerobic growth. The possibility of interaction between DctA and EIIA^{Glc} was investigated using the adenylate cyclase-based BACTH system. Both proteins were genetically fused to the T25 and T18 domains of *Bordetella pertussis* adenylate cyclase. Bacteria producing the pairs DctA and EIIA^{Glc} were tested in all combinations of fusions. Several combinations showed high β-galactosidase activity in excess of the negative control, suggesting an interaction (Fig. 47).

DcuA catalyzes an L-Asp:fumarate antiport in which AspA deaminates L-Asp to produce ammonium and fumarate, with fumarate being excreted (Strecker *et al.* 2018). C_4-dicarboxylates are energetically poor carbon sources in aerobic growth because they are fed relatively late into the central metabolic pathway. In addition, C_4-dicarboxylates are gluconeogenic substrates, since growth on these substrates is not possible without gluconeogenesis via PEP/pyruvate bypass (Miranda *et al.* 2004; Surmann *et al.* 2020). Based on current understanding, DcuA would excrete C_4-dicarboxylates, predominantly fumarate, and DctA would reuptake these C_4-dicarboxylates (Unden *et al.* 2016; Strecker *et al.* 2018). This situation would be suboptimal and unnecessary in aerobic growth, especially in the presence of carbon sources, which are fed in the upper and lower part of the glycolysis. It is known that EIIA^{Glc}, from the phosphoenolpyruvate:glucose phosphotransferase system, post-translationally inhibits transporters of secondary metabolism such as the lactose permease LacY via protein-protein interaction (Osumi and Saier 1982; Nelson *et al.* 1983; Deutscher *et al.* 2006). Noteworthy, post-translational inhibition of DctA by EIIA^{Glc} would not be a classical inducer exclusion since C_4-dicarboxylates are sensed periplasmically via the two-component

system DcuS-DcuR. Normally, $EIIA^{Glc}$ inhibits the uptake of substrates that bind cytoplasmically to specific transcriptional regulators, inducing genes of alternative metabolic pathways (Deutscher *et al.* 2006).

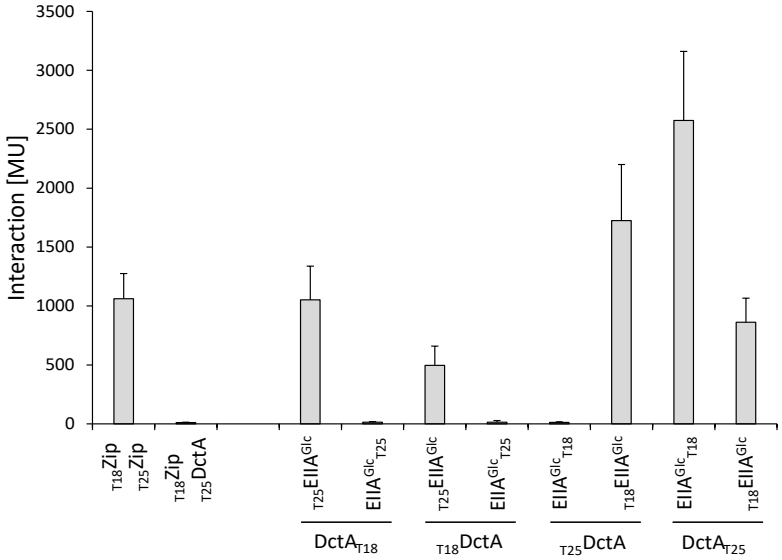

Fig. 47: DctA-$EIIA^{Glc}$ interaction *in vivo* using the BACTH system. *E. coli* BTH101 (Δ*cyaA*) was cotransformed pairwise with plasmids encoding fusions of T25 to DctA or $EIIA^{Glc}$ ($_{T25}$DctA) and fusions of T18 to DctA or $EIIA^{Glc}$ ($_{T18}$DctA). The combinations are shown on the x-axis. The leucine zipper pair $_{T18}$Zip and $_{T25}$Zip are applied as a positive control (Karimova *et al*. 1998; Karimova *et al*. 2001), the pair $_{T18}$Zip and $_{T25}$DctA as the negative control for background β-galactosidase activity. The corresponding plasmids are derivatives of pUT18C ($_{T18}$DctA), pUT18 ($DctA_{T18}$), pKT25 ($_{T25}$DctA), and pKNT25 ($DctA_{T25}$) (Tab. 1). The strains were grown aerobically in LB medium at 30°C to the exponential growth phase (OD_{578} = 0.5). The β-galactosidase activities were quantified in Miller-Units (MU).

3.5 The DctA and DcuS interaction model

The DcuS-DcuR two-component system in *E. coli* is membrane integral and represents an extracytoplasmic sensing histidine kinase (Mascher *et al.* 2006). DcuSR periplasmically senses C_4-dicarboxylates (fumarate, succinate, L-malate, and L-Asp) and induces genes involved in C_4-dicarboxylate metabolism. DcuS-DcuR and CitA-CitB belong to the CitA family of sensor kinases, whereby the two-component system CitA-CitB is specialized for the detection of citrate (Yamamoto *et al.* 2009). Contrary to DcuSR, CitAB does not require a coregulator for its functionality (Scheu *et al.* 2012). DctA or DcuB are required to convert DcuS to a responsive state by protein-protein interaction, in which DcuS is able to sense the presence of C_4-dicarboxylates. The binding of C_4-dicarboxylates to the periplasmic sensor domain results in autophosphorylation of the kinase domain, followed by the transfer of the phosphoryl group to the response regulator DcuR. In the absence of a coregulator, DcuS is constitutively active and does not require further C_4-dicarboxylate binding for activation.

The interaction between DcuS and its coregulators DctA or DcuB is essential for functionality (Davies *et al.* 1999; Janausch *et al.* 2002; Kleefeld *et al.* 2009; Witan *et al.* 2012a; Scheu *et al.* 2014; Wörner *et al.* 2016). The periplasmic sensory part and the cytoplasmic part are connected by a continuous α-helical structure, consisting of multiple domains, which are essential for signal transfer across the membrane (Stopp *et al.* 2021). The signal input site consists of a periplasmic PAS domain (PASp) anchored to the membrane by transmembrane helices 1 and 2 (TM1, TM2), while the signal output site comprises the kinase domain. The input and output sites are connected by a long α-helical structure consisting of TM2, the linker region (LR), and the N-terminal α-helix of the cytosolic PAS domain (PASc) (Stopp *et al.* 2021).

The bioinformatic approach had two objectives: First, to model a full-length structure of DcuS and second, to study the interaction between DcuS and DctA on a sequence basis. The objective was to define relevant residues for the DcuS-DctA interaction by multiple sequence alignments (MSA). Previous work suggested that domains involved in the DcuS-DctA interaction are presumably the DcuS LR and DctA helix 8b (H8b) (Witan *et al.* 2012a; Witan *et al.* 2012b; Gröpper 2013; Stopp 2021; Stopp *et al.* 2021).

3.5.1 Structural modeling of DcuS

The sensor histidine kinase DcuS is a multidomain protein of 543 amino acids and ranges across the peri- and cytoplasm. DcuS consists of a periplasmic sensory Per-ARNT-Sim (PASp) domain that is anchored to the membrane by transmembrane helices TM1 and TM2, a linker region (LR), a cytoplasmatic PAS domain, and the C-terminal histidine kinase A (HisKA)-ATPase domain (Pappalardo *et al.* 2003; Kneuper *et al.* 2005; Cheung and Hendrickson 2008; Sevvana *et al.* 2008; Scheu *et al.* 2010a). DcuS is found as dimeric or tetrameric, independent of the presence of an effector (Scheu *et al.* 2010b). Modeling of the DcuS structure is challenging, as few structural data are available from similar sensor histidine kinases, which also complicates biochemical studies. To simplify the modeling of DcuS, the protein was subdivided into several domains. The annotation of the individual domains was taken from the UniProt database and recent data (Stopp *et al.* 2021). DcuS was subdivided into the following domains: N-terminal coil, TM1, PASp, TM2, LR, PASc, and kinase (Fig. 48). Different methods were used to build a structural model of each section. For the periplasmic sensing domain PASp, the cytoplasmic signal transduction domain PASc, and

histidine kinase, either structural data or data from similar structurally resolved proteins were available (Sevvana *et al.* 2008; Podgornaia *et al.* 2013; Salvi *et al.* 2017).

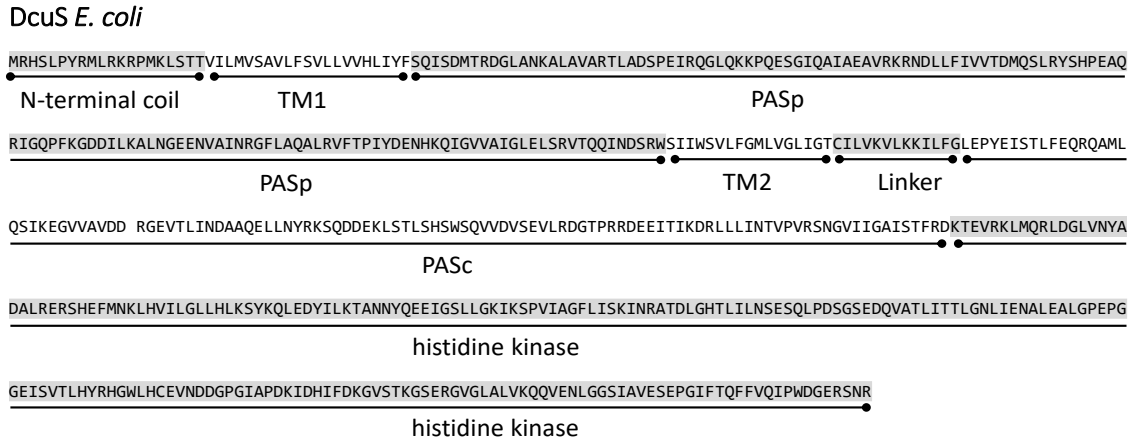

Fig. 48: DcuS sequence with annotated domains. The DcuS sequence (UniProt ID: P0AEC8) is annotated with the section used in modeling based on UniProt topology and structural data (Stopp *et al.* 2021).

The N-terminal coil was modeled *ab initio* using I-TASSER (Yang and Zhang 2015). The structural models of PASp and PASc were modeled as a homology models of CitA PASp of *Klebsiella pneumoniae* (PDB ID: 2V9A) (Sevvana *et al.* 2008) and CitA PASc of *Geobacillus thermodenitrificans* (PDB ID: 5FQ1) (Salvi *et al.* 2017) using Swiss-Model (Bordoli *et al.* 2009). TM1, TM2, and the LR were modeled manually in UCSF Chimera (Pettersen *et al.* 2004). The kinase domain was modeled by I-TASSER, using the structurally similar kinase domain HK853 of *Thermotoga maritima* (Podgornaia *et al.* 2013; Yang and Zhang 2015). The individual structural models were loaded collectively into the molecular modeling program UCSF Chimera and assembled manually (Pettersen *et al.* 2004). Structural data were available for PASp, PASc, and the kinase domain that allowed modeling of the dimeric structures (Sevvana *et al.* 2008; Podgornaia *et al.* 2013; Salvi *et al.* 2017). For the continuous α-helix connecting PASp and PASc, biochemical crosslinking data were available that identified residues involved in the homodimerization interface (Monzel and Unden 2015; Stopp *et al.* 2021). For simpler structural representation, DcuS was assumed to be a dimer (Scheu *et al.* 2010b). The DcuS model spans a length of 1.9 nm (190 Å), with a highest width of 0.6 nm (64 Å) in the periplasmic part and 0.75 nm (75 Å) in the cytoplasmic part (Fig. 49A). The continuous α-helix connecting PASp and PASc extends over a length of 0.84 nm (84 Å), with the first third being transmembrane (Fig. 49B).

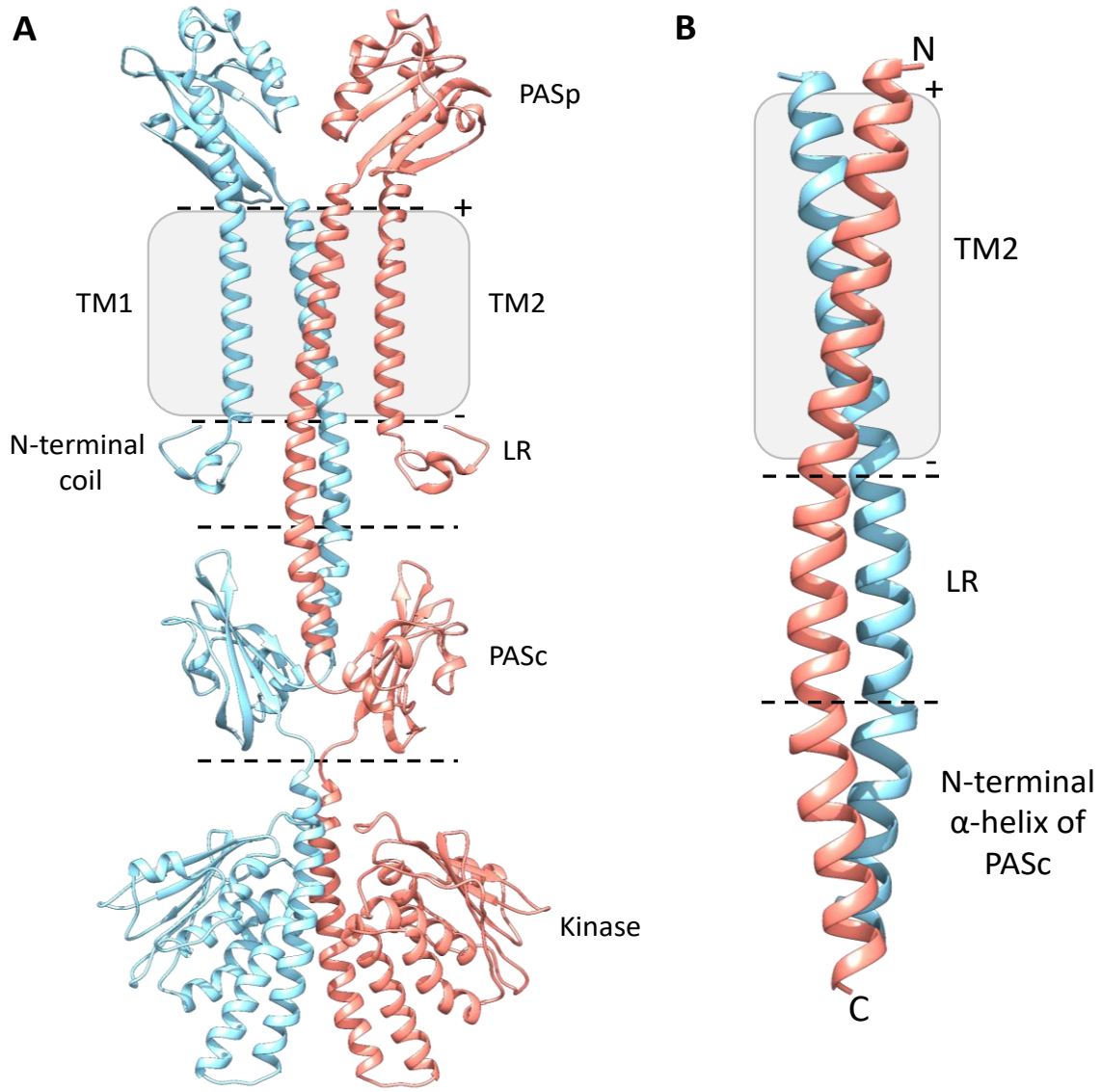

Fig. 49: Structural model of dimeric DcuS (A) and of the continuous transmembrane α-helix (B). UCSF Chimera was used to assemble the structures obtained by homology modeling (PASp, PASc, and Kinase), predicted structures (N-terminal coil), and manual modeling (TM1, TM2, and LR). The PASp dimer was obtained using the structure of DcuS homolog CitA as a template (PDB ID:2V9A) (Sevvana *et al.* 2008). The PASc dimer was modeled using the structure of CitA as a template (PDB ID: 5FQ1) (Salvi *et al.* 2017). The kinase domain was modeled using a histidine kinase of *T. maritima* (PDB ID: 4JAU) (Podgornaia *et al.* 2013). The cytoplasmic N-terminal coil were predicted by the server I-TASSER (Yang and Zhang 2015). TM1, TM2 and the LR were manually modeled using UCSF Chimera (Pettersen *et al.* 2004).

3.5.2 Multiple sequence alignment of DcuS

DcuS belongs to the CitA family of sensor histidine kinases consisting of the citrate specific sensor CitA and the C_4-dicarboxylate specific sensor DcuS (Scheu *et al.* 2010a). The CitA-CitB two-component system induces expression of genes involved in citrate fermentation in *K. pneumoniae* and *E. coli* in presence of citrate. DcuS and CitA are paralogous and share a sequence identity of 27%. The two sensors are structurally similar with a significant functional difference: $CitA_{Ec}$ does not require accessory proteins to function (Scheu *et al.* 2012). DcuS requires for function and detection of C_4-dicarboxylates, one of the two coregulators. Either DctA or DcuB convert DcuS into the C_4-dicarboxylate-responsive state through protein-protein interaction. In the absence of coregulators, DcuS would be constitutively active and induce genes involved in C_4-dicarboxylate metabolism, independent of the presence of C_4-dicarboxylates (Davies *et al.* 1999; Kleefeld *et al.* 2009; Witan *et al.* 2012b; Wörner *et al.* 2016). Previous work has experimentally narrowed down the DcuS LR as a putative interaction site for DctA (Gröpper 2013; Stopp *et al.* 2021). In this work, an LR-PASc construct showed interaction with the isolated DctA H8b region, with genetic modification, such as truncation, causing weaker interaction (Gröpper 2013). In a resulting model, the downstream PASc domain would act as a signal integration domain, combining the signals from PASp compaction (mediated by TM2 and LR), and DctA H8b interaction and converting them into a conformational change of the kinase, thereby driving autophosphorylation. DcuS and CitA are structurally and functionally similar with a significant difference that CitA does not require accessory proteins. Based on this fact, the hypothesis was formed that residues involved in DcuS LR-DctA H8b interaction could be changed in CitA. This hypothesis would help in the interpretation and identification of residues of interest.

In total, 6 DcuS and 6 CitA sequences were selected and aligned, whereby the LR and the cytoplasmic PAS domain are shown. In a previous work, DcuS homodimerization and signal transduction within PASc was investigated (Monzel *et al.* 2013). Mutations were introduced within PASc and screened for phenotypes in homodimerization and signal transduction. Based on the different phenotypes, ON and OFF mutants were defined. An ON mutant shows effector-independent activity of the kinase, whereas the OFF mutant shows no activity even in the presence of an effector. Three subgroups were defined due to the diversity of ON mutants (Tab. 3). Type I ON mutations showed a significant

Tab. 3: ON type characterization

ON type	Residue	Location
ON I	L246R	PAS core
ON I	N248D	
ON IIA	E233G	
ON IIA	F321A	β-Scaffold
ON IIB	L228A	PAS core
ON IIB	N304D	β-Scaffold
ON IIB	R322A	

restructuring of the PASc homodimer (assayed as a decrease in homodimerization) and a decrease in interaction with DctA. Type IIA ON mutations showed a slight restructuring of the homodimer and a reduced interaction with DctA. Type IIB ON mutations showed no significant restructuring of the homodimer and no decrease in interaction with DctA (Monzel *et al.* 2013). The ON mutants that were characterized in more detail are listed in Tab. 3. The mutations are annotated in the MSA and structural model of DcuS LR-PASc (Fig. 50 and Fig. 51).

The DcuS LR (C_{199}ILVKVLKKILFG$_{211}$) shows no conserved amino acid residue higher than 80% between DcuS and CitA. Within the LR of DcuS, an L-X_3-L-X_3-L sequence motif is moderately conserved, providing evidence for an α-helical structure that has already been studied in more detail biochemically (Fig. 50) (Stopp *et al.* 2021). L-X_3-L motifs are often involved in the interaction between proteins that control various cellular functions (Plevin *et al.* 2005). Overall, the LR is a relatively hydrophobic region with grand average of hydropathicity index (GRAVY) of + 1.7 (positive = hydrophobic; negative = hydrophilic). GRAVY represents the hydropathicity value of a peptide which is calculated from the sum of all hydropathy values of all amino acids of a sequence divided by the sequence length. GRAVY was calculated with the hydropathy values of Kyte and Doolittle (1982). Several positively charged amino acids, K203, K206, and K207 and two OFF (L209A and F210A) and one ON mutant (K206A) are located in the LR (Monzel *et al.* 2013). However, based on the hypothesis, no promising residues can be identified (Fig. 50).

The L-X_3-L-X_3-L motif of the LR forms a homodimerization interface of DcuS, based on biochemical crosslinking data (Stopp *et al.* 2021). Accordingly, the L_{200}-X_3-L_{204}-X_3-L_{208} motif should not have accessibility for protein-protein interaction, although residues outside this motif can be exposed. This assumption would allow the following residues to be considered (underlined) for interaction with DctA H8b:
$C_{199}I_{200}L\underline{V}_{202}\underline{K}_{203}\underline{V}_{204}L\underline{K}_{206}\underline{K}_{207}\underline{I}_{208}LF_{210}G_{211}$. C199 and I200 are unlikely due to their proximity to the membrane. Similarly, residues F210 and G211 are atypical for a protein-protein interaction. Residues K203 and K207 would be the most promising, due to a spacer residue, resulting in both residues theoretically being located opposite of the homodimerization interface (L-V$\underline{K}_{203}$V-L and L-K$\underline{K}_{207}$I-L).

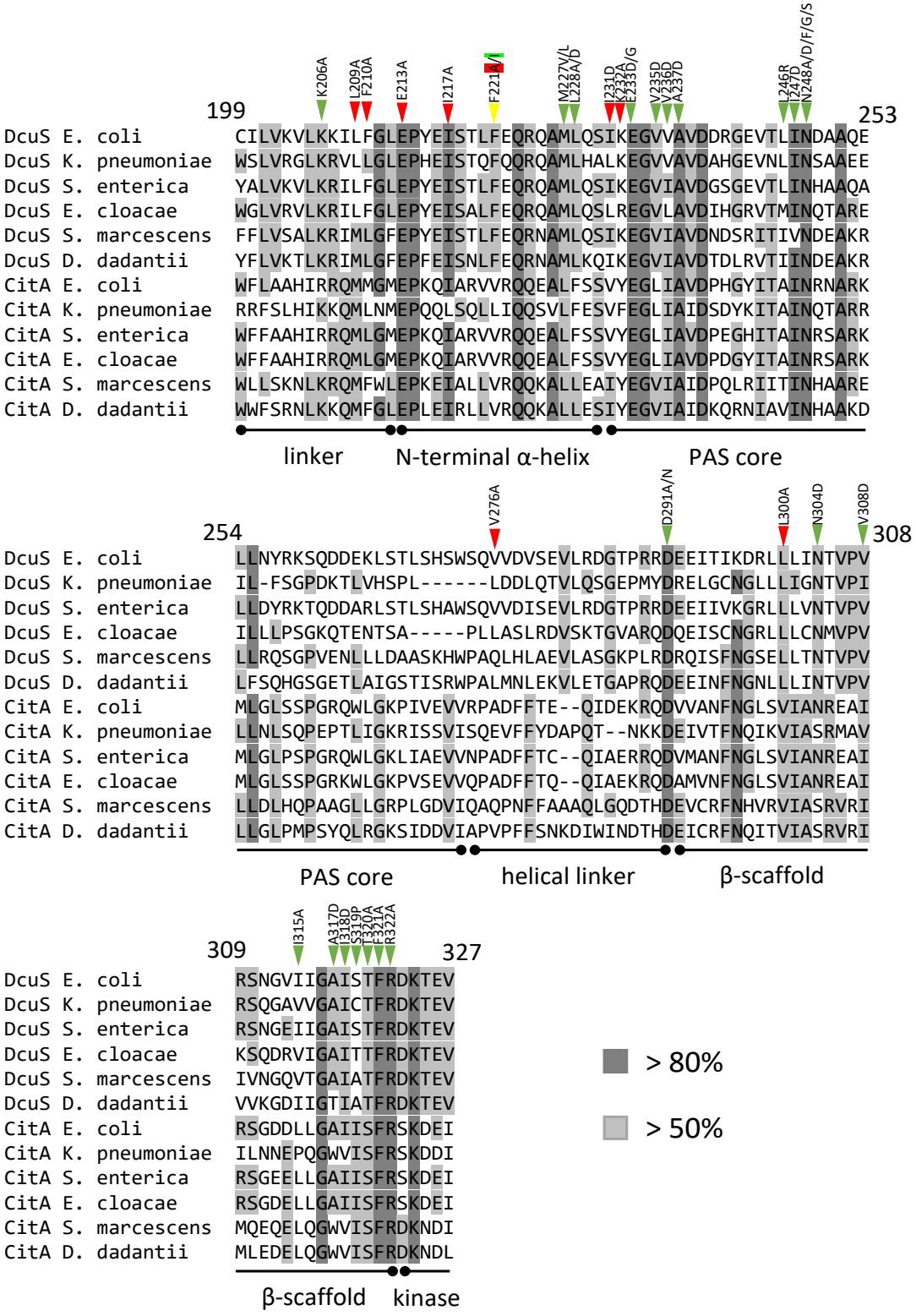

Fig. 50: Multiple sequence alignment of the LR-PASc region of DcuS and CitA. The full length DcuS and CitA sequences were obtained from UniProt (UniProt Consortium 2019) and aligned via the bioinformatics tool Unipro UGENE (Okonechnikov *et al.* 2012) using the MUSCLE algorithm in default settings (Edgar 2004). In a previous work, annotated mutations were characterized (Monzel *et al.* 2013). ON-phenotypes (green), OFF-phenotypes (red), and ON/OFF-phenotype depending on the mutation (yellow). Detailed specification of some ON mutations are given in Tab. 3.

Noteworthy, an exchange for L-Ala for K206 rendered DcuS constitutively active, which makes this residue equally interesting (Monzel *et al.* 2013). K203 showed moderate conservation of the positive charge characteristic for DcuS in the MSA, while this tendency is considerably enhanced in K206 and K207 and even conserved in CitA (Fig. 50). Overall, based on the chemical and structural properties of the LR the three L-Lys residues, K203, K206, and K207 are promising candidates for the interaction with DctA H8b.

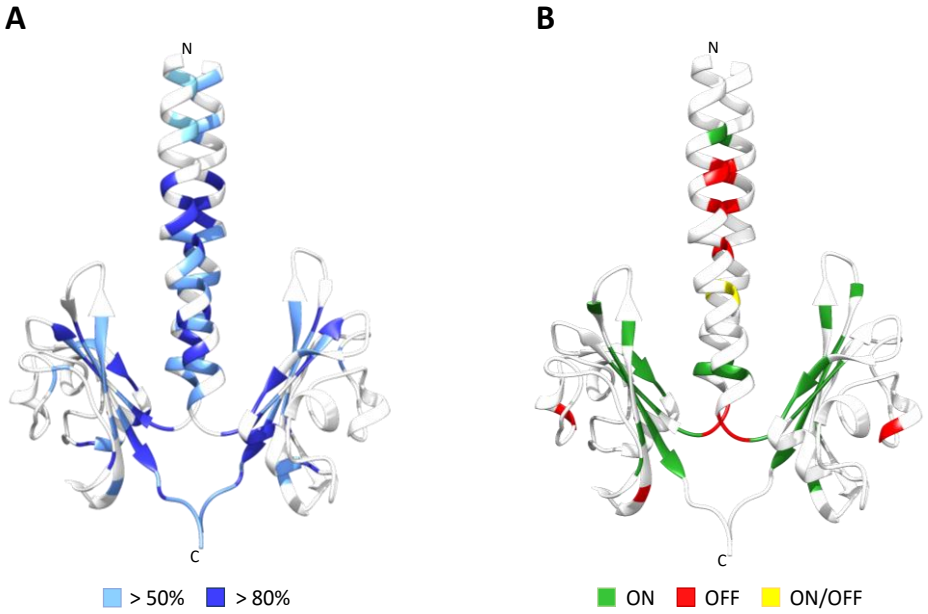

Fig. 51: Amino acid conservation (A) and ON/OFF mutations (B) mapped on the LR-PASc model. The structural model of LR-PASc is based on the crystal structure of PASc from CitA of *Geobacillus thermodenitrificans* (PCB ID: 5FQ1) modeled as a homology model with SWISS-Model. The LR is manually modeled in UCSF Chimera. (**A**) Amino acid conservation (Fig. 50), (**B**) ON, and OFF phenotypes (Monzel *et al.* 2013) were mapped on the LR-PASc model.

In the PASc region, it is noticeable that the ON and OFF mutants cluster in the N-terminal α-helix, the first half of the PAS core, and the second half of the β-scaffold, whereas only isolated mutants are found in the other regions. Interestingly, OFF mutations cluster predominantly in the N-terminal α-helix (Fig. 50 and Fig. 51). For the first half of the PASc sequence, it can be observed that an exchange to L-Ala often led to an OFF phenotype, whereas an exchange to the negatively charged amino acid L-Asp led to an ON phenotype. This assumption is no longer valid towards the end of the PASc region, at the transition from the β-scaffold to the kinase domain, where both L-Ala and L-Asp caused ON phenotypes. Structurally, a high conservation is observed in the N-terminal α-helix of PASc. Comparison of this observation with the mutants identified shows that the majority of ON and OFF phenotypes are located in the homodimerization interface (Fig. 50 and Fig. 51). Additional conservation and mutant clusters included the β-sheet structures in the PAS core and the β-scaffold, which C-terminally transitions into the kinase domain (Fig. 51 A and B). In these

domains, both a high degree of conservation and numerous mutations, especially ON mutations, are observed.

3.5.3 Structural modeling of DctA

DctA is a C_4-dicarboxylate transporter expressed under aerobic conditions and is one of the two coregulators of DcuS. DctA converts DcuS into a C_4-dicarboxylate responsive state. The protein-protein interaction between DcuS and DctA is essential for the functionality of DcuS. DctA-DcuS sensor complexes are able to induce genes involved in C_4-dicarboxylate metabolism (Davies *et al.* 1999; Kleefeld *et al.* 2009; Witan *et al.* 2012a; Wörner *et al.* 2016). Glt from *Thermococcus kodakarensis* is a sodium-dependent L-Asp transporter and orthologous to DctA. Numerous Glt crystal structures are available that allow structural prediction of DctA by homology modeling (Boudker *et al.* 2007; Jensen *et al.* 2013). DctA and Glt differ in two regions, namely DctA helix 3b and helix 8b, which are found only in DctA (Witan *et al.* 2012b). Homology modeling of DctA and *ab initio* modeling of DctA H3b and H8b were performed by Christiane Ziegler (Universität Regensburg) (Fig. 52A).

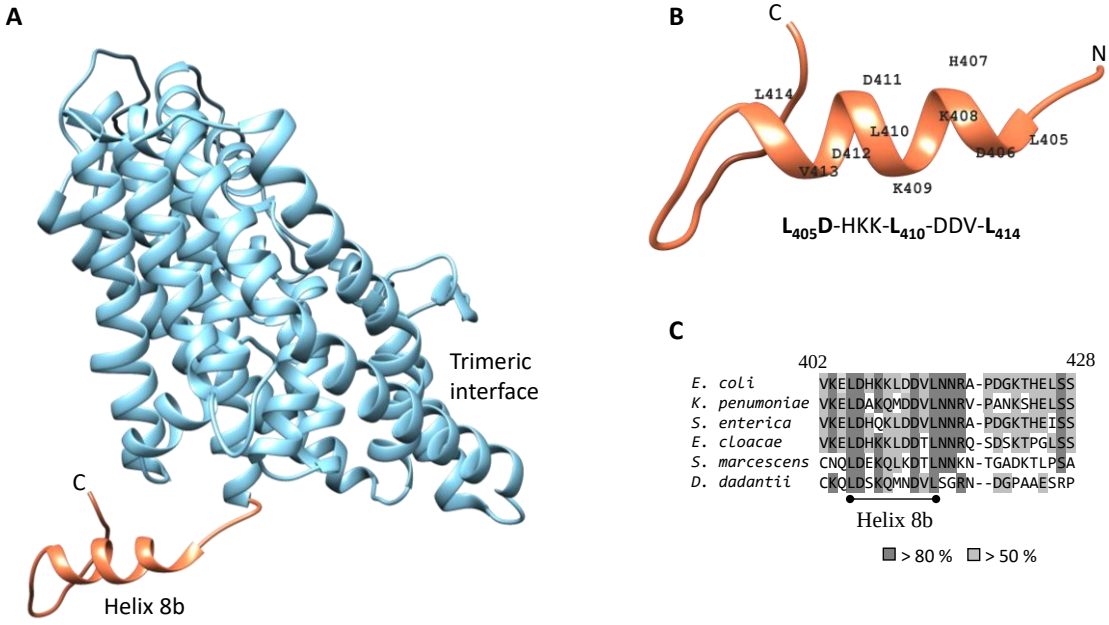

Fig. 52: Structural model of the DctA monomer (A) and DctA H8b (B) and MSA of the H8b region (C). (**A**) The homology model of DctA was modeled by Christiane Ziegler (Universität Regensburg) based on the crystal structure of Glt from *T. kodakarensis* (PCB ID: 4KY0) (Jensen *et al.* 2013). H8b region and the DctA trimeric interface are annotated. (**B**) Structural model of the H8b region, wherein the residues of the α-helical structure are annotated. (**C**) The MSA of DctA H8b was performed with full-length sequences using Unipro UGENE (Okonechnikov *et al.* 2012) with the MUSCLE algorithm in default settings (Edgar 2004). The threshold value for the color representation is > 50% (light gray) and > 80% (dark gray).

Previous work suggested that DctA H8b is essential for the DcuS-DctA interaction (Witan *et al.* 2012a; Witan *et al.* 2012b; Gröpper 2013). Helix 8b is an amphipathic α-helix with a LD-X_3-L-X_3-L motif (L_{405}D-HKK-L_{410}-DDV-L_{414}) (Fig. 52B) (Witan *et al.* 2012b). Multiple sequence alignment was performed with full-length sequences of DctA; the region containing DctA H8b is shown. The motif, with exception of L410, is highly conserved (Fig. 52C). The L-Leu residues show a spacing of 3-4 residues, indicating an α-helical structure. This LD-X_3-L-X_3-L motif could form a hydrophobic surface to allow a tilting mechanism in which H8b is repelled by the membrane (Witan *et al.* 2012b). Based on this assumption, residues located on the opposite side of the LD-X_3-L-X_3-L motif would be candidates. Another limitation is the selection of residues on the side of DcuS LR. Here, the positively charged, and hydrophilic amino acid L-Lys was selected in positions K203, K206, and K207. Only D406, D411 and D412 are qualified due to their chemical characteristics (L_{405}D$_{406}$-HKK-L_{410}-D$_{411}$D$_{412}$V-L_{414}). Structurally, D412 would be most interesting, since one residue serves as a spacer between L410 and L414, so theoretically D412 should be located on the opposite side of the hydrophobic LD-X_3-L-X_3-L motif (Fig. 52B).

3.5.4 The interaction model between DcuS and DctA

The aerobic C_4-dicarboxylate transporter DctA converts DcuS into the C_4-dicarboxylate-responsive state. Previous work has tested the interaction between DcuS and DctA in either full-length constructs or, in some cases, single domain and truncated constructs. DctA H8b (Witan *et al.* 2012a; Witan *et al.* 2012b; Gröpper 2013) and DcuS linker region (LR) (Stopp *et al.* 2021) were established as essential for DcuS functional conversion. The signal transduction of DcuS is propagated by a piston-type displacement, starting from PASp α-helix 6, through transmembrane helix 2 (TM2). This piston-type displacement is a parallel shift towards the periplasm of 4-6 Å upon activation (Monzel and Unden 2015). Biochemical data obtained from *in vivo* L-Cys crosslinking experiments, revealed a different crosslinking pattern for the LR that suggests partial resolution of the bi-helical structure of TM2 in this region. For the L-Leu residues in the L_{201}-X_3-L_{205}-X_3-L_{209} motif, a higher crosslinking efficiency was observed in the absence of fumarate (Stopp *et al.* 2021). These observations implicate that stronger DcuS homodimerization is encountered in the OFF state. The parallel piston-type displacement from PASp α6 and TM2 is translated into a different conformational change in the LR, presumably in cooperation with DctA. Similar crosslinking experiments showed that the crosslinking efficiency of the LR, apart from TM2 and the N-terminal

α-helix of PASc, is significantly changed in a *dctA*-deficient strain. The crosslinking efficiency in the LR in the *dctA*-deficient strain is almost non-quantifiable, whereas TM2 and PASc α1 are largely unchanged (Stopp 2021). Based on these observations, DcuS LR and DctA H8b represents a presumed interaction site, which is essential for signal transduction (Witan *et al.* 2012a; Witan *et al.* 2012b; Gröpper 2013; Stopp *et al.* 2021).

Bioinformatic analysis selected DcuS K203, K206, and K207 of the DcuS LR and DctA D411 and D412 of H8b as possible interacting residues. L-Lys and L-Asp are hydrophilic and oppositely charged residues that have the potential to form a salt bridge. Due to the comparatively small contact area of the interaction, a salt bridge would be advantageous. Salt bridges occur between the positively charged amino acids L-Lys/L-Arg and the negatively charged amino acids L-Asp/L-Glu. Salt bridges are a combination of non-covalent hydrogen and ionic bonding (Anslyn and Dougherty 2006).

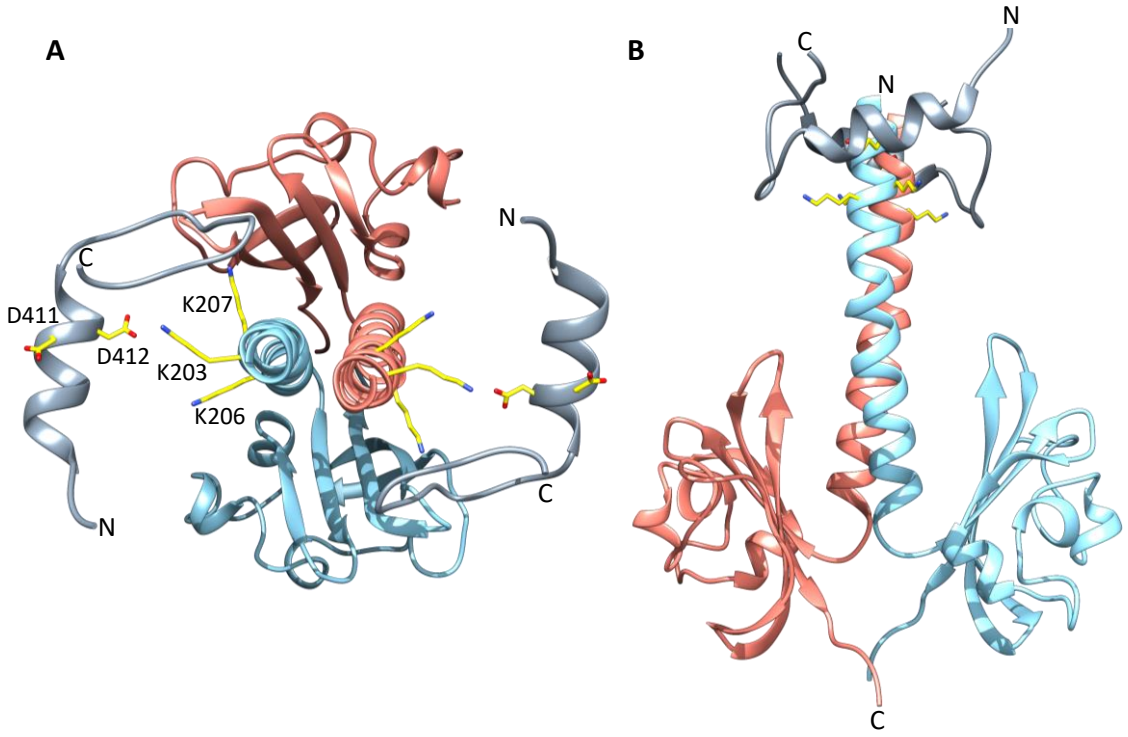

Fig. 53: Interaction model between DcuS LR and DctA H8b. The interaction between DcuS LR (light blue and light red) and DctA H8b (dark gray) was modeled based on the selected residues, DcuS K203 and DctA D412. DcuS LR is modeled in dimeric form. Important residues for interaction are annotated. The atoms are color coded as follows: carbon (yellow), oxygen (red), and nitrogen (blue).

The interaction between DcuS LR-PASc and DctA H8b were modeled based on the selected residues in UCSF Chimera. For simpler presentation, interaction between DcuS LR and DctA H8b was modeled based on DcuS K203 and DctA D412 (Fig. 53A). The salt bridge between K203 and D412 would span a distance of 2.61 Å. Structurally, K203, K206, and K207 are similarly exposed and therefore potential interaction points. For the two DctA residues D411 and D412, the selection only specifies how far H8b must be angled in order to

be in contact with K203. D411 as an interaction point would rotate the hydrophobic LD-X_3-L-X_3-L motif of DctA more toward the membrane, which would theoretically promote the tilting mechanism to repel H8b from the membrane (Witan *et al.* 2012b). Based on this interaction model, DctA H8b would interact with one DcuS monomer by a salt bridge. The salt bridge can be formed on the side of DctA H8b with D411 and D412 between DcuS LR K203, K206, and K207. Present bioinformatic and biochemical data did not allow a more precise classification between the selected residues.

To better frame the magnitude of both structural models, the interaction between full-length DcuS in dimeric form and full-length DctA in monomeric form was modeled (Fig. 54). The presumed interaction between H8b and the LR is small compared to the possible interaction regions in the transmembrane and periplasmic domains. Structurally, TM2, which is essential for transmembrane signal transduction, is shielded from DctA by TM1, suggesting that TM1 could serve as another interaction surface for DctA (Fig. 54). Nevertheless, biochemical studies with truncated constructs showed that DctA H8b is essential for an interaction between DcuS and DctA (Witan *et al.* 2012a). Overall, based on the structural modeling and the close proximity of DcuS and DctA under physiological conditions, multiple domain-specific interactions can be assumed. Bioinformatic and structural analysis suggested that a salt bridge between DctA H8b and DcuS LR might be important due to the small interaction surface in this region.

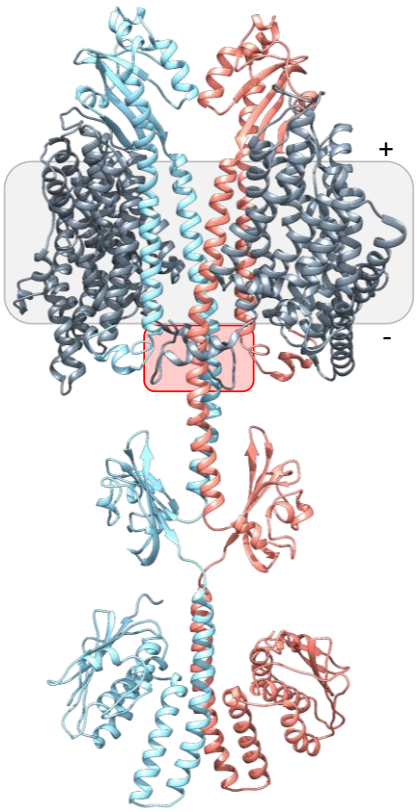

Fig. 54: Interaction model between full-length DcuS and DctA. The DcuS-DctA interaction was assembled manually. The interaction between DctA H8b and DcuS LR is highlighted (red box). Only the interacting DctA monomer is shown.

3.5.5 DcuS signal transduction and involvement of DctA

The membrane-anchored sensor histidine kinase DcuS perceives C_4-dicarboxylates in the periplasm. This stimulus is transmitted across the membrane via conformational changes involving multiple domains such as TM2, the LR, and PASc. Ultimately, this leads to a conformational change in the kinase domain that results in autophosphorylation of the

catalytic domain and transphosphorylation of the DHp domain. C_4-dicarboxylates bind to the periplasmic PASp domain of DcuS, resulting in compaction of the binding-pocket in PASp and uplifting of TM2 via PASp α-helix 6 (Pappalardo *et al.* 2003; Kneuper *et al.* 2005; Krämer *et al.* 2007). The uplift and related structural conformational changes were shown for the homologous citrate-specific sensor histidine kinase CitA (Sevvana *et al.* 2008; Salvi *et al.* 2017). This conformational change lifts the periplasmic part of TM2, which is propagated through the membrane, resulting in a piston-like motion of 4-6 Å (Monzel and Unden 2015). Biochemical data from *in vivo* L-Cys crosslinking experiments revealed a parallel shift in DcuS dimer (Monzel and Unden 2015; Stopp *et al.* 2021). Recent biochemical data suggested a change in the mode of signal transduction in the continuous α-helical structure, primarily in the LR. The piston-like motion propagating from PASp α-helix 6 and TM2 transitions to destabilization of the α-helices in the LR. Structural changes in the LR lead to reorganization of the PASc dimer, controlling kinase activity (Etzkorn *et al.* 2008; Monzel and Unden 2015; Stopp *et al.* 2021). The multiple biochemical and structural data were used for structural modeling of an ON and OFF dimeric DcuS model in the structural modeling tool UCSF Chimera. To simplify modeling, the kinase domain was removed in the signal transduction models (Fig. 55).

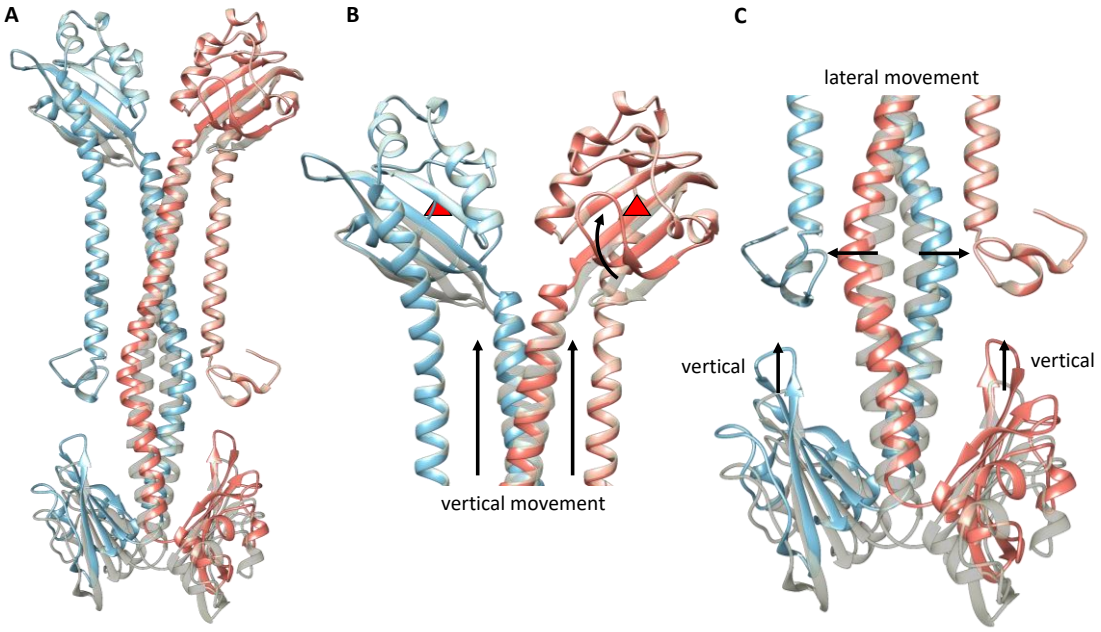

Fig. 55: Signal transduction model of DcuS in ON and OFF state. The ON (solid coloring) and OFF state (transparent) of dimeric DcuS was modeled based on numerous structural and biochemical data (Etzkorn *et al.* 2008; Sevvana *et al.* 2008; Monzel and Unden 2015; Salvi *et al.* 2017; Stopp *et al.* 2021). The kinase domain of DcuS was excluded to simplify modelling.

The compaction of the PASp binding-site upon C_4-dicarboxylate binding, triggers via PASp α-helix 6 and TM2 a parallel vertical movement (piston-like motion) in the direction of the periplasm (Fig. 55B) (Sevvana *et al.* 2008; Monzel and Unden 2015; Salvi *et al.* 2017).

Therefore, the ON and OFF states differ only minimally in crosslinking efficiency (Monzel and Unden 2015; Stopp *et al.* 2021) and, accordingly, in modeling. The structural difference between ON and OFF states is that the TM2 and PASp α6 is displaced upwards about one helical turn, which corresponds to 4-6 Å (Fig. 55B) (Monzel and Unden 2015). This conformational change presumed to provoke a lateral movement in the LR (Fig. 55C). The OFF state shows more efficient dimerization in the LR according to the L-Cys crosslinking data (Stopp *et al.* 2021). This observation is lost when DctA is absent in the deletion strain (Stopp 2021). In the ON state after C_4-dicarboxylate stimulation, the opposite is observed with a strong decrease of the crosslinking efficiency (Stopp *et al.* 2021). The decrease was interpreted as a lateral movement in the structure (Fig. 55C), possibly associated with rotation of the LR. The lateral movement causes according to Fig. 55C, tilting of the PASc domain and a vertical uplift. Incremental changes in PASc conformation are supposed to result in significant structural reorganization. The absence of a coregulator renders DcuS constitutively active, referred to as the ON state (Davies *et al.* 1999; Janausch *et al.* 2002; Kleefeld *et al.* 2009; Steinmetz *et al.* 2014). Assuming that the ON state in the absence of a coregulator has the same structural arrangement as in the presence of fumarate, the homodimerization of the LR should be destabilized. This implies that DctA H8b should stabilize the dimerization of LR, leading to the OFF state. DctA H8b acts as a kind of counterbalance that is sufficient to convert and maintain DcuS in the OFF state but does not prevent activation by binding C_4-dicarboxylates.

4 Discussion

4.1 L-Asp metabolism

4.1.1 L-Asp is a high-quality nitrogen source of *E. coli*

L-Asp is a proteinogenic amino acid and a C_4-dicarboxylate. Growth studies revealed that L-Asp is a high-quality nitrogen source that saturates nitrogen metabolism in *E. coli*. Assimilation of L-Asp requires the C_4-dicarboxylate transporter DcuA and aspartate ammonia-lyase AspA. These results are consistent with previous work identifying L-Asp as an ecological niche and DcuA-AspA as essential for exploitation for the enterohemorrhagic *E. coli* reference strain EDL933 in bovine small intestine contents (BSIC) (Bertin *et al.* 2018). Analysis of the amino acid composition in BSIC revealed high millimolar concentrations of proteinogenic amino acids, including L-Asp. Furthermore, it was shown that only L-Asp and L-Thr are degraded by EDL933 (Bertin *et al.* 2018). In growth studies with either L-Asp or L-Thr as the sole nitrogen source of *E. coli*, L-Asp provided a significantly higher growth rate than L-Thr, suggesting that L-Asp is a more important nitrogen source in the animal intestine. In addition, L-Asp is able to provide the nitrogen requirement for all nitrogen-containing compounds in *E coli* (Strecker *et al.* 2018). The significance of L-Asp is also prevalent by its high intracellular concentrations (4.2 to 9.3 mM); second highest, next to L-Glu (44.8 to 149 mM), of all amino acids (Bennett *et al.* 2009). L-Asp is a precursor of nucleic acid biosynthesis and of amino acids L-Asn, L-Lys, L-Met, L-Thr and L-Arg, which explains the necessity of a higher intracellular concentration (Fig. 56A) (Jensen *et al.* 2008; Yuan *et al.* 2009). *pyrBI* encoding aspartate carbamoyltransferase converts L-Asp to carbamoyl-aspartate the precursor for uridine monophosphate (UMP) biosynthesis, providing the cell with pyrimidines for nucleic acid synthesis (Fig. 56A). Metabolomics-driven quantitative analysis of ammonia assimilation in *E. coli* revealed that L-Asp production must considerably increase after nitrogen upshift to saturate protein and nucleic acid synthesis, underlining the importance of L-Asp (Yuan *et al.* 2009). In addition, L-Asp is a precursor for NAD^+ biosynthesis (Osterman 2009), numerous amino acids (Michal 1999), and a source of ammonium (Fig. 56A and B). Amino acids where L-Asp serves as a precursor include: L-Lys, L-Met, L-Thr, L-Arg, and L-Asn (Fig. 56A) (Michal 1999). The role of AspA and DcuA in L-Asp utilization was also confirmed by real-time quantitative PCR (RT-q-PCR) and competition assays in BSIC (Bertin *et al.* 2018). Consistent with growth studies of *dctA*- and *aspC*-deficient strains, DcuA-AspA was shown to be the main assimilation pathway for L-Asp. The *aspA*-deficient strain showed residual growth under aerobiosis when L-Asp was

the sole nitrogen source, which can be explained by the Krebs-Henseleit metabolic pathway, as discussed previously (Strecker *et al.* 2018). This pathway converts L-citrulline and L-Asp to L-Arg (Goux *et al.* 1995), while L-Arg is degraded via the arginine N-succinyltransferase (AST) pathway, releasing two ammonium and one L-Glu molecule (Schneider *et al.* 1998). The intracellular L-Asp is closely linked to the tricarboxylic acid (TCA) cycle via the reactions of AspA and AspC, producing fumarate and oxaloacetate, respectively. Thus, in a one-step reaction, *E. coli* can either produce or degrade L-Asp to supply precursors to the biosynthetic pathways or supply the cell with a nitrogen source (Fig. 56B).

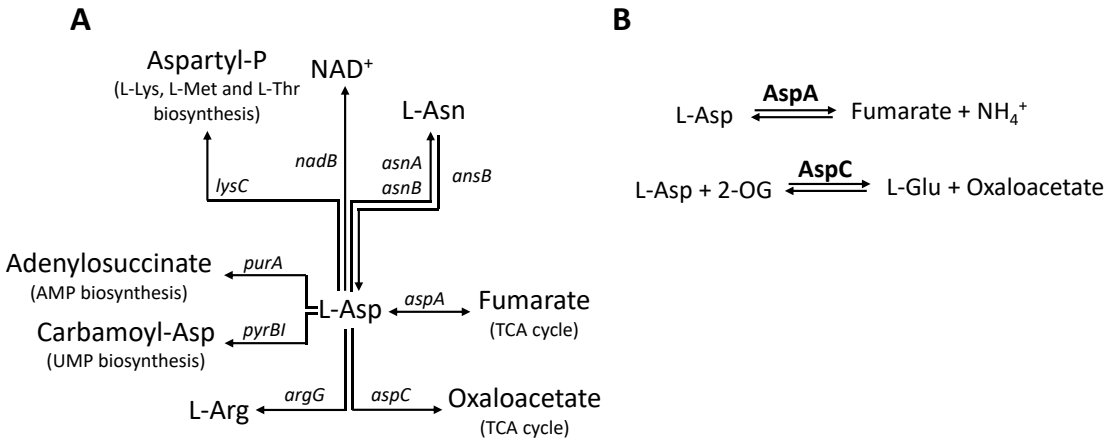

Fig. 56: L-Asp metabolism in *E. coli* (A) and reactions of AspA and AspC (B). Abbreviations: *lysC*: aspartate kinase III; *nadB*: aspartate oxidase; *asnAB*: asparagine synthetase A and B; *ansB*: asparaginase II; *pyrBI*: aspartate carbamoyltransferase; *argG*: argininosuccinate synthetase; *aspC*: aspartate aminotransferase; *aspA*: aspartate ammonia-lyase; *purA*: adenylosuccinate synthetase.

In general, free ammonium is assimilated in *E. coli* via the glutamine synthetase (GS, GlnA) and glutamine 2-oxoglutarate aminotransferase (GOGAT, GltBD) pathway, yielding L-Glu (van Heeswijk *et al.* 2013). Ammonium, and the amino acids L-Asp, L-Glu, and L-Gln that are involved in the DcuA-AspA-GS-GOGAT pathway can saturate the nitrogen requirement of *E. coli* (Michal 1999). In addition to ammonium, the β-elimination of L-Asp by AspA produces fumarate, which is of minor relevance in aerobic growth because it is excreted via an L-Asp:fumarate antiport by DcuA (Strecker *et al.* 2018). However, fumarate can be used for fumarate respiration under anaerobiosis, providing *E. coli* with an alternative electron acceptor for growth (Six *et al.* 1994). The required nitrogen for purine and pyrimidine biosynthesis is also derived from the precursor amino acids L-Asp, L-Glu, and L-Gln (Jensen *et al.* 2008). This is consistent with increased expression levels of aspartate carbamoyltransferase *pyrBI* and orotidine-5'-phophate decarboxylase *pyrF*, which are involved in UMP (pyrimidine) biosynthesis, a direct precursor for UTP and CTP (Jensen *et al.* 2008; Bertin *et al.* 2018). L-Asp is also involved in ATP biosynthesis. Inosine monophosphate (IMP) and

L-Asp are ligated through a carbon-nitrogen bond to form adenylosuccinate, a direct precursor of AMP, which is catalyzed by adenylosuccinate synthetase PurA (Jensen *et al.* 2008). Amino sugars, such as glucosamine 6-phophate which are major components of murein and the bacterial cell wall, are produced by the amination of fructose 6-phophate, with L-Gln as the ammonium donor (Michal 1999; Barreteau *et al.* 2008). L-Asp is involved in numerous biosynthetic pathways, with the most important role in nucleic acid synthesis, specifically UMP biosynthesis (Jensen *et al.* 2008; Yuan *et al.* 2009; Vogel-Scheel *et al.* 2010; Bertin *et al.* 2018). Overall, L-Asp can directly provide nitrogen for numerous biosynthetic pathways, including amino acids, nucleic acid synthesis, and NAD^+ (Fig. 56A). The DcuA-AspA-GS-GOGAT pathway with L-Asp, L-Gln, and L-Glu can provide the nitrogen precursors for all major nitrogen-containing compounds in *E. coli*, highlighting L-Asp as a high-quality nitrogen source.

4.1.2 AspA is stimulated by uridylylated GlnB bound to 2-OG and ATP

L-Asp supplies all the necessary precursors (ammonium, L-Asp, L-Glu, and L-Gln) for nitrogen assimilation in *E. coli*. *In vitro* enzymatic assays of isolated AspA showed a GlnB stimulation of the deamination reaction when the GlnB-binding pocket was either saturated with Mg-ATP and 2-OG or GlnB was modified with a UMP moiety or both. GlnB is a ubiquitous regulatory protein found in the three domains of archaea, bacteria, and eukaryotes (Son and Rhee 1987; Arcondéguy *et al.* 2001; Leigh and Dodsworth 2007; Selim *et al.* 2020). GlnB regulation of glutamine synthetase (GS) was characterized in more detail as the first GlnB target in *E. coli*. GlnB modulates the adenylyltransferase/adenylyl-removing enzyme GlnE in response to the intracellular nitrogen and energy state, resulting in either adenylylation (inactive) or deadenylylation (active) of the GS (Anderson and Stadtman 1971; Brown *et al.* 1971; van Heeswijk *et al.* 2013). The indicator of the intracellular nitrogen state is 2-oxoglutarate (2-OG), which is an intermediate of the TCA cycle

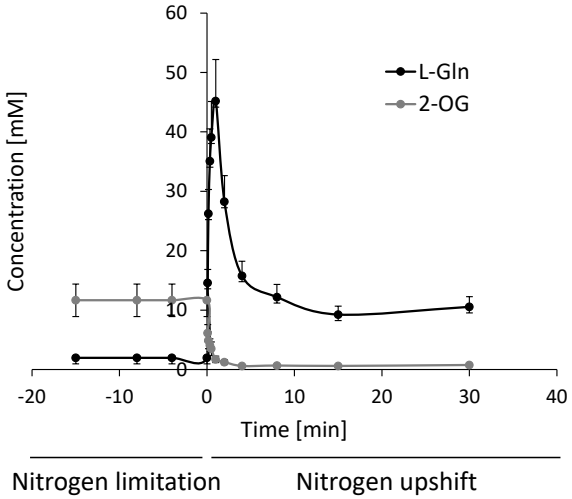

Fig. 57: L-Gln vs. 2-OG levels under nitrogen upshift. Measured and modeled dynamics of L-Gln and 2-oxoglutrate (2-OG) under nitrogen limitation and upshift, obtained from metabolomics-driven quantitative analysis of ammonia assimilation in *E. coli* (Yuan *et al.* 2009).

and provides the carbon skeleton for ammonium assimilation. Elevated 2-OG levels and low L-Gln levels represent nitrogen-limited conditions. Under nitrogen upshift, 2-OG levels decline and L-Gln levels rise, representing nitrogen-saturated conditions (Fig. 57). ATP and ADP are indicators of the energy state of the bacterial cell, although ATP has a more important role in GlnB regulation. Previous work showed that ATP concentration did not vary with the growth rate of *E. coli* (Schneider and Gourse 2004). Intracellular ATP concentration is largely constant, leaving 2-OG as the decisive substrate in nitrogen regulation (Fig. 57).

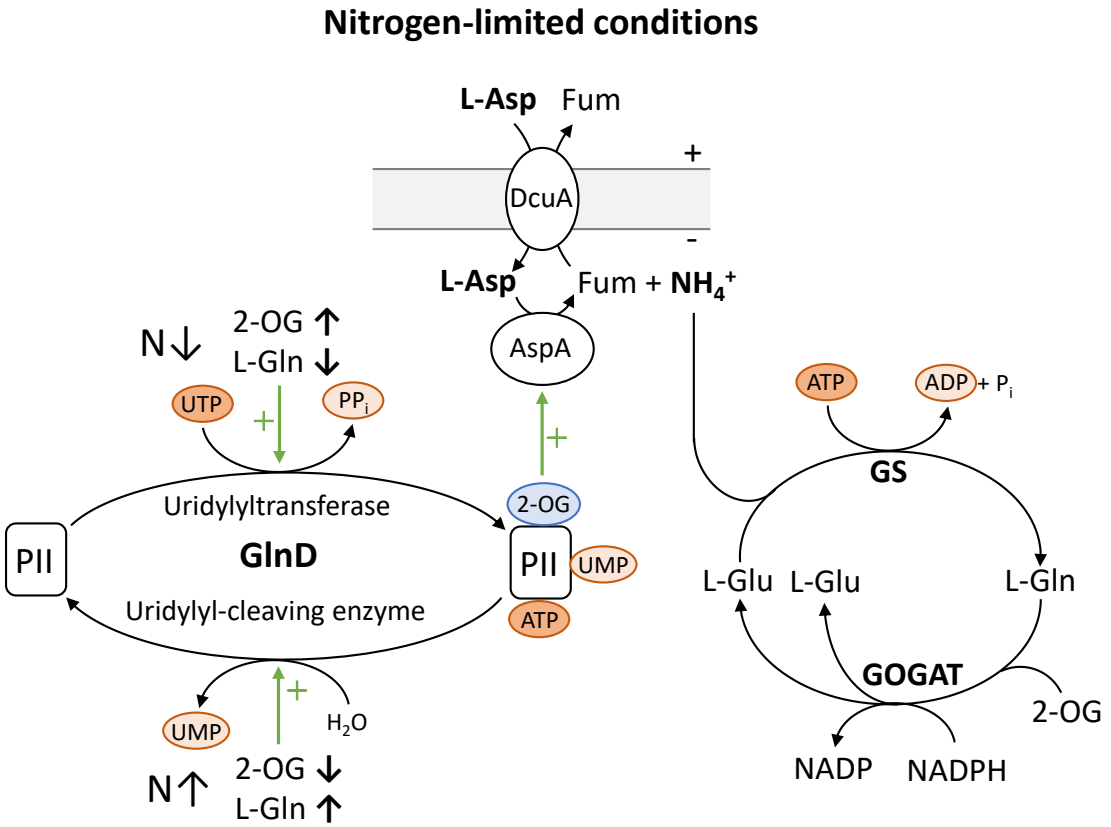

Fig. 58: GlnB-stimulation of AspA deamination reaction. Abbreviations: N↓: nitrogen-limited conditions; N↑: nitrogen-saturated conditions; 2-OG: 2-oxoglutarate; UTP: uridine-triphosphate; PP_i: diphosphate; P_i: phosphate ;UMP: uridine-monophosphate; GlnD: uridylyltransferase/uridylyl-removing enzyme; Fum: fumarate; PII: nitrogen regulator GlnB; DcuA: aerobic L-Asp transporter; AspA: aspartate ammonia-lyase; GS: glutamine synthetase GlnA; GOGAT: glutamine 2-oxoglutarate aminotransferase GltBD.

GlnB is a homotrimer and contains three characteristic T-, B- and C-loops. The B- and C-loops are involved in effector binding and modulate conformational changes in the T-loop, which is important for interaction with target proteins (Huergo *et al.* 2013). The prerequisite for 2-OG binding is the saturation of the B- and C-loop binding pocket with Mg-ATP (Huergo *et al.* 2013). In addition to binding effector molecules, GlnB can be chemically modified. GlnB Tyr51 is uridylylated by the uridylyltransferase/uridylyl-removing enzyme GlnD in response to L-Gln (Garcia *et al.* 1980; Garcia and Rhee 1983; Huergo *et al.*

2013; van Heeswijk *et al.* 2013). Under nitrogen-limited conditions GlnB is uridylylated and the binding pocket is saturated with Mg-ATP and 2-OG (Fig. 58). These different signaling inputs modulate conformational changes of the surface-exposed T-loop, allowing GlnB to positively or negatively regulate target proteins. GlnB targets in *E. coli* are involved in both nitrogen and carbon metabolism or regulation, such as NtrB of the NtrB-NtrC two-component system (Jiang and Ninfa 1999).

In recent years, the glucosamine-6-phosphate (GlcN6P) deaminase NagB and the acetyl-CoA carboxylase ACCase, or AccABCD, have been identified and characterized as GlnB targets (Gerhardt *et al.* 2015; Rodionova *et al.* 2018). NagB catalyzes the deamination of GlcN6P, generating ammonium and fructose 6-phosphate for glycolysis, which can serve as the sole carbon source for *E. coli* (Álvarez-Añorve *et al.* 2009). The utilization of GlcN6P as the nitrogen and carbon source via NagB, was stimulated up to tenfold by uridylylated GlnB (Rodionova *et al.* 2018). ACCase catalyzes the carboxylation of acetyl-CoA to produce malonyl-CoA, the building block for fatty acid elongation, which is the rate-limiting step in fatty acid biosynthesis. GlnB inhibits ACCase activity twofold, but after uridylylation of GlnB, this inhibition is abolished (Gerhardt *et al.* 2015).

Under nitrogen-limited conditions, GlnB stimulates the AspA deamination reaction twofold and increases ammonium formation, which is assimilated via the GS-GOGAT pathway (Fig. 58). Only uridylylated GlnB or GlnB bound to Mg-ATP and 2-OG or both were able to stimulate AspA deamination activity. The amination reaction of AspA was not significantly influenced by GlnB. NagB and AspA catalyze a similar reaction, providing both a carbon and nitrogen source for *E. coli* stimulated by uridylylated GlnB under nitrogen-limited conditions.

Mutations in the GlnB T-loop region, namely Ala49 and Tyr51, affected the interaction with AspA. The GlnB Ala49 residue was previously identified as important for GlnB-NtrB interaction (Martínez-Argudo and Contreras 2002), whereas Tyr51 is the site of uridylylation (Jaggi *et al.* 1996). Consistent with the *in vitro* interaction studies, the uridylylation mutant of GlnB severely suppressed the interaction with AspA. Initially, GlnK had no effect on L-Asp utilization when deleted but showed considerable interaction in the BACTH system and negligible copurification of Strep-tagged AspA. However, GlnK had no effect on either AspA amination or deamination activity.

ACCase is comprised of three modules, one of them is the biotin carboxyl carrier protein (BCCP) (Alix 1989). Previous work indicated a Mg-ATP-dependent interaction between BCCP and GlnK of *E. coli*, however, neither GlnK or GlnK-UMP affected the ACCase activity (Rodrigues *et al.* 2014). Contrary to ACCase activity of *A. thaliana*, which was reduced by GlnK up to 50% (Bourrellier *et al.* 2010), GlnB of *E. coli* reduced ACCase activity by 50%, with uridylylation abolishing this repression (Gerhardt *et al.* 2015). This situation resembles the AspA-GlnK interaction, where an interaction but no regulatory effect was observed. This may provide indications that in other organisms GlnK may exert regulation on AspA.

Overall, AspA regulation by GlnB resembles that of other GlnB-targets such as NagB (Rodionova *et al.* 2018). GlnB stimulates AspA activity when GlnB was either bound to Mg-ATP and 2-OG, uridylylated, or both. This regulation controlled the use of L-Asp as an important source for all amino acids, nucleic acid synthesis, amino sugars, and ammonium (Fig. 56A). The L-Asp degradation was induced under nitrogen-limited conditions, releasing ammonium which is assimilated in the GS-GOGAT pathway. However, AspC showed interaction with GlnB and GlnK, whereas functional evidence for an effect of GlnB or GlnK on AspC activity is not available. Nevertheless, AspA and AspC in combination with GlnB regulation would provide *E. coli* with an interesting set of tools to efficiently utilize the intracellular L-Asp pool to meet nitrogen requirements under both nitrogen-limited and nitrogen-saturated conditions. The GlnB involvement in carbon and nitrogen regulation continues to expand the role of GlnB beyond nitrogen regulation in *E. coli*.

4.1.3 Interplay between AspA and AspC in L-Asp metabolism

Aspartate aminotransferase AspC is of minor significance for L-Asp utilization in aerobic growth. The transaminase reaction by AspC is located at the interface of the TCA cycle and nitrogen metabolism, producing either L-Glu and oxaloacetate (OA), or L-Asp and 2-OG (Powell and Morrison 1978). AspC interacts with GlnB and GlnK in the adenylate cyclase-based BACTH assay. The GlnB T-loop mutant A49P shows a twofold increase in interaction, whereas the uridylylation mutant suppresses the AspC-GlnB interaction, similar to AspA-GlnB. AspC-GlnK interaction was noticeable weaker compared to AspC-GlnB. In general, these findings would indicate a specific interaction between AspC and GlnB. Consistent with the BACTH results, AspC and GlnB were clustered in a global analysis of putative interactions of *E. coli* (Hu *et al.* 2009).

Recent analysis of ammonia assimilation in *E. coli* emphasized the importance of the intracellular L-Asp pool as a precursor and nitrogen donor for protein and nucleic acid synthesis (Yuan *et al.* 2009). Metabolomics-driven simulations revealed the change in L-Glu, L-Gln, 2-OG, and L-Asp levels under nitrogen upshift. Intracellular L-Asp levels increased up to fivefold under nitrogen-saturated conditions (Tab. 4). The authors concluded that this observation is caused by net L-Asp production catalyzed by AspC (Yuan *et al.* 2009).

Tab. 4: Concentration (mM) of important metabolites under nitrogen limitation and upshift. The concentrations are based on metabolomics simulation and experimental data from Yuan *et al.* (2009).

	N-limitation	N-upshift				
Metabolites [mM]/ time [min]	-15	0.5	1	4	8	30
L-Glutamate	76.6 ± 11.6	48.3 ± 7.3	87.4 ± 13.2	163.3 ± 24.7	141.9 ± 21.5	169.5 ± 25.6
L-Glutamine	1.9 ± 0.3	39.1 ± 6.1	45.5 ± 7.0	15.8 ± 2.4	12.2 ± 2.1	10.5 ± 1.7
2-Oxoglutarate	11.6 ± 2.7	3.5 ± 1.2	1.7 ± 0.5	0.6 ± 0.1	0.7 ± 0.2	0.7 ± 0.2
L-Aspartate	1.8 ± 0.4	2.1 ± 0.6	1.5 ± 0.6	5.8 ± 2.1	8.9 ± 2.0	5.9 ± 1.9

The AspA K_M values for L-Asp and ammonium are 1 mM and 20 mM, respectively (Suzuki *et al.* 1973). This indicates that under physiological conditions AspA preferentially deaminates L-Asp, while the amination of fumarate is of minor importance. Oxaloacetate (OA) is an unstable intermediate of the TCA cycle. Intracellular L-malate levels range from 1.70 to 3.45 mM, and under equilibrium conditions, OA levels should be similar. The K_M values for AspC are saturated under physiological conditions (Bennett *et al.* 2009): L-Glu (K_M = 15 mM), OA (K_M = 0.01 mM), L-Asp (K_M = 1.3 mM), and 2-OG (K_M = 0.24 mM) (Yagi *et al.* 1985). Under nitrogen-limited conditions, ammonium formation by AspA is stimulated by uridylylated GlnB bound to Mg-ATP and 2-OG. Under nitrogen-saturated conditions, intracellular 2-OG levels severely drop, while L-Glu, L-Gln, and L-Asp levels rise (Tab. 4) (Yuan *et al.* 2009). L-Glu outcompetes 2-OG for the active site of AspC, inhibiting reflux and shifting the reaction to L-Asp production. The intracellular L-Glu pool (44.8 mM – 149 mM, Bennett *et al.* 2009) is used to synthesize L-Asp to supply nucleic acid synthesis (Jensen *et al.* 2008; Yuan *et al.* 2009). GlnB could stimulate net L-Asp production by AspC, preferably under nitrogen-saturated conditions, when GlnB is non-uridylylated, and in the apo-form (Fig. 59).

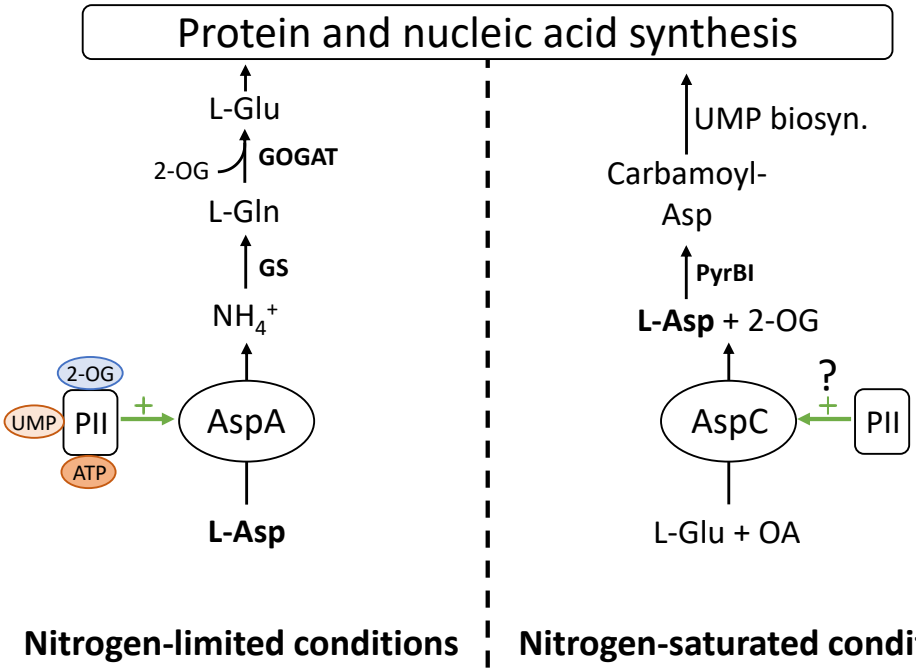

Fig. 59: GlnB regulates the intracellular L-Asp pool. Abbreviations: GS: glutamine synthetase GlnA; GOGAT: glutamine 2-oxoglutrate aminotransferase GltBD; PII: nitrogen regulator GlnB; AspA: aspartate ammonia-lyase; AspC: aspartate aminotransferase; 2-OG: 2-oxoglutarate; OA: oxaloacetate; PyrBI: aspartate carbamoyltransferase; biosyn: biosynthesis.

The postulated GlnB stimulation of AspC, would lead to a beneficial interplay between the anabolism and catabolism of L-Asp. Under nitrogen-limited conditions, the intracellular L-Asp pool would be degraded, releasing ammonium (Fig. 59). Under nitrogen-saturated conditions, L-Glu and OA are utilized to produce L-Asp for protein and especially for nucleic acid synthesis (Fig. 59). GlnB could stimulate either the increase or decrease of the intracellular L-Asp pool in response to the nitrogen and energy status of the bacterial cell, thereby fine-tuning L-Asp utilization to provide the required nitrogen precursors in exponential growth. Previous work has shown that net L-Asp production must increase significantly after the nitrogen upshift to provide *E. coli* with the required amount of L-Asp for nucleic acid synthesis to support an increased growth rate (Yuan *et al.* 2009). The interplay of AspA and AspC to efficiently utilize the intracellular L-Asp pool in response to the nitrogen state of the bacterial cell would emphasize the importance of L-Asp metabolism for *E. coli*.

4.2 Physiological role of L-Asp in the mouse intestine

4.2.1 The microbiota and substrate composition of the mouse gut

Mouse has long been established as a mammalian model organism for biological studies due to its small size, short generation time, and low cost (Carter 2007; Parker *et al.* 2018). The microbiome of the mammalian gut is also known as the second genome and shapes the development of the immune and metabolic system of the host (Round and Mazmanian 2009; Lee and Mazmanian 2010; Cani 2014). It comprises a complex community of microorganisms belonging to archaea, bacteria, eukarya, and viruses that have the potential to influence host physiology, immunity, and development (Fraune and Bosch 2010; Colombo *et al.* 2015; Bonder *et al.* 2016; Colston and Jackson 2016). The mouse intestine harbors at least several hundred bacterial species, a complex community dominated by anaerobes with essentially no aerobes (Ley *et al.* 2006; Antonopoulos *et al.* 2009; Turnbaugh *et al.* 2010). The dominant phyla are Bacteroides (class Bacteroidia) and Firmicutes (class Clostridia), while the phyla Actinobacteria, Fusobacteria, Verrucomicrobia, and facultative anaerobic Proteobacteria typically constitute minor populations in healthy adults (Hughes *et al.* 2017; Yang *et al.* 2019). The primary objective of the gut microbiota is the digestion of indigestible nutrients (Gentile and Weir 2018). In the large intestine, comprising of cecum and colon, the microbial community compete for limiting carbon and energy sources, mainly complex polysaccharides from the host diet (Martens *et al.* 2014; Cockburn and Koropatkin 2016; Hughes *et al.* 2017). In contrast to the small intestine, which contains relatively few bacteria, the majority of the microbiome resides in the large intestine (Conway *et al.* 2004), and accordingly, so is *E. coli* (Poulsen *et al.* 1994; Miranda *et al.* 2004). Nutrients derived from foods are mostly absorbed in the small intestine, while in the large intestine water and inorganic salts are ingested (Conway *et al.* 2004).

Intestinal inflammation is accompanied by a change in the composition of the intestinal microbiota called dysbiosis. Several biological mechanisms are known to cause the development of dysbiosis leading to the growth of facultative anaerobic bacteria such as *E. coli* and *S.* Typhimurium. This includes the change of the redox potential in the intestine (Albenberg *et al.* 2014), the host production of alternative electron acceptors like nitrate (Winter *et al.* 2013b; Winter *et al.* 2013a), and the nitrogen metabolism may play a role in the development of dysbiosis and thus intestinal inflammation (Lewis *et al.* 2015; Ni *et al.* 2017). Bacterial dysbiosis is characterized by the expansion of proteobacteria, especially members of the Enterobacteriaceae family, for instance the genera *Salmonella* and

Escherichia (Winter *et al.* 2013a; Shin *et al.* 2015). The generation of reactive nitrogen species (RNS) and reactive oxygen species (ROS) is an important component of the host inflammatory response (Lundberg *et al.* 1994; Winter *et al.* 2013b). Nitric oxide radicals ($NO\cdot$) and superoxide radicals ($O_2\cdot^-$) can yield peroxynitrite ($ONOO^-$) which can generate nitrate (NO_3^-), an important electron acceptor for facultative anaerobic bacteria (Szabó *et al.* 2007). In addition, *E. coli* requires cytochrome *bd* oxidase for aerobic respiration to compete successfully in the mouse intestine, indicating that the intestine is not a strictly anaerobic environment (Levitt 1970; He *et al.* 1999; Jones *et al.* 2007). Previous work has shown that oxygen is able to diffuse from the intestinal epithelium into the mucus layer (Saldeña *et al.* 2000). Presumably, facultative anaerobes such as *E. coli* scavenge oxygen in the gut to create an anaerobic environment for the numerically dominant anaerobes (Jones *et al.* 2007). Competition assays with streptomycin-treated mice revealed that *E. coli* uses nitrate and fumarate in the intestine, although fumarate is the more important electron acceptor because nitrate is limiting in the mouse intestine (Jones *et al.* 2011). In anaerobiosis, the TCA cycle is converted to a non-cyclic form, with the reductive branch producing fumarate, which fuels fumarate respiration in *E. coli* (Guest 1992). In general, fumarate can be generated endogenously from carbohydrates via glycolysis, reductive branch of the TCA cycle, and L-Asp (Unden *et al.* 2016). Analysis of mouse intestinal contents revealed an amino acid-rich environment containing almost all proteinogenic amino acids, consistent with data from bovine small intestinal contents (Bertin *et al.* 2018). C_4-dicarboxylates were only quantified in low micromolar concentrations, except for L-Asp. Competition experiments with *S.* Typhimurium mutants lacking DcuR or DcuS showed less efficient colonization of the murine gut lumen than the wild type. To successfully colonize the mouse intestine, *S.* Typhimurium utilizes H_2 as an electron donor, while C_4-dicarboxylates, predominantly L-Asp, are used as electron acceptors in fumarate respiration (Maier *et al.* 2013; Nguyen *et al.* 2020).

Besides the amino acid-rich composition of the mouse intestine, L-lactate was by far the most abundant substrate quantified. L-Lactate is produced by lactic acid fermentation from Lactobacillaceae, which are the most common family in the small intestine (Yang *et al.* 2019). In the large intestine, L-lactate and acetate are utilized for butyrate fermentation by Clostridia (Bourriaud *et al.* 2005; Detman *et al.* 2019). Short chain fatty acids (SCFA), such as butyrate, acetate, and propionate, have numerous host-beneficial roles. In ruminants, SCFA are assimilated and provide high portions of total energy gained from the diet (Mortensen and Clausen 1996; Scheppach *et al.* 2001). SCFAs are considered as a preferred

source of energy for the colon mucosa in humans and are reported to provide protection against colitis and colorectal cancer (McIntyre *et al.* 1993; Archer *et al.* 1998; Wächtershäuser and Stein 2000; Pryde *et al.* 2002). In general, SCFAs have diverse physiological roles in humans and can affect the production of lipids, energy, and vitamins, and can influence the appetite and cardiometabolic health (Brody 1998; Byrne *et al.* 2015; Canfora *et al.* 2015; Mueller *et al.* 2020). Urea, creatine, and uric acid are important nitrogen waste products, and urea was found in millimolar concentrations in the mouse intestine. In *E. coli*, for instance, urea is generated by agmatinase SpeB during L-Arg degradation (Satishchandran *et al.* 1990). *E. coli* is urease negative; urea is excreted into the environment and serves as an ammonium source for urease-positive organisms (Morris and Koffron 1967). Ammonium as the byproduct of urea hydrolysis is a major nitrogen source for bacteria in the mammalian gut. Recent data demonstrated that the presence of urease-positive microorganism led to a dysbiotic microbiota, enhancing the Proteobacteria population and a reciprocal decrease in SCFA-producing Clostridia (Shen *et al.* 2015; Ni *et al.* 2017).

4.2.2 L-Asp is a nitrogen source and electron acceptor for anaerobic growth

Analysis of the bovine and mouse intestinal contents revealed L-Asp levels in the range of 2 to 4 mM (Bertin *et al.* 2018). In the mouse intestine, L-Asp was by far the most abundant C_4-dicarboxylate present. Previous work highlighted the importance of fumarate respiration for the colonization of Proteobacteria such as *E. coli* and *S.* Typhimurium, while L-Asp is the major exogenous source of fumarate for respiration (Jones *et al.* 2011; Nguyen *et al.* 2020). DcuA and AspA were identified as essential for L-Asp utilization by EHEC strain EDL933 in bovine small intestinal contents (BSIC) (Bertin *et al.* 2018). Competition assays showed a severe growth defect for EDL933 Δ*aspA* (Bertin *et al.* 2018). Fumarate can be generated endogenously from carbohydrates via glycolysis, the reductive branch of the TCA cycle, and L-Asp, eliminating the need for exogenous fumarate (Unden *et al.* 2016). Amino acid degradation is ultimately linked to central metabolism including pyruvate and (under anaerobic conditions) to the reductive TCA cycle; thus, under anaerobic conditions an amino acid-rich environment supports endogenous fumarate production. Lrp is a global transcriptional regulator that responds to several amino acids, including L-Leu, L-Met, and L-Ala (Tani *et al.* 2002; Hart and Blumenthal 2011; Kroner *et al.* 2019). Lrp regulation is highly versatile; L-Leu binding can either potentiate or antagonize repression or activation by Lrp, or in some cases has no effect at all (Lin *et al.* 1992; Platko and Calvo 1993; Newman and

Lin 1995). Reporter gene analysis demonstrates positive Lrp regulation of DcuB and FrdA. DcuA is constitutively expressed under aerobic and anaerobic conditions (Golby *et al.* 1998b; Strecker 2018), whereby ChIP-seq analysis showed Lrp-binding in the promoter region of *aspA* (Kroner *et al.* 2019). Quantification of AspA under different growth conditions confirmed an increase in AspA molecules in response to an amino acid-rich environment (Schmidt *et al.* 2016). Lrp regulation of key genes involved in fumarate respiration would be beneficial because of the abundance of exogenous fumarate sources in the mammalian gut.

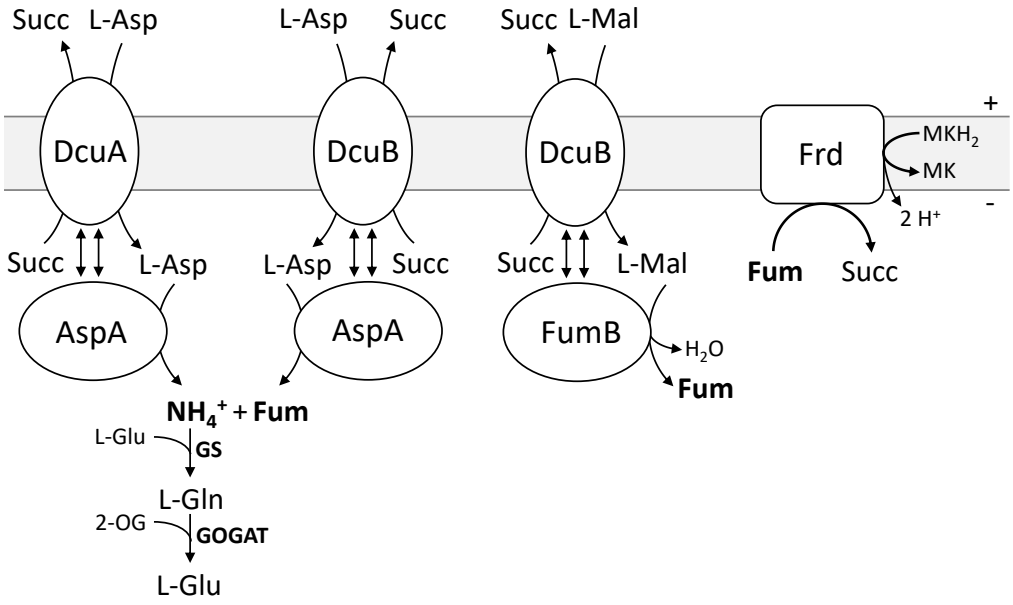

Fig. 60: L-Asp metabolism in anaerobic growth. Abbreviations: Succ: succinate; Fum: fumarate; MK/MKH_2: menaquinone/menaquinol; GS: glutamine synthetase GlnA; GOGAT: glutamine 2-oxoglutarate aminotransferase GltBD; 2-OG: 2-oxoglutarate; Frd; fumarate reductase;

L-Asp can serve as an electron acceptor in anaerobic growth, while both DcuA and DcuB can compensate for each other in L-Asp uptake (Six *et al.* 1994). These results were confirmed in growth studies with wild-type *E. coli* deficient in DcuA and DcuB. In addition, L-Asp can also serve as a nitrogen source, thus combining both a nitrogen source and an electron acceptor in one molecule. In aerobiosis, growth experiments with *dcuA*- and *aspA*-deficient *E. coli* strains showed that DcuA is aerobically more important than AspA. This observation is reversed in anaerobic growth, where an *aspA* mutant showed no noticeable growth when L-Asp was either the nitrogen source, electron acceptor, or both. The primary sequence of DcuA and DcuB share a high sequence similarity of 43%, while DcuC only shares 18% similarity to DcuA. The *dcuA dcuB* double mutant demonstrated that DcuC can compensate to some extent for fumarate uptake but not for L-Asp uptake. DcuA has a K_M of 43.3 µM for L-Asp, (Strecker *et al.* 2018), whereas DcuB has an approximate K_M of 100 µM

for fumarate (Engel *et al.* 1994). Low micromolar concentrations of L-malate and fumarate were quantified in the proximal and distal part of the small intestine, while levels in the large intestine were negligible. Commensal *E. coli* resides in the large intestine of the mammalian intestine (Poulsen *et al.* 1994; Conway *et al.* 2004; Miranda *et al.* 2004), in which L-Asp is the only C_4-dicarboxylate available in the millimolar range. DcuA would be the main L-Asp transporter, while DcuB participates also in L-Asp uptake (Fig. 60). This would result in a redundant L-Asp uptake system for *E. coli* to efficiently utilize the ecological niche of L-Asp. In addition, it is reasonable to assume that the K_M for L-Asp of DcuB is higher than that of DcuA, as the evolutionary gene duplication of the Dcu transporters and subsequent development of substrate specificity would suggest.

L-Asp as the main source of exogenous fumarate was further investigated by the interaction studies with DcuA-AspA, DcuB-AspA, and DcuB-FumB in the adenylate cyclase-based BACTH assay and in the membrane Strep protein interaction experiment (mSPINE). *aspA dcuA* and *dcuB fumB* are colocalized on the *E. coli* genome, while *dcuB fumB* cotranscripts are more common than *aspA dcuA* cotranscripts (Golby *et al.* 1998b). Both gene pairs catalyze complementary reactions to supply *E. coli* with the alternative electron acceptor fumarate. In the mSPINE experiment, significant amounts of PhoA-tagged DcuA copurified when Strep-tagged AspA was also expressed. The interaction was only observed after chemical crosslink with formaldehyde. In the BACTH assay, bacteria expressing both DcuB-AspA and DcuB-FumB showed high β-galactosidase activity which confidently exceeded the background activity. Overall, both DcuA and DcuB interacted with their respective colocalized gene product; additionally, DcuB showed interaction with AspA. The DcuA-AspA, DcuB-AspA, and DcuB-FumB metabolons would channel C_4-dicarboxylate uptake into fumarate production to efficiently drive fumarate respiration during anaerobic growth (Fig. 60).

4.2.3 The ecological niche of *E. coli* in the mammalian intestine

Environmental stimuli such as amino acids are perceived via sensory complexes consisting of a transmembrane chemoreceptor, an adaptor protein CheW, and a kinase CheA (Sourjik 2004; Hazelbauer *et al.* 2008; Yang *et al.* 2015). *E. coli* possesses two major amino acid receptors Tar and Tsr, which have the highest affinity for L-Asp and L-Ser, respectively. Recent work has shown that amino acids that attract *E. coli*, such as L-Asp, are also preferentially utilized during growth (Yang *et al.* 2015). L-Asp is by far the most effective

chemotactic ligand, which showed attractant response at 0.5 µM (Yang *et al.* 2015). Chemotaxis is essential for bacteria to maximize nutritional uptake, even in a highly competitive environment such as the mammalian gut (Celani and Vergassola 2010).

Comparison of the carbon sources of commensal and pathogenic *E. coli* revealed that L-arabinose, fucose, and N-acetylglucosamine are used by both in the mouse intestine. In addition, *E. coli* EDL933 utilized galactose, hexuronates, mannose, and ribose, whereas commensal *E. coli* utilized gluconate and N-acetylneuraminic acid (Fabich *et al.* 2008). Comparative genomics of EDL933 and commensal *E. coli* revealed no major difference in the metabolic genes involved in carbon source utilization (Perna *et al.* 2001). *E. coli* has the ability to utilize up to six sugars simultaneously in a chemostat environment, as present in the intestine (Lendenmann *et al.* 1996; Lendenmann *et al.* 1999; Flores *et al.* 2005; Ihssen and Egli 2005). This metabolic flexibility provides both commensal and pathogenic *E. coli* with a competitive advantage in the intestine (Fabich *et al.* 2008). In addition to L-Asp, ethanolamine was identified as a nitrogen source in the bovine small intestine at a concentration of 2.18 mM (Bertin *et al.* 2011). Ethanolamine-ammonia lyase converts ethanolamine to acetaldehyde and free ammonium, and acetaldehyde dehydrogenase converts acetaldehyde to acetyl-CoA, which then enters the TCA cycle (Bertin *et al.* 2011). Similar to the DcuA-AspA pathway, free ammonium is generated and assimilated in the GS-GOGAT pathway.

L-Asp is a high-quality nitrogen source for *E. coli* found in the mammalian intestine. Recent and current work specified the ecological niche of commensal and pathogenic *E. coli* that utilize a variety of different sugars, ethanolamine, and L-Asp for growth in the mammalian intestine. The L-Asp specific chemotaxis sensor Tar highlights the significance of L-Asp metabolism in *E. coli*. Interestingly, pathogenic *E. coli* is more efficient in L-Asp utilization, as *aspA* and *dcuA* showed higher fold-change (BSIC vs. M9-Glc) in expression than commensal *E. coli* (Bertin *et al.* 2018). Consistent with the importance of L-Asp, pyrimidine synthesis is a prerequisite for bacterial colonization, in which L-Asp is the precursor (Jensen *et al.* 2008; Vogel-Scheel *et al.* 2010). Overall, L-Asp is the most important C_4-dicarboxylate and vital for *E. coli* colonization in the mammalian intestine.

4.3 Metabolons of DcuAB and their colocalized genes *aspA* and *fumB*

Enzymes catalyzing consecutive reactions in metabolic pathways can be organized in weak sequential complexes (‘metabolons’). The genes encoding the enzymes of metabolons are often encoded in polycistronic operons. Metabolons are beneficial for efficient channeling of metabolic intermediates, minimize the release of toxins or labile intermediates, increase metabolic efficiency, and provide an additional layer of regulation via protein-protein interaction of enzymes involved in the metabolon (Moraes and Reithmeier 2012).The intracellular concentrations of the proteins are orders of magnitude higher than in a typical *in vitro* experiment (Srere 1967), suggesting that metabolons between a transporter and a cytosolic enzyme are more abundant in *E. coli* than functional data would suggest.

dcuA aspA and *dcuB fumB* are colocalized on the *E. coli* genome (Golby *et al.* 1998b) and catalyze complementary reactions. The interaction between DcuA-AspA, DcuB-AspA, and DcuB-FumB was demonstrated in the adenylate cyclase-based BACTH assay and in mSPINE. DcuA-AspA was investigated in a previous work, revealing a nitrogen shuttle to provide the bacterial cell with a nitrogen source without net carbon supply (Strecker *et al.* 2018). DcuB catalyzes a C_4-dicarboxylate:succinate antiport, providing the cell with an electron acceptor for fumarate respiration (Six *et al.* 1994). Fumarase B is one of five isozymes in the TCA cycle and catalyzes the reversible dehydration of L-malate to fumarate (Woods *et al.* 1988a). Akin to DcuA-AspA, DcuB-FumB would catalyze the uptake and conversion of L-malate to fumarate, driving fumarate respiration (Fig. 60). In total, *E. coli* contains five fumarases, FumA, FumB, FumC, and the recently discovered FumD and FumE (Woods *et al.* 1988b; Sévin *et al.* 2017). Presumably, DcuB is not able to interact with all fumarases present. It is more likely that DcuB interacts with some isoenzymes, while the rest are predominantly involved in the TCA cycle. Due to the high sequence similarity of DcuA and DcuB, it is possible that DcuA can also interact with FumB. In addition to C_4-dicarboxylate transporters, the major ammonium transporter AmtB showed interaction with AspA. AspA catalyzes the reversible β-elimination of L-Asp, forming ammonium and fumarate. Theoretically, an AmtB-AspA interaction would facilitate ammonium assimilation without consuming ATP. This would constitute an interesting extension of ammonium assimilation by the GS-GOGAT pathway. AspA has a relatively low affinity for ammonium (K_M = 20 mM, Suzuki *et al.* 1973), preventing amination of fumarate under physiological conditions. The AmtB-AspA metabolon could locally increase ammonium concentration, allowing ammonium assimilation by AspA and decreasing free ammonium concentration (Fig. 61A).

Data on interactions between transporters and cytosolic enzymes are scarce. Previous work was done for a postulated AmtB-GS and GlpF-GlpK interactions in *E. coli*. AmtB is the main ammonium channel and is neither dependent on ATP nor on the membrane potential (Javelle *et al.* 2005). Ammonium uptake is tightly regulated by the nitrogen regulatory protein GlnK, an orthologous of GlnB (Javelle *et al.* 2004). It was shown that significant amounts of GS are membrane-bound, although irrespective of AmtB (Javelle *et al.* 2005). Similar observation was made for GS of *A. vinelandii*, where 30% of GS activity was found to be membrane-associated (Kleinschmidt and Kleiner 1978). AmtB-GS interaction would be beneficial for ammonium assimilation to minimize free ammonium (Fig. 61B). Similarly, interaction between the glycerol facilitator GlpF and the glycerol kinase GlpK is postulated. It was demonstrated that both enzymes occur in soluble and membrane-bound forms (Seltzer and McCabe 1984), but the definitive proof of a GlpK-GlpF interaction awaits biochemical confirmation (Voegele *et al.* 1993). GlpF is a member of the major intrinsic protein (MIP) family and passively facilitates glycerol diffusion across the inner membrane. This reaction is concentration-dependent, presumably GlpK catalyzes the phosphorylation of glycerol to trap glycerol 3-phosphat in the bacterial cell to inhibit flow back (Fig. 61C). It was assumed that the glycerol kinase GlpK is activated by interaction with the glycerol facilitator GlpF (Voegele *et al.* 1993). More biochemical data was obtained for a mitochondrial glycerol kinase, where the K_M for glycerol was lowered, and the V_{Max} was increased upon interaction with the porin (Seltzer and McCabe 1984; Kaneko *et al.* 1985).

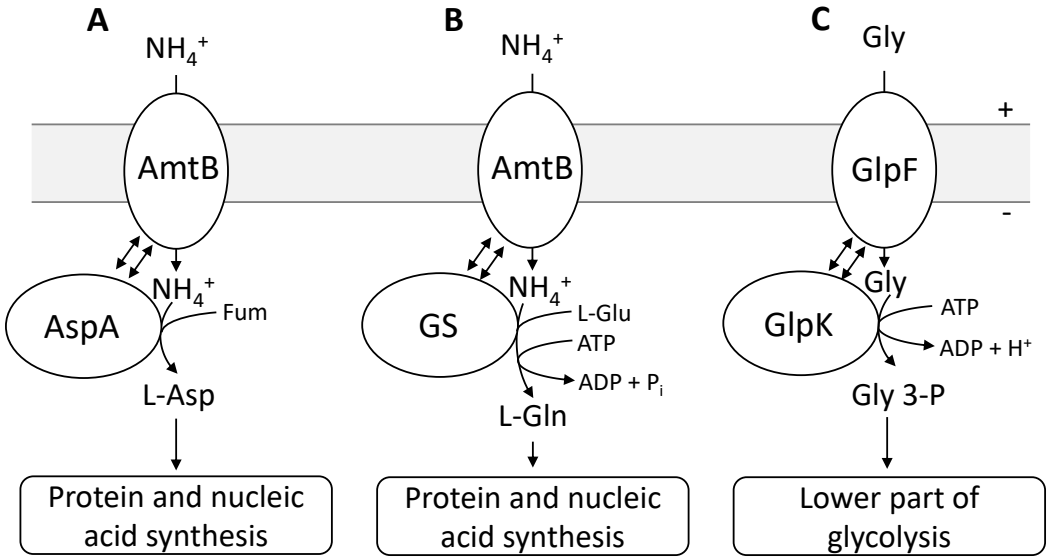

Fig. 61: Metabolic coupling between a transporter and a cytosolic enzyme. Abbreviations: NH_4^+: ammonium; Fum: fumarate; GS: glutamine synthetase GlnA; GlpF: glycerol facilitator; GlpK: glycerol kinase; Gly: glycerol; Gly 3-P: glycerol 3-phosphate.

Most of the known interactions between a transporter and a cytosolic enzyme are regulatory in *E. coli*. For instance, the inhibition of the uptake of secondary metabolites other than glucose by $EIIA^{Glc}$ of the phosphotransferase system (Deutscher *et al.* 2014), or the aforementioned GlnK-regulation of ammonium uptake by AmtB (Javelle *et al.* 2004). Recently, small proteins have been discovered which regulate the activity of large transport proteins (Hobbs *et al.* 2012). These examples have in common that one of the two interaction partners undergoes a change in activity that was measured. For the AmtB-GS and GlpF-GlpK interactions of *E. coli*, this characteristic could not be determined experimentally. Similarly, functional data for DcuA-AspA, DcuB-AspA, DcuB-FumB, and AmtB-AspA awaits to be obtained. In the case of DcuA-AspA, an *aspA*-deficiency did not change the formation of extracellular fumarate which is generated by the DcuA-AspA nitrogen shuttle (Strecker *et al.* 2018). In general, an improvement in metabolic reaction in metabolons compared with two independent reactions are difficult to demonstrate and has not been verified for most metabolons. AmtB-GS would not require modulation of activity to have a function, as this interaction would theoretically minimize free ammonium. The problem arises as to how such a function can be demonstrated experimentally. For DcuA-AspA, DcuB-AspA, DcuB-FumB, and AmtB-AspA only the interaction could be shown. However, if this interaction does not modulate the transport rate or turnover rate, biochemical verification will be difficult.

Overall, DcuA-AspA, DcuB-AspA, DcuB-FumB, and AmtB-AspA show interaction, and each pair catalyzes two consecutive reactions that could optimize the respective metabolic pathway. Interactions with Dcu transporters would efficiently supply the cell with fumarate and drive anaerobic respiration. AmtB-AspA, on the other hand, would provide an energy-saving alternative for ammonium assimilation in *E. coli*.

4.4 C_4-dicarboxylate metabolism is tightly regulated by cAMP-CRP signaling

E. coli can grow on a mixture of sugars and other carbon sources, but consumes the available substrates in sequential order through a process known as catabolite repression (CR) (Görke and Stülke 2008). The order is based among others on which substrate has the highest growth rate (Stülke and Hillen 1999; Leuze *et al.* 2012). This ensures that bacterial cells adapt their metabolic resources to the preferred carbon source, which in turn optimizes the growth rate. CR is a central regulatory mechanism that is involved in regulation of 5-10% of all genes (Stülke and Hillen 1999; Brückner and Titgemeyer 2002; Görke and Stülke 2008; Aidelberg *et al.* 2014). The classic example of CR is the biphasic growth (diauxie) of *E. coli* on a glucose and lactose-containing medium, with the bacteria initially using glucose and then lactose (Monod 1941; Loomis and Magasanik 1967). This regulation is achieved by the glucose:phosphoenolpyruvate phosphotransferase system (PTS) and cAMP-CRP signaling. Substrates, e.g., glucose and mannitol, that are transported and phosphorylated by the PTS are called PTS substrates, which affect the phosphorylation state of $EIIA^{Glc}$. The phosphorylation state determines the regulatory output. In presence of glucose, $EIIA^{Glc}$ is predominantly unphosphorylated due to the phosphoryl group translocation to the glucose transporter $EIIBC^{Glc}$, which produces glucose 6-phosphate. Unphosphorylated $EIIA^{Glc}$ inhibits transport of secondary metabolites such as lactose. In the absence of PTS substrates, $EIIA^{Glc}$ is phosphorylated; in this state $EIIA^{Glc}$ is able to stimulate cAMP production by the adenylate cyclase CyaA. The increase in intracellular cAMP leads to the formation of cAMP-CRP complexes and subsequent induction of genes involved in the catabolism of substrates other than PTS substrates. In addition, non-PTS substrates, e.g., glycerol, maltose, and melibiose, also have an effect on the phosphorylation state of $EIIA^{Glc}$ and thus on cAMP (Hogema *et al.* 1998; Eppler and Boos 1999; Eppler *et al.* 2002). CR acts at transcriptional and post-transcriptional levels to fine-tune carbon metabolism in *E. coli*.

4.4.1 *dctA* and *aspA* are class I CRP-dependent

aspA and *dctA* were identified as class I CRP-dependent promoters, requiring only cAMP-CRP for transcriptional activation, which is consistent with the reporter gene analysis in *cyaA*- and *crp*-deficient strains. Class I promoters are defined by the interaction between the activation region 1 of the CRP dimer with the α-C-terminal domain of the RNA polymerase (RNAP) (Zhou *et al.* 1994), which increases the affinity of RNAP for promoter DNA (Igarashi and Ishihama 1991; Ebright 1993; Savery *et al.* 1996) by proper positioning for

open complex formation (Browning *et al.* 2019). When cAMP-CRP signaling was impaired, the expression of *aspAp-lacZ* and *dctAp-lacZ* was drastically reduced. In the case of *dctA*, DcuR-dependent induction was not observed when cAMP-CRP signaling was interfered, indicating an inferior role in transcriptional regulation. CRP induces a nucleic acid bend of 87° for the consensus sequence (Ebright *et al.* 1989; Parkinson *et al.* 1996), the degree of the bend depends on the nucleotide sequence of the CRP-binding site. The CRP and DcuR binding sites of *dctA* are located at -81.5 and -105.5 upstream of the transcription start, respectively (Fig. 62B) (Davies *et al.* 1999; Abo-Amer *et al.* 2004). Expression data implies that DcuR induction is dependent on interaction between CRP, DcuR, and RNAP (Fig. 62B). DcuR and CRP sites for the *aspA* promoter region are inferred by sequence comparisons with known binding sites (Tsai *et al.* 2018; Surmann *et al.* 2020). Previous work observed a 2.5-fold increase in *aspAp-lacZ* expression in the presence of fumarate (Surmann *et al.* 2020). Two DcuR binding sites are located at -75 and -161, with the CRP site in between at -90.5 (Fig. 62A). Theoretically, a similar dependence on CRP for DcuR induction could be possible for the -161 site (Fig. 62A).

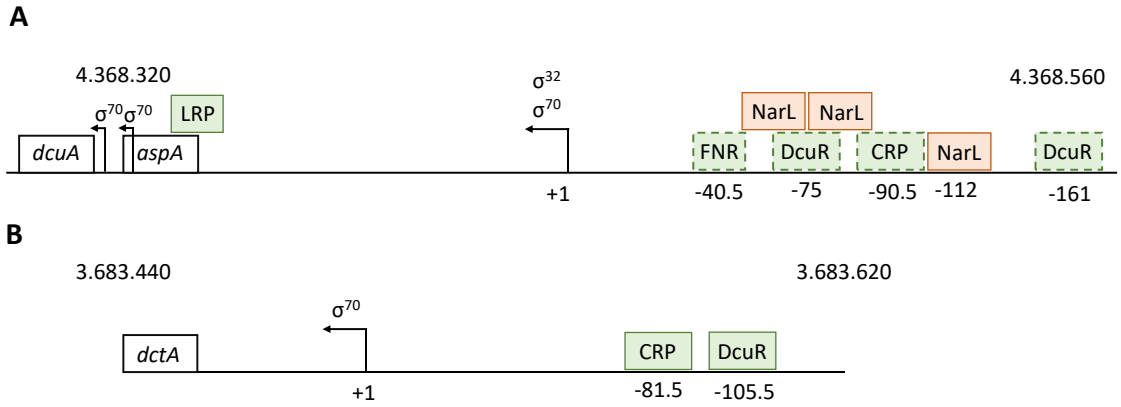

Fig. 62: Promoter region of *aspA* (A) and *dctA* (B). Binding sites are annotated based on sequence comparison (dashed lines) and on experimental data (continous lines). (**A**) LRP: Kroner *et al.* (2019); Fnr: Spiro and Guest (1991); DcuR: Surmann *et al.* (2020); CRP: Golby *et al.* (1998b) and Tsai *et al.* (2018) NarL: Goh *et al.* (2005). (**B**) CRP: Davies *et al.* (1999); DcuR: Abo-Amer *et al.* (2004).

Glycerol is often used as a carbon source because of its presumed low impact on transcriptional regulation compared to glucose and other PTS substrates. This may be the case for some genes, but in general, any carbon source, PTS sugar, or non-PTS sugar, has an impact on transcriptional regulation via cAMP-CRP signaling. Moreover, it has been shown that limitation of nitrogen, phosphorus, and other elements also negatively affects cAMP levels (Mandelstam 1962; McFall and Magasanik 1962; Clark and Marr 1964). Proteomic data from *E. coli* cultured under different carbon sources in minimal M9 medium showed that CRP was at a similar level of 2943 (±535) copies per cell (Schmidt *et al.* 2016). Quantification of absolute metabolite concentrations in *E. coli* showed that cAMP concentrations

varied widely in the presence of glucose (35 µM), glycerol (83 µM), and acetate (146 µM) (Bennett *et al.* 2009), resulting in a 4.2-fold increase in cAMP between the PTS substrate glucose and the gluconeogenic substrate acetate. This would indicate that the determining factor of cAMP-CRP signaling is primarily the intracellular cAMP concentration. In addition to the molecular concentrations of the components involved in cAMP-CRP signaling, the quality and quantity of the CRP binding site is also critical. Quality refers to the nucleotide sequence of the CRP-binding site, whereas quantity reflects the frequency of CRP-binding sites before a transcription start.

Bacterial transcription factors (TFs) are often dimeric, requiring a palindromic or symmetric TF binding site. The consensus sequence of CRP (5′-AAA**TGTGA**TCTAGA**TCACA**TTT-3′) is palindromic, with the consensus half site 5′-$A_1A_2A_3$**$T_4G_5T_6G_7A_8$**$T_9C_{10}T_{11}$-3’ (Busby and Ebright 1999; Leuze *et al.* 2012). The first half site of the CRP-binding site is dominant in TF binding and most conserved. CRP directly interacts with G_5, G_7 and A_8 in the core motif of the first half (Schultz *et al.* 1991; Chen *et al.* 2001; Leuze *et al.* 2012). Mutations in the CRP site towards the consensus lead to an enhanced ability of CRP to activate the promoter and thereby reprogram the hierarchy in sequential carbon utilization (Narang *et al.* 1997; Kovárová-Kovar and Egli 1998; Aidelberg *et al.* 2014). Glycerol and D-xylose had an unexpected strong repression on *dctAp-lacZ* activity compared to *aspAp-lacZ*. Appropriately, G_5 of the first half of CRP-binding site in *dctAp* is mutated to T_5, which presumably weakens the interaction with CRP (Fig. 63). This observation would explain why glycerol, and to some extent D-xylose, exerted much weaker repression on *aspAp-lacZ*. Both *aspA* and *dctA*, showed a mutation in the second half of the CRP-binding site, which is less important for CRP interaction (Schultz *et al.* 1991; Chen *et al.* 2001; Leuze *et al.* 2012). In addition, to the quality of the CRP-binding site, the total number of CRP-binding sites are an important characteristic in gene regulation (Leuze *et al.* 2012). The mannitol-specific PTS enzyme II MtlA transports and simultaneously phosphorylates mannitol, while mannitol-1-phosphate 5-dehydrogenase MtlD converts mannitol-1-phosphate to fructose-6-phosphate, which enters glycolysis (Mayer and Boos 2005). The *mtlAD* operon contains five CRP-binding sites (Ramseier and Saier Jr 1995) with a conservation level between 58% and 75% compared to the consensus

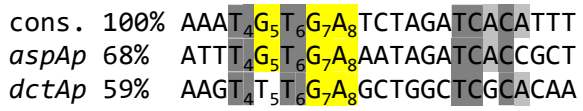

Fig. 63: Alignment of the *aspAp* and *dctAp* CRP-binding-site. The CRP consensus binding site (Ebright *et al.* 1989) was aligned against *aspA* and *dctA* CRP-binding sites. CRP-binding sites were acquired via RegulonDB (Gama-Castro *et al.* 2016). The nucleotides in direct contact with the CRP protein are annotated (yellow) (Leuze *et al.* 2012).

sequence (Ebright *et al.* 1989). However, a large fraction of CRP-controlled genes have only one CRP-binding site, consistent with *aspA* and *dctA* (Gama-Castro *et al.* 2016). 75.5% of all CRP binding sites are distributed on the peak of the Gaussian curve of sequence conservation, which represents the conservation level of all known CRP-binding sites in *E. coli*. This approach may be overgeneralized, although the CRP binding sites of *aspA* (68%) and *dctA* (59%) correspond to some extent to experimental observations. Bacteria do not have a sophisticated nucleosome structure like eukaryotes, which controls gene expression via DNA packaging. Global regulators such as CRP and IHF (integration host factor), which induce DNA bending to alter the accessibility of binding sites, mimic eukaryotic gene expression to some extent. Overall, *aspA* and especially *dctA* are unique examples of cAMP-CRP activation, which emphasize fine- tuning in response to available carbon sources and C_4-dicarboxylates which is transmitted by cAMP-CRP and specific transcriptional regulation by DcuR.

Feed-forward loops (FFL) are important regulatory networks in *E. coli* that contain two transcription factors (TF) and one or more genes. In FFL, a distinction is made between coherent and incoherent types. If the direct effect (positive or negative) of TF1 on the gene is the same as the indirect effect of TF1 via TF2 on the gene, the FFL is termed coherent (Shen-Orr *et al.* 2002; Mangan and Alon 2003; Yang *et al.* 2018). CRP directly activates *aspA*, *dctA*, and *dcuR* transcription, while DcuR positively regulates *aspA* and *dctA*. Thus, this network motif is characterized as a CRP-FFL of coherent type 1 (Fig. 64A) (Yang *et al.* 2018). In addition, Lrp, NarL, and FNR are involved in transcriptional regulation of *aspA* but neither of them is CRP-regulated. FNR directly activates *aspA* while repressing *narL*. This network motif is characterized as a coherent type 4 FFL (Fig. 64B). In conclusion, *aspA* is regulated by two FFLs and Lrp, while *dctA* is only regulated by one FFL.

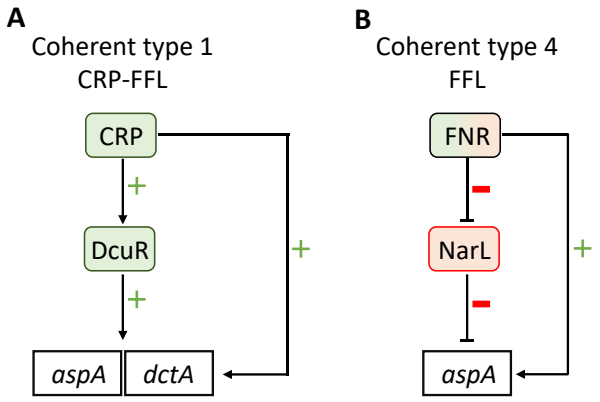

Fig. 64: Feed-forward loops of *aspA* and *dctA* regulation. Abbreviations: FFL: feed-forward loop; NarL: response regulator of the NarX-NarL two-component system; FNR: transcriptional regulator

4.4.2 *dctA* is (post-)transcriptionally regulated by cAMP-CRP and the PTS

Analysis of *dctAp-lacZ* expression showed a need for cAMP-CRP activation. Upper and lower glycolytic substrates and gluconeogenic substrates exhibited different levels of repression. When the capacity for cAMP-CRP activation was low, DcuR could not induce expression of *dctA* since both cAMP-CRP and DcuR-P are required for transcriptional activation. In addition, an interaction between DctA and $EIIA^{Glc}$ of the PTS was observed in the BACTH assay. $EIIA^{Glc}$ can inhibit transporter of secondary metabolism via protein-protein interaction in the unphosphorylated state (Deutscher *et al.* 2006). This mechanism is referred to as inducer exclusion because inhibition of the secondary transporters prevents binding of the substrate to the respective transcriptional regulator and thus induction of the associated metabolic genes. LacY is a proton-potential symporter that drives the uptake of several β-galactosides such as lactose (Kaback 1997; Kaback *et al.* 2001). LacY was identified as the first $EIIA^{Glc}$ target (Dills *et al.* 1982; Misko *et al.* 1987). $EIIA^{Glc}$ binds strongly to LacY only in the presence of a β-galactoside, this inhibits lactose uptake and subsequently prevents transcription of the *lac* operon, as allolactose is not available to abolish repression by LacI (Lewis 2005). The DctA-$EIIA^{Glc}$ interaction would be a special case since C_4-dicarboxylates are detected periplasmically by DcuS (Zientz *et al.* 1998; Golby *et al.* 1999). Therefore, inhibition of DctA by $EIIA^{Glc}$ would only affect uptake of the C_4-dicarboxylates as the substrate but not as an inducer. If the activity of DctA is indeed inhibited by binding of $EIIA^{Glc}$, DctA would be regulated at transcriptional and post-transcriptional levels by cAMP-CRP and $EIIA^{Glc}$ of the PTS, respectively (Fig. 65).

DcuA catalyzes an L-Asp:C_4-dicarboxylate (primarily fumarate) antiport, while AspA converts L-Asp to fumarate and ammonium (Strecker *et al.* 2018). Unphosphorylated $EIIA^{Glc}$ would inhibit the C_4-dicarboxylate uptake by DctA, in presence of upper or lower glycolytic substrates. Additionally, intracellular cAMP levels are low, resulting in basal expression of *dctA*, whereas DcuR is phosphorylated but fails to stimulate expression of *dctA* (Fig. 65A). In presence of C_4-dicarboxylates, $EIIA^{Glc}$ would be predominantly phosphorylated, stimulating the cAMP production by CyaA. The inhibition of DctA would be relieved and C_4-dicarboxylates could enter the bacterial cell. Moreover, sufficient amounts of cAMP-CRP would stimulate expression of *dctA* together with phosphorylated DcuR and RNAP (Fig. 65B). C_4-dicarboxylates are introduced into the TCA cycle and oxidized to CO_2. In general, C_4-dicarboxylates are gluconeogenic substrate, requiring the PEP bypass to serve as a carbon source (You *et al.* 2013; Hermsen *et al.* 2015) in addition to the pyruvate bypass

for feeding the TCA cycle. Under both conditions, the nitrogen shuttle of DcuA-AspA is active and supplies the cell with ammonium (Fig. 65).

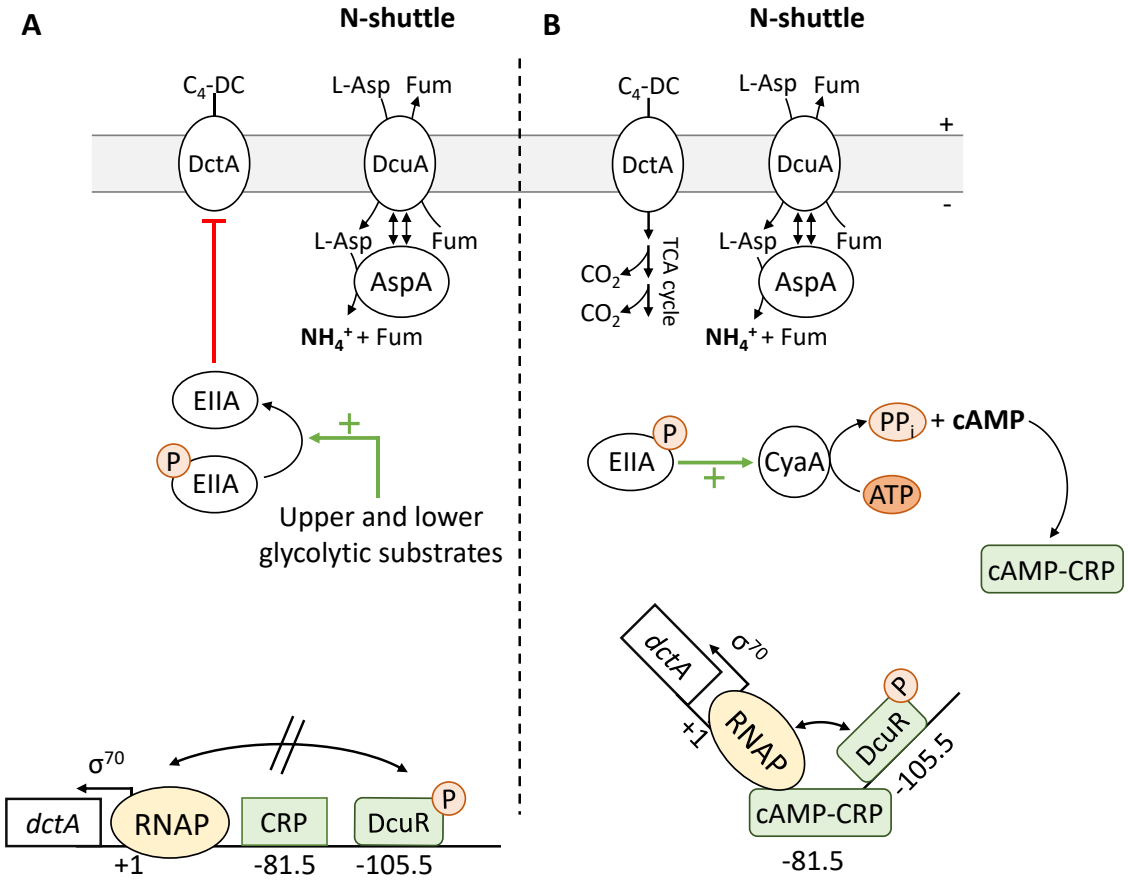

Fig. 65: C_4-dicarboxylate metabolism in aerobic growth. C_4-dicarboxylate metabolism in aerobic growth in presence (**A**) and in absence of upper and lower glycolytic substrates (**B**). Abbreviations: DctA: aerobic C_4-dicarboxylate transporter; DcuA: aerobic L-Asp transporter; C_4-DC: C_4-dicarboxlate; N-shuttle: nitrogen shuttle catalyzed by DcuA-AspA; RNAP: RNA-polymerase; CyaA: adenylate cyclase; EIIA: enzyme IIA^{Glc}

Overall, *aspAp-lacZ* was similarly dependent on cAMP-CRP activation as *dctA*. A clear distinction was observed between PTS and non-PTS sugars, while D-xylose and glycerol exerted a significantly lower repression of *aspAp-lacZ*. This hierarchical fine-tuning of genes involved in secondary metabolism via cAMP-CRP signaling allows *E. coli* to optimize metabolism in response to carbon source availability.

4.4.3 Sugar phosphates affect cAMP-CRP signaling

The *dctAp-lacZ* expression analysis emphasized that each carbon source has an effect on cAMP-CRP signaling, resulting in continuous fine-tuning of CRP-dependent genes. In general, a distinction was observed between upper and lower glycolytic substrates and

gluconeogenic substrates, with the exception of the pentose D-xylose (D-xyl) and the sugar alcohol glycerol, which showed stronger repression of *dctAp-lacZ* than expected.

The *dctA* repression in the presence of glycerol was abolished in the *glpK*-deficient strain. GlpK catalyzes the magnesium-dependent phosphorylation of glycerol to glycerol 3-phosphate (G3P), which is the rate-limiting step for glycerol utilization (Hayashi and Lin 1967; Zwaig *et al.* 1970). GlpK is inhibited by fructose 1,6-bisphosphate in a negative feedback loop (Zwaig and Lin 1966; Thorner and Paulus 1973) and by $EIIA^{Glc}$ in the presence of glycerol, causing glycerol dissimilation to halt (Boer *et al.* 1986; Hurley *et al.* 1993; Feese *et al.* 1994). Complete inhibition of GlpK occurs when four $EIIA^{Glc}$ molecules are in contact per GlpK tetramer (van der Vlag *et al.* 1994; Deutscher *et al.* 2006). The transcriptional regulator GlpR had no effect on *dctAp-lacZ* expression. These observations were similar to those obtained for *malTp-lacZ* expression (Eppler and Boos 1999). The transcriptional regulator MalT is the central regulator of the maltose metabolic pathway (Cole and Raibaud 1986). *malT* is subject to glycerol repression, which is G3P-specific (Eppler and Boos 1999). A *cyaA*-deficient mutant containing a mutant CRP protein that stimulates expression independently of cAMP abolished glycerol repression of *malT* (Eppler and Boos 1999). Accordingly, G3P-specific repression of *malT* was due to cAMP-CRP, suggesting a similar mechanism for *dctA*.

A similar observation was made for D-Xyl, where genetic inactivation of the xylulokinase XylB resolved *dctA* repression. XylB catalyzes the phosphorylation of D-xyl to xylulose 5-phosphate (X5P). Interestingly, the XylR-deficient mutant showed the same effect. Previous work has shown that *xylR*-deficiency abolished the expression of the *xylAB* and *xylFGHR* operons (Song and Park 1997), suggesting that this phenotype is due to the inability of the *xylR*-deficient strain to express *xylB*. This would indicate a X5P-specific repression, like G3P before. Sugar phosphates such as G3P and X5P affect cAMP-CRP signaling, however the exact mechanism is not known. Previous work postulated that sugar phosphates may alter the ability of phosphorylated $EIIA^{Glc}$ to stimulate CyaA (Eppler *et al.* 2002). Together with the mutation in the first half site of the CRP-binding motif (Fig. 63), which lowered the binding affinity of cAMP-CRP in the promoter region of *dctA*, the repression of D-xyl and glycerol on *dctAp-lacZ* expression is due to cAMP-CRP signaling and not to specific transcriptional regulation.

4.5 DcuS-DctA signal transduction complex

4.5.1 Modeling of the DcuS-DctA interaction

Microorganisms are in constant interaction with their environment. The ability to sense environmental parameters, such as concentrations of nutrients is essential for survival and colonization. Bacteria have evolved periplasmically exposed signal transduction systems that pass the signal across the membrane via transmembrane helices to initiate an adequate intracellular response. Classical two-component systems (TCS) consist of a membrane-bound sensor histidine kinase (HK) and a cytosolic response regulator (RR) that stimulates gene expression upon phosphorylation (Hoch *et al.* 1995; Inouye and Dutta 2002). The main biological function of TCS-mediated signal transduction is manifested in input (signal perception) and output (e.g., differential gene expression) (Mascher *et al.* 2006). The DcuS-DcuR two-component system in *E. coli* is transmembrane and represents an extracytoplasmic sensing histidine kinase (Mascher *et al.* 2006). DcuS and the citrate-specific histidine kinase CitA of the CitA-CitB TCS belong to the CitA family of sensor kinases (Bott *et al.* 1995). CitAB induces the expression of genes involved in citrate fermentation in *K. pneumoniae* and *E. coli* (Bott *et al.* 1995; Bott 1997). DcuS periplasmically senses C_4-dicarboxylates, such as L-Asp, L-malate, fumarate, and succinate, whereas DcuR induces genes involved in their metabolism (Unden *et al.* 2016). DcuS consists of a periplasmic sensory Per-ARNT-Sim (PASp) domain that binds C_4-dicarboxylates and is anchored to the membrane by the transmembrane helices TM1 and TM2 (Kneuper *et al.* 2005; Cheung and Hendrickson 2008). In the cytoplasm, TM2 is connected to a cytoplasmic PAS domain (PASc) via a short linker region (LR) (Stopp *et al.* 2021). The C-terminal histidine kinase A (HisKA)-ATPase consists of a DHp domain and catalytic active (CA) domain. The periplasmic sensory part and the cytoplasmic part are connected by a continuous α-helix, consisting of PASp α-helix 6, TM2, LR, and N-terminal α-helix 1 of PASc (Stopp *et al.* 2021). In contrast to the citrate-specific CitA-CitB TCS, DcuS requires accessory proteins to function (Scheu *et al.* 2012). Under aerobic conditions, DctA converts DcuS to the C_4-dicarboxylate-responsive state, while DcuB performs this task in the absence of oxygen. When neither DctA nor DcuB are present, DcuS is constitutively active, resulting in stimulus-independent phosphorylation of DcuR (Davies *et al.* 1999; Janausch *et al.* 2004; Kleefeld *et al.* 2009; Witan *et al.* 2012a; Steinmetz *et al.* 2014; Wörner *et al.* 2016). A structural model of DcuS was created using homology and manually created models that were joined in UCSF Chimera (Pettersen *et al.* 2004). The dimeric structures of PASp, PASc, and the kinase domain were modeled based on similar crystal structures (Sevvana *et al.* 2008; Podgornaia

et al. 2013; Salvi *et al.* 2017). Biochemical data of *in vivo* L-Cys crosslinking were available for the continuous α-helical structure consisting of PASp α6, TM2, LR, and PASc α1, which identified residues involved in homodimerization (Monzel and Unden 2015; Stopp *et al.* 2021). This information was used to identify residues that were exposed and thus accessible for interaction.

The interaction between DcuS and its coregulators DctA and DcuB are essential for function (Davies *et al.* 1999; Kleefeld *et al.* 2009; Witan *et al.* 2012a; Wörner *et al.* 2016). Previous work has identified DctA helix 8b (H8b) and DcuS LR as important for interaction (Witan *et al.* 2012b; Gröpper 2013; Stopp 2021).The combination of a structural model and multiple sequence alignment (MSA) was used to suggest residues involved in the interaction between DctA H8b and DcuS LR (Fig. 53). On the side of DcuS, the positively charged K203, K206, and K207 residues were selected, which predetermined the selection for DctA. For DctA, the negatively charged D411 and D412 residues were selected. The chemical properties indicate a salt bridge combining non-covalent hydrogen and ionic bonds. The amphipathic DctA H8b interacts with the hydrophilic head of phospholipids, initiating a tilting mechanism toward the cytoplasm, which in turn allows interaction with the LR of DcuS (Witan *et al.* 2012b). The interaction model of H8b and LR was modeled with a smaller tilt angle than theoretically possible (Fig. 53). In principle, H8b can be tilted considerably more to increase the interaction area with LR. In the current model, the interaction between H8b and LR is crossed so that only one residue can interact in each region (Fig. 53). A larger tilt angle would increase the interaction surface and therefore increase the number of residues that could be involved in a DcuS LR-DctA H8b interaction.

4.5.2 DcuS signal transduction and involvement of DctA

TCS are employed by bacteria to perceive and transmit environmental information and initiate an adaptive cellular response according to the stimulus. The ON and OFF states are two thermodynamically stable structural states in which stimulus perception shifts the equilibrium from the OFF state to the ON state. This initiates a signal cascade from the signal input to the signal output site that changes the probability of each domain switching to the alternative state (Molnar *et al.* 2014; Lesne *et al.* 2017). NarQ and NarX are paralogous sensor histidine kinases that respond to nitrate and nitrite and, together with the response regulators NarP and NarL, induce genes involved in nitrate respiration (Rabin and Stewart 1993).

NarQ consists of a periplasmic sensor domain, TM1 and TM2, a HAMP domain, a signaling helix (S-helix), a GAF-like domain, and a kinase domain (Stewart 2003; Stewart and Chen 2010; Gushchin *et al.* 2017). The sensor domain of NarQ is connected to the cytoplasmic HAMP domain via TM2. The intracellular HAMP domain, which controls the kinase activity, is connected to TM2 via a flexible L-Pro hinge (Fig. 66A). Binding of the effector to the sensor domain induces a displacement of 0.5-1 Å, resulting in a rearrangement and piston-like displacement of TM1 by 2.5 Å (not shown) and of TM2 relative to TM1. The L-Pro hinge preceding the HAMP domain translates the incoming conformational change into a lever-like rotation that results in a 7 Å displacement of the membrane distal ends of the HAMP domain (Fig. 66B) (Gushchin *et al.* 2017). The HAMP domain essentially acts as a signal amplifier and transducer for the rearrangement of TM2.

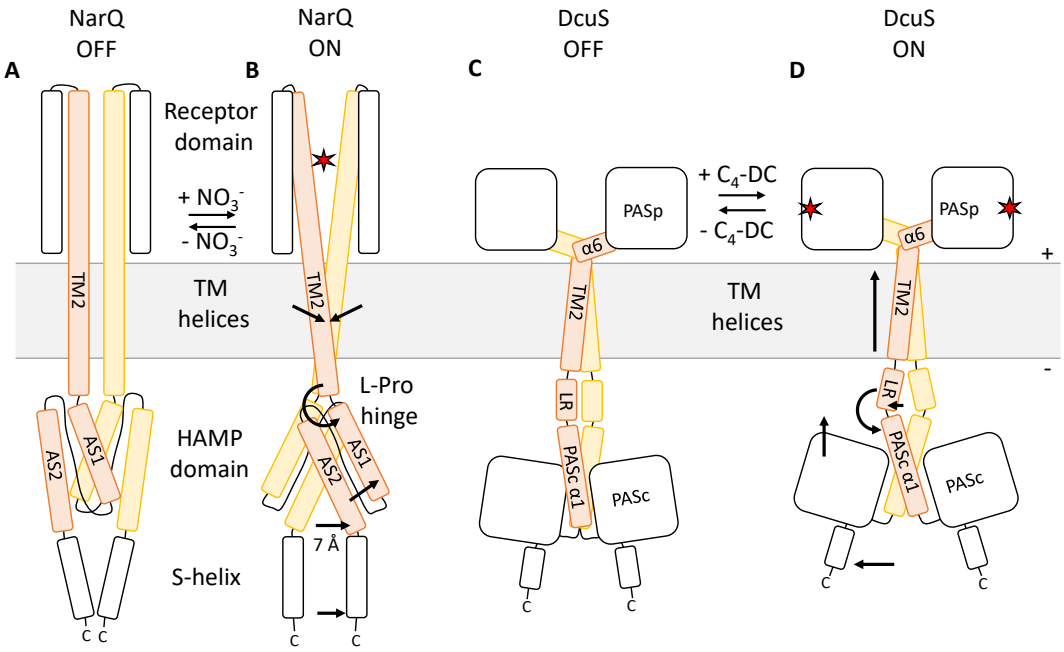

Fig. 66: Mechanism of NarQ and DcuS membrane signaling. (A and B) Binding of nitrate (NO_3^-) triggers a piston-like displacement of TM1 (not shown). The TM2-AS1 hinge (Pro179) transmits the piston-like displacement of TM1 relative to TM2 via a lever-like rotation of the HAMP domain. The lever-like rotation causes a displacement of AS2, resulting in a conformational shift of 7 Å and destabilizing the S-helix (Gushchin *et al.* 2017). **(C and B)** Binding of C_4-dicarboxylates (C_4-DC) triggers compaction of the PASp-binding domain, resulting in a piston-like displacement of TM2 via PASp α-helix 6 (α6) (Monzel and Unden 2015). The piston-like displacement destabilizes the linker region (LR), leading to a conformational rearrangement in the cytoplasmic PAS domain (PASc) (Stopp *et al.* 2021).

A different type of signal amplification is suggested for the cytoplasmic PAS domain of DcuS. The PASc α-helix 1 is connected to the periplasmic PAS domain via a continuous α-helix, comprising of PASp α6, TM2, and the LR (Fig. 66C) (Stopp *et al.* 2021). Crosslinking experiments for PASp α6 and TM2 showed a symmetric, piston-like displacement of 3-4 Å toward the periplasm upon effector binding (Monzel and Unden 2015; Stopp *et al.* 2021). Crosslinking data for the LR indicated fumarate-induced structural rearrangement,

including helical separation in the presence of fumarate (Fig. 66D) (Stopp *et al.* 2021). However, the LR is predicted to convert the piston-like displacement into a lever-like tilting of the PASc domain (Stopp *et al.* 2021). The lever-like rotation of the membrane distal ends of the NarQ HAMP domain is caused by a L-Pro hinge at position 179, which triggers a kinking mechanism of HAMP-AS1, amplifying the signal perceived in the sensor domain (Fig. 66B). Interestingly, at the interface of LR and PASc α1, there is an L-Pro residue at position 214 that is suitable for a similar kinking mechanism (Fig. 67). This conformational change would be analogous to NarQ, in which an L-Pro residue at the interface between the TM2-LR domain and PASc converts the piston-like displacement into a lever-like rotation of theC-terminal end of PASc, amplifying the conformational change and thus activating autophosphorylation of the kinase domain.

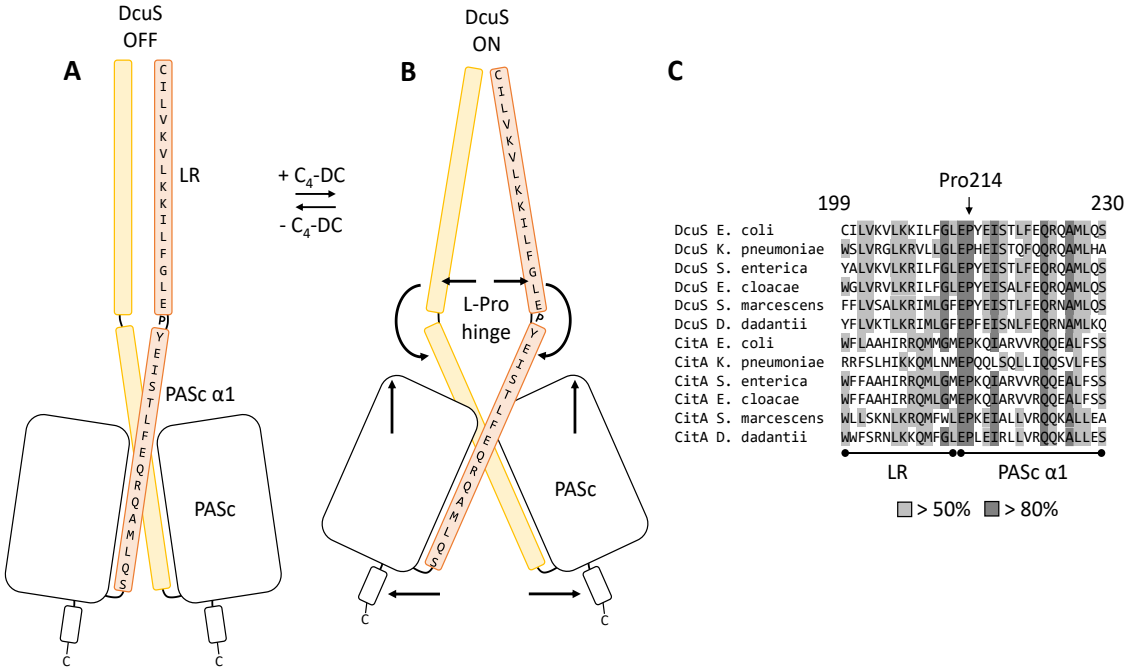

Fig. 67: Model of DcuS signal amplification via the postulated L-Pro hinge (A and B) and conservation of Pro214 in a MSA (C). (A and B) Model of LR-PASc α1 signal transduction via the predicted L-Pro hinge at the position 214. C_4-dicarboxylate (C_4-DC) binding initiates a piston-like displacement of TM2, leading to helical separation in the LR and lever-like rotation of the C-terminal end of PASc via the postulated L-Pro hinge. **(C)** The full length DcuS and CitA sequences were obtained from UniProt (UniProt Consortium 2019) and aligned via Unipro UGENE (Okonechnikov *et al.* 2012) using MUSCLE in the default settings (Edgar 2004). The region between linker and PASc α-helix 1 are shown (199-230).

L-Proline can induce special conformational characteristics to proteins, in which the backbone and sidechain are fused to a five-membered pyrrolidine ring (Senes *et al.* 2004). A database of L-Pro-induced kinks showed an average kinking angle of 21° ± 11° (Cordes *et al.* 2002). In general, L-Pro-induced kinks are more often observed in transmembrane helices than in water-soluble helices. L-Pro is not required to kink helices but L-Pro residues which are considerably conserved in helical domains are very likely kinked (Fig. 67C)

(Senes *et al.* 2004). The L-Pro hinge of NarQ is located in close proximity to the membrane (Gushchin *et al.* 2017), whereas the L-Pro residue of DcuS is presumably accessible to water. Nevertheless, both L-Pro residues are located in a similar position, upstream of a signal transducing domain that controls the autophosphorylation activity of the kinase domain. Fumarate-induced helical separation in the C-terminal part of the LR is used for a presumed lever-like rotation of the C-terminal end of PASc by a L-Pro hinge at position 214, controlling kinase activity (Fig. 67A and B). Pro214 is the only L-Pro residue in the continuous α-helix, which connects the periplasmic sensor domain to the cytoplasmic PAS domain.

DcuS and CitA are paralogous sensor histidine kinases with the main difference that DcuS requires coregulators, DctA and DcuB, for proper function (Kleefeld *et al.* 2009; Witan *et al.* 2012a; Steinmetz *et al.* 2014; Wörner *et al.* 2016). In absence of either one, the thermodynamical OFF state is not stable, leading to a constitutively active DcuS and effector-independent stimulation of DcuR regulated genes. The coregulator is necessary to convert and stabilize the DcuS OFF state. CitA signal transduction is present without any known accessory proteins that could affect the signal transduction process (Yamamoto *et al.* 2009; Scheu *et al.* 2012), suggesting that DctA is not actively involved in the signal transduction process but rather is required to transition DcuS to the OFF state. This differentiation would specify the role of DctA in signal transduction to a scaffolding function. Theoretically, it should be feasible to convert the mode of signal transduction to a CitA-like mode, in which interaction with a coregulator would be redundant.

4.6 Outlook

L-Asp is an important physiological nitrogen and electron acceptor source for commensal and pathogenic *E. coli*. Moreover, the intracellular L-Asp pool is the second highest, next to L-Glu. L-Asp is the nitrogen source for UMP (pyrimidine) biosynthesis and various other biosynthetic pathways. Recent work already postulated that the L-Asp pool must increase significantly to fuel the UMP biosynthesis in exponential growth (Yuan *et al.* 2009). The key enzyme for L-Asp production is AspC. AspC-GlnB showed an interaction in the BACTH assay but functional data still awaits to be obtained. *In vitro* enzymatic assays should be performed with AspC in the presence of GlnB and effector molecules to investigate whether a similar regulation to AspA-GlnB is observed. The expectation would be that GlnB without effector molecules or a UMP moiety would induce L-Asp production by AspC. Under nitrogen-saturated conditions, GlnB could induce L-Asp formation to boost UMP biosynthesis, allowing higher bacterial growth.

Another interesting topic would be the comparison of L-Asp metabolism of commensal and pathogenic *E. coli*. The EHEC reference strain EDL933 is able to metabolize L-Asp faster than commensal *E. coli* (Bertin *et al.* 2018). qPCR has already suggested that *aspA* and *dcuA* are more strongly induced in pathogenic *E. coli*. Whether this is sufficient to explain the increased efficiency of L-Asp degradation or whether there are additional differences, such as mutations in AspA and DcuA, or additional enzymes that increase L-Asp degradation, needs to be addressed in the future. This information would improve the understanding of L-Asp metabolism to potentially generate probiotics that minimize L-Asp concentration in the mammalian gut to counteract EHEC colonization.

Signal transduction in DcuS has been studied biochemically and structurally, and data are available for some aspects of signal transduction across the membrane. Recently, the involvement of the linker region (LR) has been elucidated, which undergoes helical separation and decrease in homodimerization in contrast to the piston-like displacement of TM2 (Monzel and Unden 2015; Stopp *et al.* 2021). The question remains which conformational change causes the LR in the cytoplasmic PAS domain. Bioinformatics and structural analysis of the model implicated a possible L-Pro hinge to induce a lever-like rotation at the membrane distal end of PASc. Electron paramagnetic resonance (EPR) spectroscopy experiments are currently underway to investigate the conformational state in ON and OFF mutants of a PASc-Kinase construct. These experiments will reveal whether a lever-like rotation of PASc is a viable mode of signal transduction.

5 Acknowledgement

My special thanks go to our cooperation partners:

Assoc. Prof. Dr. Sebastian Winter und Dr. Maria Winter (University of Texas) for their collaborative work investigating C_4-dicarboxylate metabolism in the mouse intestine, which resulted in the publication Schubert *et al*. (2021).

Dr. Maria Winter for preparing and shipping the mouse intestinal samples, which were later analyzed by MetaSysX GmbH and published in Schubert *et al*. (2021).

Dr. Sylwia Kierszniowska (MetaSysX GmbH) for the accommodation, regarding the absolute quantification of C_4-dicarboxylates in the mouse intestine.

Prof. Dr. Karl Forchhammer and Dr. Adrian Richard Schenberger Santos for theoretical assistance, regarding the uridylylation of GlnB.

I would like to thank the colleagues and students with whom I worked:

Florence Best and Marc Bohn, who provided the data for the cAMP-CRP signaling mutants in the *dctAp-lacZ* and *aspAp-lacZ* reporter strains.

Sandra Zedler, who performed the radioactive transport measurements of L-Asp and the L-Asp determination in the supernatant of *E. coli*, which were published in Schubert *et al*. (2020)

Marius Stopp for theoretical exchanges related to signal transduction of DcuS that helped model the DcuS ON and OFF state model later published in Stopp *et al*. (2021).

6 References

Abo-Amer, A.E., Munn, J., Jackson, K., Aktas, M., Golby, P., Kelly, D.J. and Andrews, S.C. 2004 DNA interaction and phosphotransfer of the C_4-dicarboxylate-responsive DcuS-DcuR two-component regulatory system from *Escherichia coli*. *J Bacteriol* **186**, 1879–1889.

Aidelberg, G., Towbin, B.D., Rothschild, D., Dekel, E., Bren, A. and Alon, U. 2014 Hierarchy of non-glucose sugars in *Escherichia coli*. *BMC Syst Biol* **8**, 1–12.

Albenberg, L., Esipova, T.V., Judge, C.P., Bittinger, K., Chen, J., Laughlin, A., Grunberg, S., Baldassano, R.N., Lewis, J.D. and Li, H. 2014 Correlation between intraluminal oxygen gradient and radial partitioning of intestinal microbiota. *Gastroenterology* **147**, 1055-1063. e8.

Alix, J.H. 1989 A rapid procedure for cloning genes from lambda libraries by complementation of *E. coli* defective mutants: application to the *fabE* region of the *E. coli* chromosome. *DNA* **8**, 779–789.

Altschul, S.F., Gish, W., Miller, W., Myers, E.W. and Lipman, D.J. 1990 Basic local alignment search tool. *J Mol Biol* **215**, 403–410.

Álvarez-Añorve, L.I., Bustos-Jaimes, I., Calcagno, M.L. and Plumbridge, J. 2009 Allosteric regulation of glucosamine-6-phosphate deaminase (NagB) and growth of *Escherichia coli* on glucosamine. *J Bacteriol* **191**, 6401–6407.

Anderson, W.B. and **Stadtman, E.R.** 1971 Purification and functional roles of the PI and PII components of *Escherichia coli* glutamine synthetase deadenylylation system. *Arch Biochem Biophys* **143**, 428–443.

Anslyn, E.V. and **Dougherty, D.A.** 2006 Modern physical organic chemistry. Mill Valley, California: University Science Books.

Antonopoulos, D.A., Huse, S.M., Morrison, H.G., Schmidt, T.M., Sogin, M.L. and Young, V.B. 2009 Reproducible community dynamics of the gastrointestinal microbiota following antibiotic perturbation. *Infect Immun* **77**, 2367–2375.

Archer, S.Y., Meng, S., Shei, A. and Hodin, R.A. 1998 p21WAF1 is required for butyrate-mediated growth inhibition of human colon cancer cells. *Proc Natl Acad Sci* **95**, 6791–6796.

Arcondéguy, T., Jack, R. and Merrick, M. 2001 P(II) signal transduction proteins, pivotal players in microbial nitrogen control. *Microbiol Mol Biol Rev* **65**, 80–105.

Atkinson, M.R., Kamberov, E.S., Weiss, R.L. and Ninfa, A.J. 1994 Reversible uridylylation of the *Escherichia coli* PII signal transduction protein regulates its ability to stimulate the dephosphorylation of the transcription factor nitrogen regulator I (NRI or NtrC). *J Biol Chem* **269**, 28288–28293.

Baba, T., Ara, T., Hasegawa, M., Takai, Y., Okumura, Y., Baba, M., Datsenko, K.A., Tomita, M., Wanner, B.L. and Mori, H. 2006 Construction of *Escherichia coli K-12* in-frame, single-gene knockout mutants: the Keio collection. *Mol Syst Biol* **2**.

Babicki, S., Arndt, D., Marcu, A., Liang, Y., Grant, J.R., Maciejewski, A. and Wishart, D.S. 2016 Heatmapper: web-enabled heat mapping for all. *Nucleic Acids Res* **44**, W147-W153.

Balsalobre, C., Johansson, J. and Uhlin, B.E. 2006 Cyclic AMP-dependent osmoregulation of crp gene expression in *Escherichia coli*. *J Bacteriol* **188**, 5935–5944.

Barreteau, H., Kovac, A., Boniface, A., Sova, M., Gobec, S. and Blanot, D. 2008 Cytoplasmic steps of peptidoglycan biosynthesis. *FEMS Microbiol Rev* **32**, 168–207.

Bauer, J. 2010 The C_4-Dicarboxylate Carriers DcuB and DctA of *Escherichia coli*: Function as Cosensors and Topology. *PhD thesis, Johannes Gutenberg-Universität Mainz, Germany*.

Bauer, J., Fritsch, M.J., Palmer, T. and Unden, G. 2011 Topology and accessibility of the transmembrane helices and the sensory site in the bifunctional transporter DcuB of *Escherichia coli*. *Biochemistry* **50**, 5925–5938.

Beer, A. 1852 Bestimmung der Absorption des rothen Lichts in farbigen Flüssigkeiten. *Ann Phys Chem* **162**, 78–88.

Bennett, B.D., Kimball, E.H., Gao, M., Osterhout, R., van Dien, S.J. and Rabinowitz, J.D. 2009 Absolute metabolite concentrations and implied enzyme active site occupancy in *Escherichia coli*. *Nat Chem Biol* **5**, 593.

Bergmeyer, H.U., Bergmeyer, J. and Grassl, M. 1983 Methods of enzymatic analysis. Vol. 8, Metabolites 3. Lipids. *Amino Acids and Related Compounds. Verlag Chemie*.

Berman, H.M., Westbrook, J., Feng, Z., Gilliland, G., Bhat, T.N., Weissig, H., Shindyalov, I.N. and Bourne, P.E. 1999 The Protein Data Bank. *Nucleic Acids Res* **28**, 235–242.

Bertin, Y., Girardeau, J.P., Chaucheyras-Durand, F., Lyan, B., Pujos-Guillot, E., Harel, J. and Martin, C. 2011 Enterohaemorrhagic *Escherichia coli* gains a competitive advantage by using ethanolamine as a nitrogen source in the bovine intestinal content. *Environ Microbiol* **13**, 365–377.

Bertin, Y., Segura, A., Jubelin, G., Dunière, L., Durand, A. and Forano, E. 2018 Aspartate metabolism is involved in the maintenance of enterohaemorrhagic *Escherichia coli* O157: H7 in bovine intestinal content. *Environ Microbiol* **20**, 4473–4485.

Best, F. 2018 Kontrolle des Transporters DctA durch das Glucose-PTS in Escherichia coli. *Bachelor thesis, Johannes Gutenberg-University, Mainz, Germany.*

Blattner, F.R., Plunkett, G., Bloch, C.A., Perna, N.T., Burland, V., Riley, M., Collado-Vides, J., Glasner, J.D., Rode, C.K. and Mayhew, G.F. 1997 The complete genome sequence of *Escherichia coli* K-12. *Science* **277**, 1453–1462.

Boer, M. de, Broekhuizen, C.P. and Postma, P.W. 1986 Regulation of glycerol kinase by enzyme III^{Glc} of the phosphoenolpyruvate:carbohydrate phosphotransferase system. *J Bacteriol* **167**, 393–395.

Bohn, M. 2019 Die Regulation der Aspartat Ammonium Lyase Aspartase in Escherichia coli. *Bachelor thesis, Johannes Gutenberg-University, Mainz, Germany.*

Bonder, M.J., Kurilshikov, A., Tigchelaar, E.F., Mujagic, Z., Imhann, F., Vila, A.V., Deelen, P., Vatanen, T., Schirmer, M. and Smeekens, S.P. 2016 The effect of host genetics on the gut microbiome. *Nat Genet* **48**, 1407–1412.

Bordoli, L., Kiefer, F., Arnold, K., Benkert, P., Battey, J. and Schwede, T. 2009 Protein structure homology modeling using SWISS-MODEL workspace. *Nat Protoc* **4**, 1–13.

Bott, M. 1997 Anaerobic citrate metabolism and its regulation in enterobacteria. *Arch Microbiol* **167**, 78–88.

Bott, M., Meyer, M. and Dimroth, P. 1995 Regulation of anaerobic citrate metabolism in *Klebsiella pneumoniae*. *Mol Microbiol* **18**, 533–546.

Boudker, O., Ryan, R.M., Yernool, D., Shimamoto, K. and Gouaux, E. 2007 Coupling substrate and ion binding to extracellular gate of a sodium-dependent aspartate transporter. *Nature* **445**(7126), 387–393.

Bourrellier, A.B.F., Valot, B., Guillot, A., Ambard-Bretteville, F., Vidal, J. and Hodges, M. 2010 Chloroplast acetyl-CoA carboxylase activity is 2-oxoglutarate–regulated by interaction of PII with the biotin carboxyl carrier subunit. *Proc Natl Acad Sci* **107**, 502–507.

Bourriaud, C., Robins, R.J., Martin, L., Kozlowski, F., Tenailleau, E., Cherbut, C. and Michel, C. 2005 Lactate is mainly fermented to butyrate by human intestinal microfloras but inter-individual variation is evident. *J Appl Microbiol* **99**, 201–212.

Bradford, M.M. 1976 A rapid and sensitive method for the quantitation of microgram quantities of protein utilizing the principle of protein-dye binding. *Anal Biochem* **72**, 248–254.

Brinkman, A.B., Ettema, T.J.G., Vos, W.M. de and van der Oost, J. 2003 The Lrp family of transcriptional regulators. *Mol Microbiol* **48**, 287–294.

Brinsmade, S.R. and **Escalante-Semerena, J.C.** 2004 The *eutD* gene of *Salmonella enterica* encodes a protein with phosphotransacetylase enzyme activity. *J Bacteriol* **186**, 1890–1892.

Brody, T. 1998 Nutritional biochemistry: Elsevier.

Brown, M.S., Segal, A. and Stadtman, E.R. 1971 Modulation of glutamine synthetase adenylylation and deadenylylation is mediated by metabolic transformation of the P II -regulatory protein. *Proc Natl Acad Sci* **68**, 2949–2953.

Browning, D.F., Butala, M. and Busby, S.J.W. 2019 Bacterial transcription factors: regulation by pick "N" mix. *J Mol Biol* **431**, 4067–4077.

Brückner, R. and **Titgemeyer, F.** 2002 Carbon catabolite repression in bacteria: choice of the carbon source and autoregulatory limitation of sugar utilization. *FEMS Microbiol Lett* **209**, 141–148.

Busby, S. and **Ebright, R.H.** 1999 Transcription activation by catabolite activator protein (CAP). *J Mol Biol* **293**, 199–213.

Byrne, C.S., Chambers, E.S., Morrison, D.J. and Frost, G. 2015 The role of short chain fatty acids in appetite regulation and energy homeostasis. *Int J Obes* **39**, 1331–1338.

Calhoun, M.W. and **Gennis, R.B.** 1993 Demonstration of separate genetic loci encoding distinct membrane-bound respiratory NADH dehydrogenases in *Escherichia coli*. *J Bacteriol* **175**, 3013–3019.

Canfora, E.E., Jocken, J.W. and Blaak, E.E. 2015 Short-chain fatty acids in control of body weight and insulin sensitivity. *Nat Rev Endocrinol* **11**, 577.

Cani, P.D. 2014 The gut microbiota manages host metabolism. *Nat Rev Endocrinol* **10**, 74–76.

Carter, A.M. 2007 Animal models of human placentation–a review. *Placenta* **28**, S41-S47.

Casino, P., Rubio, V. and Marina, A. 2010 The mechanism of signal transduction by two-component systems. *Curr Opin Struct Biol* **20**, 763–771.

Cedar, H. and **Schwartz, J.H.** 1967 Localization of the two L-asparaginases in anaerobically grown *Escherichia coli*. *J Biol Chem* **242**, 3753–3755.

Celani, A. and **Vergassola, M.** 2010 Bacterial strategies for chemotaxis response. *Proc Natl Acad Sci* **107**, 1391–1396.

Chen, S., Gunasekera, A., Zhang, X., Kunkel, T.A., Ebright, R.H. and Berman, H.M. 2001 Indirect readout of DNA sequence at the primary-kink site in the CAP-DNA complex: alteration of DNA binding specificity through alteration of DNA kinking. *J Mol Biol* **314**, 75–82.

Cheung, J. and **Hendrickson, W.A.** 2008 Crystal Structure of the *E.coli* DcuS Sensor Domain. *J Biol Chem*, **283**(20), 13762-13770.

Cheung, J. and **Hendrickson, W.A.** 2010 Sensor domains of two-component regulatory systems. *Curr Opin Microbiol* **13**, 116–123.

Cho, B.-K., Barrett, C.L., Knight, E.M., Park, Y.S. and Palsson, B.Ø. 2008 Genome-scale reconstruction of the Lrp regulatory network in *Escherichia coli*. *Proc Natl Acad Sci* **105**, 19462–19467.

Clark, D.J. and **Marr, A.G.** 1964 Studies on the repression of β-galactosidase in *Escherichia coli*. *Biochim Biophys Acta* **92**, 85–98.

Clifton, C.E. 1937 A comparison of the metabolic activities of *Aerobacter aerogenes*, *Eberthella typhi* and *Escherichia coli*. *J Bacteriol* **33**, 145.

Clifton, C.E. and **Morrow, G.** 1936 The kinetics of lysis of *Escherichia coli*. *J Bacteriol* **31**, 441.

Cockburn, D.W. and **Koropatkin, N.M.** 2016 Polysaccharide degradation by the intestinal microbiota and its influence on human health and disease. *J Mol Biol* **428**, 3230–3252.

Cole, S.T. and **Raibaud, O.** 1986 The nucleotide sequence of the *malT* gene encoding the positive regulator of the *Escherichia coli* maltose regulon. *Gene* **42**, 201–208.

Colombo, B.M., Scalvenzi, T., Benlamara, S. and Pollet, N. 2015 Microbiota and mucosal immunity in amphibians. *Front Immunol* **6**, 111.

Colston, T.J. and **Jackson, C.R.** 2016 Microbiome evolution along divergent branches of the vertebrate tree of life: what is known and unknown. *Mol Ecol* **25**, 3776–3800.

Connors, J., Dawe, N. and van Limbergen, J. 2018 The Role of Succinate in the Regulation of Intestinal Inflammation. *Nutrients* **11**.

Conway, T., Krogfelt, K.A. and Cohen, P.S. 2004 The life of commensal *Escherichia coli* in the mammalian intestine. *EcoSal Plus* **1**.

Cordes, F.S., Bright, J.N. and Sansom, M.S.P. 2002 Proline-induced distortions of transmembrane helices. *J Mol Biol* **323**, 951–960.

Cotter, P.A., Chepuri, V., Gennis, R.B. and Gunsalus, R.P. 1990 Cytochrome o (*cyoABCDE*) and d (*cydAB*) oxidase gene expression in *Escherichia coli* is regulated by oxygen, pH, and the *fnr* gene product. *J Bacteriol* **172**, 6333–6338.

Coutts, G., Thomas, G., Blakey, D. and Merrick, M. 2002 Membrane sequestration of the signal transduction protein GlnK by the ammonium transporter AmtB. *EMBO J* **21**, 536–545.

da Silva, G.P., Mack, M. and Contiero, J. 2009 Glycerol: a promising and abundant carbon source for industrial microbiology. *Biotechnol Adv* **27**, 30–39.

Davies, S.J., Golby, P., Omrani, D., Broad, S.A., Harrington, V.L., Guest, J.R., Kelly, D.J. and Andrews, S.C. 1999 Inactivation and regulation of the aerobic C_4-dicarboxylate transport (*dctA*) gene of *Escherichia coli*. *J Bacteriol* **181**, 5624–5635.

Desai, T.A. and **Rao, C.V.** 2010 Regulation of arabinose and xylose metabolism in *Escherichia coli*. *Appl Environ Microbiol* **76**, 1524–1532.

Detman, A., Mielecki, D., Chojnacka, A., Salamon, A., Błaszczyk, M.K. and Sikora, A. 2019 Cell factories converting lactate and acetate to butyrate: *Clostridium butyricum* and microbial communities from dark fermentation bioreactors. *Microb Cell Fact* **18**, 36.

Deutscher, J., Aké, F.M.D., Derkaoui, M., Zébré, A.C., Cao, T.N., Bouraoui, H., Kentache, T., Mokhtari, A., Milohanic, E. and Joyet, P. 2014 The bacterial phosphoenolpyruvate: Carbohydrate phosphotransferase system: regulation by protein phosphorylation and phosphorylation-dependent protein-protein interactions. *Microbiol Mol Biol Rev* **78**, 231–256.

Deutscher, J., Francke, C. and Postma, P.W. 2006 How phosphotransferase system-related protein phosphorylation regulates carbohydrate metabolism in bacteria. *Microbiol Mol Biol Rev* **70**, 939–1031.

Dills, S.S., Schmidt, M.R. and Saier Jr, M.H. 1982 Regulation of Lactose Transport by the Phosphoenolpyruvate-Sugar Phosphotransferase System in Membrane Vesicles of *Escherichia coli*. *J Cell Biochem* **18**, 239–244.

Doucette, C.D., Schwab, D.J., Wingreen, N.S. and Rabinowitz, J.D. 2011 α-Ketoglutarate coordinates carbon and nitrogen utilization via enzyme I inhibition. *Nat Chem Biol* **7**, 894.

Ebright, R.H. 1993 Transcription activation at class I CAP-dependent promoters. *Mol Microbiol* **8**, 797–802.

Ebright, R.H., Ebright, Y.W. and Gunasekera, A. 1989 Consensus DNA site for the *Escherichia coli* catabolite gene activator protein (CAP): CAP exhibits a 450-fold higher affinity for the consensus DNA site than for the *E. coli* lac DNA site. *Nucl Acids Res* **17**, 10295–10305.

Egan, S.M. and **Stewart, V.** 1990 Nitrate regulation of anaerobic respiratory gene expression in *narX* deletion mutants of *Escherichia coli* K-12. *J Bacteriol* **172**, 5020–5029.

Engel, P., Krämer, R. and Unden, G. 1992 Anaerobic fumarate transport in *Escherichia coli* by an *fnr*-dependent dicarboxylate uptake system which is different from the aerobic dicarboxylate uptake system. *J Bacteriol* **174**, 5533–5539.

Engel, P., Krämer, R. and Unden, G. 1994 Transport of C_4-dicarboxylates by anaerobically grown *Escherichia coli*. *FEBS J.* **222**, 605–614.

Eppler, T. and **Boos, W.** 1999 Glycerol-3-phosphate-mediated repression of *malT* in *Escherichia coli* does not require metabolism, depends on enzyme IIA^{Glc} and is mediated by cAMP levels. *Mol Microbiol* **33**, 1221–1231.

Eppler, T., Postma, P., Schutz, A., Volker, U. and Boos, W. 2002 Glycerol-3-Phosphate-Induced Catabolite Repression in *Escherichia coli*. *J Bacteriol* **184**, 3044–3052.

Etzkorn, M., Kneuper, H., Dünnwald, P., Vijayan, V., Krämer, J., Griesinger, C., Becker, S., Unden, G. and Baldus, M. 2008 Plasticity of the PAS domain and a potential role for signal transduction in the histidine kinase DcuS. *Nat Struct Mol Biol* **15**, 1031.

Fabich, A.J., Jones, S.A., Chowdhury, F.Z., Cernosek, A., Anderson, A., Smalley, D., McHargue, J.W., Hightower, G.A., Smith, J.T. and Autieri, S.M. 2008 Comparison of carbon nutrition for pathogenic and commensal *Escherichia coli* strains in the mouse intestine. *Infect Immun* **76**, 1143–1152.

Feese, M., Pettigrew, D.W., Meadow, N.D., Roseman, S. and Remington, S.J. 1994 Cation-promoted association of a regulatory and target protein is controlled by protein phosphorylation. *Proc Natl Acad Sci* **91**, 3544–3548.

Fic, E., Bonarek, P., Górecki, A., Kedracka-Krok, S., Mikolajczak, J., Polit, A., Tworzydlo, M., Dziedzicka-Wasylewska, M. and Wasylewski, Z. 2009 cAMP receptor protein from *Escherichia coli* as a model of signal transduction in proteins–a review. *J Mol Microbiol Biotechnol* **17**, 1–11.

Flores, S., Flores, N., Anda, R. de, González, A., Escalante, A., Sigala, J.C., Gosset, G. and Bolívar, F. 2005 Nutrient-scavenging stress response in an *Escherichia coli* strain lacking the phosphoenolpyruvate: carbohydrate phosphotransferase system, as explored by gene expression profile analysis. *J Mol Microbiol Biotechnol* **10**, 51–63.

Fokina, O., Chellamuthu, V.-R., Forchhammer, K. and Zeth, K. 2010 Mechanism of 2-oxoglutarate signaling by the *Synechococcus elongatus* PII signal transduction protein. *Proc Natl Acad Sci* **107**, 19760–19765.

Forchhammer, K. and **Lüddecke, J.** 2016 Sensory properties of the PII signalling protein family. *FEBS J* **283**, 425–437.

Fraune, S. and **Bosch, T.C.G.** 2010 Why bacteria matter in animal development and evolution. *Bioessays* **32**, 571–580.

Freter, R., Brickner, H., Fekete, J., Vickerman, M.M. and Carey, K.E. 1983 Survival and implantation of *Escherichia coli* in the intestinal tract. *Infect Immun* **39**, 686–703.

Fuchs, G. and **Schlegel, H.-G.** 2006 Allgemeine Mikrobiologie: Begründet von Hans-Günter Schlegel: Georg Thieme Verlag.

Gama-Castro, S., Salgado, H., Santos-Zavaleta, A., Ledezma-Tejeida, D., Muñiz-Rascado, L., García-Sotelo, J.S., Alquicira-Hernández, K., Martínez-Flores, I., Pannier, L. and Castro-Mondragón, J.A. 2016 RegulonDB version 9.0: high-level integration of gene regulation, coexpression, motif clustering and beyond. *Nucl Acids Res* **44**, D133-D143.

Garcia, D., Watts, K.J., Johnson, M.S. and Taylor, B.L. 2016 Delineating PAS-HAMP interaction surfaces and signalling-associated changes in the aerotaxis receptor Aer. *Mol Microbiol* **100**(1), 156-172.

Garcia, E., Federici, M., Rhee, S.G. and Berberich, M.A. 1980 Glutamine synthetase cascade: Enrichment of uridylyltransferase in *Escherichia coli* carrying hybrid ColE1 plasmids. *Arch Biochem Biophys* **203**, 181–189.

Garcia, E. and **Rhee, S.G.** 1983 Cascade control of *Escherichia coli* glutamine synthetase. Purification and properties of PII uridylyltransferase and uridylyl-removing enzyme. *J Biol Chem* **258**, 2246–2253.

Gentile, C.L. and **Weir, T.L.** 2018 The gut microbiota at the intersection of diet and human health. *Science* **362**, 776–780.

Gerhardt, E.C.M., Araújo, L.M., Ribeiro, R.R., Chubatsu, L.S., Scarduelli, M., Rodrigues, T.E., Monteiro, R.A., Pedrosa, F.O., Souza, E.M. and Huergo, L.F. 2012 Influence of the ADP/ATP ratio, 2-oxoglutarate and divalent ions on *Azospirillum brasilense* PII protein signalling. *Microbiology* **158**, 1656–1663.

Gerhardt, E.C.M., Rodrigues, T.E., Müller-Santos, M., Pedrosa, F.O., Souza, E.M., Forchhammer, K. and Huergo, L.F. 2015 The bacterial signal transduction protein GlnB regulates the committed step in fatty acid biosynthesis by acting as a dissociable regulatory subunit of acetyl-CoA carboxylase. *Mol Microbiol* **95**, 1025–1035.

Giraud-Panis, M.-J., Toulmé, F., Maurizot, J.C. and Culard, F. 1992 Specific binding of cyclic-AMP receptor protein to DNA. Effect of the sequence and of the introduction of a nick in the binding site. *J Biomol Struct Dyn* **10**, 295–309.

Goh, E.-B., Bledsoe, P.J., Chen, L.-L., Gyaneshwar, P., Stewart, V. and Igo, M.M. 2005 Hierarchical Control of Anaerobic Gene Expression in *Escherichia coli* K-12: the Nitrate-Responsive NarX-NarL Regulatory System Represses Synthesis of the Fumarate-Responsive DcuS-DcuR Regulatory System. *J Bacteriol* **187**(14), 4890–4899.

Golby, P., Davies, S., Kelly, D.J., Guest, J.R. and Andrews, S.C. 1999 Identification and characterization of a two-component sensor-kinase and response-regulator system (DcuS-DcuR) controlling gene expression in response to C_4-dicarboxylates in *Escherichia coli*. *J Bacteriol* **181**, 1238–1248.

Golby, P., Kelly, D.J., Guest, J.R. and Andrews, S.C. 1998a Topological analysis of DcuA, an anaerobic C_4-dicarboxylate transporter of *Escherichia coli*. *J Bacteriol* **180**, 4821–4827.

Golby, P., Kelly, D.J., Guest, J.R. and Andrews, S.C. 1998b Transcriptional Regulation and Organization of the *dcuA* and *dcuB* Genes, Encoding Homologous Anaerobic C_4-Dicarboxylate Transporters in *Escherichia coli*. *J Bacteriol* **180**, 6586–6596.

Görke, B. and **Stülke, J.** 2008 Carbon catabolite repression in bacteria: many ways to make the most out of nutrients. *Nat Rev Microbiol* **6**, 613–624.

Gosset, G., Zhang, Z., Nayyar, S., Cuevas, W.A. and Saier, M.H. 2004 Transcriptome Analysis of Crp-Dependent Catabolite Control of Gene Expression in *Escherichia coli*. *J Bacteriol* **186**, 3516–3524.

Goux, W.J., Strong, A.A., Schneider, B.L., Lee, W.N. and Reitzer, L.J. 1995 Utilization of aspartate as a nitrogen source in *Escherichia coli*. Analysis of nitrogen flow and characterization of the products of aspartate catabolism. *J Biol Chem* **270**, 638–646.

Goyal, S., Yuan, J., Chen, T., Rabinowitz, J.D. and Wingreen, N.S. 2010 Achieving optimal growth through product feedback inhibition in metabolism. *PLOS Comput Biol* **6**(6).

Graf, S., Schmieden, D., Tschauner, K., Hunke, S. and Unden, G. 2014 The sensor kinase DctS forms a tripartite sensor unit with DctB and DctA for sensing C_4-dicarboxylates in *Bacillus subtilis*. *J Bacteriol* **196**, 1084–1093.

Grainger, D.C., Hurd, D., Harrison, M., Holdstock, J. and Busby, S.J.W. 2005 Studies of the distribution of *Escherichia coli* cAMP-receptor protein and RNA polymerase along the *E. coli* chromosome. *Proc Natl Acad Sci* **102**, 17693–17698.

Gray, C.H. and **Tatum, E.L.** 1944 X-ray induced growth factor requirements in bacteria. *Proc Natl Acad Sci* **30**, 404.

Green, J., Scott, C. and Guest, J.R. 2000 Functional versatility in the CRP-FNR superfamily of transcription factors: FNR and FLP. *Advances in microbial physiology ed*. Poole, R.K. pp. 1–34. London: Academic Press.

Green, J., Trageser, M., Six, S., Unden, G. and Guest, J.R., eds. 1991 Characterization of the FNR protein of *Escherichia coli*, an iron-binding transcriptional regulator: *Proc Royal Soc B* **244**(1310), 137-144.

Griffith, K.L. and **Wolf, R.E.** 2002 Measuring β-galactosidase activity in bacteria: cell growth, permeabilization, and enzyme assays in 96-well arrays. *Biochem Biophys Res Commun* **290**, 397–402.

Gröpper, C. 2013 Bedeutung der Linker-Region der zweiten Transmembranhelix der Sensor-Histidinkinase DcuS für die Wechselwirkung mit dem C_4-Dicarboxylat-Transporter DctA als Co-Sensor von DcuS in *Escherichia coli*. *Master thesis, Johannes Gutenberg-University, Mainz, Germany.*

Guest, J.R. 1979 Anaerobic growth of *Escherichia coli* K12 with fumarate as terminal electron acceptor. Genetic studies with menaquinone and fluoroacetate-resistant mutants. *Microbiology* **115**, 259–271.

Guest, J.R. 1992 Oxygen-regulated gene expression in *Escherichia coli*. *J Gen Microbiol* **138**, 2253–2263.

Gunsalus, R.P. 1992 Control of electron flow in *Escherichia coli*: coordinated transcription of respiratory pathway genes. *J Bacteriol* **174**, 7069.

Gushchin, I., Melnikov, I., Polovinkin, V., Ishchenko, A., Yuzhakova, A., Buslaev, P., Bourenkov, G., Grudinin, S., Round, E. and Balandin, T. 2017 Mechanism of transmembrane signaling by sensor histidine kinases. *Science* **356**.

Guzman, L.M., Belin, D., Carson, M.J. and Beckwith, J. 1995 Tight regulation, modulation, and high-level expression by vectors containing the arabinose PBAD promoter. *J Bacteriol* **177**, 4121–4130.

Ha, J.-H., Hauk, P., Cho, K., Eo, Y., Ma, X., Stephens, K., Cha, S., Jeong, M., Suh, J.-Y. and Sintim, H.O. 2018 Evidence of link between quorum sensing and sugar metabolism in *Escherichia coli* revealed via cocrystal structures of LsrK and HPr. *Science advances* **4**, eaar7063.

Harman, J.G. 2001 Allosteric regulation of the cAMP receptor protein. *Biochim Biophys Acta* **1547**, 1–17.

Hart, B.R. and **Blumenthal, R.M.** 2011 Unexpected coregulator range for the global regulator Lrp of *Escherichia coli* and *Proteus mirabilis*. *J Bacteriol* **193**, 1054–1064.

Hayashi, S.I. and **Lin, E.C.** 1967 Purification and properties of glycerol kinase from *Escherichia coli*. *J Biol Chem* **242**, 1030–1035.

Hazelbauer, G.L., Falke, J.J. and Parkinson, J.S. 2008 Bacterial chemoreceptors: high-performance signaling in networked arrays. *Trends Biochem Sci* **33**, 9–19.

He, G., Shankar, R.A., Chzhan, M., Samouilov, A., Kuppusamy, P. and Zweier, J.L. 1999 Noninvasive measurement of anatomic structure and intraluminal oxygenation in the gastrointestinal tract of living mice with spatial and spectral EPR imaging. *Proc Natl Acad Sci* **96**, 4586–4591.

Hermsen, R., Okano, H., You, C., Werner, N. and Hwa, T. 2015 A growth-rate composition formula for the growth of *E. coli* on co-utilized carbon substrates. *Mol Syst Biol* **11**, 801.

Hobbs, E.C., Yin, X., Paul, B.J., Astarita, J.L. and Storz, G. 2012 Conserved small protein associates with the multidrug efflux pump AcrB and differentially affects antibiotic resistance. *Proc Natl Acad Sci* **109**, 16696–16701.

Hoch, J.A., Silhavy, T.J. and Bourret, R.B. 1995 Two-component signal transduction: ASM press Washington, DC.

Hogema, B.M., Arents, J.C., Bader, R., Eijkemans, K., Yoshida, H., Takahashi, H., Aiba, H. and Postma, P.W. 1998 Inducer exclusion in *Escherichia coli* by non-PTS substrates: The role of the PEP to pyruvate ratio in determining the phosphorylation state of enzyme IIA^{Glc}. *Mol Microbiol* **30**, 487–498.

Hu, P., Janga, S.C., Babu, M., Díaz-Mejía, J.J., Butland, G., Yang, W., Pogoutse, O., Guo, X., Phanse, S. and Wong, P. 2009 Global functional atlas of *Escherichia coli* encompassing previously uncharacterized proteins. *PLoS Biol* **7**, e1000096.

Huergo, L.F., Chandra, G. and Merrick, M. 2013 PII signal transduction proteins: nitrogen regulation and beyond. *FEMS Microbiol Rev* **37**, 251–283.

Huergo, L.F. and **Dixon, R.** 2015 The emergence of 2-oxoglutarate as a master regulator metabolite. *Microbiol Mol Biol Rev* **79**, 419–435.

Huergo, L.F., Merrick, M., Pedrosa, F.O., Chubatsu, L.S., Araujo, L.M. and Souza, E.M. 2007 Ternary complex formation between AmtB, GlnZ and the nitrogenase regulatory enzyme DraG reveals a novel facet of nitrogen regulation in bacteria. *Mol Microbiol* **66**, 1523–1535.

Huerta-Cepas, J., Szklarczyk, D., Forslund, K., Cook, H., Heller, D., Walter, M.C., Rattei, T., Mende, D.R., Sunagawa, S., Kuhn, M., Jensen, L.J., Mering, C. von and Bork, P. 2016 eggNOG 4.5: a hierarchical

orthology framework with improved functional annotations for eukaryotic, prokaryotic and viral sequences. *Nucleic Acids Res* **44**, D286-93.

Hughes, E.R., Winter, M.G., Duerkop, B.A., Spiga, L., Carvalho, T.F. de, Zhu, W., Gillis, C.C., Büttner, L., Smoot, M.P. and Behrendt, C.L. 2017 Microbial respiration and formate oxidation as metabolic signatures of inflammation-associated dysbiosis. *Cell Host Microbe* **21**, 208–219.

Hung, S., Baldi, P. and Hatfield, G.W. 2002 Global Gene Expression Profiling in *Escherichia coli* K-12 the effects of leucine-responsive regulatory protein. *J Biol Chem* **277**, 40309–40323.

Hurley, J.H., Faber, H.R., Worthylake, D., Meadow, N.D., Roseman, S., Pettigrew, D.W. and Remington, S.J. 1993 Structure of the regulatory complex of *Escherichia coli* III^{Glc} with glycerol kinase. *Science* **259**, 673–677.

Igarashi, K. and **Ishihama, A.** 1991 Bipartite functional map of the *E. coli* RNA polymerase α subunit: involvement of the C-terminal region in transcription activation by cAMP-CRP. *Cell* **65**, 1015–1022.

Igo, M.M., Ninfa, A.J., Stock, J.B. and Silhavy, T.J. 1989 Phosphorylation and dephosphorylation of a bacterial transcriptional activator by a transmembrane receptor. *Genes Dev* **3**, 1725–1734.

Ihssen, J. and **Egli, T.** 2005 Global physiological analysis of carbon-and energy-limited growing *Escherichia coli* confirms a high degree of catabolic flexibility and preparedness for mixed substrate utilization. *Environ Microbiol* **7**, 1568–1581.

Inouye, M. and **Dutta, R.** 2002 Histidine kinases in signal transduction: Elsevier.

Ishihama, A., Kori, A., Koshio, E., Yamada, K., Maeda, H., Shimada, T., Makinoshima, H., Iwata, A. and Fujita, N. 2014 Intracellular concentrations of 65 species of transcription factors with known regulatory functions in *Escherichia coli*. *J Bacteriol* **196**, 2718–2727.

Iuchi, S. and **Lin, E.C.** 1992 Mutational analysis of signal transduction by ArcB, a membrane sensor protein responsible for anaerobic repression of operons involved in the central aerobic pathways in *Escherichia coli*. *J Bacteriol* **174**, 3972–3980.

Jaggi, R., Ybarlucea, W., Cheah, E., Carr, P.D., Edwards, K.J., Ollis, D.L. and Vasudevan, S.G. 1996 The role of the T-loop of the signal transducing protein PII from *Escherichia coli*. *FEBS Letts* **391**, 223–228.

Janausch, I., Kim, O. and Unden, G. 2001 DctA-and Dcu-independent transport of succinate in *Escherichia coli*: contribution of diffusion and of alternative carriers. *Arch Microbiol* **176**, 224–230.

Janausch, I.G., Garcia-Moreno, I., Lehnen, D., Zeuner, Y. and Unden, G. 2004 Phosphorylation and DNA binding of the regulator DcuR of the fumarate-responsive two-component system DcuSR of *Escherichia coli*. *Microbiology* **150**, 877–883.

Janausch, I.G., Zientz, E., Tran, Q.H., Kröger, A. and Unden, G. 2002 C_4-dicarboxylate carriers and sensors in bacteria. *Biochim Biophys Acta* **1553**, 39–56.

Javelle, A., Severi, E., Thornton, J. and Merrick, M. 2004 Ammonium sensing in *Escherichia coli*. Role of the ammonium transporter AmtB and AmtB-GlnK complex formation. *J Biol Chem* **279**, 8530–8538.

Javelle, A., Thomas, G., Marini, A.-M., Krämer, R. and Merrick, M. 2005 *In vivo* functional characterization of the *Escherichia coli* ammonium channel AmtB: evidence for metabolic coupling of AmtB to glutamine synthetase. *Biochem J* **390**, 215–222.

Jensen, K.F., Dandanell, G., Hove-Jensen, B. and Willemoës, M. 2008 Nucleotides, Nucleosides, and Nucleobases. *EcoSal Plus* **3**.

Jensen, S., Guskov, A., Rempel, S., Hänelt, I. and Slotboom, D.J. 2013 Crystal structure of a substrate-free aspartate transporter. *Nat Struct Mol Biol* **20**, 1224–1226.

Jeske, L., Placzek, S., Schomburg, I., Chang, A. and Schomburg, D. 2019 BRENDA in 2019: a European ELIXIR core data resource. *Nucl Acids Res* **47**, D542-D549.

Jiang, P., Atkinson, M.R., Srisawat, C., Sun, Q. and Ninfa, A.J. 2000 Functional dissection of the dimerization and enzymatic activities of *Escherichia coli* nitrogen regulator II and their regulation by the PII protein. *Biochemistry* **39**, 13433–13449.

Jiang, P. and **Ninfa, A.J.** 1999 Regulation of autophosphorylation of *Escherichia coli* nitrogen regulator II by the PII signal transduction protein. *J Bacteriol* **181**, 1906–1911.

Jiang, P. and **Ninfa, A.J.** 2007 *Escherichia coli* PII signal transduction protein controlling nitrogen assimilation acts as a sensor of adenylate energy charge *in vitro*. *Biochemistry* **46**, 12979–12996.

Jiang, P. and **Ninfa, A.J.** 2009 α-ketoglutarate controls the ability of the *Escherichia coli* PII signal transduction protein to regulate the activities of NRII (NtrB) but does not control the binding of PII to NRII. *Biochemistry* **48**, 11514–11521.

Jiang, P., Peliska, J.A. and Ninfa, A.J. 1998 Enzymological characterization of the signal-transducing uridylyltransferase/uridylyl-removing enzyme (EC 2.7.7.59) of *Escherichia coli* and its interaction with the PII protein. *Biochemistry* **37**, 12782–12794.

Jones, S.A., Chowdhury, F.Z., Fabich, A.J., Anderson, A., Schreiner, D.M., House, A.L., Autieri, S.M., Leatham, M.P., Lins, J.J. and Jorgensen, M. 2007 Respiration of *Escherichia coli* in the mouse intestine. *Infect Immun* **75**, 4891–4899.

Jones, S.A., Gibson, T., Maltby, R.C., Chowdhury, F.Z., Stewart, V., Cohen, P.S. and Conway, T. 2011 Anaerobic respiration of *Escherichia coli* in the mouse intestine. *Infect Immun* **79**, 4218–4226.

Jourlin, C., Bengrine, A., Chippaux, M. and Méjean, V. 1996 An unorthodox sensor protein (TorS) mediates the induction of the tor structural genes in response to trimethylamine N-oxide in *Escherichia coli*. *Mol Microbiol* **20**, 1297–1306.

Kaback, H.R. 1997 A molecular mechanism for energy coupling in a membrane transport protein, the lactose permease of *Escherichia coli*. *Proc Natl Acad Sci* **94**, 5539–5543.

Kaback, H.R., Sahin-Tóth, M. and Weinglass, A.B. 2001 The kamikaze approach to membrane transport. *Nat Rev Mol Cell Biol* **2**, 610–620.

Kamada, N., Kim, Y.-G., Sham, H.P., Vallance, B.A., Puente, J.L., Martens, E.C. and Núñez, G. 2012 Regulated virulence controls the ability of a pathogen to compete with the gut microbiota. *Science* **336**, 1325–1329.

Kaneko, M., Kurokawa, M. and Ishibashi, S. 1985 Binding and function of mitochondrial glycerol kinase in comparison with those of mitochondrial hexokinase. *Arch Biochem Biophys* **237**, 135–141.

Kang, H.-Y., Song, S. and Park, C. 1998 Priority of pentose utilization at the level of transcription: arabinose, xylose, and ribose operons. *Mol Cells* **8**(3).

Kaper, J.B. and **O'Brien, A.D.** 2014 Overview and historical perspectives. *Microbiology spectrum* **2**.

Karimova, G., Dautin, N. and Ladant, D. 2005 Interaction network among *Escherichia coli* membrane proteins involved in cell division as revealed by bacterial two-hybrid analysis. *J Bacteriol* **187**, 2233–2243.

Karimova, G., Pidoux, J., Ullmann, A. and Ladant, D. 1998 A bacterial two-hybrid system based on a reconstituted signal transduction pathway. *Proc Natl Acad Sci* **95**, 5752–5756.

Karimova, G., Ullmann, A. and Ladant, D. 2001 Protein-protein interaction between *Bacillus stearothermophilus* tyrosyl-tRNA synthetase subdomains revealed by a bacterial two-hybrid system. *J Mol Microbiol Biotechnol* **3**, 73–82.

Karinou, E., Compton, E.L.R., Morel, M. and Javelle, A. 2013 The *Escherichia coli* SLC26 homologue YchM (DauA) is a C_4-dicarboxylic acid transporter. *Mol Microbiol* **87**, 623–640.

Kay, W.W. and **Kornberg, H.L.** 1969 Genetic control of the uptake of C_4-dicarboxylic acids by *Escherichia coli*. *FEBS Lett* **3**, 93–96.

Kay, W.W. and **Kornberg, H.L.** 1971 The Uptake of C_4-Dicarboxylic Acids by *Escherichia coli*. *FEBS J.* **18**, 274–281.

Keener, J. and **Kustu, S.** 1988 Protein kinase and phosphoprotein phosphatase activities of nitrogen regulatory proteins NtrB and NtrC of enteric bacteria: roles of the conserved amino-terminal domain of NtrC. *Proc Natl Acad Sci* **85**, 4976–4980.

Keseler, I.M., Mackie, A., Santos-Zavaleta, A., Billington, R., Bonavides-Martinez, C., Caspi, R., Fulcher, C., Gama-Castro, S., Kothari, A., Krummenacker, M., Latendresse, M., Muniz-Rascado, L., Ong, Q., Paley, S., Peralta-Gil, M., Subhraveti, P., Velazquez-Ramirez, D.A., Weaver, D., Collado-Vides, J., Paulsen, I. and Karp, P.D. 2017 The EcoCyc database: reflecting new knowledge about *Escherichia coli* K-12. *Nucleic Acids Res* **45**, D543-D550.

Khoroshilova, N., Beinert, H. and Kiley, P.J. 1995 Association of a polynuclear iron-sulfur center with a mutant FNR protein enhances DNA binding. *Proc Natl Acad Sci* **92**, 2499–2503.

Kibbe, W.A. 2007 OligoCalc: an online oligonucleotide properties calculator. *Nucl Acids Res* **35**, W43-W46.

Kim, J., Adhya, S. and Garges, S. 1992 Allosteric changes in the cAMP receptor protein of *Escherichia coli*: hinge reorientation. *Proc Natl Acad Sci* **89**, 9700–9704.

Kim, O.B. and **Unden, G.** 2007 The L-tartrate/succinate antiporter TtdT (YgjE) of L-tartrate fermentation in *Escherichia coli*. *J Bacteriol* **189**, 1597–1603.

Kleefeld, A. 2006 Der Carrier DcuB als zweiter Sensor des Zweikomponentensystems DcuSR in *Escherichia coli*. *PhD thesis, Johannes Gutenberg-University, Mainz, Germany.*

Kleefeld, A., Ackermann, B., Bauer, J., Krämer, J. and Unden, G. 2009 The fumarate/succinate antiporter DcuB of *Escherichia coli* is a bifunctional protein with sites for regulation of DcuS dependent gene expression. *J Biol Chem* **284**, 265–275.

Kleinschmidt, J.A. and **Kleiner, D.** 1978 The glutamine synthetase from *Azotobacter vinelandii*: purification, characterization, regulation and localization. *FEBS J* **89**, 51–60.

Kneuper, H., Janausch, I.G., Vijayan, V., Zweckstetter, M., Bock, V., Griesinger, C. and Unden, G. 2005 The nature of the stimulus and of the fumarate binding site of the fumarate sensor DcuS of *Escherichia coli*. *J Biol Chem* **280**, 20596–20603.

Kolb, A., Busby, S., Buc, H., Garges, S. and Adhya, S. 1993 Transcriptional regulation by cAMP and its receptor protein. *Annu Rev Biochem* **62**, 749–797.

Körner, H., Sofia, H.J. and Zumft, W.G. 2003 Phylogeny of the bacterial superfamily of Crp-Fnr transcription regulators: exploiting the metabolic spectrum by controlling alternative gene programs. *FEMS Microbiol Rev* **27**, 559–592.

Koropatkin, N.M., Cameron, E.A. and Martens, E.C. 2012 How glycan metabolism shapes the human gut microbiota. *Nat Rev Microbiol* **10**, 323–335.

Kovárová-Kovar, K. and **Egli, T.** 1998 Growth kinetics of suspended microbial cells: from single-substrate-controlled growth to mixed-substrate kinetics. *Microbiol Mol Biol Rev* **62**, 646–666.

Krämer, J., Fischer, J.D., Zientz, E., Vijayan, V., Griesinger, C., Lupas, A. and Unden, G. 2007 Citrate sensing by the C_4-dicarboxylate/citrate sensor kinase DcuS of *Escherichia coli*: binding site and conversion of DcuS to a C_4-dicarboxylate-or citrate-specific sensor. *J Bacteriol* **189**, 4290–4298.

Kroner, G.M., Wolfe, M.B. and Freddolino, P.L. 2019 *Escherichia coli* Lrp regulates one-third of the genome via direct, cooperative, and indirect routes. *J Bacteriol* **201**.

Kunkel, T.A. 1985 Rapid and efficient site-specific mutagenesis without phenotypic selection. *Proc Natl Acad Sci* **82**, 488–492.

Kyte, J. and **Doolittle, R.F.** 1982 A simple method for displaying the hydropathic character of a protein. *J Mol Biol* **157**.

Laemmli, U.K. 1970 SDS-page Laemmli method. *Nature* **227**, 680–685.

Lee, Y.K. and **Mazmanian, S.K.** 2010 Has the microbiota played a critical role in the evolution of the adaptive immune system? *Science* **330**, 1768–1773.

Leigh, J.A. and **Dodsworth, J.A.** 2007 Nitrogen regulation in bacteria and archaea. *Annu Rev Microbiol* **61**, 349–377.

Lendenmann, U., Snozzi, M. and Egli, T. 1999 Growth kinetics of *Escherichia coli* with galactose and several other sugars in carbon-limited chemostat culture. *Can J Microbiol* **46**, 72–80.

Lendenmann, U.R.S., Snozzi, M. and Egli, T. 1996 Kinetics of the simultaneous utilization of sugar mixtures by *Escherichia coli* in continuous culture. *Appl Environ Microbiol* **62**, 1493–1499.

Lesne, E., Dupré, E., Locht, C., Antoine, R. and Jacob-Dubuisson, F. 2017 Conformational changes of an interdomain linker mediate mechanical signal transmission in sensor kinase BvgS. *J Bacteriol* **199**.

Leuze, M.R., Karpinets, T.V., Syed, M.H., Beliaev, A.S. and Uberbacher, E.C. 2012 Binding motifs in bacterial gene promoters modulate transcriptional effects of global regulators CRP and ArcA. *Gene Regul Syst Biol* **6**, GRSB. S9357.

Levitt, M.D. 1970 Oxygen tension in the gut. *Mass Medical Soc*.

Lewis, J.D., Chen, E.Z., Baldassano, R.N., Otley, A.R., Griffiths, A.M., Lee, D., Bittinger, K., Bailey, A., Friedman, E.S. and Hoffmann, C. 2015 Inflammation, antibiotics, and diet as environmental stressors of the gut microbiome in pediatric Crohn's disease. *Cell Host Microbe* **18**, 489–500.

Lewis, M. 2005 The lac repressor. *C R Biol* **328**, 521–548.

Ley, R.E., Turnbaugh, P.J., Klein, S. and Gordon, J.I. 2006 Human gut microbes associated with obesity. *Nature* **444**, 1022–1023.

Lin, R., D'Ari, R. and Newman, E.B. 1992 Lambda placMu insertions in genes of the leucine regulon: extension of the regulon to genes not regulated by leucine. *J Bacteriol* **174**, 1948–1955.

Lin, S.-H. and **Lee, J.C.** 2003 Determinants of DNA bending in the DNA− cyclic AMP receptor protein complexes in *Escherichia coli*. *Biochemistry* **42**, 4809–4818.

Liu, D. and **Reeves, P.R.** 1994 *Escherichia coli* K12 regains its O antigen. *Microbiology* **140 (Pt 1)**, 49–57.

Liu, F., Qimuge, Hao, J., Yan, H., Bach, T., Fan, L. and Morigen 2014 AspC-mediated aspartate metabolism coordinates the *Escherichia coli* cell cycle. *PLOS ONE* **9**, e92229.

Liu, J. and **Magasanik, B.** 1995 Activation of the dephosphorylation of nitrogen regulator I-phosphate of *Escherichia coli*. *J Bacteriol* **177**, 926–931.

Loomis, W.F. and **Magasanik, B.** 1967 Glucose-lactose diauxie in *Escherichia coli*. *J Bacteriol* **93**, 1397–1401.

Lundberg, J.O.N., Lundberg, J.M., Alving, K. and Hellström, P.M. 1994 Greatly increased luminal nitric oxide in ulcerative colitis. *The Lancet* **344**, 1673–1674.

Ma, C.-W., Lüddecke, J., Forchhammer, K. and Zeng, A.-P. 2014 Population shift of binding pocket size and dynamic correlation analysis shed new light on the anticooperative mechanism of PII protein. *Proteins* **82**, 1048–1059.

Maier, L., Vyas, R., Cordova, C.D., Lindsay, H., Schmidt, T.S.B., Brugiroux, S., Periaswamy, B., Bauer, R., Sturm, A. and Schreiber, F. 2013 Microbiota-derived hydrogen fuels *Salmonella* typhimurium invasion of the gut ecosystem. *Cell Host Microbe* **14**, 641–651.

Maloney, P.C., Kashket, E.R. and Wilson, T.H. 1974 A protonmotive force drives ATP synthesis in bacteria. *Proc Natl Acad Sci* **71**, 3896–3900.

Mandelstam, J. 1962 The repression of constitutive β-galactosidase in *Escherichia coli* by glucose and other carbon sources. *Biochem J* **82**, 489.

Mangan, S. and **Alon, U.** 2003 Structure and function of the feed-forward loop network motif. *Proc Natl Acad Sci* **100**, 11980–11985.

Mao, X.-J., Huo, Y.-X., Buck, M., Kolb, A. and Wang, Y.-P. 2007 Interplay between CRP-cAMP and PII-Ntr systems forms novel regulatory network between carbon metabolism and nitrogen assimilation in *Escherichia coli*. *Nucleic Acids Res* **35**, 1432–1440.

Martens, E.C., Kelly, A.G., Tauzin, A.S. and Brumer, H. 2014 The devil lies in the details: how variations in polysaccharide fine-structure impact the physiology and evolution of gut microbes. *J Mol Biol* **426**, 3851–3865.

Martínez-Argudo, I. and **Contreras, A.** 2002 PII T-loop mutations affecting signal transduction to NtrB also abolish yeast two-hybrid interactions. *J Bacteriol* **184**, 3746–3748.

Mascher, T., Helmann, J.D. and Unden, G. 2006 Stimulus perception in bacterial signal-transducing histidine kinases. *Microbiol Mol Biol Rev* **70**, 910–938.

Mayer, C. and **Boos, W.** 2005 Hexose/Pentose and Hexitol/Pentitol Metabolism. *EcoSal Plus* **1**.

McFall, E. and **Magasanik, B.** 1962 The effects of thymine and of phosphate deprivation on enzyme synthesis in *Escherichia coli*. *Biochim Biophys Acta* **55**, 900–908.

McIntyre, A., Gibson, P.R. and Young, G.P. 1993 Butyrate production from dietary fibre and protection against large bowel cancer in a rat model. *Gut* **34**, 386–391.

McKay, D.B., Weber, I.T. and Steitz, T.A. 1982 Structure of catabolite gene activator protein at 2.9-Å resolution. Incorporation of amino acid sequence and interactions with cyclic AMP. *J Biol Chem* **257**, 9518–9524.

Mellerowicz, E.J. and **Gorshkova, T.A.** 2012 Tensional stress generation in gelatinous fibres: a review and possible mechanism based on cell-wall structure and composition. *J Exp Bot* **63**, 551–565.

Michal, G. 1999 Biochemical pathways: Spektrum, Akad. Verlag Heidelberg.

Miller, J.H. 1992 A short course in bacterial genetics: a laboratory manual and handbook for *Escherichia coli* and related bacteria.

Miranda, R.L., Conway, T., Leatham, M.P., Chang, D.E., Norris, W.E., Allen, J.H., Stevenson, S.J., Laux, D.C. and Cohen, P.S. 2004 Glycolytic and gluconeogenic growth of *Escherichia coli* O157: H7 (EDL933) and *E. coli* K-12 (MG1655) in the mouse intestine. *Infect Immun* **72**, 1666–1676.

Miroux, B. and **Walker, J.E.** 1996 Over-production of proteins in *Escherichia coli*: mutant hosts that allow synthesis of some membrane proteins and globular proteins at high levels. *J Mol Biol* **260**, 289–298.

Misko, T.P., Mitchell, W.J., Meadow, N.D. and Roseman, S. 1987 Sugar transport by the bacterial phosphotransferase system. Reconstitution of inducer exclusion in *Salmonella* typhimurium membrane vesicles. *J Biol Chem* **262**, 16261–16266.

Molnar, K.S., Bonomi, M., Pellarin, R., Clinthorne, G.D., Gonzalez, G., Goldberg, S.D., Goulian, M., Sali, A. and DeGrado, W.F. 2014 Cys-scanning disulfide crosslinking and bayesian modeling probe the transmembrane signaling mechanism of the histidine kinase, PhoQ. *Structure* **22**, 1239–1251.

Monod, J. 1941 Recherches sur la croissance des cultures bacteriennes.

Monzel, C., Degreif-Dünnwald, P., Gröpper, C., Griesinger, C. and Unden, G. 2013 The cytoplasmic PASC domain of the sensor kinase DcuS of *Escherichia coli*: role in signal transduction, dimer formation, and DctA interaction. *MicrobiologyOpen* **2**, 912–927.

Monzel, C. and **Unden, G.** 2015 Transmembrane signaling in the sensor kinase DcuS of *Escherichia coli*: A long-range piston-type displacement of transmembrane helix 2. *Proc Natl Acad Sci* **112**, 11042–11047.

Moore, W.E.C. and **Holdeman, L.V.** 1974 Special problems associated with the isolation and identification of intestinal bacteria in fecal flora studies. *Am J Clin Nutr* **27**, 1450–1455.

Moraes, T.F. and **Reithmeier, R.A.F.** 2012 Membrane transport metabolons. *Biochim Biophys Acta* **1818**, 2687–2706.

Morris, D.R. and **Koffron, K.L.** 1967 Urea production and putrescine biosynthesis by *Escherichia coli*. *J Bacteriol* **94**, 1516–1519.

Mortensen, P.B. and **Clausen, M.R.** 1996 Short-chain fatty acids in the human colon: relation to gastrointestinal health and disease. *Scand J Gastroenterol* **31**, 132–148.

Mueller, N.T., Zhang, M., Juraschek, S.P., Miller, E.R. and Appel, L.J. 2020 Effects of high-fiber diets enriched with carbohydrate, protein, or unsaturated fat on circulating short chain fatty acids: results from the OmniHeart randomized trial. *Am J Clin Nutr* **111**, 545–554.

Mühldorfer, I. and **Hacker, J.** 1994 Genetic aspects of *Escherichia coli* virulence. *Microb Pathog* **16**, 171–181.

Müller-Hill, B. and **Oehler, S.** 1996 The *lac* operon: A Short History of a Genetic Paradigm. *Walter de Gruyter New York*.

Narang, A., Konopka, A. and Ramkrishna, D. 1997 New patterns of mixed-substrate utilization during batch growth of *Escherichia coli* K12. *Biotechnol Bioeng* **55**, 747–757.

Narang, A. and **Pilyugin, S.S.** 2007 Bacterial gene regulation in diauxic and non-diauxic growth. *J Theor Biol* **244**, 326–348.

Nelson, S.O., Wright, J.K. and Postma, P.W. 1983 The mechanism of inducer exclusion. Direct interaction between purified III^{Glc} of the phosphoenolpyruvate: sugar phosphotransferase system and the lactose carrier of *Escherichia coli*. *EMBO J* **2**, 715–720.

Newman, E.B. and **Lin, R.** 1995 Leucine-responsive regulatory protein: a global regulator of gene expression in *E. coli*. *Annu Rev Microbiol* **49**, 747–775.

Nguyen, B.D., Cuenca, M., Hartl, J., Gül, E., Bauer, R., Meile, S., Rüthi, J., Margot, C., Heeb, L. and Besser, F. 2020 Import of Aspartate and Malate by DcuABC Drives H_2/Fumarate Respiration to Promote Initial *Salmonella* Gut-Lumen Colonization in Mice. *Cell Host Microbe* **27**(6), 922-936.

Ni, J., Shen, T.-C.D., Chen, E.Z., Bittinger, K., Bailey, A., Roggiani, M., Sirota-Madi, A., Friedman, E.S., Chau, L. and Lin, A. 2017 A role for bacterial urease in gut dysbiosis and Crohn's disease. *Sci Transl Med* **9**(416).

Ninfa, A.J. and **Magasanik, B.** 1986 Covalent modification of the *glnG* product, NRI, by the *glnL* product, NRII, regulates the transcription of the *glnALG* operon in *Escherichia coli*. *Proc Natl Acad Sci* **83**, 5909–5913.

Okonechnikov, K., Golosova, O. and Fursov, M. 2012 Unipro UGENE: A unified bioinformatics toolkit. *Bioinformatics* **28**, 1166–1167.

Oliveira, M.A.S., Gerhardt, E.C.M., Huergo, L.F., Souza, E.M., Pedrosa, F.O. and Chubatsu, L.S. 2015 2-Oxoglutarate levels control adenosine nucleotide binding by *Herbaspirillum seropedicae* PII proteins. *FEBS J* **282**, 4797–4809.

Olivera, B.C.L., Ugalde, E. and Martínez-Antonio, A. 2010 Regulatory dynamics of standard two-component systems in bacteria. *J Theor Biol***264**, 560–569.

Ortet, P., Whitworth, D.E., Santaella, C., Achouak, W. and Barakat, M. 2015 P2CS: updates of the prokaryotic two-component systems database. *Nucleic Acids Res* **43**, D536-41.

Oshima, T., Aiba, H., Masuda, Y., Kanaya, S., Sugiura, M., Wanner, B.L., Mori, H. and Mizuno, T. 2002 Transcriptome analysis of all two-component regulatory system mutants of *Escherichia coli* K-12. *Mol Microbiol* **46**, 281–291.

Osterman, A. 2009 Biogenesis and Homeostasis of Nicotinamide Adenine Dinucleotide Cofactor. *EcoSal Plus* **3**.

Osumi, T. and **Saier, M.H.** 1982 Regulation of lactose permease activity by the phosphoenolpyruvate: sugar phosphotransferase system: evidence for direct binding of the glucose-specific enzyme III to the lactose permease. *Proc Natl Acad Sci* **79**, 1457–1461.

Oyamada, T., Yokoyama, K., Morinaga, M., Suzuki, M. and Makino, K. 2007 Expression of *Escherichia coli* DcuS-R two-component regulatory system is regulated by the secondary internal promoter which is activated by CRP-cAMP. *Korean J Microbiol* **45**, 234.

Pappalardo, L., Janausch, I.G., Vijayan, V., Zientz, E., Junker, J., Peti, W., Zweckstetter, M., Unden, G. and Griesinger, C. 2003 The NMR structure of the sensory domain of the membranous two-component fumarate sensor (histidine protein kinase) DcuS of *Escherichia coli*. *J Biol Chem* **278**, 39185–39188.

Park, S.-J., Tseng, C.-P. and Gunsalus, R.P. 1995 Regulation of succinate dehydrogenase (*sdhCDAB*) operon expression in *Escherichia coli* in response to carbon supply and anaerobiosis: role of ArcA and Fnr. *Mol Microbiol* **15**, 473–482.

Parker, K.D., Albeke, S.E., Gigley, J.P., Goldstein, A.M. and Ward, N.L. 2018 Microbiome composition in both wild-type and disease model mice is heavily influenced by mouse facility. *Front Microbiol* **9**, 1598.

Parkinson, G., Wilson, C., Gunasekera, A., Ebright, Y.W., Ebright, R.E. and Berman, H.M. 1996 Structure of the CAP-DNA complex at 2.5 Å resolution: a complete picture of the protein-DNA interface. *J Mol Biol* **260**, 395–408.

Pereira, C.S., Santos, A.J.M., Bejerano-Sagie, M., Correia, P.B., Marques, J.C. and Xavier, K.B. 2012 Phosphoenolpyruvate phosphotransferase system regulates detection and processing of the quorum sensing signal autoinducer-2. *Mol Microbiol* **84**, 93–104.

Perna, N.T., Plunkett, G., Burland, V., Mau, B., Glasner, J.D., Rose, D.J., Mayhew, G.F., Evans, P.S., Gregor, J. and Kirkpatrick, H.A. 2001 Genome sequence of enterohaemorrhagic *Escherichia coli* O157: H7. *Nature* **409**, 529–533.

Pettersen, E.F., Goddard, T.D., Huang, C.C., Couch, G.S., Greenblatt, D.M., Meng, E.C. and Ferrin, T.E. 2004 UCSF Chimera—a visualization system for exploratory research and analysis. *J Comput Chem* **25**, 1605–1612.

Pioszak, A.A., Jiang, P. and Ninfa, A.J. 2000 The *Escherichia coli* PII signal transduction protein regulates the activities of the two-component system transmitter protein NRII by direct interaction with the kinase domain of the transmitter module. *Biochemistry* **39**, 13450–13461.

Platko, J.V. and **Calvo, J.M.** 1993 Mutations affecting the ability of *Escherichia coli* Lrp to bind DNA, activate transcription, or respond to leucine. *J Bacteriol* **175**, 1110–1117.

Plevin, M.J., Mills, M.M. and Ikura, M. 2005 The LxxLL motif: a multifunctional binding sequence in transcriptional regulation. *Trends Biochem Sci* **30**, 66–69.

Podgornaia, A.I., Casino, P., Marina, A. and Laub, M.T. 2013 Structural basis of a rationally rewired protein-protein interface critical to bacterial signaling. *Structure* **21**, 1636–1647.

Popovych, N., Tzeng, S.-R., Tonelli, M., Ebright, R.H. and Kalodimos, C.G. 2009 Structural basis for cAMP-mediated allosteric control of the catabolite activator protein. *Proc Natl Acad Sci* **106**, 6927–6932.

Poulsen, L.K., Lan, F., Kristensen, C.S., Hobolth, P., Molin, S. and Krogfelt, K.A. 1994 Spatial distribution of *Escherichia coli* in the mouse large intestine inferred from rRNA *in situ* hybridization. *Infect Immun* **62**, 5191–5194.

Powell, J.T. and **Morrison, J.F.** 1978 The purification and properties of the aspartate aminotransferase and aromatic-amino-acid aminotransferase from *Escherichia coli*. *FEBS J.* **87**, 391–400.

Prohl, C., Wackwitz, B., Vlad, D. and Unden, G. 1998 Functional citric acid cycle in an *arcA* mutant of *Escherichia coli* during growth with nitrate under anoxic conditions. *Arch Microbiol* **170**, 1–7.

Pryde, S.E., Duncan, S.H., Hold, G.L., Stewart, C.S. and Flint, H.J. 2002 The microbiology of butyrate formation in the human colon. *FEMS Microbiol Lett* **217**, 133–139.

Pyles, E.A., Chin, A.J. and Lee, J.C. 1998 *Escherichia coli* cAMP Receptor Protein− DNA Complexes. 1. Energetic Contributions of Half-Sites and Flanking Sequences in DNA Recognition. *Biochemistry* **37**, 5194–5200.

Pyles, E.A. and **Lee, J.C.** 1998 *Escherichia coli* cAMP Receptor Protein− DNA Complexes. 2. Structural Asymmetry of DNA Bending. *Biochemistry* **37**, 5201–5210.

Rabin, R.S. and S**tewart, V.** 1993 Dual response regulators (NarL and NarP) interact with dual sensors (NarX and NarQ) to control nitrate-and nitrite-regulated gene expression in *Escherichia coli* K-12. *J Bacteriol* **175**, 3259–3268.

Radchenko, M. and **Merrick, M.** 2011 The role of effector molecules in signal transduction by PII proteins: *Biochem Soc Trans* **39**(1), 189-194.

Radchenko, M.V., Thornton, J. and Merrick, M. 2010 Control of AmtB-GlnK complex formation by intracellular levels of ATP, ADP, and 2-oxoglutarate. *J Biol Chem* **285**, 31037–31045.

Ramseier, T.M. and **Saier Jr, M.H.** 1995 cAMP-cAMP receptor protein complex: five binding sites in the control region of the *Escherichia coli* mannitol operon. *Microbiology* **141**, 1901–1907.

Rhee, S.G., Chock, P.B. and Stadtman, E.R. 1989 Regulation of *Escherichia coli* glutamine synthetase. *Adv Enzymol Relat Areas Mol Biol* **62**, 37–92.

Rodionova, I.A., Goodacre, N., Babu, M., Emili, A., Uetz, P. and Saier, M.H. 2018 The nitrogen regulatory PII protein (GlnB) and N-acetylglucosamine 6-phosphate epimerase (NanE) allosterically activate glucosamine 6-phosphate deaminase (NagB) in *Escherichia coli*. *J Bacteriol* **200**, e00691-17.

Rodrigues, T.E., Gerhardt, E.C.M., Oliveira, M.A., Chubatsu, L.S., Pedrosa, F.O., Souza, E.M., Souza, G.A., Müller-Santos, M. and Huergo, L.F. 2014 Search for novel targets of the PII signal transduction protein in Bacteria identifies the BCCP component of acetyl-CoA carboxylase as a PII binding partner. *Mol Microbiol* **91**, 751–761.

Rosenberg, A.H., Lade, B.N., Dao-shan, C., Lin, S.-W., Dunn, J.J. and Studier, F.W. 1987 Vectors for selective expression of cloned DNAs by T7 RNA polymerase. *Gene* **56**, 125–135.

Round, J.L. and **Mazmanian, S.K.** 2009 The gut microbiota shapes intestinal immune responses during health and disease. *Nat Rev Immunol* **9**, 313–323.

Roy, V., Fernandes, R., Tsao, C.-Y. and Bentley, W.E. 2010 Cross species quorum quenching using a native AI-2 processing enzyme. *ACS Chem Biol* **5**, 223–232.

Saldeña, T.A., Saraví, F.D., Hwang, H.-J., Cincunegui, L.M. and Carra, G.E. 2000 Oxygen Diffusive Barriers of Rat Distal Colon. *Dig Dis Sci* **45**, 2108–2114.

Salem, M.A., Jüppner, J., Bajdzienko, K. and Giavalisco, P. 2016 Protocol: a fast, comprehensive and reproducible one-step extraction method for the rapid preparation of polar and semi-polar metabolites, lipids, proteins, starch and cell wall polymers from a single sample. *Plant Methods* **12**, 1–15.

Salvi, M., Schomburg, B., Giller, K., Graf, S., Unden, G., Becker, S., Lange, A. and Griesinger, C. 2017 Sensory domain contraction in histidine kinase CitA triggers transmembrane signaling in the membrane-bound sensor. *Proc Natl Acad Sci*, 201620286.

Sambrook, J., Fritsch, E.F. and Maniatis, T. 1989 Molecular cloning: a laboratory manual/J. Sambrook, EF Fritsch, T. Maniatis.

Satishchandran, C., Markham, G.D., Moore, R.C. and Boyle, S.M. 1990 Locations of the *speA*, *speB*, *speC*, and *metK* genes on the physical map of *Escherichia coli*. *J Bacteriol* **172**, 4748.

Sauer, U. and **Eikmanns, B.J.** 2005 The PEP-pyruvate-oxaloacetate node as the switch point for carbon flux distribution in bacteria. *FEMS Microbiol Rev* **29**, 765–794.

Savery, N., Rhodius, V. and Busby, S.J.W. 1996 Protein-protein interactions during transcription activation: the case of the *Escherichia coli* cyclic AMP receptor protein. *Philos Trans R Soc Lond B Biol Sci* **351**, 543–550.

Scheppach, W., Luehrs, H. and Menzel, T. 2001 Beneficial health effects of low-digestible carbohydrate consumption. *Br J Nutr* **85**, S23-S30.

Scheu, P.D., Kim, O.B., Griesinger, C. and Unden, G. 2010a Sensing by the membrane-bound sensor kinase DcuS: exogenous versus endogenous sensing of C_4-dicarboxylates in bacteria. *Future Microbiol* **5**, 1383–1402.

Scheu, P.D., Liao, Y.-F., Bauer, J., Kneuper, H., Basche, T., Unden, G. and Erker, W. 2010b Oligomeric sensor kinase DcuS in the membrane of *Escherichia coli* and in proteoliposomes: chemical cross-linking and FRET spectroscopy. *J Bacteriol* **192**, 3474–3483.

Scheu, P.D., Steinmetz, P.A., Dempwolff, F., Graumann, P.L. and Unden, G. 2014 Polar Localization of a Tripartite Complex of the Two-Component System DcuS/DcuR and the Transporter DctA in *Escherichia coli* Depends on the Sensor Kinase DcuS. *PLoS One,* **9**(12), e115534.

Scheu, P.D., Witan, J., Rauschmeier, M., Graf, S., Liao, Y.-F., Ebert-Jung, A., Basche, T., Erker, W. and Unden, G. 2012 CitA/CitB two-component system regulating citrate fermentation in *Escherichia coli* and its relation to the DcuS/DcuR system in vivo. *J Bacteriol* **194**, 636–645.

Schmidt, A., Kochanowski, K., Vedelaar, S., Ahrné, E., Volkmer, B., Callipo, L., Knoops, K., Bauer, M., Aebersold, R. and Heinemann, M. 2016 The quantitative and condition-dependent *Escherichia coli* proteome. *Nat Biotechnol* **34**, 104–110.

Schneider, B.L., Kiupakis, A.K. and Reitzer, L.J. 1998 Arginine catabolism and the arginine succinyltransferase pathway in *Escherichia coli*. *J Bacteriol* **180**, 4278–4286.

Schneider, D.A. and **Gourse, R.L.** 2004 Relationship between growth rate and ATP concentration in *Escherichia coli* a bioassay for available cellular ATP. *J Biol Chem* **279**, 8262–8268.

Schryvers, A., Lohmeier, E. and Weiner, J.H. 1978 Chemical and functional properties of the native and reconstituted forms of the membrane-bound, aerobic glycerol-3-phosphate dehydrogenase of *Escherichia coli*. *J Biol Chem* **253**, 783–788.

Schubert, C. 2016 Der C_4-Dicarboxylat Stoffwechsel von *E. coli* Die physiologische Funktion von *aspA* und *dcuA*. *Bachelor thesis, Johannes Gutenberg-University, Mainz.*

Schubert, C. and **Unden, G.** 2021 C_4-dicarboxylate metabolons: Interaction of C_4-dicarboxylate transporters of *Escherichia coli* with cytosolic enzymes and regulators. *bioRxiv* Preprint publication.

Schubert, C., Zedler, S., Strecker, A. and Unden, G. 2020 L-Aspartate as a high-quality nitrogen source in *Escherichia coli*: Regulation of L-aspartase by the nitrogen regulatory system and interaction of L-aspartase with GlnB. *Mol Microbiol*.

Schultz, S.C., Shields, G.C. and Steitz, T.A. 1991 Crystal structure of a CAP-DNA complex: the DNA is bent by 90 degrees. *Science* **253**, 1001–1007.

Selim, K.A., Ermilova, E. and Forchhammer, K. 2020 From cyanobacteria to Archaeplastida: new evolutionary insights into PII signalling in the plant kingdom. *New Phytol* **227**, 722–731.

Seltzer, W.K. and **McCabe, E.R.B.** 1984 Subcellular distribution and kinetic properties of soluble and particulate-associated bovine adrenal 21vcerol kinase. *Mol Cell Biochem* **64**, 51–61.

Senes, A., Engel, D.E. and DeGrado, W.F. 2004 Folding of helical membrane proteins: the role of polar, GxxxG-like and proline motifs. *Curr Opin Struct Biol* **14**, 465–479.

Senior, A.E. 1990 The proton-translocating ATPase of *Escherichia coli*. *Annu Rev Biophys Biophys Chem* **19**, 7–41.

Sévin, D.C., Fuhrer, T., Zamboni, N. and Sauer, U. 2017 Nontargeted in vitro metabolomics for high-throughput identification of novel enzymes in *Escherichia coli*. *Nat Methods* **14**, 187–194.

Sevvana, M., Vijayan, V., Zweckstetter, M., Reinelt, S., Madden, D.R., Herbst-Irmer, R., Sheldrick, G.M., Bott, M., Griesinger, C. and Becker, S. 2008 A ligand-induced switch in the periplasmic domain of sensor histidine kinase CitA. *J Mol Biol* **377**, 512–523.

Sharma, H., Yu, S., Kong, J., Wang, J. and Steitz, T.A. 2009 Structure of apo-CAP reveals that large conformational changes are necessary for DNA binding. *Proc Natl Acad Sci* **106**, 16604–16609.

Shen, T.-C.D., Albenberg, L., Bittinger, K., Chehoud, C., Chen, Y.-Y., Judge, C.A., Chau, L., Ni, J., Sheng, M. and Lin, A. 2015 Engineering the gut microbiota to treat hyperammonemia. *J Clin Investig* **125**, 2841–2850.

Shen-Orr, S.S., Milo, R., Mangan, S. and Alon, U. 2002 Network motifs in the transcriptional regulation network of *Escherichia coli*. *Nat Genet* **31**, 64–68.

Shin, N.-R., Whon, T.W. and Bae, J.-W. 2015 Proteobacteria: microbial signature of dysbiosis in gut microbiota. *Trends Biotechnol* **33**, 496–503.

Silhavy, T.J., Berman, M.L. and Enquist, L.W. 1984 Experiments with gene fusions. *Cold Spring Harbor Laboratory*.

Six, S., Andrews, S.C., Unden, G. and Guest, J.R. 1994 *Escherichia coli* Possesses Two Homologous Anaerobic C_4-Dicarboxylate Membrane Transporters (DcuA and DcuB) Distinct from the Aerobic Dicarboxylate Transport System (Dct). *J Bacteriol* **176**, 6470–6478.

Smith, H.W. 1975 Survival of orally administered *E. coli* K12 in alimentary tract of man. *Nature* **255**, 500–502.

Son, H.S. and **Rhee, S.G.** 1987 Cascade control of *Escherichia coli* glutamine synthetase. Purification and properties of PII protein and nucleotide sequence of its structural gene. *J Biol Chem* **262**, 8690–8695.

Song, S. and **Park, C.** 1997 Organization and regulation of the D-xylose operons in *Escherichia coli* K-12: XylR acts as a transcriptional activator. *J Bacteriol* **179**, 7025–7032.

Sourjik, V. 2004 Receptor clustering and signal processing in *E. coli* chemotaxis. *Trends Microbiol* **12**, 569–576.

Spiro, S. and **Guest, J.R.** 1990 FNR and its role in oxygen-regulated gene expression in *Escherichia coli*. *FEMS Microbiol Lett* **75**, 399–428.

Spiro, S. and **Guest, J.R.** 1991 Adaptive responses to oxygen limitation in *Escherichia coli*. *Trends Biochem Sci* **16**, 310-314.

Sprenger, G.A. 1995 Genetics of pentose-phosphate pathway enzymes of *Escherichia coli* K-12. *Arch Microbiol* **164**, 324–330.

Srere, P.A. 1967 Enzyme concentrations in tissues. *Science* **158**, 936–937.

Starai, V.J., Garrity, J. and Escalante-Semerena, J.C. 2005 Acetate excretion during growth of *Salmonella enterica* on ethanolamine requires phosphotransacetylase (EutD) activity, and acetate recapture requires acetyl-CoA synthetase (Acs) and phosphotransacetylase (Pta) activities. *Microbiology* **151**, 3793–3801.

Steinmetz, P.A., Worner, S. and Unden, G. 2014 Differentiation of DctA and DcuS function in the DctA/DcuS sensor complex of *Escherichia coli*: function of DctA as an activity switch and of DcuS as the C_4-dicarboxylate sensor. *Mol Microbiol* **94**, 218–229.

Stewart, V. 2003 Nitrate-and nitrite-responsive sensors NarX and NarQ of proteobacteria. *Biochem Soc Trans* **31**(1), 1–10.

Stewart, V., Chen, L.-L. and Wu, H.-c. 2003 Response to culture aeration mediated by the nitrate and nitrite sensor NarQ of *Escherichia coli* K-12. *Mol Microbiol* **50**, 1391–1399.

Stojiljkovic, I., Bäumler, A.J. and Heffron, F. 1995 Ethanolamine utilization in *Salmonella* typhimurium: nucleotide sequence, protein expression, and mutational analysis of the *cchA cchB eutE eutJ eutG eutH* gene cluster. *J Bacteriol* **177**, 1357–1366.

Stopp, M. 2021 Intramolecular signal transduction of the sensor histidine kinase DcuS and the aerobic and anaerobic fumarate proteom in the regulation of the *Escherichia coli* C_4-dicarbixylate metabolism. *PhD thesis, Johannes Gutenberg-University, Mainz, Germany.*

Stopp, M., Steinmetz, P.A., Schubert, C., Griesinger, C., Schneider, D. and Unden, G. 2021 Transmembrane signaling and cytoplasmic signal conversion by dimeric transmembrane helix 2 and a linker domain of the DcuS sensor kinase. *J Biol Chem* **269**, 100148.

Strecker, A. 2018 Der C_4-Dicarboxylat-Metabolismus von *Escherichia coli* Die Rolle von DcuA und von DcuS im Signaltransfer. *PhD thesis, Johannes Gutenberg-University, Mainz, Germany.*

Strecker, A., Schubert, C., Zedler, S., Steinmetz, P. and Unden, G. 2018 DcuA of aerobically grown *Escherichia coli* serves as a nitrogen shuttle (L-aspartate/fumarate) for nitrogen uptake. *Mol Microbiol* **109**, 801–811.

Studier, F.W. and **Moffatt, B.A.** 1986 Use of bacteriophage T7 RNA polymerase to direct selective high-level expression of cloned genes. *J Mol Biol* **189**, 113–130.

Studier, F.W., Rosenberg, A.H., Dunn, J.J. and Dubendorff, J.W. 1990 Use of T7 RNA polymerase to direct expression of cloned genes. *Methods Enzymol* **185**, e89.

Stülke, J. and **Hillen, W.** 1999 Carbon catabolite repression in bacteria. *Curr Opin Microbiol* **2**, 195–201.

Surmann, K., Stopp, M., Wörner, S., Dhople, V.M., Völker, U., Unden, G. and Hammer, E. 2020 Fumarate dependent protein composition under aerobic and anaerobic growth conditions in *Escherichia coli*. *J Proteomics* **212**, 103583.

Sutherland, B.W., Toews, J. and Kast, J. 2008 Utility of formaldehyde cross-linking and mass spectrometry in the study of protein-protein interactions. *J Mass Spectrom* **43**, 699–715.

Suzuki, S., Yamaguchi, J. and Tokushige, M. 1973 Studies on aspartase. I. Purification and molecular properties of aspartase from *Escherichia coli*. *Biochim Biophys Acta* **321**, 369–381.

Szabó, C., Ischiropoulos, H. and Radi, R. 2007 Peroxynitrite: biochemistry, pathophysiology and development of therapeutics. *Nat Rev Drug Discov* **6**, 662–680.

Tani, T.H., Khodursky, A., Blumenthal, R.M., Brown, P.O. and Matthews, R.G. 2002 Adaptation to famine: a family of stationary-phase genes revealed by microarray analysis. *Proc Natl Acad Sci* **99**, 13471–13476.

Tebbutt, J., Rhodius, V.A., Webster, C.L. and Busby, S.J.W. 2002 Architectural requirements for optimal activation by tandem CRP molecules at a class I CRP-dependent promoter. *FEMS Microbiol Lett* **210**, 55–60.

Thorner, J.W. and **Paulus, H.** 1973 Catalytic and allosteric properties of glycerol kinase from *Escherichia coli*. *J Biol Chem* **248**, 3922–3932.

Tong, L. 2013 Structure and function of biotin-dependent carboxylases. *Cell Mol Life Sci* **70**, 863–891.

Towbin, H. and **Gordon, J.** 1984 Immunoblotting and dot immunobinding - Current status and outlook. *J Immunol Methods* **72**, 313–340.

Tran, Q.H., Bongaerts, J., Vlad, D. and Unden, G. 1997 Requirement for the proton-pumping NADH dehydrogenase I of *Escherichia coli* in respiration of NADH to fumarate and its bioenergetic implications. *FEBS J.* **244**, 155–160.

Trchounian, A. 2004 *Escherichia coli* proton-translocating F0F1-ATP synthase and its association with solute secondary transporters and/or enzymes of anaerobic oxidation–reduction under fermentation. *Biochem Biophys Res* **315**, 1051–1057.

Tsai, M.-J., Wang, J.-R., Yang, C.-D., Kao, K.-C., Huang, W.-L., Huang, H.-Y., Tseng, C.-P., Huang, H.-D. and Ho, S.-Y. 2018 PredCRP: predicting and analysing the regulatory roles of CRP from its binding sites in *Escherichia coli*. *Sci Rep* **8**, 1–9.

Turnbaugh, P.J., Quince, C., Faith, J.J., McHardy, A.C., Yatsunenko, T., Niazi, F., Affourtit, J., Egholm, M., Henrissat, B. and Knight, R. 2010 Organismal, genetic, and transcriptional variation in the deeply sequenced gut microbiomes of identical twins. *Proc Natl Acad Sci* **107**, 7503–7508.

Unden, G., Strecker, A., Kleefeld, A. and Kim, O.B. 2016 C_4-Dicarboxylate Utilization in Aerobic and Anaerobic Growth. *EcoSal Plus* **7**.

UniProt Consortium 2019 UniProt: a worldwide hub of protein knowledge. *Nucleic Acids Res* **47**, D506-D515.

Vadder, F. de, Kovatcheva-Datchary, P., Zitoun, C., Duchampt, A., Bäckhed, F. and Mithieux, G. 2016 Microbiota-Produced Succinate Improves Glucose Homeostasis via Intestinal Gluconeogenesis. *Cell Metab* **24**, 151–157.

van der Vlag, J., van Dam, K. and Postma, P.W. 1994 Quantification of the regulation of glycerol and maltose metabolism by IIA^{Glc} of the phosphoenolpyruvate-dependent glucose phosphotransferase system in *Salmonella typhimurium*. *J Bacteriol* **176**, 3518–3526.

van Heeswijk, W.C., Hoving, S., Molenaar, D., Stegeman, B., Kahn, D. and Westerhoff, H.V. 1996 An alternative PII protein in the regulation of glutamine synthetase in *Escherichia coli*. *Mol Microbiol* **21**, 133–146.

van Heeswijk, W.C., Stegeman, B., Hoving, S., Molenaar, D., Kahn, D. and Westerhoff, H.V. 1995 An additional PII in *Escherichia coli*: a new regulatory protein in the glutamine synthetase cascade. *FEMS Microbiol Lett* **132**, 153–157.

van Heeswijk, W.C., Westerhoff, H.V. and Boogerd, F.C. 2013 Nitrogen assimilation in *Escherichia coli*: putting molecular data into a systems perspective. *Microbiol Mol Biol Rev* **77**, 628–695.

Venditti, V., Ghirlando, R. and Clore, G.M. 2013 Structural basis for enzyme I inhibition by α-ketoglutarate. *ACS Chem Biol* **8**, 1232–1240.

Voegele, R.T., Sweet, G.D. and Boos, W. 1993 Glycerol kinase of *Escherichia coli* is activated by interaction with the glycerol facilitator. *J Bacteriol* **175**, 1087–1094.

Vogel-Scheel, J., Alpert, C., Engst, W., Loh, G. and Blaut, M. 2010 Requirement of purine and pyrimidine synthesis for colonization of the mouse intestine by *Escherichia coli*. *Appl Environ Microbiol* **76**, 5181–5187.

Wächtershäuser, A. and **Stein, J.** 2000 Rationale for the luminal provision of butyrate in intestinal diseases. *Eur J Nutr* **39**, 164–171.

Wadolkowski, E.A., Burris, J.A. and O'Brien, A.D. 1990 Mouse model for colonization and disease caused by enterohemorrhagic *Escherichia coli* O157: H7. *Infect Immun* **58**, 2438–2445.

Wallace, B.J. and **Young, I.G.** 1977 Role of quinones in electron transport to oxygen and nitrate in *Escherichia coli*. Studies with a *ubiA*− *menA*− double quinone mutant. *Biochim Biophys Acta* **461**, 84–100.

Willis, R.C. and **Woolfolk, C.A.** 1974 Asparagine utilization in *Escherichia coli*. *J Bacteriol* **118**, 231–241.

Winter, S.E., Lopez, C.A. and Bäumler, A.J. 2013a The dynamics of gut-associated microbial communities during inflammation. *EMBO Rep* **14**, 319–327.

Winter, S.E., Winter, M.G., Xavier, M.N., Thiennimitr, P., Poon, V., Keestra, A.M., Laughlin, R.C., Gomez, G., Wu, J. and Lawhon, S.D. 2013b Host-derived nitrate boosts growth of *E. coli* in the inflamed gut. *Science* **339**, 708–711.

Witan, J., Bauer, J., Wittig, I., Steinmetz, P.A., Erker, W. and Unden, G. 2012a Interaction of the *Escherichia coli* transporter DctA with the sensor kinase DcuS: presence of functional DctA/DcuS sensor units. *Mol Microbiol* **85**, 846–861.

Witan, J., Monzel, C., Scheu, P.D. and Unden, G. 2012b The sensor kinase DcuS of *Escherichia coli*: two stimulus input sites and a merged signal pathway in the DctA/DcuS sensor unit. *Biol Chem* **393**, 1291–1297.

Woods, S.A., Miles, J.S. and Guest, J.R. 1988a Sequence homologies between argininosuccinase, aspartase and fumarase: a family of structurally-related enzymes. *FEMS Microbiol Lett* **51**, 181–186.

Woods, S.A., Schwartzbach, S.D. and Guest, J.R. 1988b Two biochemically distinct classes of fumarase in *Escherichia coli*. *Biochim Biophys Acta* **954**, 14–26.

Wörner, S., Strecker, A., Monzel, C., Zeltner, M., Witan, J., Ebert-Jung, A. and Unden, G. 2016 Conversion of the sensor kinase DcuS of *Escherichia coli* of the DcuB/DcuS sensor complex to the C_4-dicarboxylate responsive form by the transporter DcuB. *Environ Microbiol* **18**, 4920–4930.

Wörner, S., Surmann, K., Ebert-Jung, A., Völker, U., Hammer, E. and Unden, G. 2017 Cellular concentrations of the transporters DctA, DcuB, and the sensor DcuS of *Escherichia coli* and the contributions of free and complexed DcuS to transcriptional regulation by DcuR. *J Bacteriol* **200**(4).

Wrong, O. 1978 Nitrogen metabolism in the gut. *Am J Clin Nutr* **31**, 1587–1593.

Yagi, T., Kagamiyama, H., Nozaki, M. and Soda, K. 1985 [17] Glutamate-aspartate transaminase from microorganisms. *Meth Enzymol* **113**, 83–89.

Yamamoto, K., Matsumoto, F., Minagawa, S., Oshima, T., Fujita, N., Ogasawara, N. and Ishihama, A. 2009 Characterization of CitA-CitB signal transduction activating genes involved in anaerobic citrate catabolism in *Escherichia coli*. *Biosci Biotechnol Biochem* **73**, 346–350.

Yang, C.-D., Huang, H.-Y., Shrestha, S., Chen, Y.-H., Huang, H.-D. and Tseng, C.-P. 2018 Large-scale functional analysis of CRP-mediated feed-forward loops. *Int J Mol Sci* **19**, 2335.

Yang, J., Park, J., Park, S., Baek, I. and Chun, J. 2019 Introducing Murine Microbiome Database (MMDB): A Curated Database with Taxonomic Profiling of the Healthy Mouse Gastrointestinal Microbiome. *Microorganisms* **7**(11), 480.

Yang, J. and **Zhang, Y.** 2015 I-TASSER server: new development for protein structure and function predictions. *Nucleic Acids Res* **43**, W174-W181.

Yang, Y., M. Pollard, A., Hoefler, C., Poschet, G., Wirtz, M., Hell, R.??d. and Sourjik, V. 2015 Relation between chemotaxis and consumption of amino acids in bacteria. *Mol Microbiol* **96**, 1272–1282.

Yanisch-Perron, C., Vieira, J. and Messing, J. 1985 Improved M13 phage cloning vectors and host strains: nucleotide sequences of the M13mpl8 and pUC19 vectors. *Gene* **33**, 103–119.

Yeh, J.I., Chinte, U. and Du, S. 2008 Structure of glycerol-3-phosphate dehydrogenase, an essential monotopic membrane enzyme involved in respiration and metabolism. *Proc Natl Acad Sci* **105**, 3280–3285.

You, C., Okano, H., Hui, S., Zhang, Z., Kim, M., Gunderson, C.W., Wang, Y.-P., Lenz, P., Yan, D. and Hwa, T. 2013 Coordination of bacterial proteome with metabolism by cyclic AMP signalling. *Nature* **500**, 301–306.

Yuan, J., Doucette, C.D., Fowler, W.U., Feng, X.-J., Piazza, M., Rabitz, H.A., Wingreen, N.S. and Rabinowitz, J.D. 2009 Metabolomics-driven quantitative analysis of ammonia assimilation in *E. coli*. *Mol Syst Biol* **5**(1), 302.

Zeth, K., Fokina, O. and Forchhammer, K. 2014 Structural basis and target-specific modulation of ADP sensing by the *Synechococcus elongatus* PII signaling protein. *J Biol Chem* **289**, 8960–8972.

Zhang, Y., Pu, H., Wang, Q., Cheng, S., Zhao, W., Zhang, Y. and Zhao, J. 2007 PII is important in regulation of nitrogen metabolism but not required for heterocyst formation in the Cyanobacterium *Anabaena sp.* PCC 7120. *J Biol Chem* **282**, 33641–33648.

Zheng, D., Constantinidou, C., Hobman, J.L. and Minchin, S.D. 2004 Identification of the CRP regulon using *in vitro* and *in vivo* transcriptional profiling. *Nucleic Acids Res* **32**, 5874–5893.

Zhou, Y., Pendergrast, P.S., Bell, A., Williams, R., Busby, S. and Ebright, R.H. 1994 The functional subunit of a dimeric transcription activator protein depends on promoter architecture. *EMBO J* **13**, 4549–4557.

Zientz, E., Bongaerts, J. and Unden, G. 1998 Fumarate Regulation of Gene Expression in *Escherichia coli* by the DcuSR (*dcuSR* Genes) Two-Component Regulatory System. *J Bacteriol* **180**, 5421–5425.

Zientz, E., Janausch, I.G., Six, S. and Unden, G. 1999 Functioning of DcuC as the C_4-dicarboxylate carrier during glucose fermentation by *Escherichia coli*. *J Bacteriol* **181**, 3716–3720.

Zientz, E., Six, S. and Unden, G. 1996 Identification of a Third Secondary Carrier (DcuC) for Anaerobic C_4-Dicarboxylate Transport in *Escherichia coli*: Roles of the Three Dcu Carriers in Uptake and Exchange. *J Bacteriol* **178**, 7241–7247.

Zschiedrich, C.P., Keidel, V. and Szurmant, H. 2016 Molecular Mechanisms of Two-Component Signal Transduction. *J Mol Biol* **428**, 3752–3775.

Zubay, G., Schwartz, D. and Beckwith, J. 1970 Mechanism of activation of catabolite-sensitive genes: a positive control system. *Proc Natl Acad Sci* **66**, 104–110.

Zwaig, N., Kistler, W.S. and Lin, E.C. 1970 Glycerol kinase, the pacemaker for the dissimilation of glycerol in *Escherichia coli*. *J Bacteriol* **102**, 753–759.

Zwaig, N. and **Lin, E.C.C.** 1966 Feedback Inhibition of Glycerol Kinase, a Catabolic Enzyme in *Escherichia coli*. *Science* **153**, 755–757.

I Appendix

2.1 Oligonucleotide primers

Tab. 5: Oligonucleotide primers used for site-directed mutagenesis and PCR amplification. Restrictions sites and amino acid exchange positions are red.

Primer	Sequence (5'→3')	Amino acid exchange/restriction site
BACTH experiments		
pKT25 pUT18C *aspA* for	CGCGTCTAGAAGCCATGTCAAACAAC	XbaI
pKT25 pUT18C *aspA* rev	CGTTCCCGGGTCTGTTCGCTTTC	SmaI
pKNT25 pUT18 *aspA* for	GCTTGAAAAAGAGGATCCACATGTCAAACAAC	BamHI
pKNT25 pUT18 *aspA* rev	GTACTGAGCTCTTCGATTCCTGTTCGCTTTC	SacI
BACTH *fumB* for	CATCATGGATCCGATGTCAAACAAACCC	BamHI
BACTH *fumB* rev	GTAGTAGGTACCTTCTTAGTGCAGTTCG	KpnI
BACTH *aspC* for	CCCGGGGAGCTCATGTTTGAGAACATTAC	SacI
BACTH *aspC* rev	GTAGTAGGATCCCAGCACTGCCACAATCGC	BamHI
BACTH *glnK* for	GCTATAGGATCCCATGAAGCTGGTGACCGTG	BamHI
BACTH *glnK* rev	GATATAGGTACCGGCAGCGCCGCTTCGTC	KpnI
BACTH *glnB* for	GCGCGCGGATCCTATGAAAAAGATTGATGCG	BamHI
BACTH *glnB* rev	GCTATAGGTACCGGAATTGCCGCGTCGTCC	KpnI
glnB A49P for	CTGTACCGCGGCCCGGAGTATATGGTG	A49P
glnB A49P rev	CACCATATACTCCGGGCCGCGGTACAG	A49P
glnB Y51F for	GCGGCGCGGAGTTTATGGTGGATTTTC	Y51F
glnB Y51F rev	GAAAATCCACCATAAACTCCGCGCCGC	Y51F
Expression plasmids		
pASK IBA3plus *aspA* for	CATCATGAGCTCATGTCAAACAACATTC	SacI
pASK IBA3plus *aspA* rev	GTAGTAGGATCCCTGTTCGCTTTCATC	BamHI
pASK IBA3plus *glnB* for	CGCGCGGGTACCATGAAAAAGATTGATG	KpnI
pASK IBA3plus *glnB* rev	GTTTAAGGATCCAATTGCCGCGTCGTC	BamHI
pASK IBA3plus *glnK* for	CATCATGGTACCATGAAGCTGGTGAC	KpnI
pASK IBA3plus *glnK* rev	CAAAAAGGATCCCAGCGCCGCTTCG	BamHI
pET28a *glnD* for	CATCATGGATCCATGAATACCCTTCCAGAAC	BamHI
pET28a *glnD* rev	GTAGTAAAGCTTCCCTTTATCGTTTGGATTG	HindIII
pET28a *aspC* for	CGCGCGGGATCCATGTTTGAGAACATTAC	BamHI
pET28a *aspC* rev	GTAGTAAAGCTTCAGCACTGCCACAATCGC	HindIII
pET28a *glnB* for	GAAAGGGGATCCATGAAAAAGATTGATG	BamHI
pET28a *glnB* rev	GTAGTAAAGCTTAATTGCCGCGTCGTC	HindIII
pET28a *glnK* for	GAAAGGGGATCCATGAAGCTGGTG	BamHI
pET28a *glnK* rev	GTAGTAAAGCTTCAGCGCCGCTTC	HindIII

Tab. 6: Oligonucleotide primers used for sequencing.

Primer	Sequence (5'→3')
BACTH Seq for	GGAAACAGCTATGACCAT
pKT25 Seq rev	GGATGTGCTGCAAGGCGATT
IBA3plus Seq rev	CAGTAGCGGTAAACGGCAGAC
pET28a Seq for	CCGCGAAATTAATACGACTCACTATAG
pET28a Seq rev	GTTATGCTAGTTATGCTCAGC

2.2 Chemicals

Tab. 7:Chemicals

Chemicals	Manufacturer
2-(4-(2-hydroxyethyl)-1-piperazinyl)-ethanesulfonic acid (HEPES)	Roth
30% Acrylamide / 0,8% bis-acrylamide (37,5:1)	Roth
3-Morpholinopropane sulfonic acid (MOPS)	Roth
Acid hydrolyzed casein (AHC)	Gibco
Adenosine diphosphate (ADP)	Thermo Fisher Scientific
Adenosine triphosphate (ATP)	Thermo Fisher Scientific
Agar agar, Kobe I	Roth
Agarose NEEO Ultra Quality	Roth
Albumin Fractone V, (Bovine Albumin Serum, BSA)	BioFroxx
Ammonium chloride (NH_4Cl)	Fluka
Ammonium persulfat (APS)	Sigma-Aldrich
Ampicillin sodium salt	Roth
Bacto-Trypton	BD
Bromphenol blue	AppliChem
Calcium chloride ($CaCl_2$)	AppliChem
Chloroform	Roth
Cetyltrimethylammoniumbromid (CTAB)	Serva
Citrate	Roth
Coomassie® brilliant blue G 250	Serva
D(+)-Xylose	Fluka
D-Desthiobiotin	Sigma-Aldrich
Dimethyl sulfoxide (DMSO)	Roth
Disodium hydrogen phosphate (Na_2HPO_4)	Roth
Dithiothreitol (DTT)	Sigma-Aldrich
D-Maltose	Fluka
dNTP Mix	Thermo Fisher Scientific
D-Xylose	Fluka
Ethanol (100%)	Sigma-Aldrich
Ethylenediaminetetraacetic acid (EDTA)	Roth
GBX developer/replenisher	Carestream Healthcare
GBX fixer/replenisher	Carestream Healthcare
Glycerol (100%)	Roth
His magnetic beads	Promega
Hydrochloric acid, > 37 % (HCl)	Sigma-Aldrich
Immobilon Western Chemiluminescence HRP Substrate	Millipore
Isopropyl β-D-1-thiogalactopyranoside (IPTG)	Thermo Fisher Scientific
Kanamycin sulfate	Roth
L-[$U^{14}C$]Aspartate (40 Bq/nmol)	Hartmann Analytics
Lactose	Fluka
L-Alanine	Roth

L-Arabinose	Roth
L-Asparagine	Sigma-Aldrich
LB-Medium	Sigma-Aldrich
L-Glutamine	Fluka
L-Glycine	Roth
Lithium chloride (LiCl)	Roth
L-Malate	Fluka
L-Serine	Roth
L-Threonine	Sigma-Aldrich
L-Tryptophan	Serva
Magnesium chloride ($MgCl_2$)	Roth
Magnesium sulfate ($MgSO_4$)	Roth
Mannitol	Roth
N,N,N',N'- Tetramethylethylenediamine (TEMED)	Fluka
Na_2-Fumarate	Roth
Na_3-Citrate	Roth
ortho-Nitrophenyl-β-galactoside (ONPG)	Roth
Polyethylene glycol (PEG) 6000	Roth
Polysorbate 20 (Tween 20)	Roth
Potassium chloride (KCl)	Roth
Potassium dihydrogen phosphate (KH_2PO_4)	Roth
Pyruvate	Fluka
Red-Safe™ Nucleic Acid Staining Solution	iNtRON Biotechnologies
Rhamnose	Fluka
Rotiszint Ecoplus	Roth
SOB-Medium	Roth
Sodium carbonate (Na_2CO_3)	Fluka
Sodium chloride (NaCl)	Roth
Sodium deoxycholate (SDC)	Fluka
Sodium dodecyl sulfate (SDS)	Roth
Sodium lactate	Sigma-Aldrich
Sorbitol	Roth
Succinate	Roth
Tricin	Roth
Tris(hydroxymethyl)aminomethane (Tris)	Roth
Uridine-5'-triphosphate (UTP)	Thermo Fisher Scientific
Yeast extract	Roth
D(+)-Glucose	Roth

2.3 Media, solutions, and buffers

2.3.1 Media and buffers

All media were autoclaved, or filter sterilized prior to use.

Lysogeny broth (LB)-medium (Sambrook *et al.* 1989)

Finished mixture (Sigma-Aldrich):

10 g/l Casein

5 g/l Yeast extract

5 g/l Sodium chloride (NaCl)

LB agar

LB medium with 15 g/l Agar agar Kobe I

SOC-medium

26.64 g/l Super optimal broth (SOB)-medium

20 mM Glucose

Glycerol-MOPS-buffer

1 mM 3-(N-Morpholino)-Propansulfaonsäure (MOPS)

15% (v/v) Glycerol

TSB-buffer

LB-Medium with

100 g/l Polyethylene glycol (PEG) 6000

2,46 g/l $MgSO_4$ x H_2O

2,03 g/l $MgCl_2$ x 6 H_2O

100 ml/l DMSO

The components were dissolved in H_2O and sterile filtered.

10x M9-Medium (Miller 1992; Kim and Unden 2007)

10x stock solution:	75 g/l Na_2HPO_4 x 2 H_2O
	30 g/l KH_2PO_4
	5 g/l NaCl
	10 g/l NH_4Cl

pH value adjusted to 7.0

Supplements:	10 ml/l 10 mM $CaCl_2$
	1 ml/l 2 M $MgSO_4$
Enriched:	10 ml/l 10 % AHC
	5 ml/l 1% L-Tryptophan

As stated in the experiment:

Carbon sources:	50 mM
Electron acceptors:	20 mM
Effectors:	20 mM

Agarose gel

1% (w/v) Agarose solubilized in 1x TAE-Puffer

25 µl/l RedSafe™ nucleic acid staining solution

2.3.2 Antibiotics

Tab. 8: Antibiotics

Antibiotic	Stock solution	Final concentration
Ampicillin	50 mg/ml in H_2O	100 µg/ml
Kanamycin	50 mg/ml in H_2O	50 µg/ml

2.3.3 β-Galaktosidase assay (Miller 1992)

β-Galaktosidase-Puffer (Monzel *et al.* 2013)

100 mM Potassium phosphate buffer, pH 7.0

10 mM KCl

1 mM $MgCl_2$

0.005% (w/v) Cetyltrimethylammonium bromide (CTAB)

0.0025% (w/v) Sodium deoxycholate (SDC)

8 mM Dithiothreitol (DTT)

Solutions for the β-Galaktosidase assay

4 mg/ml *ortho*-Nitrophenyl-β-galactoside (ONPG)

1 M Na_2CO_3

2.3.4 SDS-PAGE and semi-dry Western blotting

according to Laemmli (1970), Towbin and Gordon (1984)

Resolving gel buffer

1.5 M Tris-HCl, pH 8.8

Stacking gel buffer

0.5 M Tris-HCl, pH 6.8

Resolving gel:

	Resolving gel		Stacking gel
	10%	15%	4%
H_2O	1.978 ml	1.145 ml	1.191 ml
30% Acrylamide, 0,8% bis-acrylamide mix	1.667 ml	2.5 ml	0.267 ml
Gel buffer	1.25 ml	1.25 ml	0.5 ml
SDS (10% w/v)	50 µl	50 µl	20 µl
TEMED	5 µl	5 µl	2 µl
APS (10% w/v)	50 µl	50 µl	20 µl

SDS running buffer (10x)

250 mM Tris base

1.92 M L-Glycine

1% (w/v) SDS

SDS sample buffer (2x) (Laemmli 1970)

100 mM Tris-HCl, pH 7.7

200 mM DTT

4% (w/v) SDS

0.2% (w/v) Bromophenol blue

20% (w/v) Glycerol

Tris-glycine transfer buffer

25 mM Tris base

192 mM L-Glycine

20% (v/v) Ethanol

10x PBS, pH 7.5

1.37 M NaCl

27 mM KCl

100 mM Na_2HPO_4

20 mM KH_2PO_4

Buffer for immunostaining

	Blocking	Washing	Antibody
BSA (w/v)	3%		1%
Tween 20 (v/v)	0.1%	0.1%	0.1%

solubilized in 1x PBS

Primary antibodies (Dilution 1:10,000)

Anti-Strep, fused to HRP (IBA-Life-Sciences)

Anti-His, fused to HRP (Roth)

Anti-PhoA produced in mouse (Sigma-Aldrich)

Anti-IgG-mouse-HRP polyclonal (Sigma-Aldrich)

Developer solution

Millipore Immobilon Western Chemiluminescent HRP Substrate (Merck Millipore)

2.3.5 Isolation of His-tagged Proteins

Component	Resuspension	Equilibration/Wash	Elution
Tris-HCl, pH 7.7	50 mM	50 mM	50 mM
$MgCl_2$	10 mM		
NaCl		500 mM	500 mM
Imidazole		20 mM	250-500 mM
Glycerol (10% w/v)		10%	10%

2.3.6 Isolation of Strep-tagged Proteins

Component	Resuspension	Equilibration/Wash	Elution
Tris-HCl, pH 7.7	20 mM	100 mM	100 mM
NaCl		150 mM	150 mM
EDTA		1 mM	1 mM
D-Desthiobiotin			2.5 mM

2.3.7 Transport assay

Transport buffer

100 mM Na_2HPO_4/KH_2PO_4-buffer, pH 7

1 mM MgSO4, pH 7

Solutions

0.1 M LiCl

1 M Glucose

Rotiszint Ecoplus (Roth)

L-[U^{14}C]-Aspartate (40 Bq/nmol, Hartmann Analytics)

2.3.8 Strain construction

R-Agar

10 g/l Bacto-Tryptone

1 g/l Yeast extract

8 g/l NaCl

1 g/l Glucose

12 g/l Agar agar Kobe I

After autoclaving add sterile $CaCl_2$ (2 mM)

R-Top agar

6.5 g/l Agar-Agar

solubilized in LB medium.

After autoclaving $CaCl_2$ (5 mM) and $MgSO_4$ (10 mM) were added.

MC buffer

5 mM $CaCl_2$

10 mM $MgSO_4$

3.1 Results

3.1.7 AspC-GlnK interaction in BACTH assay

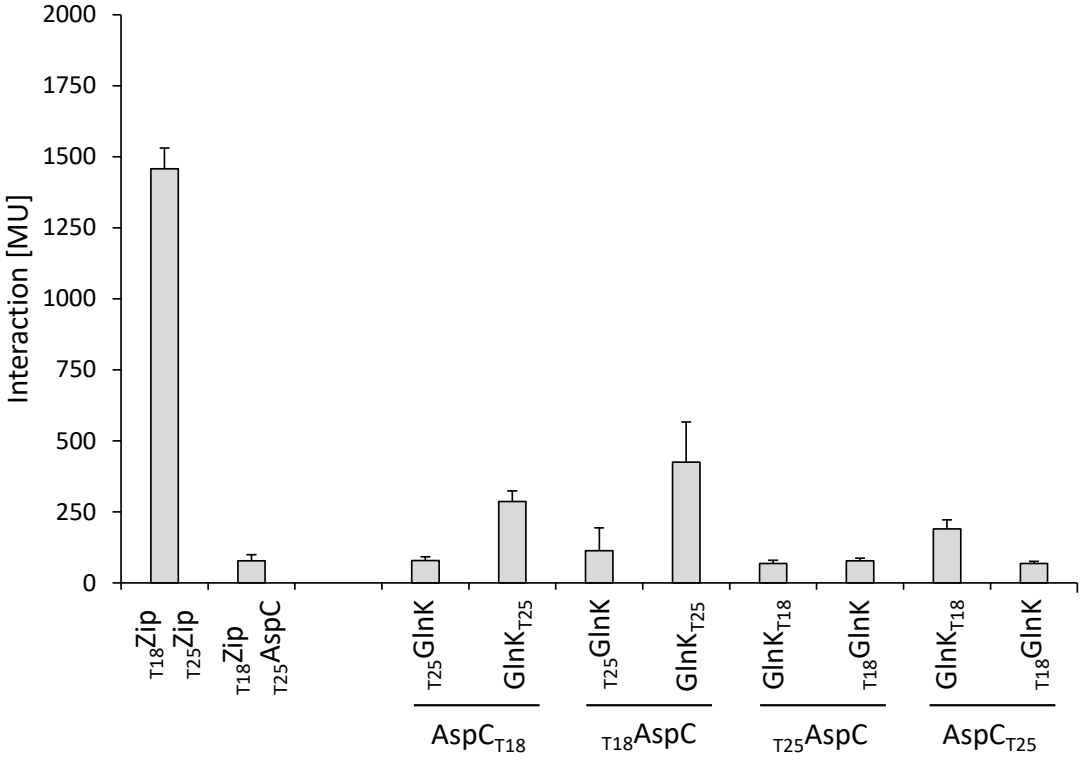

Fig. 68: Interaction of AspC with the nitrogen regulator proteins GlnK. *E. coli* BTH101 (Δ*cyaA*) was cotransformed pairwise with plasmids encoding fusions of T25 to AspC or GlnK ($_{T25}$AspC) and fusions of T18 to AspC or GlnK ($_{T18}$AspC). The combinations are shown on the x-axis. The leucine zipper pair $_{T18}$Zip and $_{T25}$Zip are applied as a positive control (Karimova *et al*. 1998; Karimova *et al*. 2001), the pair $_{T18}$Zip and $_{T25}$AspC as the negative control for background β-galactosidase activity. The corresponding plasmids are derivatives of pUT18C ($_{T18}$AspC), pUT18 (AspC$_{T18}$), pKT25 ($_{T25}$AspC), and pKNT25 (AspC$_{T25}$) (Tab. 1). The strains were grown aerobically in LB medium at 30°C. β-Galactosidase activities were quantified in Miller-Units (MU).

II Talks and Poster

Talks

Schubert, C. 2019. The role of the C_4-dicarboxylate transporter DcuA and of aspartate ammonia-lyase AspA in nitrogen assimilation by *Escherichia coli*. *2nd Rhineland-Palatinate symposium, Kaiserslautern*.

Poster

Schubert, C., Strecker, A. and Unden, G. 2019. The role of the C_4-dicarboxylate transporter DcuA and the aspartase AspA in N-assimilation by *Escherichia coli*. *VAAM annual conference, Mainz.*

Schubert, C. and Unden, G. 2020.The N-shuttle catalyzed by DcuA and AspA is regulated in *E. coli* by the nitrogen-regulator protein GlnB (PII). *6th Joint Conference of the DGHM and VAAM, Leipzig*.

III Lebenslauf

Persönliche Daten

Name	Christopher Schubert
Anschrift	
Telefon	
E-Mail	chris.schubert.93@live.de
Geburtsdatum	04.11.1993
Geburtsort	
Familienstand	
Staatsangehörigkeit	Deutsch

Promotion

04/18 – 03/21	Johannes Gutenberg-Universität Mainz Institut für Molekulare Physiologie, Mikrobiologie und Weinforschung Arbeitsgruppe Prof. Dr. G. Unden

Studium

10/16 - 02/18	Johannes Gutenberg-Universität Mainz Master of Science (M.Sc.) Biologie (Note: 1,0) Thema: Kontrolle des Sensors DcuS aus *Escherichia coli* durch den Transporter DctA und das Glucose-PTS-System Arbeitsgruppe Prof. Dr. G. Unden
10/13 – 08/16	Johannes Gutenberg-Universität Mainz Bachelor of Science (B.Sc.) Biologie (Note: 2,0) Thema: Der C_4-Dicarboxylat Stoffwechsel von *E. coli* Die physiologische Funktion von *aspA* und *dcuA* Arbeitsgruppe Prof. Dr. G. Unden

Schule

08/04 - 03/13	Goethe Gymnasium, Bensheim Allgemeine Hochschulreife (Note: 2,7)

IV Danksagung

V Eidesstattliche Erklärung

Hiermit erkläre ich, dass die vorliegende Dissertation mit dem Titel: L-Aspartate is a high-quality nitrogen source of *Escherichia coli*: regulation and physiology, von mir selbst angefertigt wurde und ich keine anderen als die angegebenen Quellen und Hilfsmittel verwendet habe. Weiterhin wurden keine entgeltliche Hilfe Dritter, insbesondere Promotionsberatung oder -vermittlung in Anspruch genommen.

_____ _____

Ort, Datum Unterschrift